REDUCED-ORDER MODELLING FOR PREDICTION OF AIRCRAFT FLIGHT DYNAMICS

BASED ON INDICIAL STEP RESPONSE FUNCTIONS INVESTIGATING AGILE AIRCRAFT UNDERGOING RAPID MANOEUVRES

by

M.J.M. Ketelaars

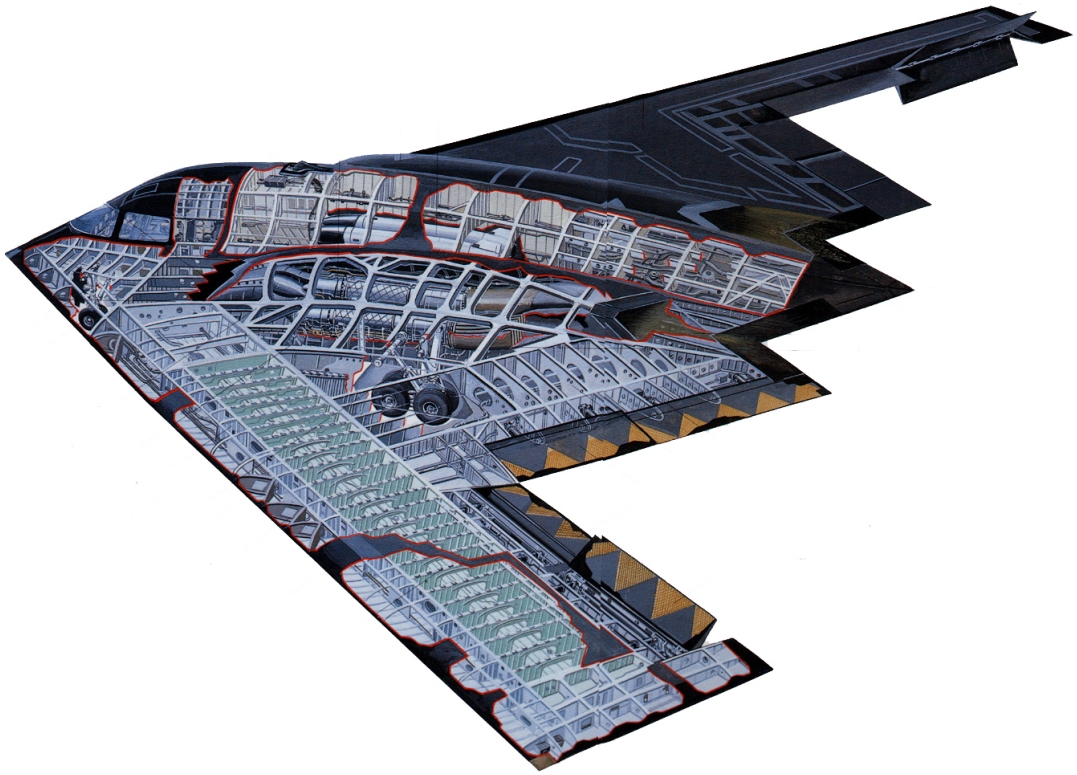

July, 2017

TU Delft

nlr Dedicated to innovation in aerospace

REDUCED-ORDER MODELLING FOR PREDICTION OF AIRCRAFT FLIGHT DYNAMICS

BASED ON INDICIAL STEP RESPONSE FUNCTIONS INVESTIGATING AGILE AIRCRAFT UNDERGOING RAPID MANOEUVRES

by

M.J.M. Ketelaars

in partial fulfilment of the requirements for the degree of

Master of Science

in Aerospace Engineering

at the Delft University of Technology,

to be defended publicly on Thursday, July 27, 2017 at 13:00 PM.

Supervisors:	Dr. Ir. Mark Voskuijl,	TU Delft
	Dr. Ir. Michel van Rooij,	NLR
Thesis committee:	Prof. Dr. Ing. Georg Eitelberg,	TU Delft
	Dr. Ir. Mark Voskuijl,	TU Delft
	Dr. Ir. Michel van Rooij,	NLR
	Dr. Jurij Sodja,	TU Delft

July, 2017

Thesis number: 140#17#MT#FPP
An electronic version of this thesis is available at http://repository.tudelft.nl/.

TU Delft

nlr Dedicated to innovation in aerospace

PREFACE

Hereby, I present my master's thesis about reduced-order modelling for flight dynamics predictions. This is a result of nine months of hard work by exploring multiple disciplines within the fields of aerospace engineering. This research has been conducted in collaboration with the Netherlands Aerospace Centre in Amsterdam. Commuting every day between Delft and Amsterdam was very worth the effort. I am very proud of the report and to present the knowledge gained for the scientific community.

Foremost, I would like to express my sincere gratitude to my supervisors, Dr. Ir. Michel van Rooij and Dr. Ir. Mark Voskuijl, for their great support and guidance during my thesis. I especially liked their enthusiasm for the project and their willingness to help me communicate findings to the outside world. I would also like to thank the other members of the committee, Prof. Dr. Ing. Georg Eitelberg and Dr. Jurij Sodja, for their time and effort in assessing this thesis.

I would also like to thank the NLR, my great colleagues at the department and the work-group AVT-251, for providing me the opportunity and resources to make a relevant contribution to the aerospace community.

Lastly, I am grateful for my family and friends in supporting me. You have been a great source of strength and inspiration to me.

Martijn
Delft, July 2017

SUMMARY

During aircraft design, multiple tools are utilised to inspect the performance of the configuration. As the design matures, higher fidelity analyses are conducted to predict the flight dynamics of the aircraft. These analyses are conducted by using semi-empirical relations, numerically analysing flow behaviour, conducting wind-tunnel tests and performing scaled test flights. However, Semi-empirical relations might not hold for next generation aircraft and wind tunnel testing and scaled test flights are extensive and are also prone to accuracy issues. A best of both worlds can be found in numerical analysis. However, an increase in flow fidelity modelling comes with an increase in computational cost. Besides, complete analysis of all possible manoeuvres of a design increases the number of computations significantly. Current methods cope with this issue by using flight dynamics models based on so called stability derivatives, instantaneous values which couple flight state parameters to aerodynamic loads to predict aircraft flight dynamics. However, these models do not take into account time dependency. Therefore, these methods do not accurately predict the flight dynamics of agile aircraft, such as unmanned combat aerial vehicles, undergoing rapid manoeuvres where unsteadiness dominates flow behaviour. This conventional reduced-order modelling method, in which samples of the full-order model are taken in the form of stability derivatives, causes design iterations to be analysed inaccurately.

The objective of this report is to investigate reduced-order modelling for flight dynamics prediction, thereby comparing conventional techniques to a method which does take into account unsteadiness in flow behaviour. The method investigated is based on indicial step response functions, which are samples in the form of unsteady aerodynamic flow behaviour functions of the full-order model. The idea is that once these samples are known, any flight manoeuvre can be analysed within minutes. Research found in literature has assessed some of the capabilities and limitations of this method, but not yet applied this to flight dynamics prediction. The research described within this report will address this gap by using two test cases.

The first testcase is used to assess the assumptions made in literature, on aerodynamics loads modelling, by applying the method on a two-dimensional airfoil in subsonic flow conditions. It was found that the indicial step response functions are indeed representing the full-order model, thereby taking into account unsteady flow behaviour in aerodynamic loads prediction. In longitudinal motions, the angle of attack and pitch rate effect need to be taken into account to predict lift, drag and pitching moments. Multiple frequencies of the same manoeuvre can be analysed within minutes once the samples are calculated. Results show that the accuracy of the predictions becomes a trade-off issue between samples calculated and accuracy required.

The second testcase is used to apply the indicial response functions to flight dynamics prediction of an agile unmanned bomber aircraft undergoing fast manoeuvres. A longitudinal-directional climbing manoeuvre was calculated by developing a flight dynamics model based on stability derivatives. The flow behaviour encountered during this manoeuvre was analysed to include highly unsteady and non-linear phenomena(e.g. vortices and flow separation) at higher angles of attack. By comparing the results of the method under investigation to the full-order solutions, it was shown that aerodynamic flight dynamics predictions were accurate in capturing unsteady behaviour and weak non-linear flow behaviour. However, the samples proved to be inaccurate in representing behaviour in highly non-linear regions.

Concluding, this means that indicial step response functions provide more accurate flight dynamics predictions than conventional stability derivatives in representing unsteady flow behaviour. The accuracy of the predictions are highly dependent on the samples chosen. Several samples suffice to predict the unsteady behaviour for linear and weak non-linear flow regions of the flight manoeuvre. If surrogate modelling is applied, the method can become more computational efficient than conducting multiple full-order time-marching numerical calculations. It is recommended that more research is performed on indicial step response functions in capturing highly non-linear flow behaviour, as the research showed that the size of the samples affects the flow behaviour representation.

NOMENCLATURE

Acronyms

AGARD	Advisory Group for Aerospace Research and Development
AOA	Angle of Attack
AVT	Applied Vehicle Technology
CFD	Computational Fluid Dynamics
CPU	Central Processing Unit
DATCOM	Data Compendium
DLR	Deutsches Zentrum für Luft- und Raumfahrt
EARSM	Explicit Algebraic Reynolds Stress Model
IPS	Indicial Prediction System
LARC	Langley Research Center
MAC	Mean Aerodynamic Centre
MDO	Multi-Disciplinary Optimisation
MIL-STD	Military Standard
MTOM	Maximum Take-Off Mass
MTOW	Maximum Take-Off Weight
MULDICON	Multi-Disciplinary Configuration
NACA	National Advisory Committee for Aeronautics
NASA	National Aeronautics and Space Administration
NATO	North Atlantic Treaty Organization
NLR	Netherlands Aerospace Centre
POD	Proper-Orthogonal Decomposition
RANS	Reynolds-Averaged Navier-Stokes
RBF	Radial Basis Functions
ROM	Reduced-Order Model
SACCON	Stability and Control Configuration
STO	Science and Technology Organization
UCAV	Unmanned Combat Aerial Vehicle
URANS	Unsteady Reynolds-Averaged Navier-Stokes
USAFA	United States Air Force Academy
VLM	Vortex Lattice Method

Greek Symbols

α	Angle of attack	$^\circ$
β	Side-slip angle	$^\circ$
Δ	Absolute difference	
δ	Deflection	$^\circ$

γ	Climb angle	°
Ω	Angular frequency	rad/s
ϕ	Roll angle	°
ψ	Heading angle	°
ρ	Air density	kg^3/m
τ	Transformed time variable	
θ	Pitch attitude	°

Roman Symbols

C_L	Lift coefficient	
C_{A_α}	Axial force coefficient as a function of angle of attack	1/rad
C_{A_q}	Axial force coefficient as a function of pitch rate	s/rad
C_A	Axial force coefficient	
C_D	3D Drag coefficient	
C_d	2D Drag coefficient	
C_{l_0}	2D Lift coefficient value at start	
C_{L_α}	3D Lift coefficient as a function of angle of attack	1/rad
C_{l_α}	2D Lift coefficient as a function of angle of attack	1/rad
C_{l_q}	2D Lift coefficient as a function of pitch rate	s/rad
C_L	3D Lift coefficient	
C_l	2D Lift coefficient	
C_{m_α}	Pitching moment coefficient as a function of angle of attack	1/rad
C_{m_q}	Pitching moment coefficient as a function of pitch rate	s/rad
C_m	Pitching moment coefficient	
C_{N_α}	Normal force coefficient as a function of angle of attack	1/rad
C_{N_q}	Normal force coefficient as a function of pitch rate	s/rad
C_N	Normal force coefficient	
C_{X_u}	X coefficient with respect to a change in u	
F_a	Aerodynamic reference frame	
F_b	Body-fixed reference frame	
F_E	Earth-fixed reference frame	
F_I	Inertial reference frame	
F_s	Stability reference frame	
T_{bE}	Earth to body frame transformation matrix	
V_∞	Inflow velocity	m/s
X_u	Derivative of X with respect to u	
A	Axial force vector	N
a	Acceleration	m/s^2
c	Chord length	m
D	Drag force vector	N
de	Elevator deflection	rad
F	Force	N
f	Function output	

g	Gravitational acceleration	m/s^2
H	Unit step function	
I	Moment of inertia	$kg \cdot m^2$
L	Lift force vector	N
L	Moment over body frame x-axis	$N \cdot m$
M	Mach number	
M	Moment over body frame y-axis	$N \cdot m$
m	Mass	kg
N	Moment over body frame z-axis	$N \cdot m$
N	Normal force vector	N
n	Load factor	
p	Roll rate	°/s
q	Dynamic pressure	Pa
q	Pitch rate	°/s
R	Resultant force vector	N
r	Yaw rate	°/s
S	Surface area	m^2
s	Non-dimensionalised time	
t	Time	s
u	Velocity component in x-direction	m/s
V	Flow speed	m/s
v	Velocity component in y-direction	m/s
w	Velocity component in z-direction	m/s
X	Force in x-direction	N
Y	Force in y-direction	N
Z	Force in z-direction	N

Subscripts

g	Gravitational force
$aero$	Aerodynamic forces
a	Aileron
e	Elevator
ref	Reference
req	Required
r	Rudder
t	Thrust

CONTENTS

1

INTRODUCTION

Aircraft design is a complex and highly iterative process. Engineers use analysis techniques combining semi-empirical design methods, numerical simulations, wind tunnel tests and experimental test flights to determine the flight mechanics of aircraft [1]. However, even while using these iterative techniques with existing tools available nearly every major fighter program since 1960 has had aerodynamic problems not discovered until flight testing [2] [3][4]. For example, the F-15 exhibited significant aero-elastic flutter [5] and the B-2 bomber (cover page [6]) experienced a residual pitch oscillation [7]. Costs might be reduced if these problems are discovered in earlier design phases. This means that using high fidelity tools, able to predict flight dynamics more accurately, earlier on in the design process are of great interest to the aerospace community.

Several methods of predicting the flight dynamics of aircraft exist. The most accurate is the use of experimental test flights, however this is also the most expensive. Besides, these are not used in the earlier design phases. Wind tunnel tests are also expensive, although cheaper than flight tests, but cope with scaling issues. Lower fidelity methods include analytic approaches and the use of semi-empirical methods such as the DATCOM method [8]. However, these techniques are not accurate enough for designs involving non-linear and unsteady aerodynamics, e.g vortices and flow separation. A compromise between high fidelity modelling and relatively low computational costs is the use of numerical methods such as computational fluid dynamics (CFD) [9]. A drawback of CFD is that a high computational effort is required when for example wanting to simulate hundreds of manoeuvres in a realistic time frame [10]. This means that there is a need for high fidelity aerodynamic loads prediction tools such as CFD while keeping the computational costs low [11]. Recent efforts in CFD based aerodynamic modelling are in the area of so called Reduced-Order Modelling [12]. These methods build a Reduced-Order Model (ROM) of the flight dynamics of the aircraft design based on several flow samples. In the ROM method investigated these exist in the form of indicial step response functions which capture the unsteady aerodynamic flow behaviour of an aircraft in several flight conditions. A ROM can then be build to accurately simulate any flight condition and aircraft manoeuvre in a relatively low time frame [13]. Currently, modelling limitations exist in taking into account unsteady and non-linear flow behaviour associated with vortices and flow separation which might occur when agile aircraft undergoing rapid manoeuvres are analysed [14]. To meet the future modelling demands and requirements, this research will therefore explore the topic of Reduced-Order Modelling based on indicial step response functions.

In the first chapter, Chapter 2, the project background as well as some required fundamentals will be given. A first testcase will explore ROM building based on indicial step response functions and address capabilities and limitations of the method in Chapter 3. Afterwards, in Chapter 4, a second testcase will apply lessons learnt to an actual agile aircraft design undergoing a rapid manoeuvre to trade-off prediction accuracy and computational effort and to make a comparison to a conventional ROM technique involving stability derivatives. The conclusions of the research will be drawn in Chapter 5, whereas recommended future research on the topic will be discussed in Section 5.4 concluding the project.

2

PROJECT BACKGROUND

This chapter will cover the project background. Before the conducted research is described it is essential for the reader to understand the terminology used. The main topic of the research is Reduced-Order Modelling for prediction of aircraft flight dynamics. Flight dynamics is the discipline concerned with the study of aircraft and their orientation and control in three dimensional space. It includes the studies of aerodynamic loads acting on aircraft, how this affects the flight path, and the other way around. Therefore, the prediction of flow behaviour resulting in the acting flight loads is highly relevant for aircraft flight dynamics. The fundamentals of these topics are found within this chapter.

The chapter will start off with a brief background on flight loads prediction in section 2.1. Here conventional modelling techniques are explored as well as the need for and challenges in accurate flight loads modelling. The associated fundamentals of flight dynamics are given in section 2.2. As mentioned in the introduction of this report multiple ROM techniques exist. Therefore section 2.3 will describe existing methods and address why indicial step response function theory is the preferred method in this research. The theorem of this method will be explained within section 2.4. To get up-to-date with past and recent developments in this method, the relevant literature is also reviewed within the section. Following this, a project plan will finally be given in section 2.5 which will address the gaps in literature and forms the structure of the research described.

2.1. FLIGHT LOADS PREDICTION

Accurate flight load prediction depends on the ability to capture the necessary amount of relevant flow phenomena. This highly affects the flight dynamics prediction as the loads affect the aircraft flight path and vice versa. When designing an aircraft it is important to assess how the design will perform during the mission and whether it meets the mission requirements. At steady conditions and low angles of attack the well-known simplified equations of motion, which will be given later on this chapter, can be used to analyse flight dynamics. Based on the flow conditions and flight parameters the aerodynamic coefficients, which represent forces and moments acting on the aircraft, are calculated. These can for example be used to check whether an aircraft is statically stable in manoeuvring flight. However, in reality flight loads are unsteady, meaning the states of an aircraft are time dependent. A vortex created at the leading edge of a wing can affect flight controls downstream. At this point more extensive numerical methods, wind-tunnel tests and experimental test-flights are required to predict whether the design meets the mission requirements. Validation and iterations are then needed in order to assess the predicted flying qualities of the aircraft.

Wind tunnel tests and experimental test flights are generally not available in the conceptual phase of aircraft design. Besides, they are more expensive than numerical methods, while CFD can predict flow behaviour relatively accurately. A drawback of numerical methods is that they cope with an increase in computational costs when more accurate results are needed as visualised in fig. 2.1. At higher angles of attack and rapid manoeuvres regions of non-linearity appear due to vortices and flow separation in the flow. These phenomena need to be captured accurately in order to model how the aircraft design will perform during flight. In order to reduce the costs of using CFD while maintaining the required accuracy, a ROM can be used. The goal of the ROM is to accurately represent flow behaviour of the full-order model, but at a lower computational effort. By successfully building a ROM the drawback of the increase in computational time of complex flow physics simulation can be taken away. One well known and conventional ROM building method is based on using stability derivatives in a flight dynamics model. These couple the flights loads to the aircraft flight path in order to predict the aircraft flight dynamics. This will be discussed in more detail within the next part.

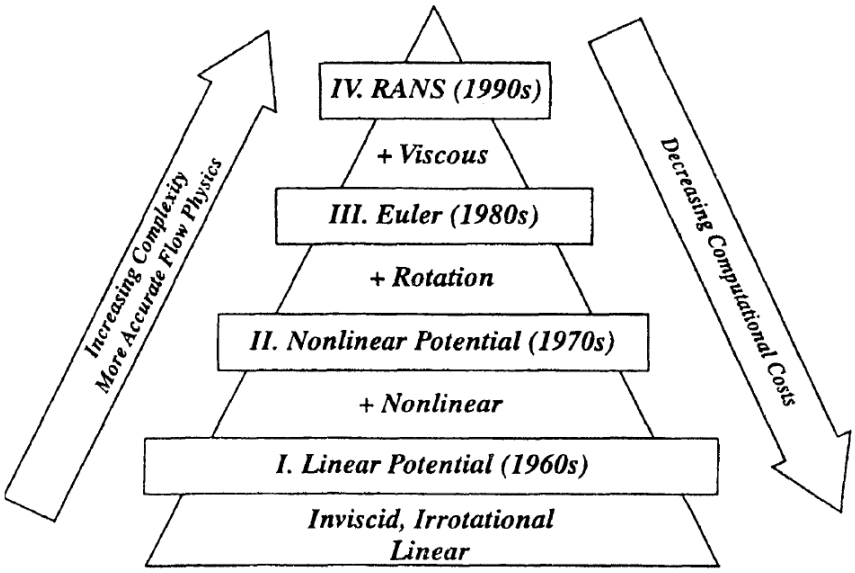

Figure 2.1: Hierarchy of fluid flow models [15]

2.1.1. Conventional flight dynamics modelling

One method to reduce computational effort while capturing relevant flow phenomena is to use stability derivatives stored in so called aerodynamic look-up tables. Samples in the form of static and dynamic stability derivatives, taking into account steady and unsteady aerodynamic effects, are calculated using high-fidelity CFD such as unsteady Reynolds-Averaged Navier-Stokes (URANS) calculations [16]. In theory this forms a dataset able to predict aircraft flight dynamics in any given flow condition. Inter- and extrapolation techniques are then used to fill in the remaining sample space. The validity of these look-up tables is then investigated by replaying simulated manoeuvres, including complex vortical flow, through the full-order time-marching CFD solutions. These tables are also often used in flight simulators for real time flight dynamics prediction.

Da Ronch et al. [17] described an approach for the generation of high-fidelity aerodynamic look-up tables using CFD. A surrogate model based on Kriging (an interpolation method) was used to generate remaining table data. The method was validated for several test cases and it was shown that the tables can efficiently be adapted for iterative aircraft design changes based on several high-fidelity CFD calculations. However, the major computational cost remains the prediction of non-linear regions (vortices) in the flight envelope. Besides, Ghoreyshi et al. [18] showed that there is a time-lag difference between the use of look-up tables and the time-marching solution for the calculation of a fast manoeuvring aircraft at high angles of attack.

This shows that aerodynamic look-up tables can be an efficient method to reduce computational time of high-fidelity CFD calculations in steady and linear flow behaviour. However, when modelling time-dependency and non-linear flow the computational efficiency declines for this method. Neglecting computational efficiency, brute-force look-up table filling is still being done [19]. However, the modelling of flight dynamics is still inaccurate. The predictions for models do not hold due to unsteady aerodynamic effects [20]. More research (Greenwell et al. [21]) states that conventional stability derivative models break down for modern agile aircraft in rapid manoeuvres. This concludes that conventional methods of reducing computational time while maintaining the required accuracy in flight prediction are lacking. To properly implement ROMs in the design it is essential to understand what the difficulties and challenges are in modelling unsteady and non-linear flow.

2.1.2. Unsteady aerodynamics

To explain the relationship between accuracy in aerodynamic flow modelling and computational effort it is essential to understand the fundamentals of (un)steady and (non)-linear flow prediction. This part will give an overview of those topics using the classical analytical approach.

It is well known that it is relatively straightforward to calculate aerodynamic loads of an aircraft in steady conditions using the equations of motion (see section 2.2). In these conditions the aircraft state variables, e.g. angles of attack and pitch rate, do not depend on previous conditions. However, to predict flight dynamics of an aircraft performing rapid manoeuvres it is essential to understand whether this is a valid assumption. To validate whether an aircraft can perform the mission requirements, an analysis of the dynamic behaviour of the configuration is required. This involves analysing unsteady effects, meaning that flight states are dependent on the time-history. This significantly increases computational effort as the complete time-history is needed to predict flow behaviour over the design.

For many years unsteady aerodynamics has been involved in the estimation of dynamic stability derivative identification. Cowley and Glauert [22] were the first to include unsteady effects into a dynamic stability analysis. It was shown that there is a delay before the down-wash of the wing reaches the tail, which is important for dynamic stability [12]. In 1925, Wagner [23] was the first to model unsteady lift of incompressible attached flow over airfoils undergoing a step change in angle of attack. Wagner's function showed that the unsteady lift asymptotically reaches a steady state value at one degree angle of attack as seen in fig. 2.2. Lomax et al. [24] continued this work and the result is also seen in the same figure. It was stated that a sudden increase in angle of attack induced a flow disturbance near the leading edge, resulting in a higher flow velocity and thereby increased suction peak. Other classical methods of two dimensional airfoils in incompressible flow followed [25][26]. Kussner's function described the response to a sharp-edge gust in incompressible flow [27]. Theodorsen's function described the frequency response of the 2D airfoil to a sinusoidal motion [28] and Sear's function gave the frequency response to a sinusoidal gust [29]. Over time, as the complexity of aircraft geome-

try increased, is was no longer practical to use analytical methods limited to 2D airfoils. A transition occurred where the numerical computation of linear unsteady aerodynamics responses in the frequency domain became the preferred method [30]. The non-linear models were calculated through a time integration. With the increasing complexity of a multi-disciplinary approach to aircraft design, there has been a transition from using simple analytical methods to numerical descriptions as described by Silva [31].

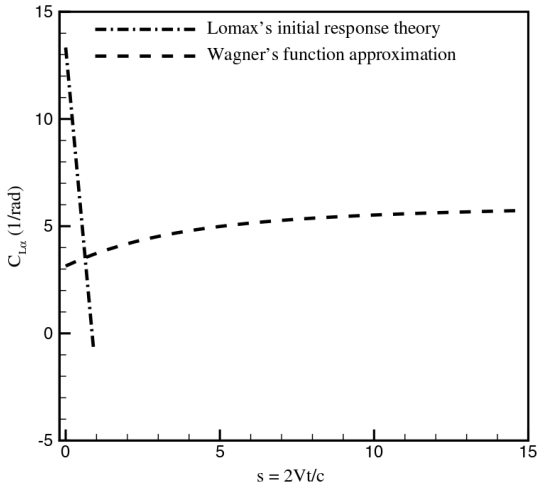

Figure 2.2: Classical analytical approximation of the lift coefficient of a 2D airfoil to a forced step response in angle of attack [32]

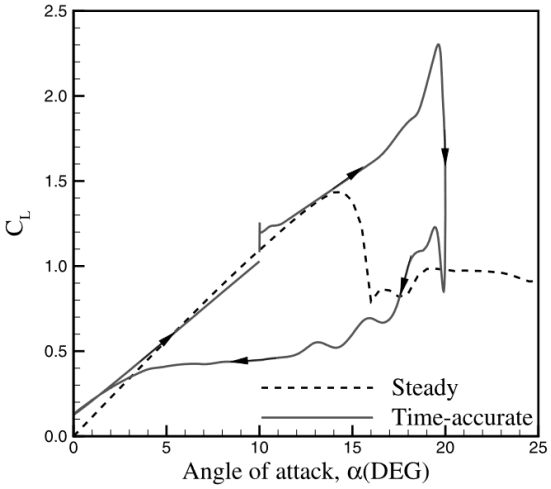

Figure 2.3: Aerodynamic load comparison between a steady and time-accurate (unsteady) CFD analysis of a NACA0012 airfoil undergoing a pitching motion [33]

2.1.3. Numerical based analysis

A numerical flow analysis using CFD is often conducted to investigate how the flow over an aircraft or airfoil configuration behaves. These algorithms approximate the loads acting on the pre-defined configuration based on the input flow conditions provided. These CFD methods can be divided into several levels of accuracy, which are already seen in fig. 2.1. These can range from low-fidelity approximations of the flow used in the Vortex lattice method (VLM) [34], to high-fidelity approximations of the Navier-Stokes equations including turbulence models able to take into account non-linear effects such as vortices, flow separation and turbulence [35] [36] [37]. What can also be seen in the figure of fluid flow models hierarchy, increasing accuracy and complexity of flow physics comes with an increase in computational costs. This research will identify capabilities and accuracy of Reduced-Order Modelling for a non-conventional configuration undergoing rapid manoeuvres at high angles of attack. It is therefore chosen to compare the validity of ROMs to the time-marching (unsteady) RANS equations including turbulence models to cope with non-linear flow phenomena. The mathematical derivation will not be elaborated further, but it is important to know that these unsteady RANS equations can be used to approximate unsteady flow behaviour and non-linear effects such as turbulence at the highest level of fidelity required.

In aircraft design, these unsteady RANS simulations are often used to validate whether the configuration meets the mission requirements. These requirements can come in the form of structural load limits or stability and control limits. As already mentioned, at higher angles of attack and rapid manoeuvres the computational cost significantly increases due to vortices and flow separation. Simulating hundreds of manoeuvres for each configuration and flight condition within a reasonable timespan is unrealistic. As a result trade offs between the number and accuracy of simulations and computational time are made. A ROM can be used to get the best of both worlds as it is a description of the aerodynamic behaviour in the form of a small number of spatial/temporal modes (typically less than one hundred) extracted from the full-order model which can reach up to an order of millions [38][39]. Basically, the ROMs are able to significantly reduce the computational effort by reducing the required number of full-order simulations while still capturing the full-order model accuracy for any given flight condition. Once this ROM is established it can be used to calculate manoeuvres much faster than it would take the full-order Navier-Stokes solution. The capabilities and limitations of different ROM types are explored later on, but first some final remarks on challenges found in accurate flow prediction based on CFD are given.

2.1.4. Challenges in prediction accuracy

To highlight the relevance of this research the challenges in current flight dynamics prediction methods will be quickly addressed again. As mentioned in chapter 1 many fighter aircraft have aerodynamic problems not discovered during flight simulation in the design. These agile aircraft often perform at high angles of attack and high rates of change due to the need to manoeuvre fast. In these conditions regions of high non-linearities and unsteadiness may appear in the flow due to vortices and flow separation. As aircraft become more unconventional [40] and operate at higher angles of attack, the accurate modelling of unsteady and non-linear flow behaviour using CFD methods becomes more relevant to flight dynamics prediction. Besides, Greenwell [2004] [21] stated that: ' for modern combat aircraft with highly non-linear aerodynamic characteristics undergoing agile manoeuvres at high angles of attack, the stability derivative model breaks down completely '. Strengthening the relevance of accurate CFD prediction methods.

As mentioned before, conventional methods are able to efficiently reduce computational time at maintained accuracy for flight dynamics prediction at low angles of attack and linear flow behaviour. Recent research [41] assessed the ability of tabular data filling, applied to an unmanned combat aerial vehicle (UCAV). At high angles of attack the predictions were inaccurate. It was shown that flow hysteresis has a large role in the decrease in accuracy of this method. Flow hysteresis is the phenomenon in which an aircraft load path during equal flight conditions might differ at different frequencies [42]. This means that in order to have accurate flow prediction at higher angles of attack more samples are needed to built an accurate ROM. Ghoreyshi and Cummings [33] investigated challenges in oscillating an airfoil at high incidence angles and whether a ROM based on indicial functions could accurately predict results compared to a full-order time-marching CFD solution. The results showed that a hysteresis loop was developed which significantly changed at different frequencies. Figure 2.3 shows the discrepancies between a steady and time-marching (unsteady) CFD solution due to flow hysteresis. This shows that there are clearly challenges in modelling accurate unsteady non-linear flow. The ability of ROMs to capture these phenomena should be validated against the time-marching CFD solution in order to investigate limitations and capabilities in more detail. In order to conduct research on modelling flight dynamics and accurate flow behaviour sampling it is essential to have a basic understanding of the fundamentals. This will therefore follow in the next section.

2.2. FLIGHT DYNAMICS FUNDAMENTALS

To understand the concepts of Reduced-Order Modelling and the link between flight path manoeuvres and aerodynamic loads, it is essential to understand the fundamentals on flight dynamics. This section discusses the sign conventions used in flight parameter identification to clarify how the aerodynamic forces and moments are defined. To model flight dynamics it is of importance to understand the concept of reference frames. These will be described in section 2.2.1. When the fundamentals on aerodynamic loads modelling are given the equations of motion can be derived. They describe how the flight parameter states affect aerodynamic flight loads, basically the aircraft flight dynamics. This will be done in section 2.2.2. Finally, in section 2.2.3, some brief basics on flight dynamics prediction and stability derivative methods are presented. The objective of this section is to provide the reader a basic understanding of definitions used in the remainder of this report and conducted research.

2.2.1. REFERENCE FRAMES

To predict the flight path and determine loads acting on the aircraft, flight path parameters are needed. The definition of these parameters are dependent on reference frames. In aircraft flight dynamic analysis multiple reference frames exist. This part will discuss the most relevant frames used during the research. Once the conventions and definitions used are given, the equations of motion are derived in section 2.2.2.

The first reference system described is the so called Earth-fixed reference frame (F_E). The origin of this system is an arbitrary location on the Earth ground. The x-axis is directed North, the y-axis is directed East and the z-axis is directed down in accordance with the right-hand rule. This frame is assumed to be the Inertial reference frame (F_I).

The second reference system is called the Body-fixed reference frame (F_b) and is often used when dealing with aircraft. The origin of the frame is the centre of gravity of the aircraft. The x-axis lies in the symmetry plane of the aircraft and points towards the nose. The z-axis points down. The y-axis can be determined using the right-hand rule and (conventionally) points towards the starboard (right) wing of the aircraft. The two frames are visualised in fig. 2.4.

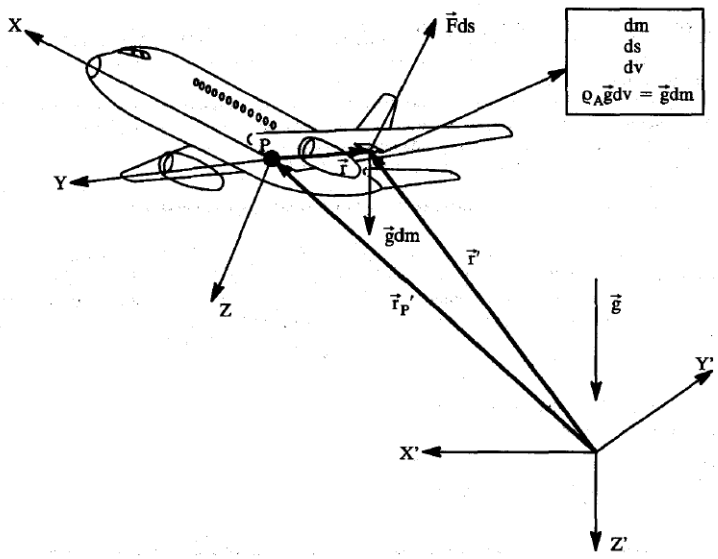

Figure 2.4: Earth- (Inertial-) and Body-reference frames [43]

To transform between these two frames the so called Euler angles are used. These angles, heading angle ψ, pitch attitude θ and roll angle ϕ , define how the body frame rotates with respect to the Earth frame (or Inertial frame). The sequence used is rotation about the z-axis, y-axis and finally the x-axis. Performing this transformation results in the following transformation matrix:

$$T_{bE} = \begin{pmatrix} \cos\theta\cos\psi & \cos\theta\sin\psi & -\sin\theta \\ \sin\phi\sin\theta\cos\psi - \cos\phi\sin\psi & \sin\phi\sin\theta\sin\psi + \cos\phi\cos\psi & \sin\phi\cos\theta \\ \cos\phi\sin\theta\cos\psi + \sin\phi\sin\psi & \cos\phi\sin\theta\sin\psi - \sin\phi\cos\psi & \cos\phi\cos\theta \end{pmatrix} \tag{2.1}$$

It is now possible to define rotation of an aircraft with respect to the Earth-fixed reference frame. The velocity in an F_E frame consists out of an u, v, and a w component in the direction of the x, y and z-axis respectively. The rotational velocity in this F_E frame is described by $\dot{\phi}$, $\dot{\theta}$ and $\dot{\psi}$. However, the rotational velocity with respect to the F_b frame is described by the rates of change p (roll rate), q (pitch rate) and r (yaw rate). Using the transformation matrix in eq. (2.1) the kinematic equations in eq. (2.2) to eq. (2.4) can be derived, showing the relation between the rotational velocities of the two frames. It is important to note that this implies that in general $\dot{\phi}$, $\dot{\theta}$ and $\dot{\psi}$ are not equal to p, q and r, only for small perturbations.

$$p = \dot{\phi} - \dot{\psi}\sin\theta \tag{2.2}$$

$$q = \dot{\theta}\cos\phi + \dot{\psi}\cos\theta\sin\phi \tag{2.3}$$

$$r = -\dot{\theta}\sin\phi + \dot{\psi}\cos\theta\cos\phi \tag{2.4}$$

A third reference frame described is the Stability reference frame (F_s). This reference frame is obtained by first rotating over the y_b-axis. This rotation angle is the well known angle of attack α. To describe the flight path and get the so called Flight-path (or Aerodynamic) reference frame (F_a) the Stability reference frame is rotated over the z-axis by the side-slip angle β. This transformation results in the frame x-axis being aligned with the velocity vector. These two angles are frequently used in aerodynamic load modelling and the relation between the angles and the velocity vector components are given in eq. (2.5) and eq. (2.6). Now that the conventions and relevant flight parameters are given, the equations of motion can be set up. These relate the flight parameters to the loads acting on the aircraft and can now be used to describe the flight path of an aircraft The equations of motion will be given in the next section.

$$\alpha = atan(\frac{w}{u}) \tag{2.5}$$

$$\beta = atan(\frac{v}{u}) \tag{2.6}$$

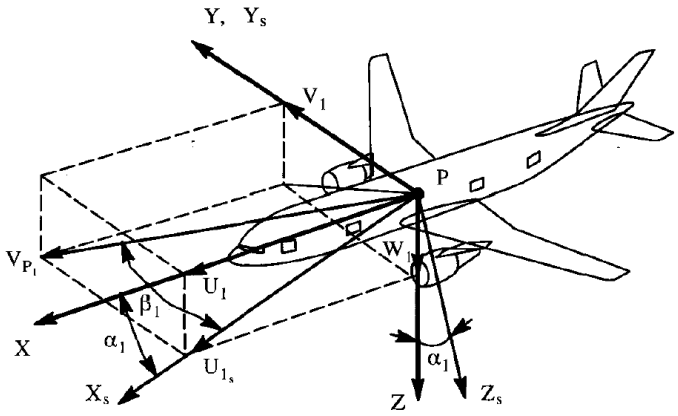

Figure 2.5: Body- and Stability-reference frames [43]

2.2.2. Equations of motion

To determine how the aircraft will behave at any given flight condition, the relation between flight parameters and forces and moments acting on the aircraft must be determined. These are called the equations of motion and describe the flight dynamics of an aircraft. Under the assumption that the aircraft is a rigid body, has a constant mass and the velocity is measured from the centre of gravity of the aircraft, the three forces on the six degree of freedom aircraft can be determined from the accelerations. Starting from the well known Newton's Second Law (eq. (2.7)):

$$\mathbf{F} = m\frac{d\mathbf{V}}{dt} = m\mathbf{a} \tag{2.7}$$

First take a look at the left hand side of this equation, to what forces the aircraft is subjected to. Two important kind of forces can be distinguished (neglecting a third thrust force). The gravity forces and the aerodynamic forces acting on the aircraft. It is well know that the gravitational force is defined as the mass multiplied by the gravitational acceleration. However, this is conventionally defined in the Earth reference frame, whereas the forces acting on the aircraft are conventionally defined in the Body reference frame. This force must therefore be given as a function of the latter one. By using the transformation matrix between the two frames of interest given in eq. (2.1), the following relation holds:

$$\mathbf{F_g^b} = mg\begin{bmatrix} -sin\theta \\ sin\phi cos\theta \\ cos\phi cos\theta \end{bmatrix} \tag{2.8}$$

The second and last kind of forces, the aerodynamic forces acting on the aircraft, are a lot harder to define and form one of the main research topics of this report. Therefore these will for now be given as X^b_{aero}, Y^b_{aero} and Z^b_{aero} and will be discussed in more detail in the next part. This results in the following (eq. (2.9)) forces acting on the aircraft during any flight manoeuvre (neglecting thrust forces):

$$\mathbf{F^b} = \mathbf{F_g^b} + \mathbf{F_{aero}^b} = mg\begin{bmatrix} -sin\theta \\ sin\phi cos\theta \\ cos\phi cos\theta \end{bmatrix} + \begin{bmatrix} X^b_{aero} \\ Y^b_{aero} \\ Z^b_{aero} \end{bmatrix} \tag{2.9}$$

Now looking at the right hand terms of eq. (2.7) the accelerations of the aircraft must be defined. These can be expressed in terms of the rotational velocities (u,v,w) and the Euler rates (p,q,r) in the Body reference frames. This results in the following equations of motion for the three forces acting on the aircraft during any flight manoeuvre, where the assumptions made still apply:

$$mg\begin{bmatrix} -sin\theta \\ sin\phi cos\theta \\ cos\phi cos\theta \end{bmatrix} + \begin{bmatrix} X^b_{aero} \\ Y^b_{aero} \\ Z^b_{aero} \end{bmatrix} = m\begin{bmatrix} \dot{u}+qw-rv \\ \dot{v}+ru-pw \\ \dot{w}+pv-qu \end{bmatrix} \tag{2.10}$$

The three non-linear equations of motion for the moments acting on the aircraft can be derived in a similar way. The resulting relations are given in eq. (2.11). These describe the three moments L, M and N over the X_b, Y_b and Z_b axis respectively. The moments depend on the inertia tensors. Using the assumption that only symmetric (over the X_b-axis) configurations will be investigated in the research, the assumption is made that $I_{xy} = I_{yz} = 0$.

$$\mathbf{M^b} = \begin{bmatrix} I_{xx}\dot{p}+(I_{zz}-I_{yy})qr-I_{xz}(pq+\dot{r}) \\ I_{yy}\dot{q}+(I_{xx}-I_{zz})pr+I_{xz}(p^2-r^2) \\ I_{zz}\dot{r}+(I_{yy}-I_{xx})pq+I_{xz}(qr-\dot{p}) \end{bmatrix} \tag{2.11}$$

How these equations of motion are applied in flight path predictions, together with a more detailed elaboration on the aerodynamic forces will be discussed next.

2.2.3. Stability derivatives

At this point the six non-linear equations of motions along with the kinematic equations, relating the transformation between reference frames, are known. These equations describe the flight dynamics of the aircraft, concerning how the forces acting on the aircraft influence the flight path in time. When looking back at eq. (2.9) the terms $\mathbf{F^b_{aero}}$ describe this relation between flight parameters and aerodynamic loads. These are highly dependent on the current state of the aircraft as well as previous states. For example, a change in angle of attack could create a disturbance near the leading edge of the wing which later occurs near the trailing edge or even the tail wing of the aircraft. The investigation on how to capture these effects with respect to accuracy and computational time is one of the main research topics in this report.

The conventional method in analysing flight dynamics is by representing the aircraft loads as a Taylor's series. Theoretically this will result in an infinite large Taylor's series expansion as the loads are dependent on all states as well as their derivatives. However, from literature [43][44] it can be generally assumed that the six forces and moments depend on the flight parameters given by table 2.1. For example, the aerodynamic forces in the X-axis of the body reference system only depend on the velocity vectors u and w, the rotational velocity q (the pitch rate), and the change in elevator and thrust deflections δ_e and δ_t. Note that this is a preliminary assumption of which the validity will be the focus point when drawing conclusions on the results later on. For example, often also the first derivatives of the flight velocities are taken into account when analysing the loads in X and Z direction [44].

Table 2.1: The six aircraft forces and moments and their flight parameter dependency assumption in the form of flight velocities, rotational velocities and control surface deflections δ [43][44]

	Flight parameters									
Loads	u	v	w	p	q	r	δ_a	δ_e	δ_r	δ_t
X	x		x		x			x		x
Y		x		x		x	x		x	
Z	x		x		x			x		x
L		x		x		x	x		x	
M	x		x		x			x		x
N		x		x		x	x		x	

The resulting dependencies are conventionally described in their non-dimensional forms. For example, the effect of the velocity vector u is given by eq. (2.12). The convention for describing the non-dimensional coefficient is given by eq. (2.13), where q is the dynamic pressure and S is the reference surface of the aircraft. These coefficients are the well known and so called stability, or control, derivatives. In short these values describe how particular forces or moments change with a change in the corresponding flight parameter. The values and signs contain the information on stability and control of the aircraft configuration, hence the name. Conventionally these derivatives can be divided in static and dynamic components concerned with the time-invariant and time dependent changes in flight parameters respectively.

$$X_u = \frac{\delta X}{\delta u} \tag{2.12}$$

$$C_{X_u} = \frac{X_u}{S_{ref} \cdot q} \tag{2.13}$$

Having the equations of motion and the effect of the flight states on the aircraft loads described by the stability derivatives, the loads acting on an aircraft during a manoeuvre can be calculated. The equations of motion can be linearised for small changes in motion. These result in a flight dynamics model where any flight manoeuvre, as well as the stability of the aircraft, can be determined. The manoeuvre can than be started by deflecting the control surfaces, the input states of the model. However, for more complex and realistic manoeuvres, where unsteady effects and non-linearities dominate flow behaviour, the equations cannot be linearised. Conventionally the stability coefficients are determined using either semi-empirical relations, wind-tunnels test, CFD or test flights in order to create look-up tables, which are used in a numerical flight dynamics model of the aircraft. This results in the conventional method of ROM building. Having the fundamentals on flight dynamics and how conventional methods fit in the bigger picture of Reduced-Order Modelling, more details on other ROM building methods are explored within the next section.

2.3. Reduced-order modelling

The principle on which reduced-Order modelling rests is that the method approximates the full-order model with the same, or at least necessary, accuracy at a reduced computational cost. To keep focus on the subject, the research will limit itself to ROMs that predict aerodynamic loads of aircraft, applied to flight dynamics, specifically to reduce computational cost of CFD while maintaining the required fidelity in model prediction. Several ROM building techniques on the topic of aerodynamic load and flow simulation will be discussed. The proposed technique explored within the main research will be discussed in more detail in section 2.4.

2.3.1. Model building techniques

Reduced-Order Modelling in general is a broad concept. One can theoretically replace every full-order model with a ROM in order to change the efficiency of processes. With the increasing focus of the aerospace industry on Multi-Disciplinary Optimisation (MDO) this has led to an increase in ROM building techniques research. For example, Parrish et al. [45] investigated how ROMs based on Proper-Orthogonal Decomposition (POD) and ROMs based on Radial Basis Functions (RBF) can reduce computational effort in finding the optimum in lift over drag for an airfoil at different angles of attack. It was found that the use of ROMs based on these techniques can indeed reduce total CPU time and thereby decrease computational effort.

POD and RBF techniques are basically complex methods of inter- and extrapolation optimisation. Research [46] [26] using POD to set up ROMs involves eigenmode analysis on the simulated flow. A ROM is set up by constructing an aerodynamic model of these dominant modes of the flow [47]. The ROMs are specifically used to analyse (dynamic) non-linear flow models, aero-acoustics and turbulence models. However, as in the use of RBF [48], this type of ROM building is a mathematical intensive method, requiring manipulation of the CFD solver code. To simulate flight dynamics using ROM aerodynamic load prediction a more flexible and less complex ROM building technique is preferred.

When investigating ROMs to improve upon the computational efficiency of aerodynamic load prediction to predict aircraft flight dynamics it has been found that Volterra Theory [49] can provide an answer. As explained in section 2.2.3 a well known conventional ROM method is to approximate the flight dynamics of an aircraft using a Taylor series expansion. The aerodynamic parameters of interest, e.g. the lift coefficient, can then be represented as an infinite sum of terms of the functions derivatives. However, this method does not take into account state history. This leads to issues in finding accurate approximations of unsteady effects present in certain flight dynamics problems. The Volterra theorem is basically similar to a Taylor series expansion, but is able to capture these unsteady effects. These are captured in so called Volterra Kernels and can model the time-history of a function [50] [51]. ROMs based on this Volterra theory have been successfully used in aero-elastic studies [52] [53]. However, calculating the Volterra Kernels is not trivial. Due to the demanding calculations of the second order kernels and higher it is not feasible to build a ROM based on Volterra theory for high non-linear flow. It is more suited for modelling weak non-linear and unsteady flow.

The above brief summary on ROM building shows that many techniques exist, each having its own strengths and weaknesses in their area of interest. The area of interest of this research requires a ROM building technique able to approximate (highly) unsteady and non-linear flow behaviour, specifically to predict aircraft flight dynamics by analysing flow behaviour of agile aircraft undergoing rapid manoeuvres. A building technique which might be able to fulfil these requirements is found in the indicial response theorem. Details on this preferred sampling method follows in the next section.

2.4. INDICIAL RESPONSE THEOREM

Reduced order models can be built using so called indicial response theory. This ROM building technique is based on indicial response functions. A detailed exploration of this ROM building technique and why it is most suitable for the conducted research is presented in this section. First the fundamentals of the theorem are given in section 2.4.1. This will give the reader a basic understanding of the mathematics and concepts involved. Secondly, the details on how to generate the indicial response functions, the dataset required for the ROMs, are given in section 2.4.2. Some final notes regarding the number of indicial response functions required to built an accurate ROM are given in section 2.4.3. When the fundamentals are provided an extensive literature review on the subject is given in section 2.4.4. Lastly, an example on how to implement the mathematics in a numerical analysis is described in section 2.4.5. This will give a complete and thorough understanding of the proposed ROM building technique when it is applied to flight dynamics analysis further on in this report.

2.4.1. FUNDAMENTALS

A response is the output of a system to a general input. This is different from an indicial response. An indicial response is the specific response of a system due to a unit step change in the input (for example in the angle of attack). The mathematical representation of the unit step function in the time domain is defined in eq. (2.14).

$$H(t) = \begin{cases} 1 & \text{for} \quad t \geq 0 \\ 0 & \text{for} \quad t < 0 \end{cases} \tag{2.14}$$

These functions are samples of the full-order model. For example, the angle of attack is forced as an input to the aircraft to investigate the indicial effect it has on the lift coefficient. Now consider one has multiple indicial response functions of a system and wants to use these samples, containing the information of the full-order system, to create a ROM. By combining the calculations of the parameter effects on the system as well as the described parameter history in the forms of functions, this might logically lead to the use of a convolution integral. By applying a convolution on the indicial effect the angle of attack has on the lift coefficient with the angle of attack history, one obtains a reduced-order model of the lift coefficient over time. The mathematics of such an integral is seen in eq. (2.15). The function shows the general response y to a forcing function f using Duhamels's superposition integral (eq. (2.15))[54]. The forcing function f might be considered to be an indicial response function of the system, e.g. lift as a function of angle of attack C_{l_α}, whereas a represents the relevant parameter, e.g. the angle of attack history during flight.

$$y(t) = f(0)a(t) + \int_0^t \frac{df(\tau)}{d\tau} a(t-\tau)d\tau \tag{2.15}$$

It was shown by Findeisen [55] using "differential theorem of the convolution integral" that eq. (2.15) can be written as:

$$y(t) = f(0)a(t) + \frac{d}{dt}\left(\int_0^t f(\tau)a(t-\tau)d\tau\right) \tag{2.16}$$

For a non-zero initial value y_0 must be added, the first term in the equation. This value represents the steady state value at which the aerodynamic load in the manoeuvre starts. Using this method one can approximate all six aerodynamic loads (coefficients) by summing the separate Duhamel's integrals. For example, Ghoreyshi et al. [2] assumed that the unsteady (linear) lift depends on angle of attack and pitch rate effects alone. Equation (2.16) can be adapted to calculate the unsteady lift, resulting in eq. (2.17), where $C_{l\alpha}$ and C_{lq} in the equation represent two indicial step response functions. Also note that the equation starts from a steady state, which is added to the total lift (coefficient) in the first term of the equation in the form of C_{l_0}.

$$C_l(t) = C_{l0} + \frac{d}{dt}\left(\int_0^t \alpha(\tau) C_{l\alpha}(t-\tau)d\tau\right) + \frac{d}{dt}\left(\int_0^t q(\tau) C_{lq}(t-\tau)d\tau\right) \tag{2.17}$$

This equation is limited to linear flow behaviour as the indicial response functions do not depend on flow conditions or angle of attack and pitch rate. This means that only two indicial response functions are used, one to take into account each effect. Tobak [56] extended this model to approximate non-linear flow behaviour. This was done by calculating the indicial functions at different angles of attack and Mach number and implementing them in Duhamel's integrals. The resulting equation is shown in eq. (2.18).

$$C_l(t) = C_{l0}(M) + \frac{d}{dt}\left(\int_0^t \alpha(\tau) C_{l\alpha}(t-\tau,\alpha,M)d\tau\right) + \frac{d}{dt}\left(\int_0^t q(\tau) C_{lq}(t-\tau,\alpha,M)d\tau\right) \tag{2.18}$$

This equation forms the basis for calculating the ROMs. The information of the full-order model is stored in the indicial step response functions and these are then used to create a reduced-order model calculating the six aerodynamic load coefficients of an aircraft during flight. The unsteady effects of each flight parameter on the aerodynamic loads, represented by the indicial functions, are convoluted in the Duhamel's integrals. In this representation the indicial response functions depend on the free stream Mach number and angle of attack, meaning more indicial response functions will be used to take into account non-linearities. This quick example shows how to make a ROM of the unsteady lift based on the assumption that it is only dependent on the angle of attack and pitch rate. To calculate the six aerodynamic forces and moments all the relevant individual indicial response functions need to be calculated. An increase in non-linearities and effects taken into account means more indicial step response functions are needed. Eventually, the computational efficiency becomes a trade-off between accuracy in full-order model representation using indicial functions and computational effort required to calculate the samples. The capabilities and limitations, together with this efficiency, form the main topic of this research. However, before the project plan and existing literature are described, first the fundamentals of the generation of the indicial step response functions are provided.

2.4.2. Indicial step response functions

As mentioned before, indicial step response functions are samples taken from the full-order model. Once these responses are known any manoeuvre can be quickly calculated by adding all the relevant Duhamel's integrals. This is very much different from conventional full-order CFD, which uses all the input parameters to find a solution to the flow equations at each time step, resulting in the six aerodynamic loads. However, the strength of building ROMs based on indicial response theory is also its weakness. The input parameters need to be uncoupled such that only one input parameter is excited, resulting in the specific system response instead of the general system response. Earlier methods for calculating these responses use small perturbations [57] or a surface transpiration approach [58]. However, these methods both need access to the CFD solvers source code which increases the complexity and lowers flexibility of calculating the solutions. More recently, Ghoreyshi et al. [32] developed a method to calculate the indicial step response function using a CFD grid motion technique. This grid motion allows the uncoupling of input parameters, e.g. the angle of attack and pitch rate, for the indicial function calculations. The fundamentals of uncoupling these two parameter effects are shown in 2.6.

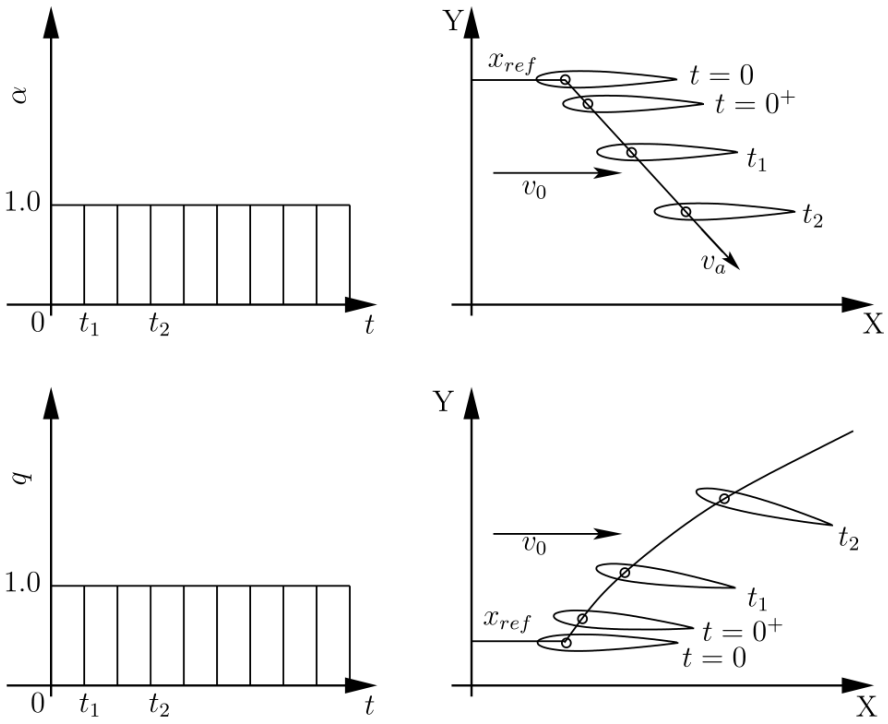

Figure 2.6: CFD grid motion technique to uncouple angle of attack and pitch rate effects by invoking a step input on the specific flight parameter resiling in the wanted indicial step response function [32]

In the left side of the picture either the angle of attack or pitch rate is given a specific step input at $t = 0$. To achieve this response using grid motion the grid is either translated downwards and to the right, for the angle of attack, or rotated to the upper right for the pitch rate. This specific input should be invoked on the CFD solution by grid motion. Details on how this indicial response is achieved by grid motion is given in fig. 2.7 and fig. 2.8 for static (angle of attack) and dynamic (pitch rate) flight parameters respectively.

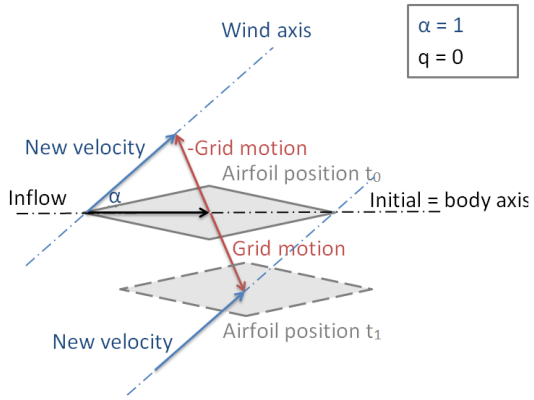

Figure 2.7: CFD grid motion technique showing detailed flow vector transformation to achieve a specific unit step input on the angle of attack while keeping the pitch rate zero

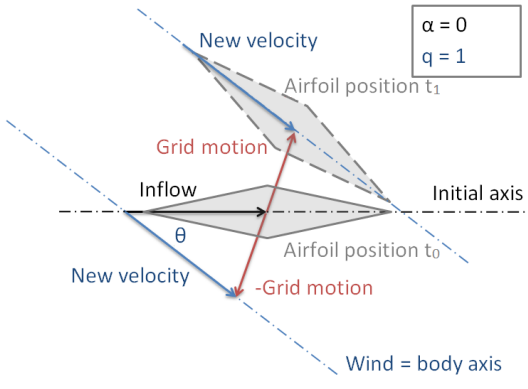

Figure 2.8: CFD grid motion technique showing detailed flow vector transformation to achieve a specific unit step input on the pitch rate while keeping the angle of attack zero

The air is flowing at a constant velocity stream wise to the initial x-axis. Translating the grid to a new position adds a new velocity vector to the CFD solution opposite to the velocity of the grid motion. By simple vector calculation of these two vectors, the original inflow and opposing grid motion vector, this results in a new total actual velocity acting upon the grid. For an angle of attack response this means translating the grid such that the new wind axis is moved while keeping the initial and body axis equal. Since there is no rotation, all effects in aerodynamic loads must come from the change in angle of attack. The same grid motion technique also applies to the side-slip angle. In order to get a pitch rate response, the grid is translated and rotated such that the new wind axis equals the body axis, resulting in a pitch attitude, but zero change in angle of attack. The magnitude of the grid motion speed results in the magnitude of the pitch rate step size. This method applies for all Euler rates. For each time step, translation and rotation are chosen so that the inflow velocity magnitude stays the same. This means that the indicial step response functions are calculated without affecting the velocity magnitudes.

This technique has been tested successfully for indicial function calculation of several aircraft configurations [59] [60] [61]. The main advantage of this grid motion approach is that it is available in most CFD solvers and does not require access to the source code. It is merely based on grid manipulation. This provides the fundamentals on ROM building based on the previously discussed samples, as well as the generation of these samples. However, one can imagine that the accuracy of a ROM highly depends on the number of samples taken into account. Therefore, a small discussion follows on system identification and how this translates in choosing the sampling space.

2.4.3. Sample space

So far the concepts of reduced-order modelling, which will be used during the research, have been explained. It was stated that once the samples in the form of indicial step responses are known the aerodynamic loads of the aircraft in any given manoeuvre can be calculated in a much lower time-frame than it would take the time-marching CFD solution. However, the accuracy of the ROM approximation is dependent on the chosen samples. For example, continuing previous sections, consider that the lift coefficient is dependent on the angle of attack and pitch rate as described by eq. (2.17). When a linear model is assumed only 2 indicial response functions are needed to predict what the lift will be for any given flight condition (disregarding validity of the assumption). However, when the angle of attack is assumed to be non-linear and dependent on the Mach number extra indicial response functions are needed. To have a fully accurate ROM every combination of angle of attack and Mach number must be calculated. This might not be computational efficient and can result in the ROM taking more time to set up than it would take the calculation of the time-marching CFD solution for a given manoeuvre. To reduce the number of computations a surrogate model can be set up based on a number of sample indicial response functions [2]. The minimum number of samples taken can then be used to fill up the remaining sample space.

Picking the samples from the complete sample space to identify the required responses of the system is not a trivial task. Samples must be chosen such that an accurate surrogate model can be set up. Several sample strategies have already been investigated. Using the previous example of the lift coefficient being dependent on the combinations of Mach number and angle of attack, three existing sampling strategies are given in fig. 2.9 [13]. The figure shows three methods to pick 144 samples from the full-order model. These samples are then used to calculate the relevant indicial response functions. Design space reduction based on Kriging has been shown to be an efficient way in surrogate modelling to approximate the indicial response functions needed to build ROMs [62] [63] [60]. This shows that a system identification is needed in order to know which samples need to be taken. For example, it might be the case that only one or several indicial responses are sufficient to represent part of any flight manoeuvre. Also, steady calculations on assumed flow behaviour will help in identifying full-order model flow behaviour. To help in the investigation of ROM building based on these functions a thorough literature review follows.

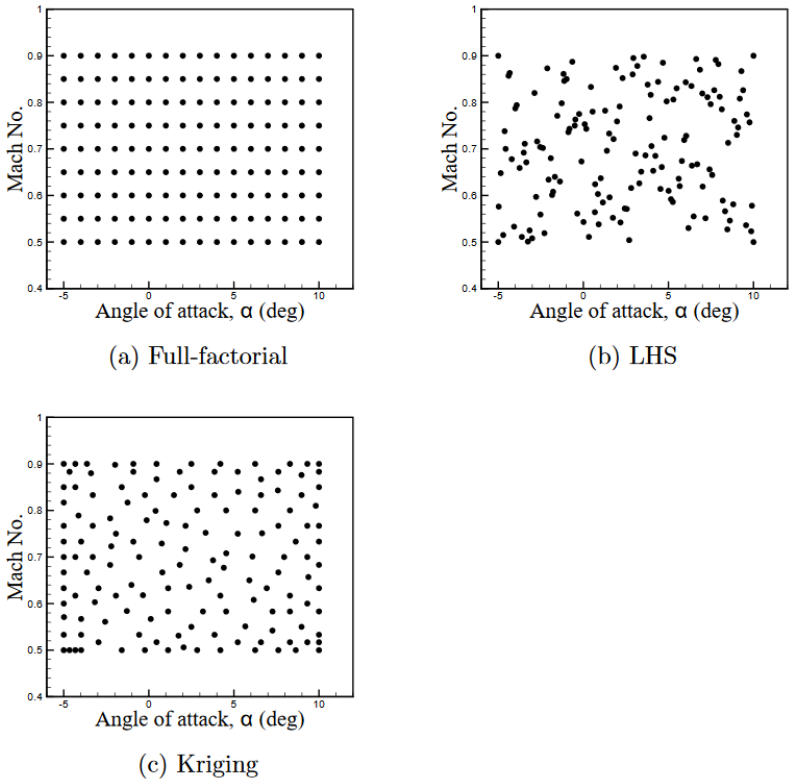

Figure 2.9: Three different sampling strategies showing 144 design space data-points [13].

2.4.4. Literature review

To asses the capabilities and limitations of the method, the relevant literature needs to be reviewed. This will help in identifying gaps in literature and clarify where more research is needed. First, the earlier work on indicial response theory is reviewed. This is followed by more recent developments, where relatively simple ROMs are built using this theorem. The gaps in literature found, will help in identifying future research required, which will be further addressed by the research proposed in section 2.5.

Earlier work

The review of earlier work will start off with the fundamentals on the indicial response theorem, given in section 2.4. The classical description of the building of a ROM, based on indicial step response functions, starts with Tobak et al. [64] in 1954. The concept of superposition and convolution was applied to an aircraft undergoing a short period manoeuvre. This was extended in 1976 [56], leading to the fundamental equation on indicial response theory to model unsteady and non-linear flow behaviour (eq. (2.18)). It was shown that the previously assumed linear aerodynamic indicial functions and superposition principles could be extended, using the theory of functionals. This led to integral forms (Duhamel's integrals) for aerodynamic responses which capture non-linearities.

Ballhaus et al. [57] investigated the use of Tobak's indicial method for the computation of unsteady transonic force and moment coefficients for a flutter analysis. The research compares this method with two other methods for computing the unsteady aerodynamic coefficients. These two methods use the conventional approach of harmonic and time-integration calculation of the complete flow field for each frequency, for each eigenmode of interest, to predict unsteady flow behaviour. The indicial method makes use of the principle of superposition which resulted in obtaining aerodynamic responses for multiple degree of freedom systems in a much faster way. This showed that unsteady and non-linear aerodynamics can be modelled faster when applying the indicial response method.

More research on the applications of this indicial method to predict unsteady flow behaviour followed [65] [66]. This was done in the fields of predicting unsteady and separated flow in transonic and supersonic regions for missiles [67][68], as well as prediction of aero-elastic effects [69]. However, these earlier works on reduced-order modelling were based on lower fidelity CFD methods and complex ways of calculating the indicial response functions. Lesieutre et al. [70] looked at a practical approach in calculating the indicial functions with a Navier-Stokes solver. The paper concludes that as long as the fundamental phenomena do not change, the indicial method is able to accurately and efficiently approximate the unsteady aerodynamic loads. When the flow phenomena change, more indicial functions are needed at different combinations of sample space (e.g. Mach number and angle of attack combination). Other results show that the indicial method works extremely well for supersonic flow ($M = 2$) at small angles of attack for inviscid flow (Euler). These papers show that the method of ROMs based on indicial response functions is a powerful way to predict unsteady and non-linear flow behaviour in a reduced computational time when compared to conventional methods. However, it also became clear that the challenge of this method lies in calculating these indicial response functions.

One of the earlier methods of directly calculating indicial response functions using computational fluid dynamics was done by Singh and Baeder [58]. A surface transpiration approach, which adds extra non-physical flows to the airfoil surface such that streamlines are changed [71], was used to uncouple the angle of attack and pitch rate effects. An unsteady Euler solver was used to produce the numerical results of a rectangular wing to a step change in angle of attack. The results were validated against 2D analytical results. It was found that indicial response functions can provide very accurate results based on directly calculated CFD solutions.

Knowing that indicial response theory can be used to predict flow behaviour based on several sample indicial response functions, Reisenthel et al. [72] performed research to verify whether new manoeuvres can be approximated once certain indicial functions are known. It was stated that with the increase in technology, and aircraft manoeuvring faster and at higher angles of attack, conventional methods such as stability derivatives might not be accurate enough in the future. Research was performed to assess whether flow behaviour can be predicted using the indicial theorem [72][73][74]. Based on experimental data extraction several indicial response function were calculated and used to predict the empty sample space [75]. Also non-linear flow phenomena such as bifurcations and flow hysteresis were taken into account [76]. The results led to the development of a tool called the Indicial Prediction System (IPS) [77] [78]. A specific example used to demonstrate the capabilities of the Indicial Prediction System (IPS) is the aerodynamic loads modelling on a 65-degrees sweep delta wing, undergoing rolling motions at high angles of attack. This is an effort to combine the research done in predicting flow behaviour of new manoeuvres based on indicial response theory and kernels obtained from extracted experimental data.

The earlier work on indicial response theorem showed the capabilities and possibilities of the method. However, as aircraft tend to perform at higher angles of attack at higher rates of change there is a need for more accurate flow prediction using the full capabilities of numerical analysis. This resulted in work-group formations such as NATO-AVT-161 [79], assessing state-of the art flight dynamics prediction methods. More recent developments on ROMs based on indicial response functions follows in the next part.

Recent developments

Recent developments in ROMs based on indicial response functions were mainly done in collaboration under the NATO STO Task Group AVT-201 "Extended Assessment of Reliable Stability & Control Prediction Methods for NATO Air Vehicles" [80]. This work-group's main objective was to "Determine an overall strategy for creating S&C databases for vehicle simulation at full-scale conditions, including the deflection of control surfaces, throughout the operational envelope of the vehicle."[81]. The research included ROMs based on several building techniques. However, the following part will only review the literature sources on indicial response theorem. Most of the found literature is a contribution or at least closely related to this work-group.

Ghoreyshi [32] investigated in 2012 the use of response functions to model aerodynamic loads using a grid motion technique. This technique is already explained in section 2.4.2. The relevant indicial response functions are calculated using the grid motion technique in unsteady RANS CFD solutions. Only the longitudinal loads were considered. The grid motion method ensures uncoupling of pitch rate and angle of attack. The unsteady lift based on the pitching moments and angles of attack of a 2D airfoil and a generic UCAV were approximated

using this ROM and validated against the full-order CFD model. Several different time-steps were investigated and it was shown that there is a peak in the initial time for the response functions. This peak reduced when the free stream Mach number is increased. This reduction is due to compressibility effects. The results of this paper are seen in fig. 2.10. The linear ROMs were able to accurately predict the unsteady lift at low angles of attack. For higher angles of attack the non-linear ROMs were able to accurately approximate the unsteady lift compared to the full-model URANS.

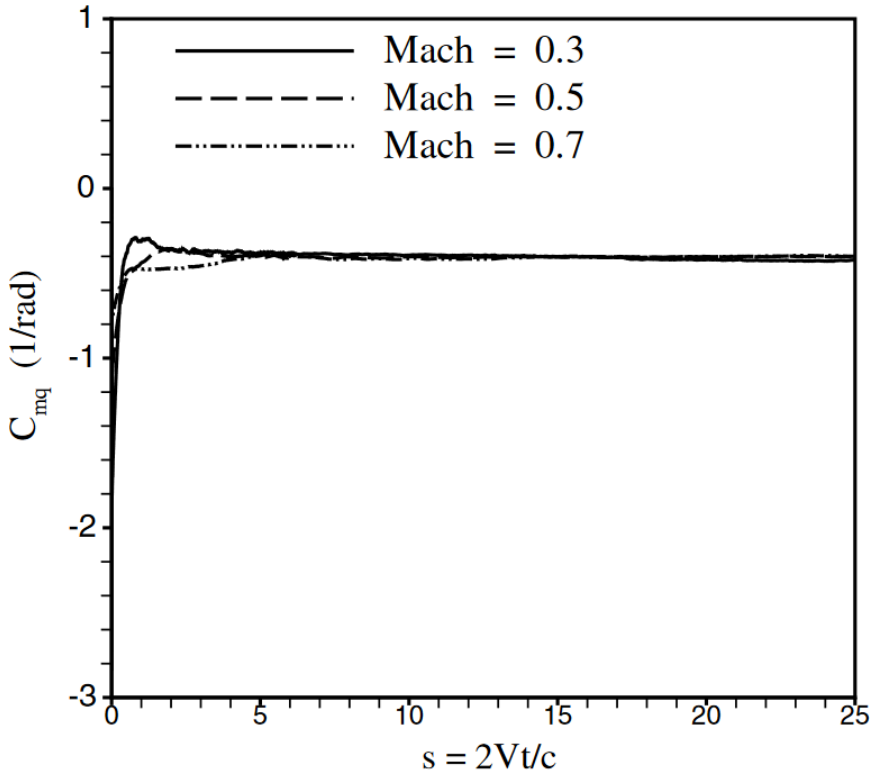

Figure 2.10: Effect of Mach number on the NACA0012 pitching moment indicial function with unit step change in pitch rate [32]

The research was followed by more work done on reduced-order modelling based on indicial response functions. The aerodynamic loads of the same generic UCAV called SACCON were analysed for manoeuvres at moderate angles of attack [12]. The six forces and moments were approximated using a ROM and compared to the unsteady RANS solutions, both based on the grid motion tool. Linear ROMs were build for highly unsteady manoeuvres, one of them was the Immelmann Turn as seen in fig. 2.11. It was shown that longitudinal loads were well predicted using the ROMs, but the lateral loads were off. This result can be seen in fig. 2.12. This is probably because of non-linearities observed. It will be an important issue to investigate whether the dependencies matter in approximating the full-order model. This will be addressed in the project plan following this section.

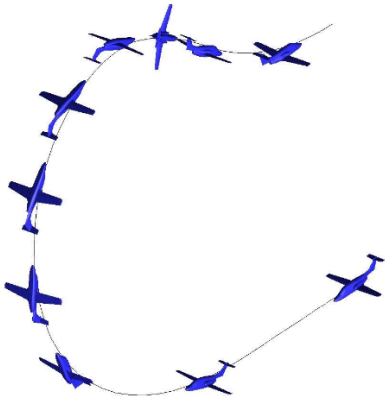

Figure 2.11: Immelmann Turn manoeuvre [82]

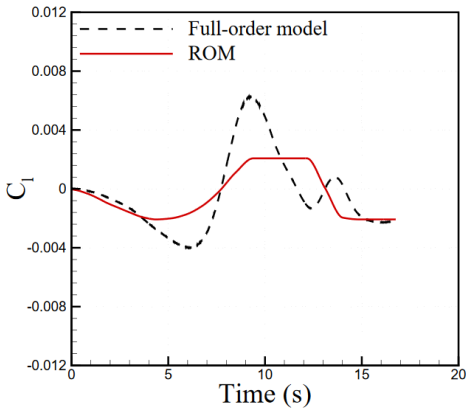

Figure 2.12: URANS and ROM solutions of the rolling-moment coefficient during an Immelmann Turn manoeuvre. [12]

Ghoreyshi et al. [59] also applied the research done on indicial response functions based ROMs on a generic fighter configuration, called X-31, in transonic flow regimes. This configuration has highly swept slender wings which results in complex vortical flow at high angles of attack. The built ROMs were validated against the full-order unsteady RANS solutions. Furthermore, a surrogate model was created to estimate the remaining sample space (combinations of Mach number and angles of attack) solutions based on some calculated samples (indicial response functions). The research explored several ROM building techniques, but the non-linear model based on indicial functions yielded the best accuracy. The predictions based on the ROMs were obtained in a matter of seconds, compared to the 52 hours using 256 processors (2.3 GHz) of the unsteady RANS solutions. Note that these results were only obtained for the longitudinal forces and moments. Lateral forces and moments and sampling strategies were not researched.

Ghoreyshi and Cummings [33] investigated the challenges in oscillating an airfoil at high incidence angles and whether a ROM based on indicial functions could accurately predict results compared to a full-order CFD solution. The results obtained showed that a hysteresis loop was developed at different angles of attack which significantly changed at different frequencies. It clearly described that current unsteady modelling methods has its limitations. Even as this relates the accuracy of full-order models with experimentally obtained data, it is important in understanding the fidelity limitations of reduced-order models.

In 2014 Ghoreyshi, Jirásek and Cummings [35] published an article about the developments and challenges in the generation of reduced-order modelling using Computational Fluid Dynamics. Several ROM building techniques were presented, including surrogate models to generate remaining design points based on number of samples. This surrogate model is important as it was able to compute remaining indicial response functions in lower computational time. Furthermore, it was stated that these ROMs can predict the initial transient behaviour seen in CFD solution, but are limited to weakly non-linear systems. Overall, the research validated that all ROM building techniques are able to predict accurate solutions for low angles of attack at a reasonable computational time when using a surrogate model.

The research conducted by Ghoreyshi et al. [61] continued the work on unsteady aerodynamic modelling using ROMs based on indicial response functions by adding control surfaces on a generic aircraft inspired by the T-38 jet trainer. Only longitudinal forces and moments were approximated using a time-dependent surrogate model. The linear ROMs predicted accurate results compared to the unsteady RANS solutions for small-amplitude deflection motions. Larger amplitude motions could only be accurately predicted using non-linear ROMs. However, this was also more expensive due to the amount of indicial responses needed at different combinations of angles of attack and Mach number. It was shown that unsteady effects due to surface deflection angles resulted in a lagging effect which led to inaccurate non-linear ROMs. This study showed that ROMs based on indicial response functions applied to configurations including control surfaces need more research to improve solution accuracy.

Part of the research done by the mentioned NATO work-group was comparing ROM results of different CFD solvers [83]. This in order to validate robustness of the ROM building technique. Linear and non-linear models were created using the grid motion approach and compared to the unsteady RANS solutions based on the same grid motion technique. A 2D NACA 0012 airfoil and a generic UCAV configuration were taken as test cases. Overall, the results matched for low to medium angles of attack. At higher angles of attack there were some discrepancies, probably due to differences in grid and solver algorithms. As shown before the initial peaks due to the step inputs decreased in magnitude at higher Mach numbers. The solvers used for the 2D case were Cobalt and Kestral at United States Air Force Academy (USAFA), USM3D at NASA Langley Research Center (LaRC) and ENSOLV at the Netherlands National Aerospace Laboratories. The 3D UCAV called SACCON was only tested using the first three solvers. All showed accurate ROM approximations of the unsteady RANS as seen in fig. 2.13. This research is important for the project proposed as it addresses the importance of choosing the right grid.

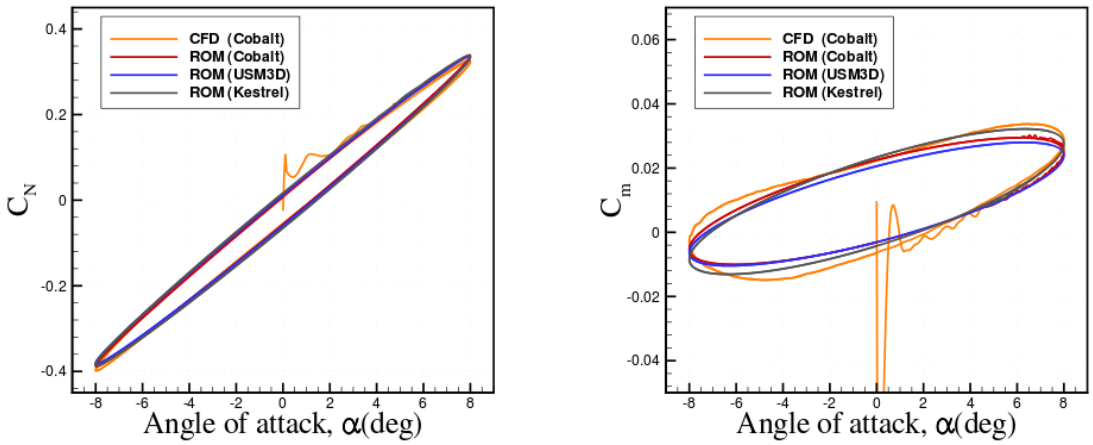

Figure 2.13: Multi-code comparison of ROM and full URANS CFD with SACCON sinusoidal motions with 8 degrees amplitude and zero mean pitch angle at M = 0.3 [83]

The work done in 2016 [84], as a contribution to the NATO STO Group AVT-201, investigated the stability and control of a generic UCAV. Besides the ROM building based on response functions and comparing them to the URANS solutions in two different CFD solvers, the results were also compared to wind tunnel data. For the ROM building different grid solvers were employed. The results of the two grids were comparable. However, discrepancies were found between the full-order CFD and wind tunnel test data, probably due to a lack in unsteady effects modelling in the CFD solutions. This is slightly less relevant to the project proposed as it will revolve around the accuracy of ROMs compared to the full-order model instead of the CFD model to the 'real' life data from wind tunnel tests. Nevertheless, the linear ROMs were able to accurately approximate the solutions for static control surface deflections at low angles of attack. However, at higher angles of attack non-linear ROMs were needed. They showed an improved accuracy, but at a higher computational cost. This leads to wondering whether the non-linear ROM based on response functions is computational efficient compared to calculating the full-order URANS for this test case. No datasets were created for a dynamic surface deflection.

Lastly, the grid motion technique was used to estimate longitudinal dynamic derivatives of a generic missile configuration [85]. The input space for the generation of the non-linear indicial step responses consisted out of several angles of attack, pitch rates and Mach numbers ranging from sub- to high supersonic. Results showed that the technique based on step responses are more accurate than traditional harmonic solution techniques for the estimation of the dynamic derivatives. Furthermore, the build ROMs were able to approximate the solution faster than the full-order unsteady RANS solutions.

Based on the literature sources reviewed, one can conclude that lots has been done in ROM building based on indicial response functions in the last years. However, this is all research not directly related to the aircraft flight dynamics prediction as a whole. The research addresses abilities and accuracy of ROMs in different cases for several aircraft configurations. Therefore it might be interesting to combine found results in a flight dynamics analysis of one interesting test case to see whether the proven ROM method is computational efficient in a design process. Research questions will be formed later on, but first the above knowledge on ROM building based on indicial step response functions will be combined in an example where a ROM will be built in a numerical manner. This will provide all the fundamentals on dataset generation and ROM building itself needed when describing the research conducted.

2.4.5. Numerical approach

Consider the equation for the ROM of the lift coefficient as a function of the two indicial step response functions of angle of attack and pitch rate, assumed by Ghoreyshi [2], in eq. (2.19). The unsteady flow behaviour effects are stored within the functions, which are taken from the full-order model. How this equation is solved in detail using a numerical approach now follows.

$$C_l(t) = C_{l0} + \frac{d}{dt}\left(\int_0^t \alpha(\tau) C_{l\alpha}(t-\tau)d\tau\right) + \frac{d}{dt}\left(\int_0^t q(\tau) C_{lq}(t-\tau)d\tau\right) \tag{2.19}$$

Starting from the assumption by Tobak et al. [64] that the time history of an aircraft motion can be broken down into an infinite number of infinitesimally small step changes in angle of attack. This assumption is visualised in fig. 2.14. The y-axis (vertical) holds the variation in angle of attack during a pitch oscillating motion, whereas the x-axis (horizontal) holds the time history. The figure shows that the history in angle of attack can be discretised, where indicial response functions are visualised within each step for convenience. Assuming that these functions are the indicial lift responses $C_{L\alpha}$, it clearly follows that the lift at time t' is the sum of the increments in lift of each time step. Alternatively, in the case of a linear lift response where the functions in each step are equal, the increments in lift for the various time steps are equivalent to the increments in the first step at time $t' - t'_1$ as is evident from the figure. This leads to the lift being written as:

$$C_L(t') = C_{L\alpha}(t')\alpha(0) + \sum_0^{t'} C_{L\alpha}(t'-t'_1)\frac{\Delta\alpha}{\Delta t'}(t'_1)\Delta t'_1 \tag{2.20}$$

Transforming the term $t' - t'_1$ to τ and letting the increment in time approach zero, Duhamel's integral (already given in eq. (2.16)) follows:

$$C_L(t') = \frac{d}{dt'}\int_0^{t'} C_{L\alpha}(\tau)\alpha(t'-\tau)d\tau \tag{2.21}$$

The integral in eq. (2.21) is basically a convolution operation (see eq. (2.22)) where the angle of attack is convoluted with the indicial response of the relevant flight parameter on the load of interest. An example will be used to show the numerical procedure of implementing this ROM building process. A flow diagram to solve this equation in a numerical manner is given in fig. 2.15. An explanation now follows based on the numbering system used in the diagram.

$$(f \star g)(t) \triangleq \int_{-\infty}^{\infty} f(\tau)g(t-\tau)d\tau = \int_{-\infty}^{\infty} f(t-\tau)g(\tau)d\tau \tag{2.22}$$

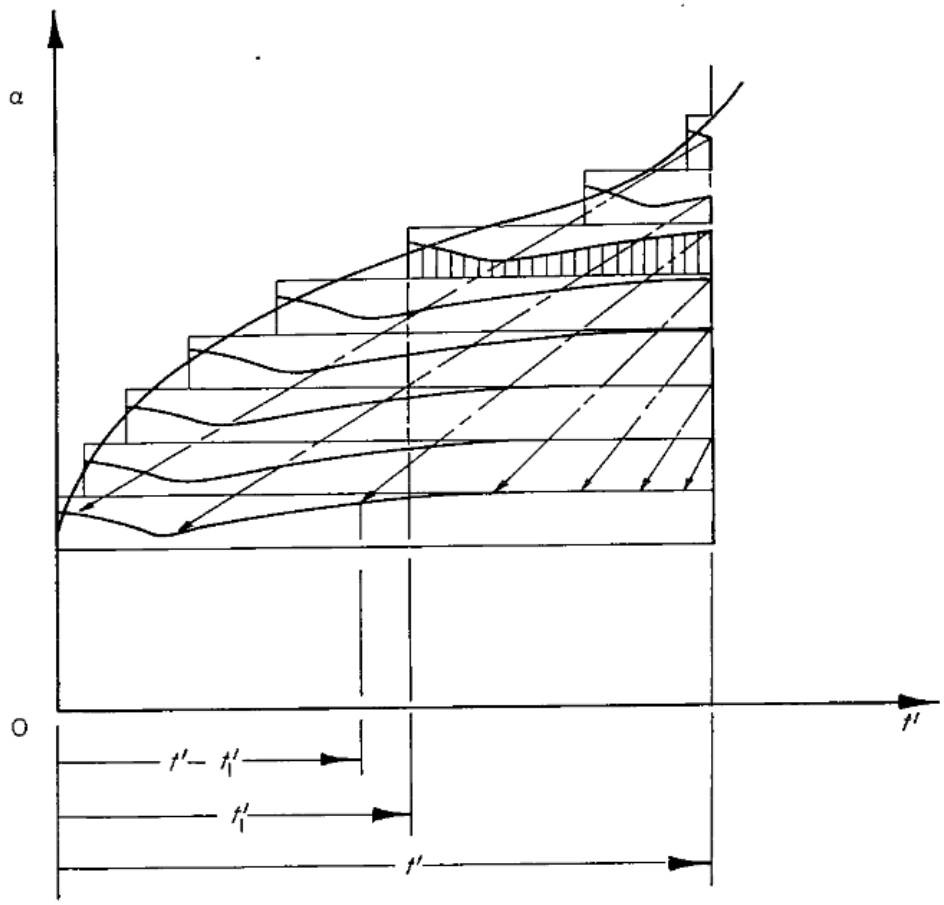

Figure 2.14: Illustration of the superposition process by Tobak et al. [64]

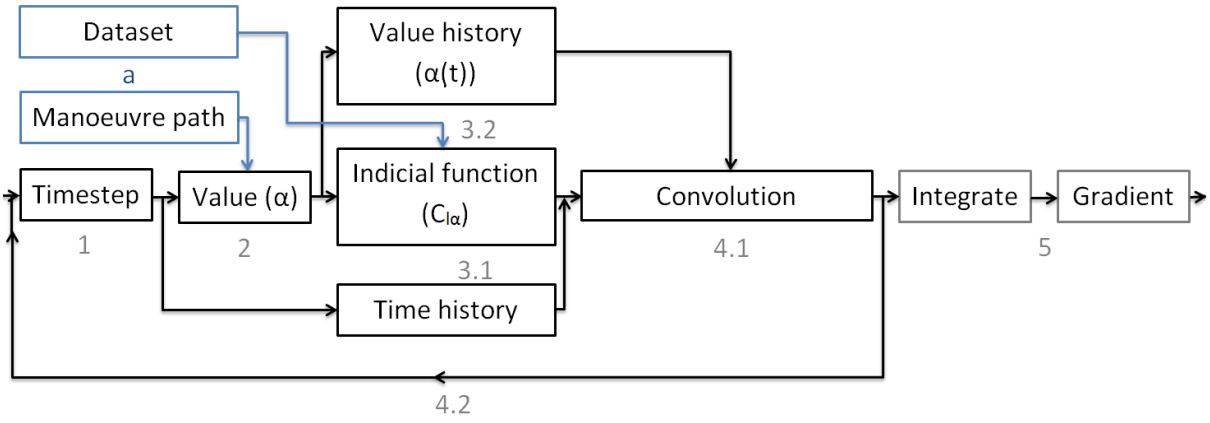

Figure 2.15: Flow diagram visualising how eq. (2.21), where the lift (coefficients) is approximated based on the unsteady C_{l_α} functions convoluted with the angle of attack history, is solved in a numerical procedure

(a) The assumption is made that the manoeuvre path is fixed and that the configuration follows a sinusoidal angle of attack motion. For now, this means that flight dynamics prediction is not considered as the loads will not affect the manoeuvre path. This is done because first a basic understanding of the ROM method to predict aerodynamic flight loads is needed. In the second testcase, in Chapter 4, the flight path will also vary by applying the method to a flight dynamics model. Secondly, assume that the lift coefficient of that configuration can be approximated by the variation in angle of attack only, as given by eq. (2.21). This ensures one sample of the full-order model being contained within the ROM building dataset. An example indicial step response function C_{L_α} is shown in fig. 2.16 together with the motion history.

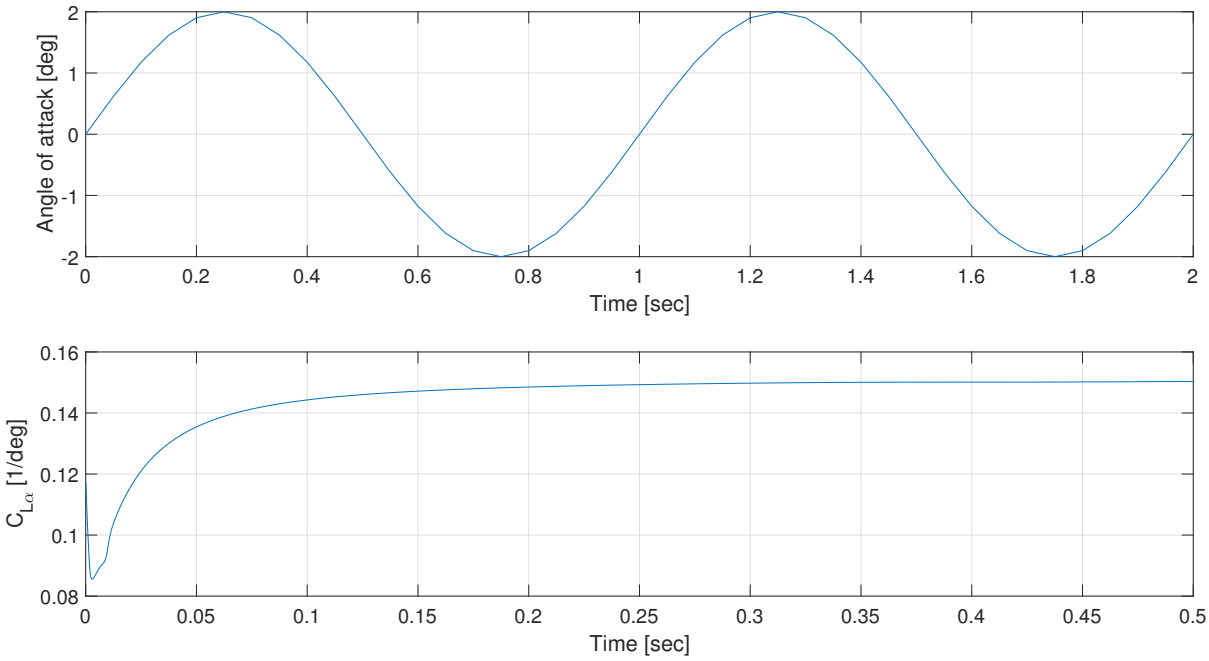

Figure 2.16: Example motion at a frequency of 1 [Hz] showing two periods where the manoeuvre path is given (top) and an example indicial step response functions is shown (bottom) making up the ROM building dataset

(1) The time history of the manoeuvre is split up into time steps. So logically the start of the loop starts at the first time step.

(2) From the manoeuvre path, the value of interest at that time step is taken. In the example this means that the angle of attack has a certain value at the time step of interest. When another flight parameter is analysed (another Duhamel's integral), say the pitch rate, this value is taken from the fixed manoeuvre path description.

(3) At this step the dataset containing the full-order model samples are used. In a conventional flight dynamics model the relevant stability derivative would be used and multiplied with the parameter value to get an aerodynamic load value, thereby neglecting unsteadiness. In this method, instead of taking an instantaneous value, the whole indicial function of interest is taken (3.1), together with the value history from start up to the current time step (3.2). In a linear model one would have one function for the whole range of angles of attack, meaning multiplying the fiction by the angle of attack. However, for a non-linear model one would have multiple functions starting at different angles of attack. For example, considering step responses sizes of one degree, if a value of 2.3 degrees is reached this means that the first degree is multiplied by the relevant step function moving from 0 to 1 degree, the second with the function for 2 to 3 and the remainder of 0.3 degrees by the indicial function moving from 2 to 3 degrees angle of attack.

(4) The next step in the process is to convolute the two functions α or C_{L_α}. This is done by flipping one of the functions, sliding one function over the other, and multiply the values in a manner described in step (3). This process is looped until a value for all time steps in the manoeuvre is found. Note that in order to ensure this method works, the indicial function needs to be as long in time as the motion takes. In the above case the indicial function is only 0.5 second long compared to the motion of 2 seconds. However, it can be assumed that the lift as function of angle of attack has reached a steady state value after 0.5 seconds so the datasets can be extrapolated to fit the motion time history.

(5) The last step is to find the sum of the integral of the complete value vector of the time history. Having the convolution solution, the last step is to find the gradient of step values in time as is described by eq. (2.20). This is the basic procedure on which the method of ROM building relies on. When multiple effects are needed, for example the pitch rate effect on the lift coefficient, the flow diagram is re-executed, now using the pitch rate values and functions over time. The resulting ROM can be seen in fig. 2.17. Note that in this case the first term on the right hand side of eq. (2.19), the steady state value at which the manoeuvre starts, is zero. In the case of a non-zero angle of attack steady flight start it is obvious that this value should be added to the final ROM.

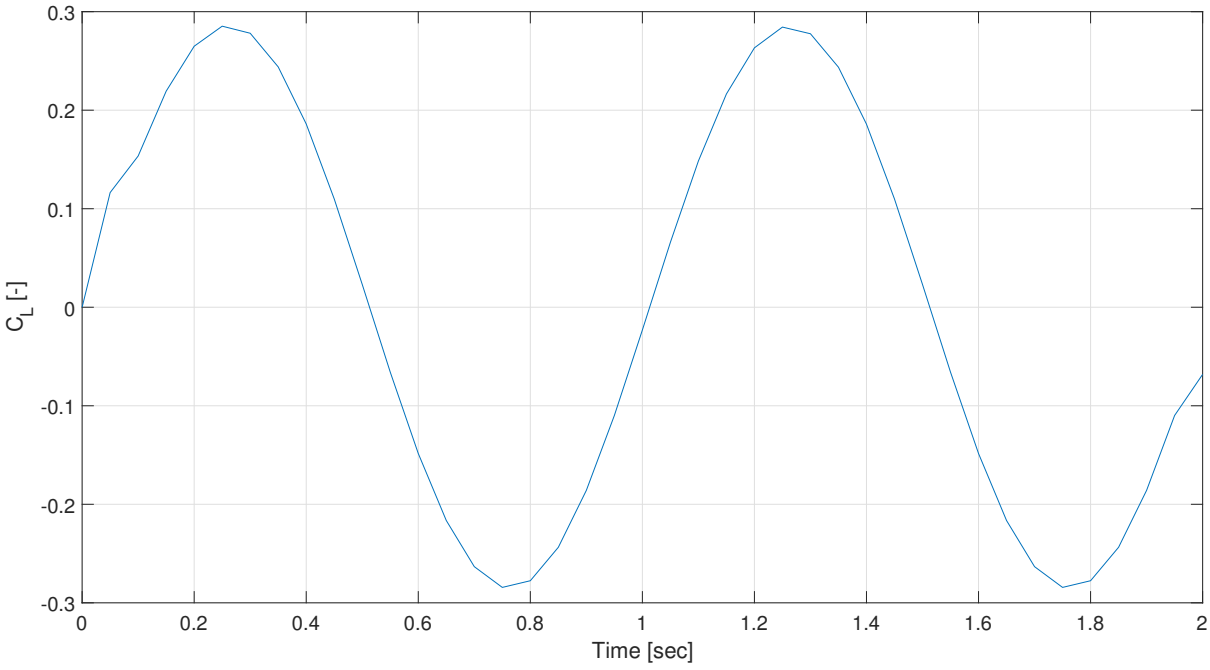

Figure 2.17: Example ROM of the lift (coefficient) load prediction only being dependent on changes in angle of attack while taking into account the unsteady behaviour of the full-order model

This motion oscillates at a frequency of 1 [Hz] showing two periods. Due to the nature of the C_{L_α} behaviour it is obvious that the resulting ROM reaches the values of the steady state relatively quickly. The unsteady effect is present in the whole motion, but only noticeable in the results in the first tenth of a second in the ROM (the small 'bump'). This is in line with physical flow behaviour. As the motion starts oscillating from a steady state flow condition, a leading edge disturbance appears, which flows downstream. These disturbances keep appearing during the whole motion (dependent on the discretization), but have the highest impact on the flow behaviour at the start of the motion. This is due to the fact that the disturbance is suddenly introduced to a steady state solution at the start, in contrast to the disturbance being present at all times in later stages of the motion. Whether this is actually the case is part of the main research, but at least the unsteadiness can directly be seen from the results in this example.

The research will focus on the benefits and limitation of this method combining flight dynamics and CFD calculations. This means that the flight path will eventually be dependent on the predicted aerodynamic loads. The basic MATLAB script for building the ROMs of the CFD calculations which also reads in additional experimental and full-order model CFD data is added in appendix A. A flow diagram showing how the individual functions work is visualised in fig. 2.18. First, some constants such as the airspeed are assumed. Then the core ROM building code is performed by initialising the manoeuvre path (ROMInit). The calculated indicial response functions are read in, redimensioned and stored within a dataset (storeIndicialData) after which the ROM is built using the described procedure in the ROMBuilder function. Afterwards, the results are plotted and a validation can be conducted by adding experimental (wind-tunnel) results (readExpData) and the full-order time-marching URANS solution (CFDReader). This concludes the fundamentals and background on ROM building of the aerodynamic loads based on indicial step response functions. The next section will present the project plan together with the research objective and research questions.

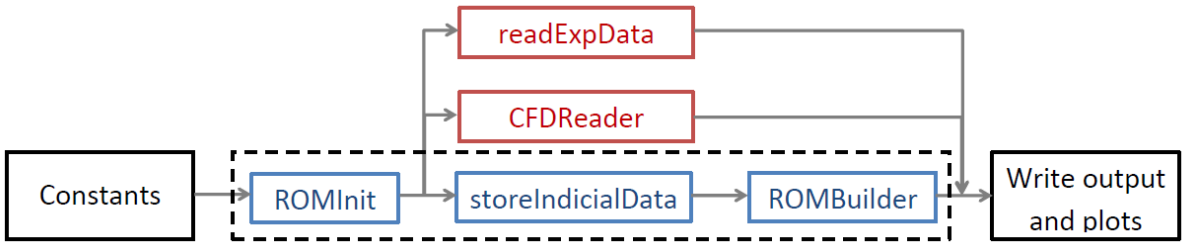

Figure 2.18: Flow diagram of the ROM building method as implemented by using separate Matlab functions

2.5. PROJECT PLAN

The goal of this research is to continue ROM research, combining lessons learnt from literature, and thereby apply the method based on indicial step response functions to flight mechanics of rapid and agile manoeuvres. A research objective will be formed using a main research question. Throughout the project an answer will be found by answering three sub-questions. The resulting project plan is described in this section.

2.5.1. RESEARCH OBJECTIVE

As is clear from the background presented in previous chapters ROMs might cope with the need to reduce computational time of accurate CFD flow predictions. However, most research was performed under assumed flight path descriptions. In a design process this flight path is not known. Stability and control of the aircraft needs to be analysed in order to assess whether the design meets the requirements or needs to be optimised. Therefore, interesting research would be to combine literature and apply this method in a more realistic flight dynamics analysis. Thereby assessing whether a ROM can improve upon existing techniques such as conventional stability derivative models. Therefore, the main research question will be:

How can Reduced-Order Modelling based on indicial step response functions improve flight dynamics prediction?

To conduct any research on flight dynamics prediction the requirements in modelling aerodynamics loads are needed. For example, modern fighter aircraft operate at high angles of attack during rapid manoeuvres which might introduce strong vortices and other non-linearities in the flow. It is essential to understand which parameters affect the flow and what degree of flow modelling is required to meet the qualifications and eventually the requirements of designs. Therefore, the first sub-question which needs answering is:

What are the requirements in modelling aerodynamic loads for agile aircraft undergoing rapid manoeuvres?

The answer to this first sub-question will provide a strong basis for the research. It will clarify what range of flight parameters are needed to model a manoeuvre such as a pitching oscillation and whether other effects might play a role on flight dynamics prediction. However, knowing the requirements in flow analysis does not automatically mean that the ROM method is able to grasp every phenomenon in the flow. Complete flow separation and unsteady vortices might be able to be predicted using full-order URANS, but might not be captured using the proposed functions. It is therefore needed to conduct research by finding an answer to the second sub-question:

What are the limitations of indicial response functions in accurately sampling flow behaviour?

The answer to the first two sub-questions will limit the research on prediction requirements and limitations. The next logical step is to define a manoeuvre and research whether the proposed ROM method is able to grasp the accuracy acquired if a conventional flight dynamics analysis was done. This give rise to the question whether a ROM based on indicial response functions is able to predict the same, or even more accurate, flight dynamics as conventional methods such as the stability derivative model given in section 2.2. If this is the case another question arises whether this method does this in a computational efficient way. Therefore, to guide the research it is needed to answer the third sub-question:

When are ROMs based on indicial step response functions more useful than conventional flight dynamics prediction methods in terms of accuracy and computational effort?

By answering the presented three sub-questions the research will show how ROMs based on indicial step response functions can improve flight dynamics analyses of new generation aircraft. Having the fundamentals, background and a project plan the research can be conducted. In order to perform a well-structured research the methodology in finding answer to the research question(s) is finally described.

2.5.2. METHODOLOGY

From literature it is known that most fundamental research of this ROM building method is conducted on a NACA0012 airfoil profile. By analysing relative simple 2D subsonic flow behaviour over such an airfoil the capabilities and limitations of indicial step response functions and ROM building itself will become clear. Therefore, a first testcase consisting out of this airfoil will be used to validate some of the research performed in literature. This will help in finding an answer to the first two sub-questions by investigating prediction requirements and assessing limitations of the ROM method. The research performed on Reduced-Order Modelling in this two-dimensional subsonic flow is described in chapter 3.

To continue the research an answer must be found to last sub-question. In order to make a comparison to conventional aerodynamic loads prediction methods in a flight dynamics analysis it is useful to have a more realistic testcase. This is found in the MULDICON baseline design as created by the the NATO AVT-251 workgroup which is concerned with the multi-disciplinary design and performance assessment of effective, agile NATO air vehicles [40]. This baseline design is a next generation lambda shape bomber Unmanned Combat Aerial Vehicle (UCAV). More details on the testcase and setup will be provided when the research is described in chapter 4. This testcase will be used to further investigate limitations of the ROM building method as well as implementing the method in a more complete flight dynamics prediction analysis. The results obtained and observations made of these two testcase will lead to an answer to the main research question thereby concluding this project. The conclusions drawn by answering these research question(s) are provided in chapter 5. The following two chapters will describe the conducted research.

3

REDUCED-ORDER MODELLING FOR AERODYNAMIC LOADS PREDICTION

The first part of the research will focus on the verification, validation and exploration of the creation of ROMs, based on the indicial step response functions. The goal of this chapter is to create a thorough understanding of the capabilities and limitations of the method, by investigating the ability of ROMs to predict aerodynamic loads on a two-dimensional NACA profile in subsonic flow conditions. The reasoning behind the chosen test case will be provided in section 3.1. After the investigation set-up has been described, the conducted research will be given. A summary of all investigations can be found in table 3.1.

The ROM building method, which uses indicial step response functions to sample the full-order model, is used to predict aerodynamic flight loads. The basic calculations, where six samples are calculated and used in ROM prediction, are given in section 3.2. By reproducing results found in literature, more accurate ROMs are calculated. These final ROM results are found in section 3.3. The accuracy of the ROMs will be further investigated in section 3.4, by using the calculated samples to predict aerodynamic loads at different frequencies of the motion. The accuracy of the samples calculated, to capture full-order model flow behaviour, will be investigated during a sensitivity analysis described in section 3.5. The last section of this chapter, section 3.6, is added to combine and discuss found results during the test case investigation. Intermediate conclusions regarding ROM accuracy, sampling space effects and computational efficiency will be given.

Table 3.1: Research conducted within this chapter to assess capabilities and limitations of ROM building based on indicial step response functions

Analysis	**Section**	**Investigation**
Sampling and ROM building	3.2	ROM building, based on angle of attack and pitch rate effects
Linearity assumptions	3.3	Reproduce and analyse ROMs created in literature
Motion frequency	3.4	Investigation of ROM accuracy
Pitch rate effect sampling	3.5.1	Flow state dependency and step size magnitude
Angle of attack effect sampling	3.5.2	Negative step responses and flow hysteresis prediction

3.1. TEST CASE DESCRIPTION

In line with literature and to reduce complexity, the first testcase will be the NACA0012 airfoil. As this setup is a 2D case, only the longitudinal loads (lift, drag and pitching moment) need to be taken into account during aerodynamic loads analysis. Extending the model to a 3D case will be relatively straightforward as the procedure for the generation of the indicial step response functions and the ROMs are similar for the other three aircraft loads in a six degree of freedom flight dynamics model.

The size and shape of the profile can be seen in fig. 3.1. In convention with the used CFD solver ENSOLV, the leading edge of the airfoil points towards the left. The height of the airfoil is in the positive z-axis direction and the air flows towards the trailing edge in the positive x-axis direction. As this is a symmetric airfoil, the centre of pressure and aerodynamic centre lie at one quarter of the chord length behind the leading edge. Sign conventions are identical for all reference systems, but will be given explicitly in this report when required. As the datasets will be generated using CFD, a detailed description of the numerical setup in the CFD solver ENSOLV will be given next.

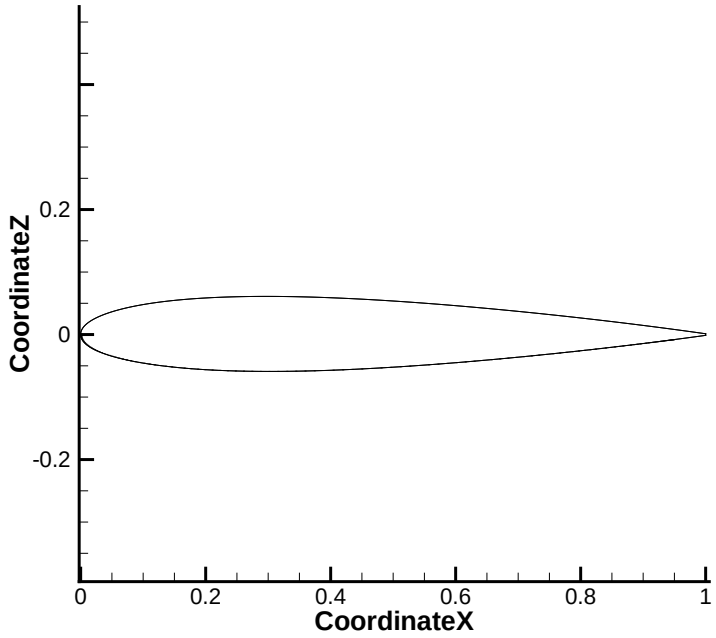

Figure 3.1: Shape of the NACA0012 airfoil as interpreted by CFD solver ENSOLV

3.1.1. NUMERICAL SETUP

To limit complexity of the results several assumptions are made. The flow speed is assumed to be constant, having a value of 0.6 for the Mach number. In line with the literature reviewed in section 2.4.4, the proposed ROMs are able to predict aerodynamic loads correctly in subsonic flow. Due to this assumption the effect of changing speed during the flight motion is not taken into account at first. Furthermore, even as the NACA0012 airfoil might not induce high non-linearity and unsteadiness in the flow at low to medium angles of attack, it is decided to analyse the flow by solving the URANS equations. To cope with possible turbulence in the flow an Explicit Algebraic Reynolds Stress Model (EARSM) in K-omega form is added [86]. This might increase computational time, but as this testcase will only be used to apply the theory and verify the method, this is less relevant than the accuracy investigation. The computational effort will be more relevant in the second testcase. By applying the URANS in the 2D testcase, the accuracy in CFD results will be consistent when considering the 3D testcase in the next chapter such that lessons learnt from the NACA airfoil can be applied directly.

GRID

The grid used in ENSOLV is fully structured and given in fig. 3.2. The grid was produced by NLR using NLR's in-house domain modeller and grid generation tools Endomo [87] and Engrid [88] respectively. The grid consists of a total of 54,272 cells, with 96 cells placed along the chord. The dimensionless wall distance for proper turbulence modelling $y+ \approx 1$. This grid will be used to approximate the RANS solutions and calculate the samples of the full-order model, the indicial step response functions. The time steps for unsteady calculations in ENSOLV are non-dimensionalised by the constant speed and reference length of the airfoil. A value of 0.01 for these time steps, with the combination of roughly 30 to 50 sub-iterations per time step (depending on the calculation), proved to be a valid size in order to have reliable accuracy in the CFD solution. Under these assumptions, a manoeuvre can be selected which will be used to investigate the accuracy of the ROMs versus the full-order model. This will be done in the next part.

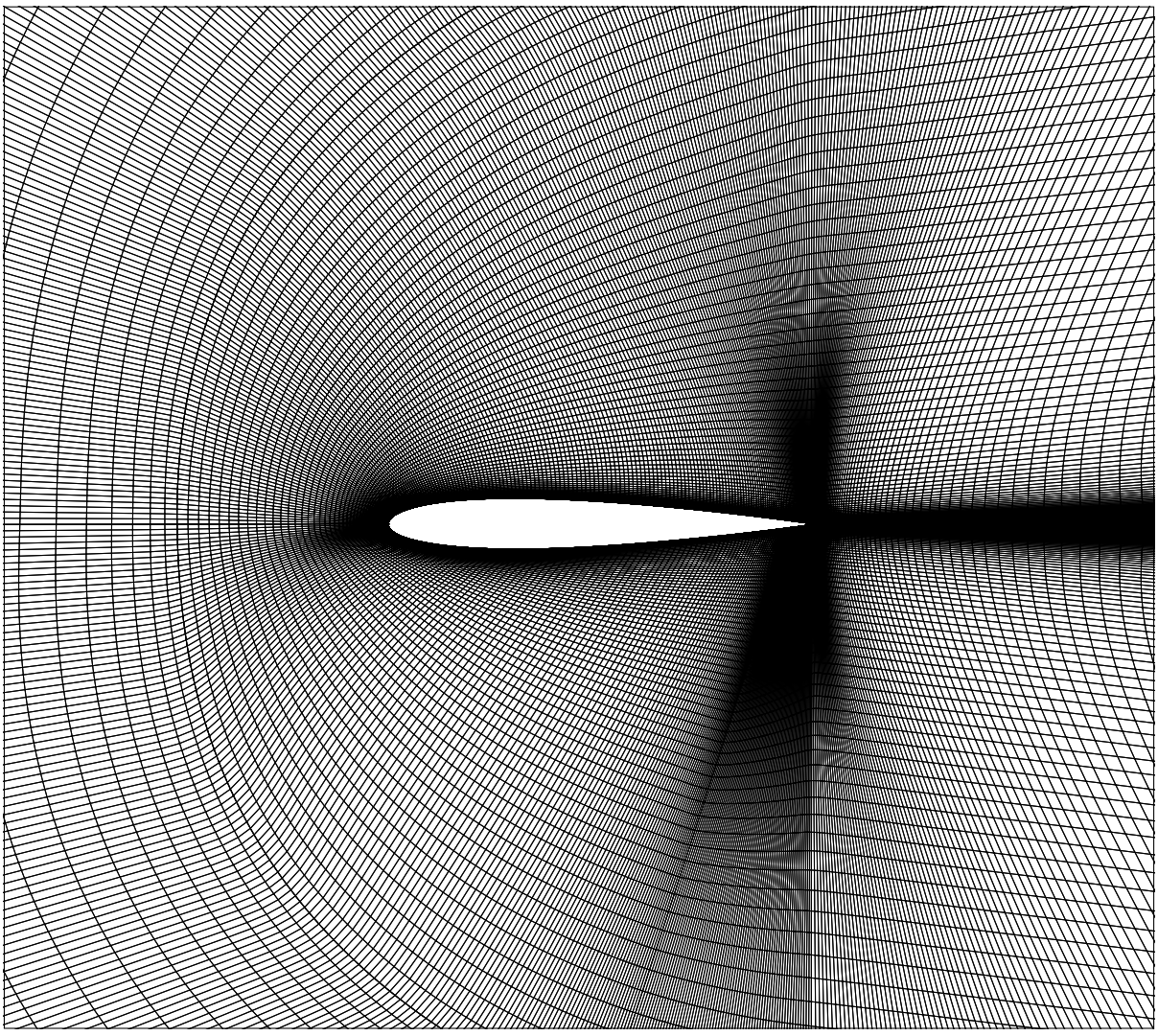

Figure 3.2: Fully structured NACA0012 grid consisting of 54,272 cells

3.1.2. MANOEUVRE SELECTION

Before the indicial response functions are generated it is required to know which indicial responses are necessary. The test case is focused on a two-dimensional constant subsonic flow, limiting the manoeuvres to longitudinal motion. The manoeuvre which will be used to verify the built ROMs with the full-order model is strongly related to the first sub-question proposed:

What are the requirements in modelling aerodynamic loads for agile aircraft undergoing rapid manoeuvres?

To make a relevant statement regarding the requirements in longitudinal load analysis (lift, drag and pitching moment) of this testcase, it is necessary to get a basic understanding of the flow behaviour. Therefore, first the steady behaviour of the test case is considered. These values are calculated by setting the airfoil at a certain angle of attack with respect to the inflow air and finding the steady RANS solution. The lift coefficient as well as the drag coefficient as a function of the angle of attack is given in fig. 3.3. The pitching moment over angle of attack is given in fig. 3.4. The flow behaviour is as expected in these conditions. Due to the relatively high Reynolds number and Mach number, non-linearities already appear from angles of attack of four degrees and onward. What can be seen is that separation starts to occur after 8 degrees angle of attack. A manoeuvre covering the range from 0 to roughly 8 degrees angle of attack would therefore be a suitable candidate to test the ROM method and see whether unsteady effects can be taken into account. In theory, unsteady effects would postpone separation and increase the lift coefficient at higher angles of attack as the flow disturbance moves downstream. Higher frequencies would therefore be more interesting to investigate. This leads to the testcase being similar to those in literature [89]. Here, the assumption is made that the three longitudinal loads only depend on changes in angle of attack and pitch rate, thereby disregarding higher order terms of these effects. This research will therefore start with the same assumptions. Later in this chapter it will become clear whether these assumptions hold for the manoeuvre chosen.

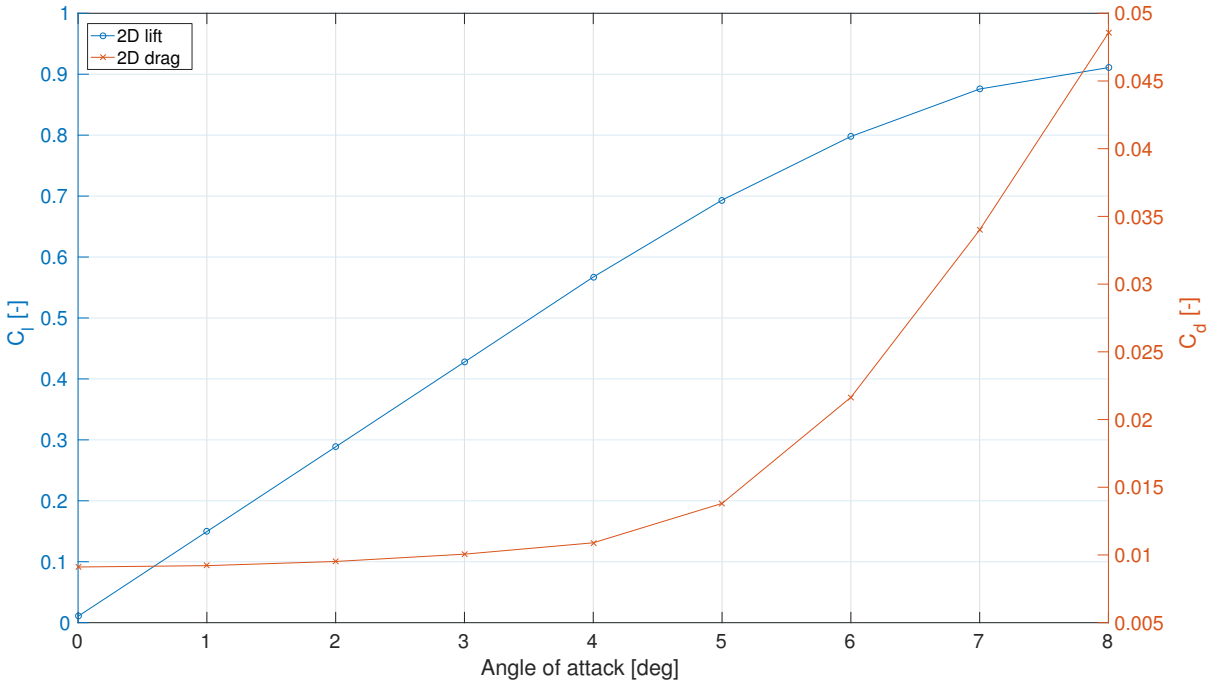

Figure 3.3: Steady RANS 2D lift and drag coefficients as a function of angle of attack of a NACA0012 profile at a Mach number of 0.6 and Reynolds number of 4,800,000

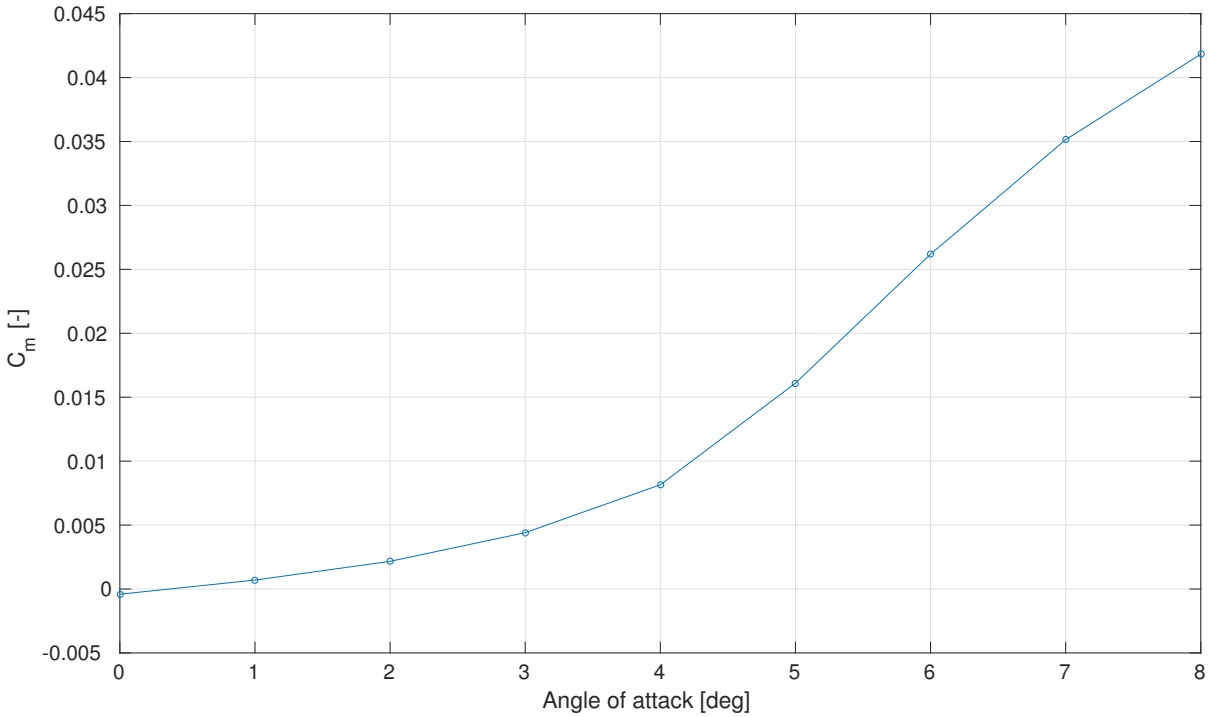

Figure 3.4: Steady RANS 2D pitching moment coefficient as a function of angle of attack of a NACA0012 profile at a Mach number of 0.6 and Reynolds number of 4,800,000

In order to reduce complexity the pitch oscillation will occur from a standstill position, meaning the flight path axis system does not move with respect to the inertial axis system. This implies that the angle of attack and pitch attitude are equal during the motion. This will also make sure that derivatives of the effects are the same for angle of attack and pitch attitude, thereby minimising an increase in complexity if these are incorporated. In line with literature and experiments already conducted in wind-tunnels [90], the manoeuvre given in eq. (3.1) is investigated. This pitch oscillation motion is described by fig. 3.5. The frequency will be 5.27 [Hz] and the timespan is chosen such that two periods can be analysed.

Now that the setup for the ROM code development is known, in the next part the first ROMs will be built by first generating the indicial step response functions.

$$\theta = \alpha = 3.16^\circ + 4.59^\circ sin(\omega t) \tag{3.1}$$

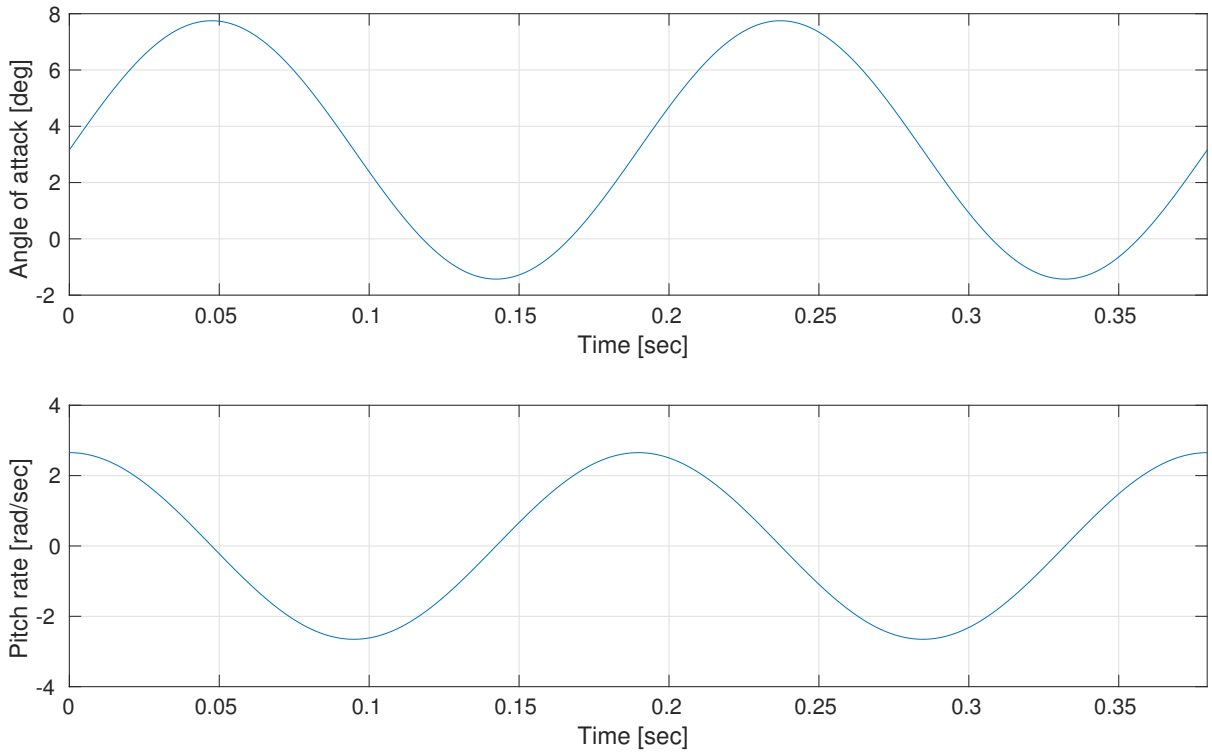

Figure 3.5: Longitudinal flight parameters of a two period pitching oscillation manoeuvre for the 2D NACA0012 testcase at a frequency of 5.27 [Hz]

3.2. BASIC CALCULATIONS

Having a motion to investigate and knowing the requirements on modelling the three longitudinal loads, the resulting ROMs can be created. As assumed before, the loads are dependent on the effects of angle of attack and pitch rate. Mach number is considered to be constant during the motion. This section will provide the basic calculations of ROM building to predict aerodynamic loads. Therefore, first the minimum required number of functions in the dataset in order to build a ROM is calculated and the results are given in section 3.2.1. The so called resulting 'linear' ROMs will be given in section 3.2.2. The linearity in these models will become clear during the generation of the datasets and the discussion of the results.

3.2.1. INDICIAL STEP RESPONSES

ROMs are generated using the fact that a reduced-order model can be built based on samples from the full-order model. In this method these samples come in the form of indicial step response functions, which together form the dataset from which the ROMs are built. The assumptions made require that the ROMs are based on a minimum of 6 indicial step responses: The indicial effect of a step input in angle of attack on the three longitudinal flight loads and the indicial effect of a step input in pitch rate on the aerodynamic loads.

Before the step responses are generated, the conventions used should be clear. Details on the reference systems are already given in section 2.2.1, but for clarity purposes a brief recap of longitudinal forces in the frames follows. From common knowledge on aerodynamics it is clear that a resulting total aerodynamic force vector can be calculated from the pressure distribution over an airfoil. This resultant vector may de decomposed into two vectors in the x- and z-axes. This is visualised in fig. 3.6. However, these two vectors can be divided either in the wind-axis frame or the body-frame. When the resultant force is divided into components on the wind-axis frame one gets the conventional lift and drag force vectors. Lift acts on the airfoil in a direction perpendicular to the relative wind vector. Drag is the resistance that opposes the motion of the airfoil trough the air, parallel to the relative wind vector. These are calculated using the angle between the body- and wind-frame reference axes, the angle of attack. However, when the resultant force vector is decomposed in two components on the body-frame reference axis, one gets a normal force perpendicular to the x_b axis and an axial force parallel to the x_b axis as shown in the figure. The mathematical relationship between these two aerodynamic forces, defined in two reference frames is given by eq. (3.2). Due to the nature of the grid motion (see section 2.4.2) to calculate the indicial step responses, the dependency on angle of attack increases complexity, therefore the normal and axial forces are used directly instead of converting these to the conventional lift and drag forces. This will not affect the results when the full-order model and the ROM are compared as it is just a matter of definition. Thus from now on the normal and axial forces are used to represent the two longitudinal aerodynamic forces acting on the airfoil.

$$\begin{bmatrix} C_l \\ C_d \end{bmatrix} = \begin{bmatrix} cos(\alpha) & -sin(\alpha) \\ sin(\alpha) & cos(\alpha) \end{bmatrix} \begin{bmatrix} C_N \\ C_A \end{bmatrix} \tag{3.2}$$

The third and last load acting on the airfoil in a longitudinal motion is the pitching moment. In theory, the total resultant aerodynamic force can be acting anywhere on the airfoil depending on the flow conditions. However, it is convention to position this resultant force on the aerodynamic centre of the configuration. In the case of a symmetric NACA0012 this force is placed at a quarter chord length behind the leading edge. The moment, with respect to this position when the resultant force is placed on its actual location (the centre of pressure), is compensated for by adding this so called pitching moment. By definition this is automatically defined in the body-axis frame. Now understanding how the three aerodynamic loads, the normal and axial force and the pitching moment are defined, the dataset can be generated by calculating the first indicial step responses.

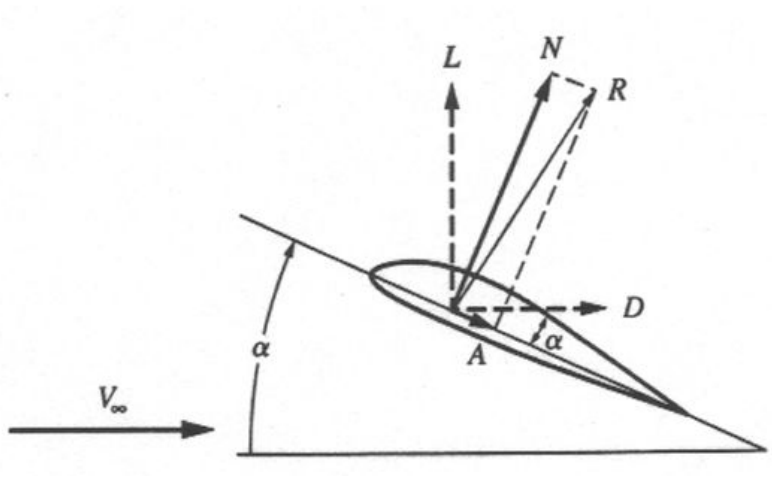

Figure 3.6: Total resultant aerodynamic force vector (R) divided in two components either in the wind-axis frame (Lift and Drag) or in the body-axis frame (Normal and Axial) [91]

An indicial response is the specific response of a system due to a unit step change in the input. In this first testcase, the system is the full-order model of the NACA0012 by calculating the URANS solution. This means by that exciting a unit step change in one of the flight parameters, e.g. angle of attack, one gets the indicial step response of the specified flight load, e.g. normal force, for that specific effect. This is done by decoupling the effects using the grid motion technique described earlier. In line with literature (see section 2.4.4), the indicial step responses of the three loads, by forcing a one degree angle of attack step change to account for the angle of attack effect are calculated. To account for the pitch rate effect a step input of one radians per second is applied to the system to calculate the pitch rate effect. This results in the first dataset consisting of six indicial step response functions seen in fig. 3.7 to fig. 3.12.

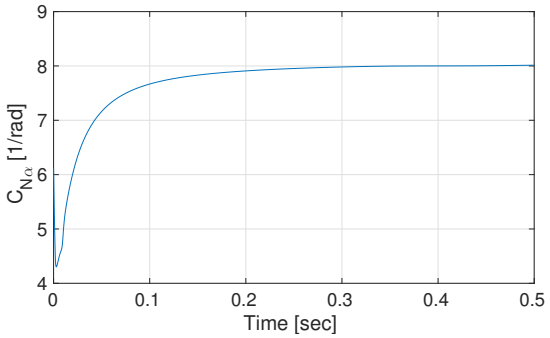

Figure 3.7: Indicial step response function of the angle of attack effect on the normal force coefficient by applying a one degree step change on a steady RANS solution at zero angle of attack and pitch rate

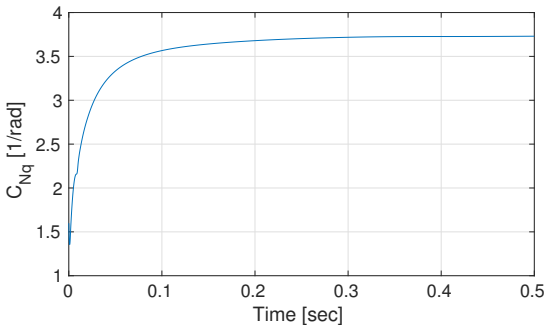

Figure 3.8: Indicial step response function of the pitch rate effect on the normal force coefficient by applying a one radians per second step change on a steady RANS solution at zero angle of attack and pitch rate

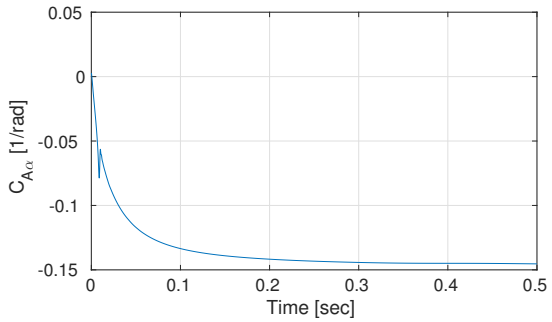

Figure 3.9: Indicial step response function of the angle of attack effect on the axial force coefficient by applying a one degree step change on a steady RANS solution at zero angle of attack and pitch rate

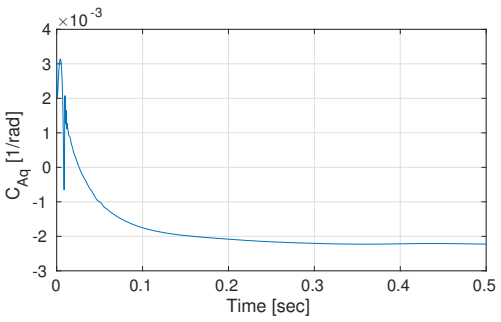

Figure 3.10: Indicial step response function of the pitch rate effect on the axial force coefficient by applying a one radians per second step change on a steady RANS solution at zero angle of attack and pitch rate

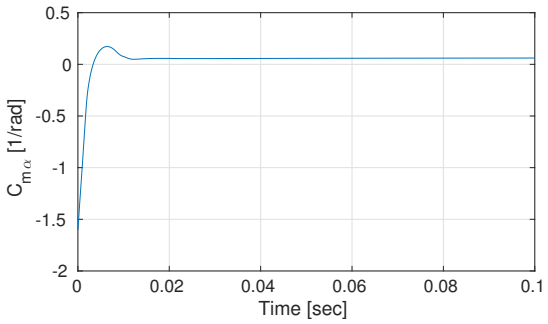

Figure 3.11: Indicial step response function of the angle of attack effect on the pitching moment coefficient by applying a one degree step change on a steady RANS solution at zero angle of attack and pitch rate

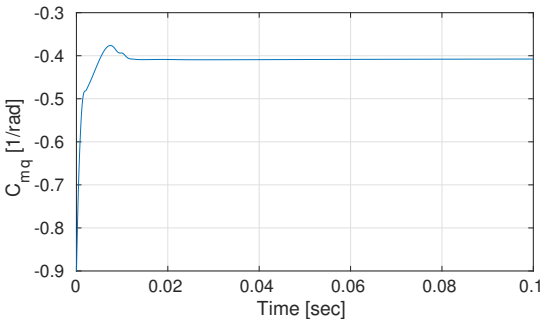

Figure 3.12: Indicial step response function of the pitch rate effect on the pitching moment coefficient by applying a one radians per second step change on a steady RANS solution at zero angle of attack and pitch rate

First look at the indicial response function of the angle of attack on the normal force coefficient in fig. 3.7. This condition is the airfoil being positioned at one degree angle of attack and zero pitch rate. The function seen is the solution of the converged unsteady RANS solution over a timespan of 0.5 seconds. Starting from a steady RANS flow at zero angles of attack and zero pitch rate, a step input of one degree is given to the angle of attack while keeping the pitch rate zero. What can be seen is that, in accordance with unsteady aerodynamics theory, the normal force coefficients first undergoes a negative peak and roughly needs 0.5 seconds to settle at a steady state condition. This corresponds to the air flowing roughly 10 times over the one metre chord length of the airfoil at a speed of Mach 0.6. This behaviour can be physically explained. When the airfoil is immediately positioned in its new position the flow over the leading edge increases. This higher velocity over the leading edge leads to a higher suction peak. Over time, as the flow settles, the non-linearity created at the start propagates towards the trailing edge and eventually disappears. Conventional flight dynamics models would take the final value of this function in the form of a static stability derivative C_{N_α}, thereby neglecting the unsteady effect of the non-linearity flowing over the chord length A similar phenomenon can be seen in the effect of a step input on the pitch rate on the normal force coefficient in fig. 3.8. When the pitch rate is suddenly set at one radians per second a (slightly less big) suction peak appears which is followed by a transient solution, eventually settling at the condition where the angle of attack is zero degree and the pitch rate is one radians per second. One can imagine that this indicial step response function is challenging to simulate in a wind tunnel, but relatively easily calculated using CFD. These two functions are used to build a ROM in section 3.2.2. When using one function to approximate the whole unsteady behaviour of an effect, these effects on the load are considered linear, hence the term 'linear' ROM. For example, the unsteady behaviour from an angle of attack from four to five degrees can easily be approximated by adding the steady state solution at four degrees angle of attack to the indicial step response functions seen in fig. 3.14. Whether it is an accurate representation is another question which will be answered when the number of samples in the dataset are extended in the next section.

Similar unsteady behaviour can be seen for the two remaining loads in fig. 3.9 to fig. 3.12. In general the unsteady effect of a change in angle of attack is larger than the effect of a change in pitch rate. Also when looking at the pitching moment effects it can be seen that the unsteady effects are less than for the other two loads as the URANS reaches a steady state much earlier in time. When these functions are used to build a ROM is it expected that the linear approximation for the effect in angle might cause discrepancies at higher angles of attack due to the non-linear flow behaviour at that region as seen in fig. 3.3.

3.2.2. Preliminary models

As mentioned before, two indicial step response functions will be used for each flight load to build a ROM. To reduce the amount of figures and as the flow behaviour and analysis is similar for both forces, it is chosen to only discuss the results of the ROMs of the normal force and pitching moment coefficients. The ROMs and additional indicial functions of the axial force coefficient can be found in appendix B.

A ROM of the normal force (coefficient) is built using the method described in section 2.4.5 and is visualised in fig. 3.13. Also the full-order CFD motion is calculated and shown in the same figure in order to asses the accuracy of the ROM. This solution is considered to be the full-order model which the ROM should approximate. In the same figure some experimental data can be seen for validation purposes. The experimental data is acquired by performing the same pitching oscillation manoeuvre on a NACA0012 airfoil under the same flow conditions in a wind-tunnel test [90]. The full-order CFD URANS solution and the experimental AGARD CT2 data are in good agreement, meaning the full-order model is a reasonable accurate representation of the actual flow behaviour during the motion. The linear ROM and the full-order solution are also in good agreement at the lower angles of attack. As expected, the normal force predicted by the ROM at higher angles of attack is off.

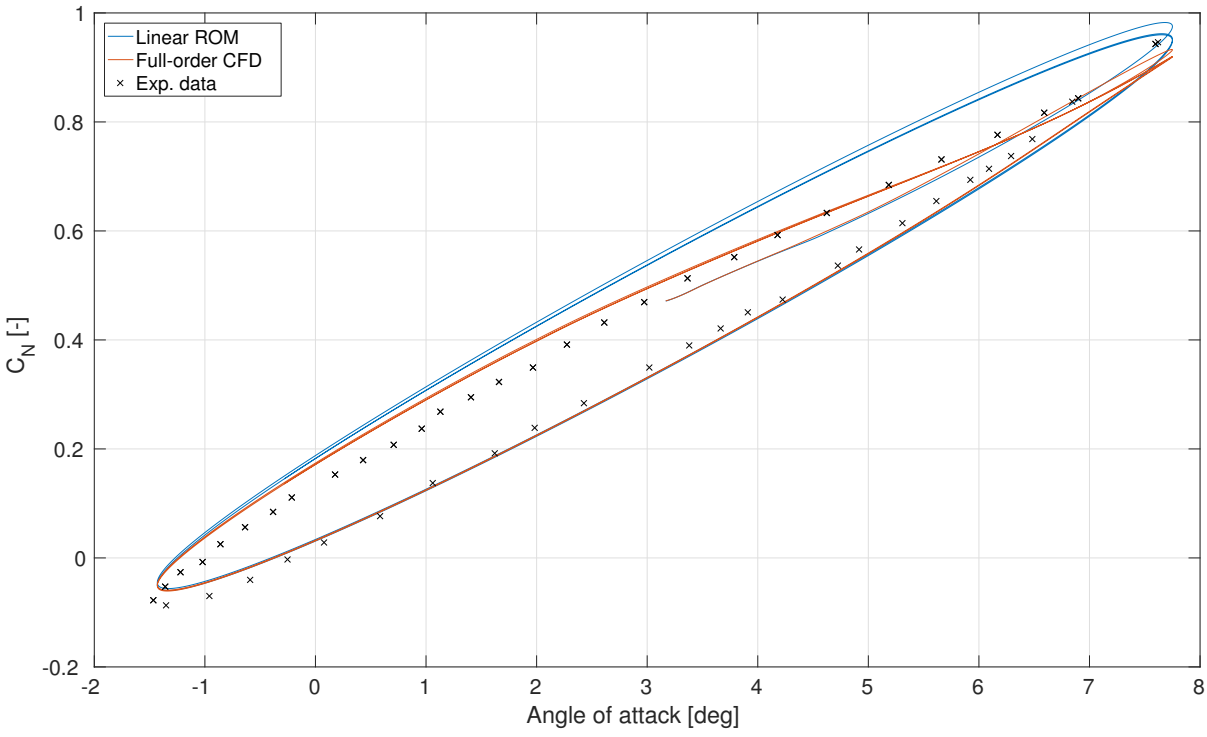

Figure 3.13: Comparison between AGARD CT2 wind-tunnel data, the full-order CFD URANS and the linear ROM normal force coefficient solutions undergoing a pitching oscillation at a frequency of 5.27$[Hz]$, Mach of 0.6 and a Reynolds number of 4.8$E6$

The results on the pitching moment (coefficient) are visualised in fig. 3.14. Again, the full-order CFD and the experimental data are in reasonable agreement. The same discrepancies are found when comparing the linear ROM to the full-order model. Near higher angles of attack the ROM predicts the pitching moment magnitude too low. Also at lower angles of attack there is a small offset between the models. Differences during the URANS convergence at each time step might be a cause, but this will be investigated in more detail later on in this chapter. The same discrepancies can be found for the axial force (coefficient) found in the appendix. Overall it can be said that the linear ROMs show a reasonable accurate approximation of the full-order model at lower angles of attack. The dataset needs to be extended to include unsteady flow behaviour at higher angles of attack in order to have a more accurate ROM. The results on more accurate ROMs, in accordance with literature, are given in the next section.

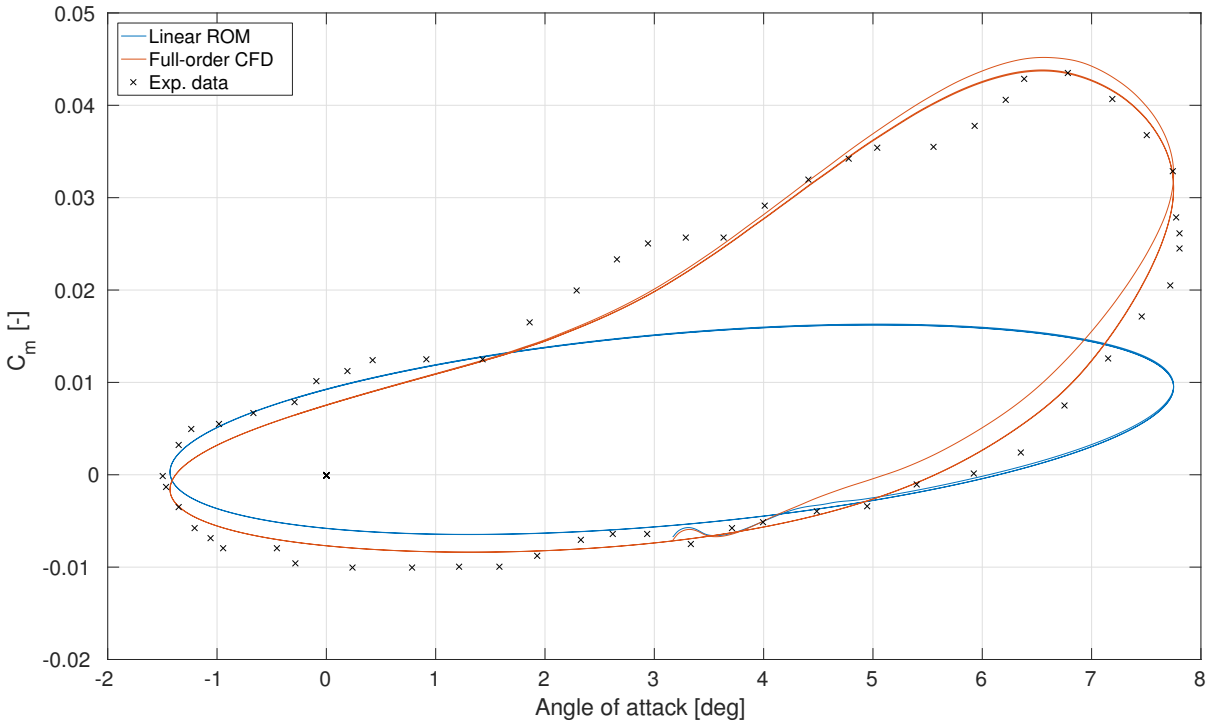

Figure 3.14: Comparison between AGARD CT2 wind-tunnel data, the full-order CFD URANS and the linear ROM pitching moment coefficient solutions undergoing a pitching oscillation at a frequency of 5.27$[Hz]$, Mach of 0.6 and a Reynolds number of 4.8E6

3.3. Resulting reduced-order models

The dataset is extended using more indicial response functions in section 3.3.1 in order to take into account non-linearities. The datasets are then verified in section 3.3.2 and finally in section 3.3.3 the resulting non-linear ROMs are given. This section of the report will eventually provide the fundamental ROMs which can be used to compare against the full-order model and provide data to answer the research questions.

3.3.1. Sample space extension

At higher angles of attack non-linearities begin to occur in the flow such that more than one indicial response function is needed to improve accuracy of the ROMs. For sake of completeness, the full span of angles of attack encountered during the motion will be represented by its specific indicial function. This means that besides the response from zero to one degree angle of attack (while keeping the pitch rate zero), also the indicial responses from one to two degrees up to eight degrees are calculated. The results are shown in fig. 3.15 and fig. 3.16. The axial force responses are found in appendix B.

The assumption of linearity holds for lower angles of attack for the normal force coefficient as can be seen from fig. 3.15. The unsteady behaviour shown by the indicial step response functions from zero to four degrees is similar. This explains the accurate approximations of the ROMs compared to the full-order model at this region of angles of attack. At higher angles of attack the unsteady behaviour rapidly changes, resulting in lower steady state values for the normal coefficient, corresponding to the observations made on the linear ROMs at higher angles of attack. From fig. 3.16 similar changes in unsteady behaviour towards higher angles of attack can be seen. A slight difference is found for these indicial functions at lower angles of attack. This would explain the discrepancies found for the pitching moment ROM at lower angles of attack compared to the full-order model. However, these are just suspicions which needs to be proven by using the extended sample space datasets to build a new 'non-linear' ROM. Before this can be done the extended dataset needs to be verified.

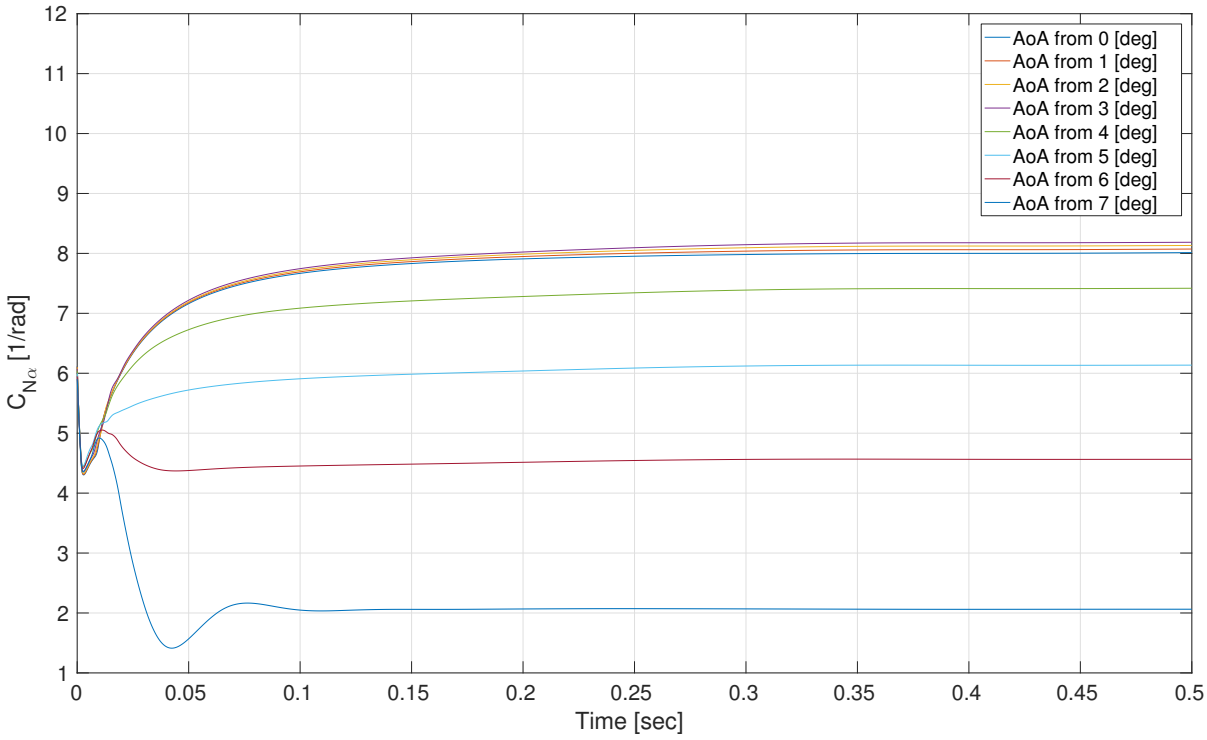

Figure 3.15: Additional indicial step response functions of the angle of attack effect on the normal force coefficient to capture the non-linear unsteady flow behaviour by applying a one degree step change on a steady RANS solution at various angles of attack while keeping the pitch rate zero

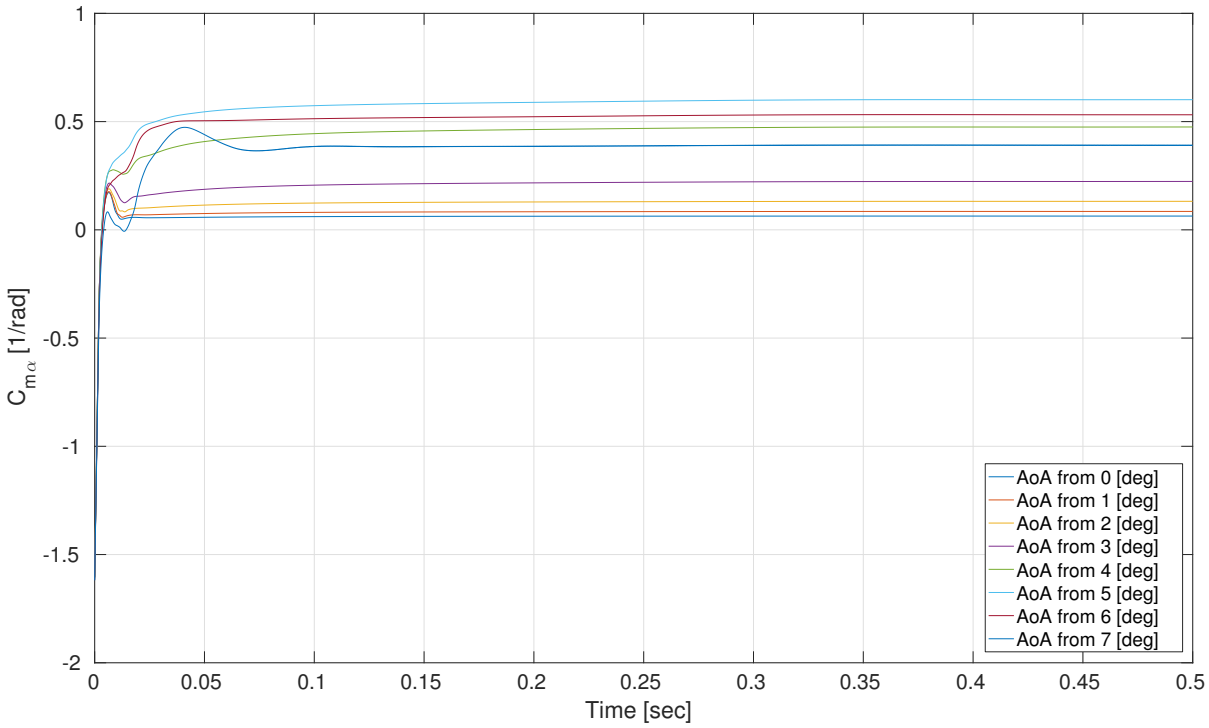

Figure 3.16: Additional indicial step response functions of the angle of attack effect on the pitching moment coefficient to capture the non-linear unsteady flow behaviour by applying a one degree step change on a steady RANS solution at various angles of attack while keeping the pitch rate zero

3.3.2. Dataset verification

Before the generated functions can be used, the datasets need to be verified in order to assess the accuracy of the samples of the full-order model itself. Consider the first indicial step response generated for the dataset. A step response of one degree angle of attack was given to the airfoil at an angle of attack of zero degrees at constant speed and zero pitch rate. As is clear from the unsteady behaviour in previous section the solution for all three aircraft loads asymptotically reach a steady state value. This value should, in theory, correspond to the found value when the steady RANS is approximated for the configuration in an angle of attack of one degree. This comparison can be made for all angle of attack effect functions. The results on the normal and pitching moment comparison can be seen in fig. 3.17 and fig. 3.18 respectively.

It can be seen that for all three longitudinal loads, the final values of the indicial step responses are in agreement with the steady RANS solutions when the airfoil is positioned in the same flow conditions. The explanation for the plots not having the exact similar values is that the URANS might not have converged to the exact same values as the steady RANS. The results show that the grid motion technique and the generated datasets are verified for this test case.

In order to emphasise the non-linearity at higher angles of attack and show that both normal and axial force are verified take a look at fig. 3.19. The values found are transformed to the wind-axis system to include a dependency on angle of attack and compare the lift and drag coefficients during the verification process. It can be seen that also these values show accurate agreement, verifying that it is still sufficient to only look at the ROMs for the normal and axial forces.

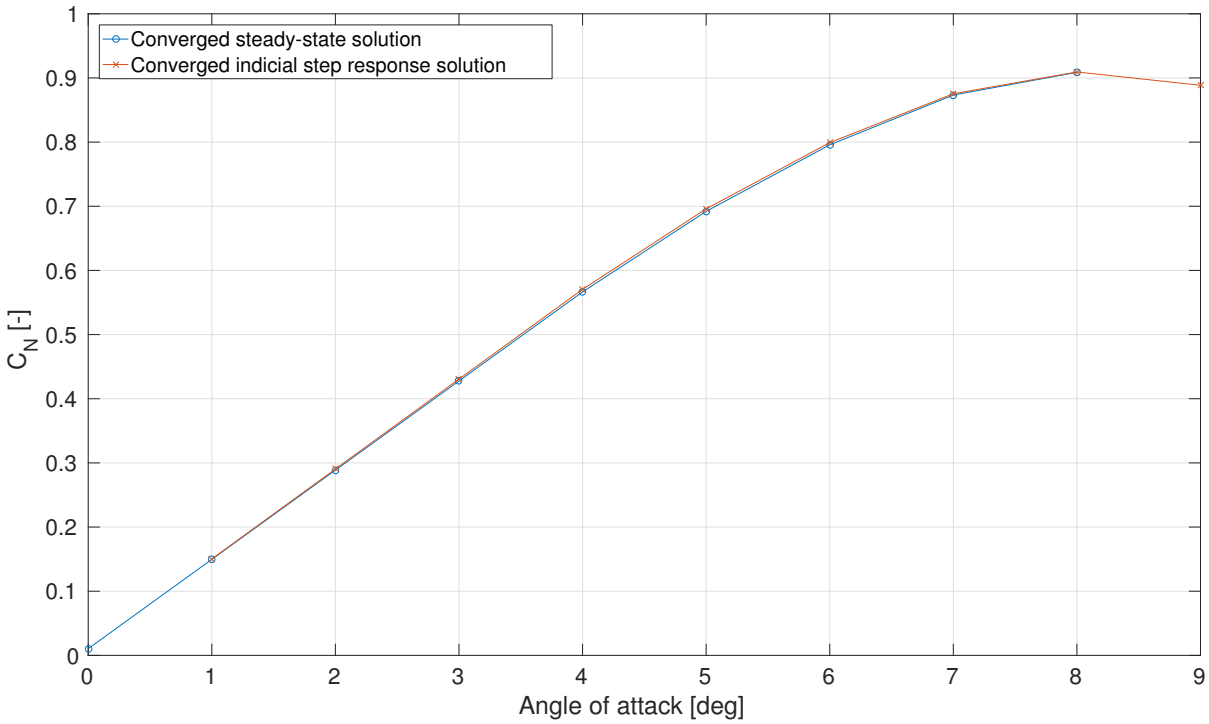

Figure 3.17: Final values of the angle of attack indicial step response functions on the normal force coefficient generated by approximating the unsteady RANS compared to the airfoil directly configuring in the angle of attack of interest and finding the steady RANS solution

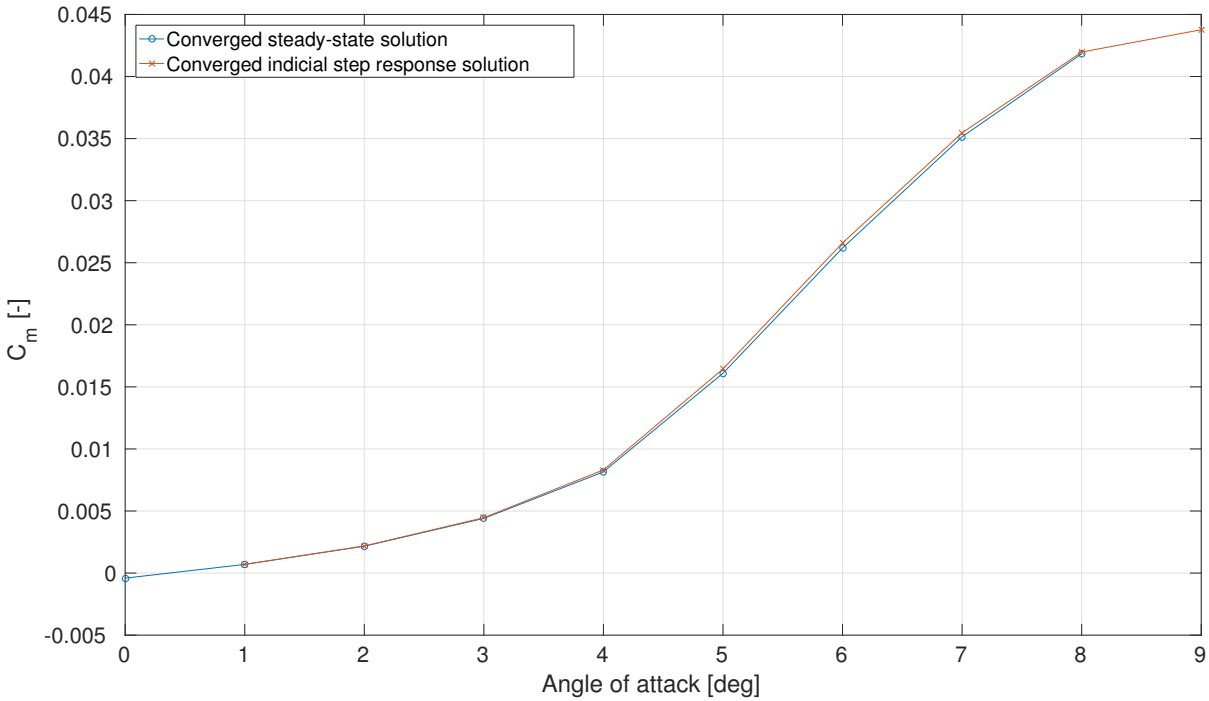

Figure 3.18: Final values of the angle of attack indicial step response functions on the pitching moment coefficient generated by approximating the unsteady RANS compared to the airfoil directly configuring in the angle of attack of interest and finding the steady RANS solution

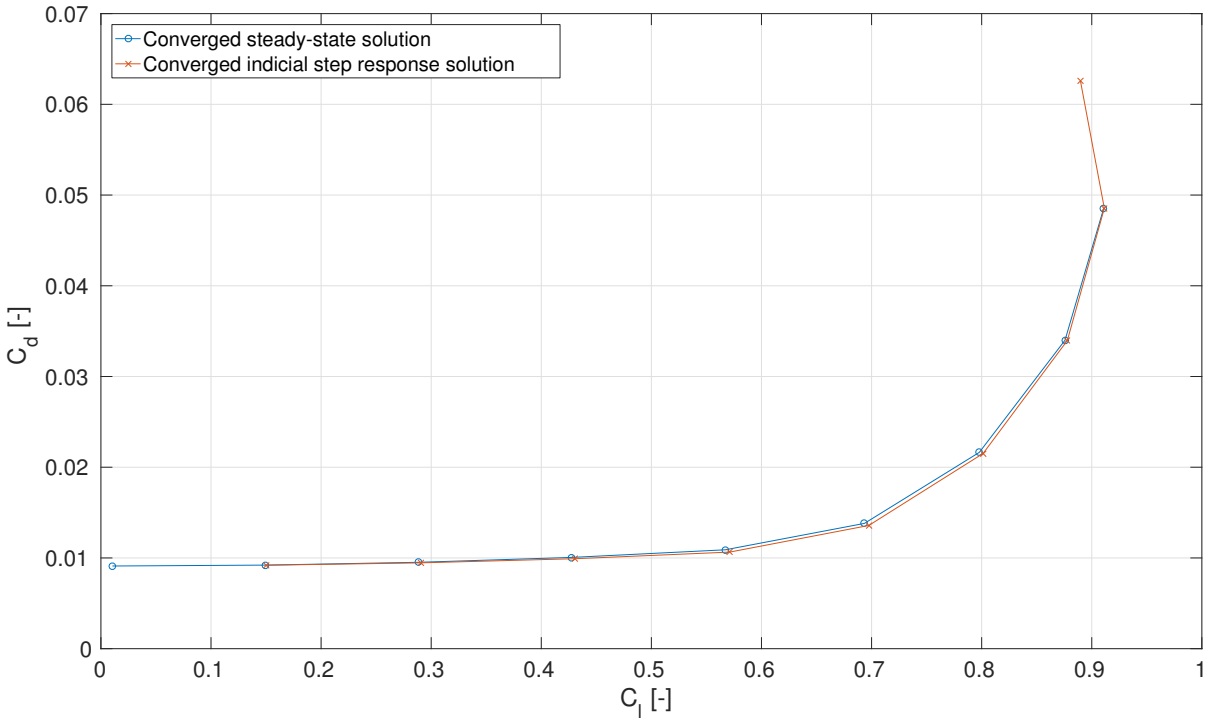

Figure 3.19: Transformed normal and axial force values to the wind-axis systems by adding a dependency on the angle of attack resulting in the lift and drag values verification of the datasets

3.3.3. Non-linear reduced-order models

Having an extended dataset with more samples from the full-order model new ROMs can be built, which in theory should take unsteady effects at higher angles of attack into account more accurately. As assumed before, the three flight loads will only be dependent on two effects, the change in angle of attack and pitch rate during the pitch oscillation motion. The pitch rate effect is still assumed to be independent of angle of attack and pitch rate magnitude such that one indicial step response function will suffice for this linear effect. However, in contrast to the dataset used to built linear ROMs, the angle of attack effect is now considered to be non-linear and is approximated using 8 indicial response functions. Again, the new ROMs are built using the numerical procedure already given in section 2.4.5. The results, including the full-order CFD URANS solution, are visualised in fig. 3.20 and fig. 3.21.

First take a look at the ROM approximation of the normal force (coefficient) in fig. 3.20. It is clear that the non-linear ROM is a far more accurate approximation of the full-order model than the linear ROM built in the previous section. At higher angles of attack the values of the ROM now seem an reasonable accurate approximation of the full-order model. Besides, noticing that the motion covers two periods, the behaviour of the models find good agreement , meaning that flow hysteresis might be taken into account using this ROM building method. Now look at fig. 3.21 for the pitching moment (coefficient) ROM compared to the full-order CFD URANS solution. Again, in contrast to the linear ROM, the non-linear ROM finds good agreement with the full-order model, even at higher angles of attack. However, there is a still a small offset when the motion moves from higher angles of attack to lower values.

Overall it can be stated that these non-linear ROMs show a reasonable accurate approximation of the full-order model. Besides, it is clear that this ROM building method effectively takes unsteady effects into account. To investigate why the ROMs do not exactly correspond to the full-order model, thereby validating the assumptions made, and investigate to what order this ROM method can take unsteady aerodynamics into account a frequency analysis has been performed.

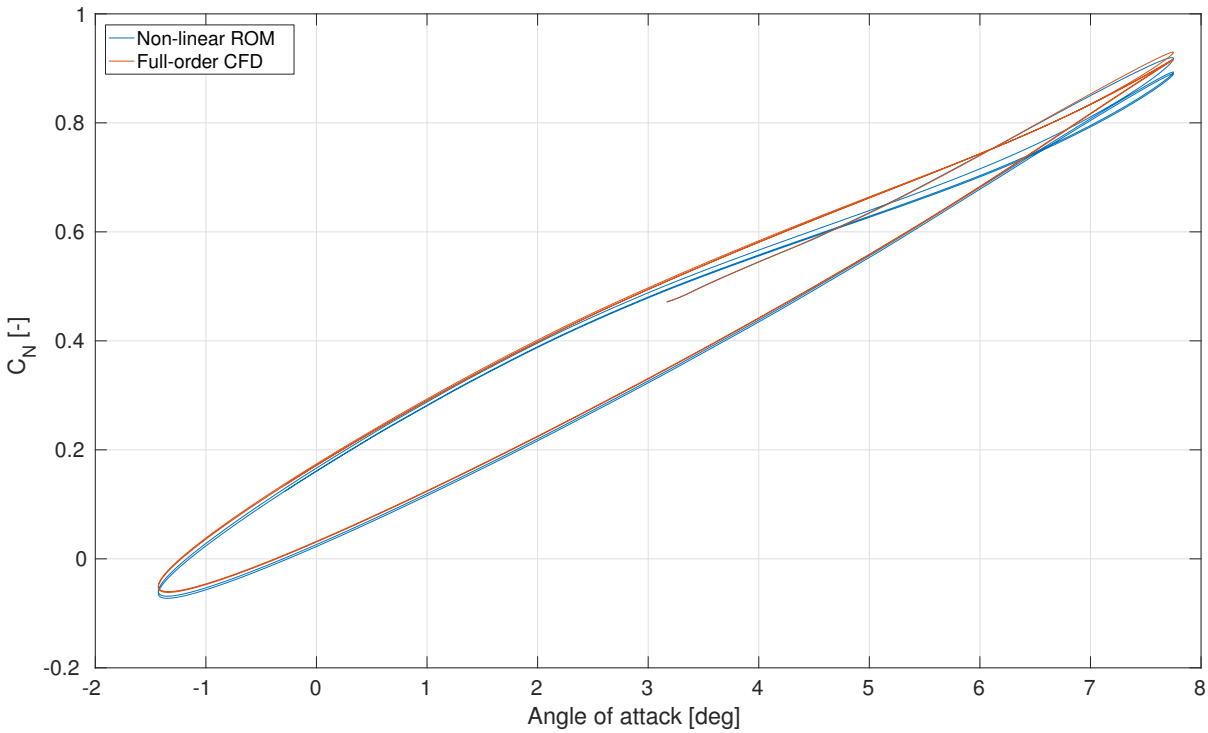

Figure 3.20: Comparison between the full-order CFD URANS and the non-linear ROM normal force coefficient solutions undergoing a pitching oscillation at a frequency of 5.27$[Hz]$, Mach of 0.6 and a Reynolds number of 4.8E6

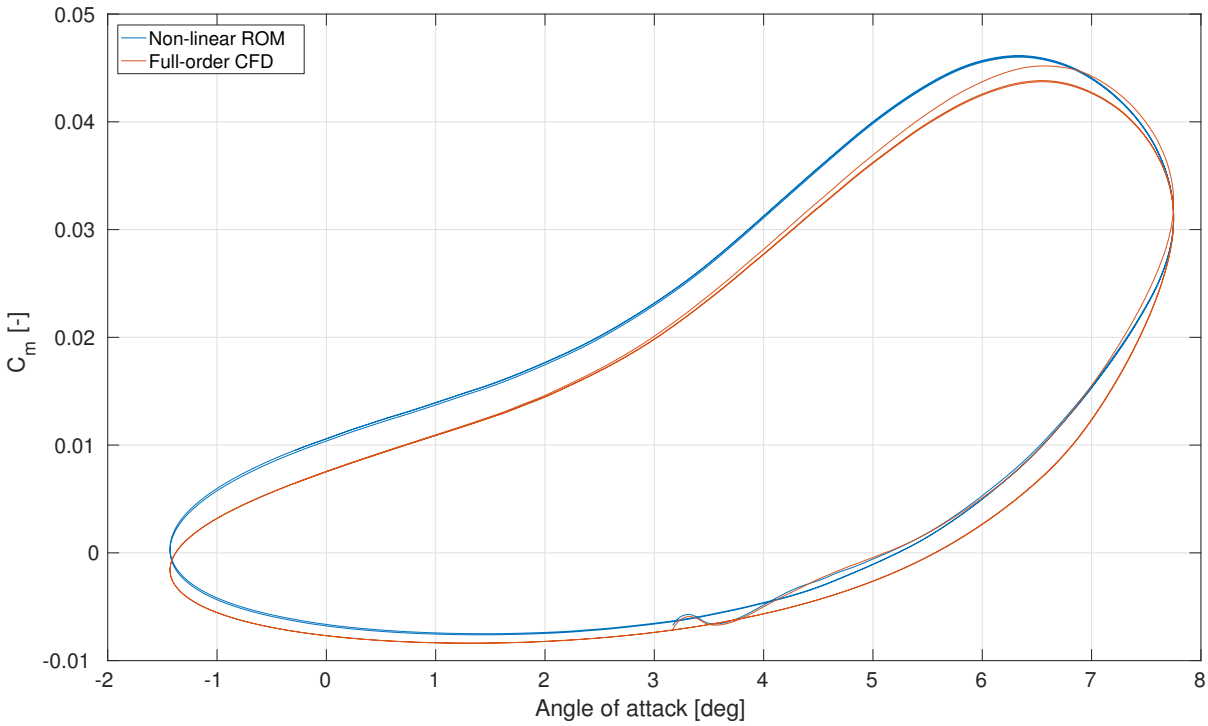

Figure 3.21: Comparison between the full-order CFD URANS and the non-linear ROM pitching moment coefficient solutions undergoing a pitching oscillation at a frequency of 5.27$[Hz]$, Mach of 0.6 and a Reynolds number of 4.8E6

3.4. FREQUENCY ANALYSIS

In previous sections it is made clear that the ROM accuracy depends on the samples used in the dataset. The angle of attack effect on the three loads clearly has a non-linear effect on the three flight loads such that more indicial response functions are needed to accurately capture unsteady flow behaviour. The motion considered was a pitch oscillation at a constant frequency of 5.27 [Hz]. One can imagine that changing this frequency has a big impact on the unsteady flow behaviour over the airfoil. The time lag in reaching a steady state value for a motion might be much higher than one complete period of the motion for example. Of course an attempt has been made to capture this effect by calculating the indicial response of the full-order model by applying a step input on the pitch rate. So far, in accordance with literature, this has been assumed to be linear and approximated by one indicial function. However, the non-linear ROMs still show differences between their solutions and the full-order URANS solutions. This might be a calculation error in convergence at each time step, but in order to investigate this in a more scientific manner, a frequency analysis is conducted. First a lower frequency (2.63 [Hz]) of the motion (eq. (3.1)) will be investigated which, in theory, should include less unsteady aerodynamic flow behaviour. Afterwards, a higher frequency (10.54 [Hz]) will be investigated such that a more accurate error analysis can be conducted in section 3.4.3. The chosen frequencies are in accordance with literature [83] such that the results can be compared as this is the first time this analysis is conducted with the ENSOLV CFD solver, which also needs validation itself for optimal results and conclusions. Again, the normal force and pitching moments ROMs are analysed in detail whereas the axial force ROMs can still be found in appendix B.

3.4.1. LOWER FREQUENCY

The resulting ROMs and the full-order CFD solutions for the normal force and pitching moment coefficient can be found in fig. 3.22 and fig. 3.23 respectively. It can be seen that the ROMs and full-order CFD solutions show good agreement. Still, some discrepancies are found at higher angles of attack for the normal force and at lower angles of attack for the pitching moment when the motion comes from a higher angle of attack. Similar difference were found for the axial force ROMs. Using the same dataset as for the previously calculated motion at 5.27 [Hz] this means that this motion, at a lower frequency of 2.63 [Hz], is in better agreement with the indicial step responses calculated. A more detailed investigation of the pitch rate changes between the frequencies and the time-lag of the indicial responses is conducted in the error analysis later on, but first a higher frequency of the motion is analysed to acquire more data.

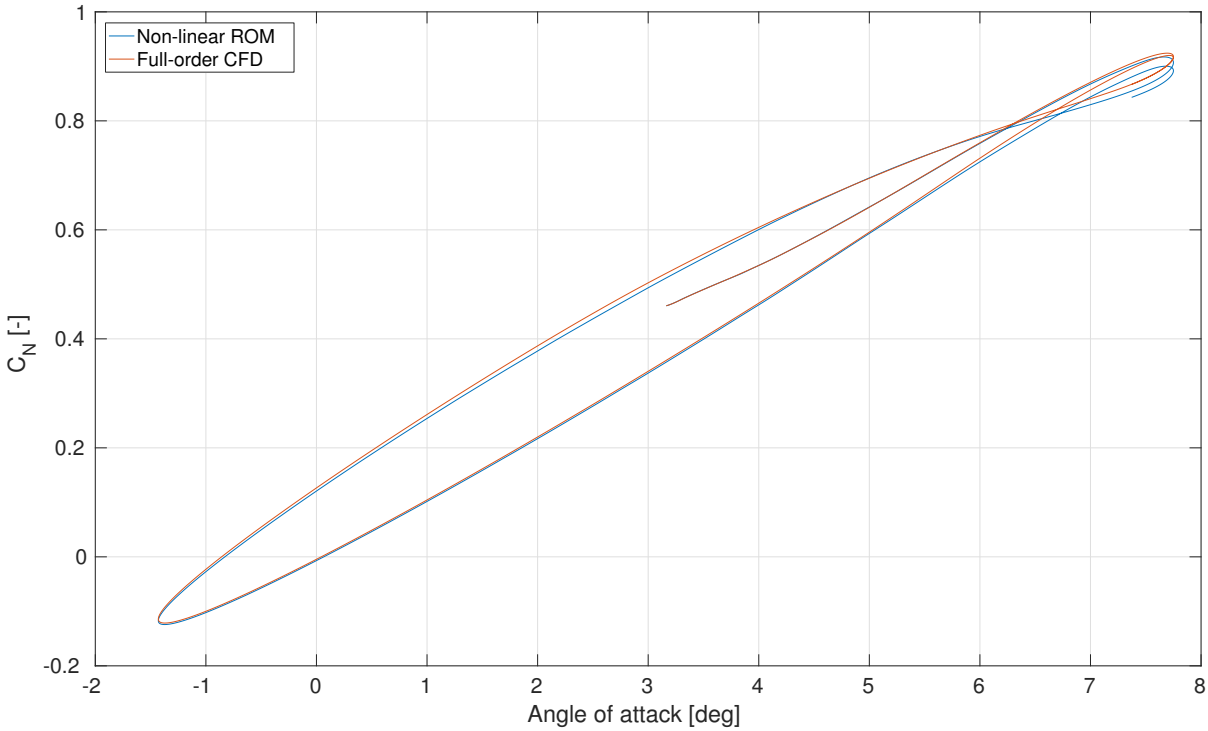

Figure 3.22: Comparison between the full-order CFD URANS and the non-linear ROM normal force coefficient solutions undergoing a pitching oscillation at a frequency of 2.63$[Hz]$, Mach of 0.6 and a Reynolds number of 4.8E6

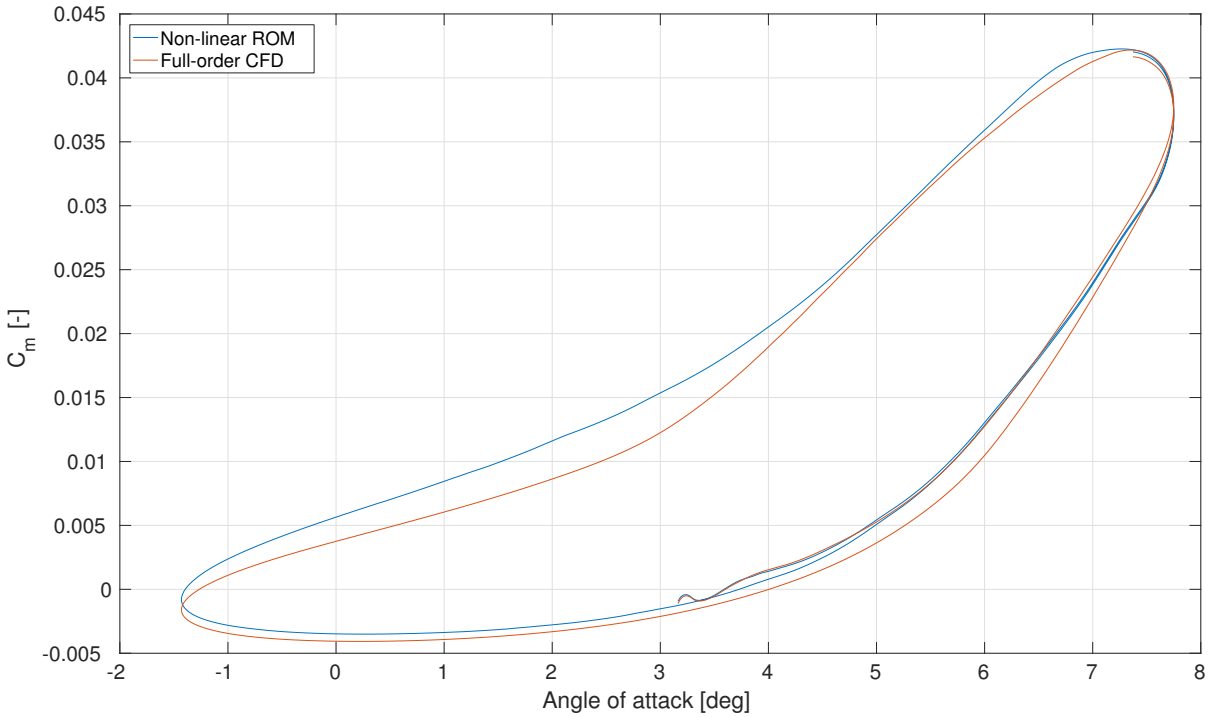

Figure 3.23: Comparison between the full-order CFD URANS and the non-linear ROM pitching moment coefficient solutions undergoing a pitching oscillation at a frequency of 2.63$[Hz]$, Mach of 0.6 and a Reynolds number of 4.8E6

3.4.2. HIGHER FREQUENCY

The resulting ROMs of the motion undergoing a higher frequency of 10.54 [Hz] for the normal force and pitching moment are visualised in fig. 3.24 and fig. 3.25 respectively. The differences between the ROMs and full-order models are clearly bigger than for the lower frequencies. As only the effects of pitch rate and angle of attack are assumed to affect the loads, and having the same range in angles of attack for all frequencies, this means that the pitch rate effect might be a cause for the errors. At the start of the motion, from 3.16 [deg] up to roughly 7.8 [deg] the ROM is in good agreement with the full-order solution. However, as the motion starts to reduce its angle of attack the ROMs show the biggest differences in the loop. To investigate this change in pitch rate as the frequency changes and the effect on the unsteadiness in the motion a thorough error analysis is conducted in the next part. It should be noted that found ROMs and full-order CFD data are in accordance with results found in literature having performed similar research with other CFD solvers, showing the flexibility of this method [83].

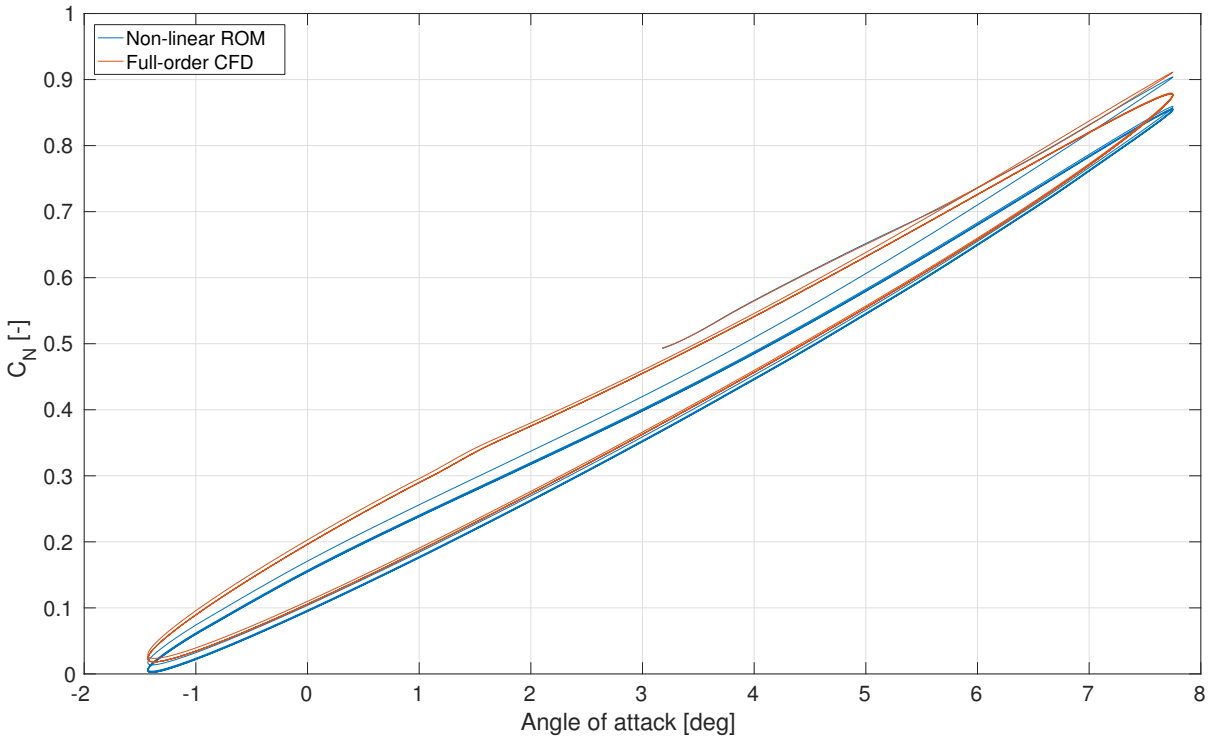

Figure 3.24: Comparison between the full-order CFD URANS and the non-linear ROM normal force coefficient solutions undergoing a pitching oscillation at a frequency of 10.54$[Hz]$, Mach of 0.6 and a Reynolds number of 4.8E6

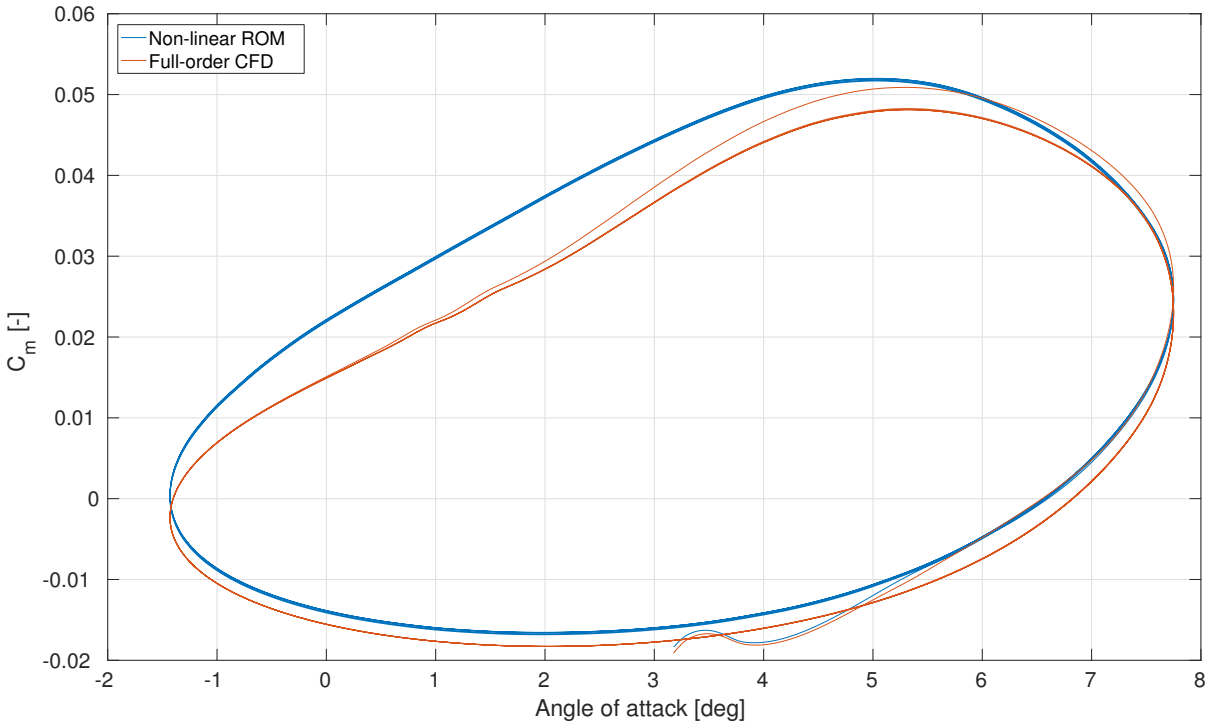

Figure 3.25: Comparison between the full-order CFD URANS and the non-linear ROM pitching moment coefficient solutions undergoing a pitching oscillation at a frequency of 10.54$[Hz]$, Mach of 0.6 and a Reynolds number of 4.8$E6$

3.4.3. Error analysis

Having the ROM results at different frequencies makes it possible to analyse the origin of the ROM discrepancies in more detail. To keep the analysis effort at a reasonable level only the errors in normal force (coefficient) results will be evaluated. The results for the axial and pitching moment coefficients can be found in appendix B. Nevertheless, the observations made from these ROMs are similar to the ones obtained from the normal force ROM error analysis. As seen from fig. 3.22 and fig. 3.24 there are clear differences between the full-order CFD manoeuvre and the approximation of the reduced-order model. These differences will be analysed in a qualitatively manner in the upcoming part to better understand the limitations and capabilities of ROMs.

One method of analysing the results is using the so called absolute error. This will give the difference between the measured value, the ROM dataset in this case, and the target value, the full-motion CFD to which the method should validate against. The calculation (eq. (3.3)) is a very straightforward and fast way to analyse the error produced. However, even as this method quickly shows where the largest error is produced, it says nothing regarding the relative error. For example, consider the following case. The CFD full-order C_N might have a value of $2e-4$ at lower angles of attack whereas the ROM predicted the value to be $1e-4$. This absolute error of $1e-4$ is low compared to an absolute error of $0.8-0.83=0.03$ at higher angles of attack. However, the value relative to the target value of $2e-4$ is 100% lower in contrast to the relative error produced by the difference between 0.8 and 0.83. Therefore, the absolute error will be used to validate the ROM in a quantitative manner whereas the relative error (eq. (3.4)) will be used to validate the ROM in a qualitatively manner and truly check where the discrepancies originate from. This relative error will be multiplied by 100% to get the so called percentage error for ease of interpretation.

$$\Delta C_N \equiv C_{N_{CFD}} - ROM \tag{3.3}$$

$$\delta C_N = \frac{\Delta C_N}{C_{N_{CFD}}} * 100\% \tag{3.4}$$

The results of the validation between the ROM and the full-order CFD calculation at a frequency of 2.63 [Hz] are visualised in fig. 3.26. The two flight parameters, angle of attack and pitch rate, can be seen as a function of the full 0.5 [sec] timespan of the motion in the top of the figure. The resulting absolute and relative error as a function of the time are seen in the bottom of the figure. What stands out is the difference between absolute and relative error, showing the significance of the use of both error analysis methods.

First the absolute error will be analysed. Clearly the error is zero at the start of the manoeuvre as both the ROM and full-order start at a steady RANS value of 3.16 degree angle of attack. However, as the angle of attack increases, the error also increases. The error decreases again as the angle of attack is lowered. As the individual indicial functions C_{N_α} should effectively approximate the normal coefficient for the effect in angle of attack, the origin must lie in the fact that only one pitch rate step change is calculated at an angle of attack of zero degrees. However, it is interesting that the error increases again when the angle of attack decrease is halfway around 0.15 [sec]. At this point the aircraft is pitching with a negative pitch rate meaning that the sign of the pitch rate has an relative strong effect on the accuracy of the ROM. The motion continues in the lower angles of attack region which corresponds to a minimum error as expected. As the angle of attack increases again the error also significantly increases again as expected using the previous explanation. When looking at the relative error the history roughly corresponds to the absolute error history. Except for two points where the error increases to over 100%. These peaks occur at negative angles of attack meaning that the zero angle of attack condition is of importance in this configuration. To further analyse the origins of the differences and to check if the predicted behaviour can be seen in other manoeuvres the higher frequency motion is analysed.

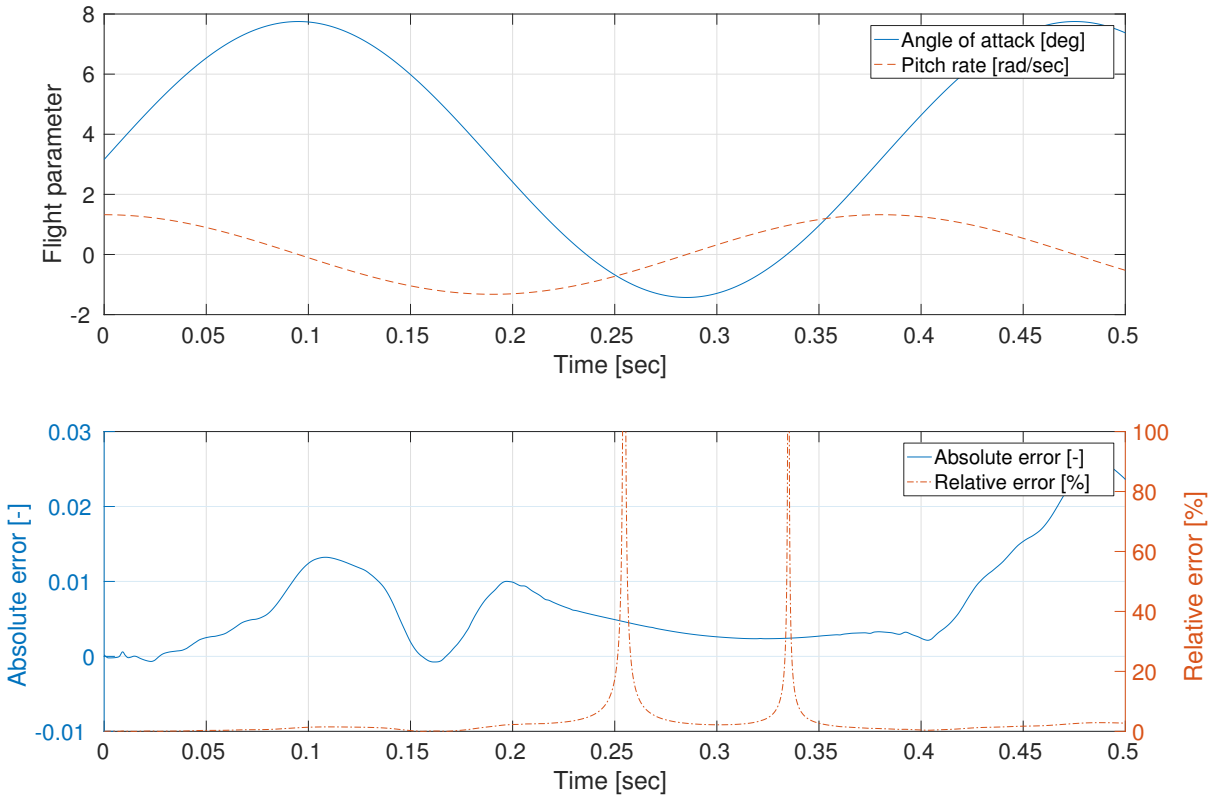

Figure 3.26: Flight parameter history (top) during the oscillating motion at a frequency of 2.63 [Hz] including the differences between the normal force ROM and the full-order model (bottom) expressed in the absolute and relative error histories

The validation between the predicted (ROM) and target (full-order CFD) values at a higher frequency of 10.54 [Hz] can be seen in fig. 3.27. Again, the flight parameters can be seen in the top figure whereas the two error histories are seen in the lower part of the figure. Note that the same timespan of 0.5 [sec] has more oscillations as the frequency is higher. When looking at the first period of the motion several similarities between the two frequencies can be spotted. Again, as the angle of attack increases the absolute error increases. However, in contrast to the lower frequency, the error keeps increasing even as the angle of attack decreases again. The difference in frequencies can be found in the pitch rate change. At a higher frequency the pitch rate changes much higher than in lower frequencies. As the indicial function to approximate the pitch rate effect only steps from zero to 1 [rad/sec] at an angle of attack of zero degrees, the step size might have an effect on the ROM accuracy. Keeping this in mind the motion is further analysed. It can be seen that the absolute error is relatively low at parts of the motion where the pitch rate is roughly 1 [rad/sec], the step size of the indicial function. Looking at the relative error it can again be noted that this error increases at roughly zero angles of attack. Three big differences between the frequencies can be noted. First, the error increases much earlier. This may be due to the fact that the pitch rate attains higher values at a higher frequency, leading to more unsteadiness which might not all be captured using only one indicial function for the pitch rate effect. The second difference is the absence of the second relative error peak in the first oscillation. This reduction in error can be explained by the high pitch rate having a higher unsteady effect on the normal force behaviour which might compensate the error at the transition between positive and negative angles of attack due to the time-lag in the transient part of the indicial functions. This would also explain the third difference, the relative error peaks being lower at higher frequencies. The 'regular' frequency of 5.27 [Hz] was also analysed and these observations can clearly be seen in the relevant error analysis which is added in appendix B

Summarising, several discrepancies can be explained by the assumptions made and therefore sampling space used in approximating the ROMs. The assumption on the pitch rate being linear might cause errors as well as the effect on the size and sign of the steps. Therefore a more detailed sensitivity analysis will be performed on the indicial functions used in the next part. This will further help in identifying the origins of the discrepancies and investigate the effect of the assumptions made in limiting the samples taken from the full-order model.

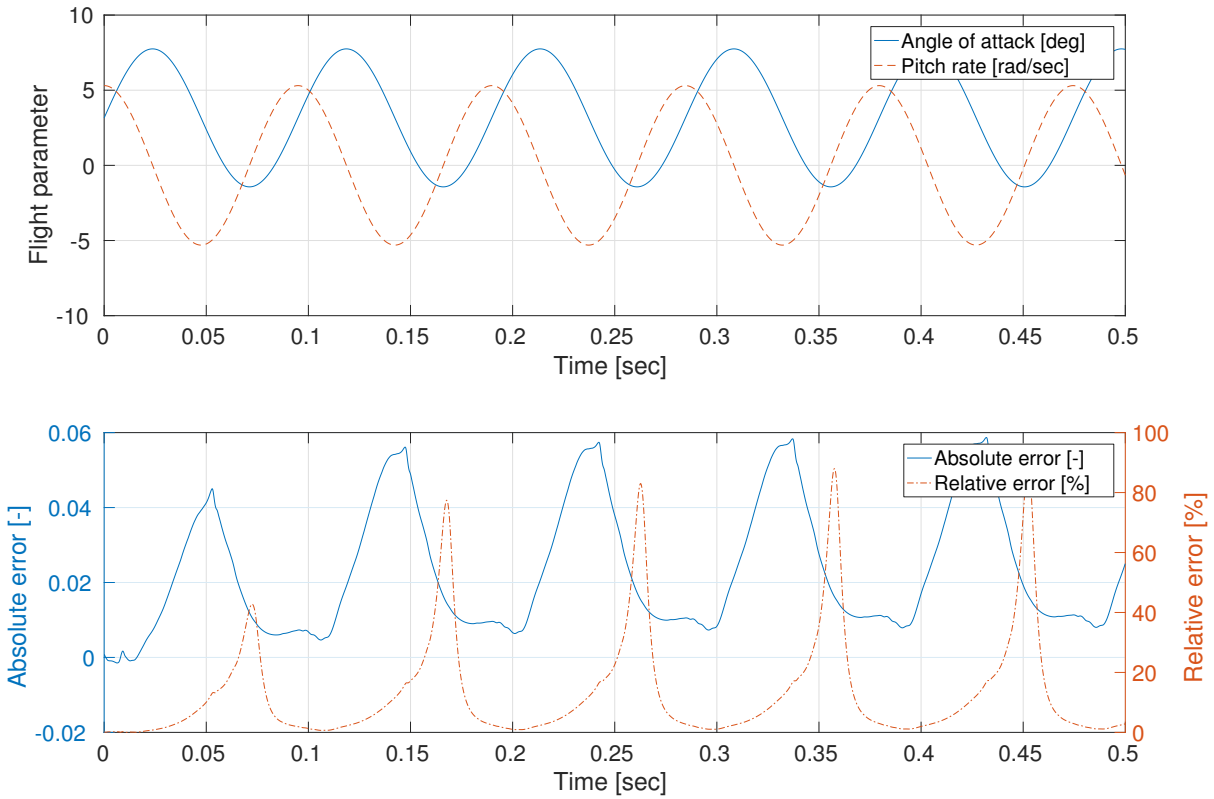

Figure 3.27: Flight parameter history (top) during the oscillating motion at a frequency of 10.54 [Hz] including the differences between the normal force ROM and the full-order model (bottom) expressed in the absolute and relative error histories

3.5. Sensitivity analysis

To investigate whether the suspected errors in the frequency analysis can be scientifically substantiated a sensitivity analysis on the dataset is performed. In the produced ROMS 9 indicial functions were used to approximate the full-order model. As explained before, the assumption was made that the pitch rate effect is linear with angle of attack. This validity of this assumption will be investigated in section 3.5.1. Secondly, the differences between positive and negative steps in angle of attack will be shown in section 3.5.2. This section will therefore strengthen the suspicions on the origins of the ROM errors found in previous error analysis and show how sensitive the resulting ROMs are to differences in the indicial functions included within the dataset.

3.5.1. Pitch rate linearity

Recapping, two effects are taken into account to approximate the full-order model. The effect of angle of attack and the effect of pitch rate. Eight functions were used to take into account the first effect. Due to the definition of the motion, the angle of attack and the pitch attitude are the same throughout the manoeuvre. Therefore, together with the assumption on having a pure longitudinal motion it is clear from the kinetic equations previously derived (see eq. (2.3)) that the effect of the first derivative of the angle of attack is in fact the effect on a change in pitch rate. This effect was assumed to be linear, but discrepancies were found at higher angles of attack and higher pitch rates. Based on already conducted research the assumption was that one indicial step response function in pitch rate from zero to one [rad/sec] at a constant angle of attack of zero degrees can be used to approximate the pitch rate effect during the whole motion. The validity of this assumption now follows.

Dependency on angle of attack

As is clear from the error analysis, an error between ROM and full-order model may originate from the fact that a change in pitch rate might cause different behaviour in the flow at higher angles of attack. Several steps responses at low angles of attack as well as a step response at a higher angle of attack of five degrees, where the steady lift plots become non-linear can be seen in fig. 3.28. The function, previously used in the dataset, is plotted first and corresponds with fig. 3.8. It can be seen that the C_{N_α} effect is linear as all functions reach a final steady value of roughly 0.03 at this angle of attack range. However, as the angle of attack increases, the peak in the beginning of the normal force coefficient also increases significantly. As the method in calculating the indicial response of pitch rate using grid motion it is hard to explain this behaviour in a physical manner. However, one can imagine that if the pitch rate effect is linear with angle of attack, and the normal coefficient increases with increasing angle of attack, a bigger difference and thus a higher peak is unavoidable at higher angles of attack. This means that unsteady effects in pitch rate behaviour becomes more important at higher angles of attack up to a certain point. One can argue that this effect is a numerical problem instead of a physical problem, which in theory could be solved. However, starting from an increasing steady state value a higher change in velocity fields is introduced which needs to be solved by CFD as fast as possible to decrease the (suspected small) non-physically existing peak. The computational time significantly increases when more sub-iterations and smaller time steps are needed. At this point it becomes a trade-off between computational accuracy of the ROM approximation and time needed to take into account the numerical convergence of the change in flow behaviour. Due to the fact that the time steps and number of sub-iterations are finite, the flow behaviour at the start of the responses might be less accurate. It is thus suspected that the unsteady behaviour at higher angles of attack causes the normal force to obtain slightly higher values, which is in line with the differences between the ROM and full-order model found in all frequencies. This means that the assumption that the pitch rate is independent on angle of attack might be wrong, but is unknown due to the fact that this is a numerical problem. Similar observations are made from the axial force and pitching moment coefficients and are added in appendix C.

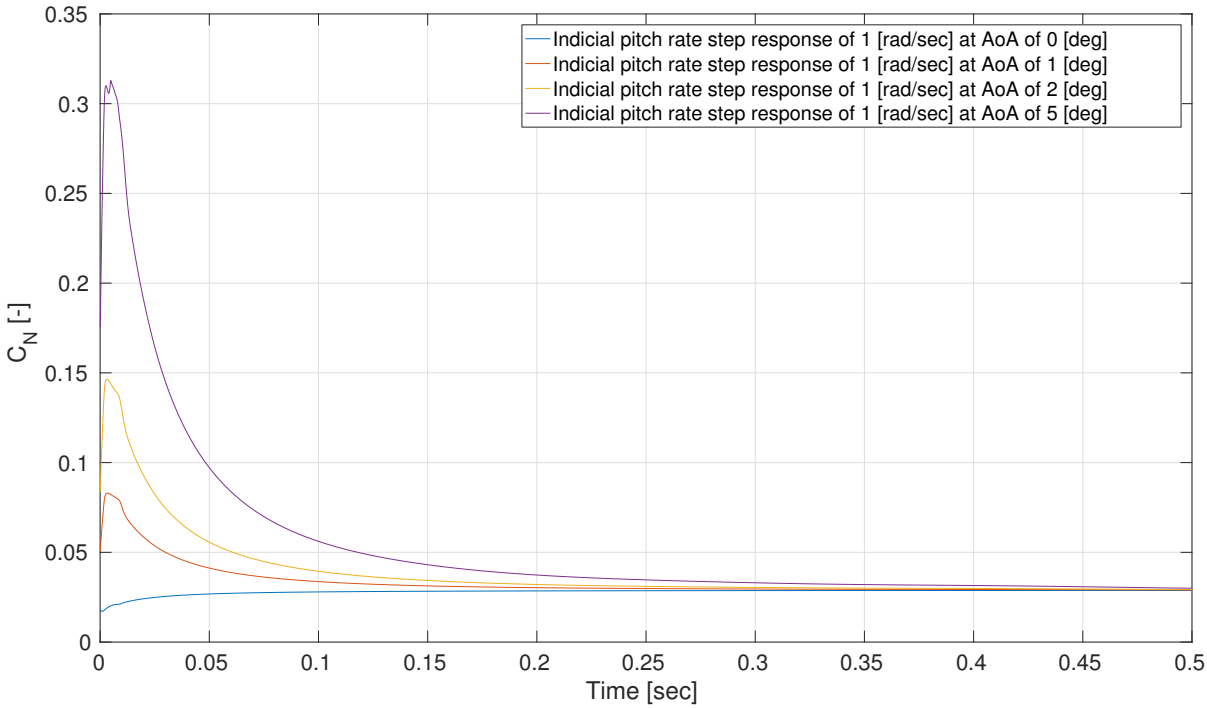

Figure 3.28: Indicial step response function of the pitch rate effect on the normal force coefficient by applying a one radians per second step change on a steady RANS solution at various starting angles of attack having a constant pitch rate

Pitch rate step size

Instead of changing the point at which the change in step occurs, one can also change the magnitude of the step itself. This effect is seen in fig. 3.29. The assumption that the pitch rate can be assumed linear with step size seems correct, at least for the low angles of attack region. It can be seen that doubling the step size at 1 [rad/sec] does correspond to the indicial function with a step size of 2 [rad/sec]. The same is found to be the case for the pitching moment coefficient, but is slightly different for the axial force coefficients. The visualisation of these results can be found in appendix C. However, as this assumption seems correct for the normal force and pitching moment, with small differences found for the axial force, the pitch rate step size of 1 [rad/sec] is still sufficient for all pitch rate step sizes.

Strictly speaking it can be stated that the assumption of linearity in pitch rate indicial responses is wrong. At higher angles of attack there appears a higher suction peak when a pitch rate step input is given. The step size magnitude of the input does not have an effect on the indicial response of the full-order model. However, as differences between the ROM and full-order model are small due to this assumption, it can be assumed that this still holds.

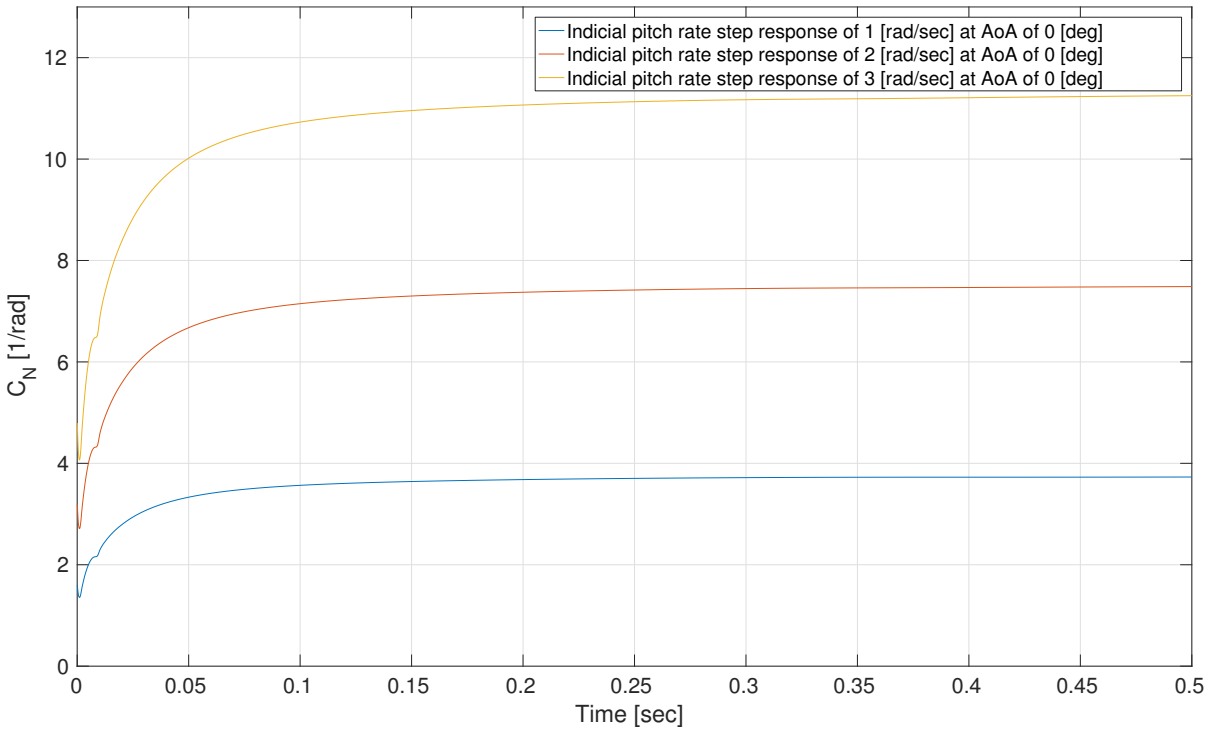

Figure 3.29: Indicial step response function of the pitch rate effect on the normal force coefficient by applying various radians per second step changes on a steady RANS solution at zero angle of attack having a constant pitch rate

3.5.2. Negative step responses

The biggest errors in the ROM approximation of the loads appear when the motion decreases its angle of attack and pitch rate. This gives rise to the question whether the negative indicial responses have different flow behaviour than the positive indicial responses. Logically there would be a difference, otherwise flow phenomena such as flow hysteresis would not exist. Flow hysteresis usually appears at higher angles of attack where laminar flow begins to transition into turbulent flow and even starts separating, resulting in a different flight load path when the airfoil is rotated back to its original position. To investigate whether this method is able to capture this phenomenon the positive step indicial functions at high angles of attack are compared to its negative step responses. The results on the normal load are seen in fig. 3.30. Again, the results on the other two loads are in appendix C.

There are clear differences between the positive and negative step indicial response behaviours. As expected, the 'suction peak' in a negative and positive response shows an increasing difference as the angles of attack increases. Including these negative step indicial functions to approximate the flow hysteresis could increase the ROM accuracy compared to the full-order URANS solutions. It should be investigated whether this extended dataset then accurately approximates the real flow hysteresis behaviour. The second testcase is chosen such that this research can be conducted, as this is a question on how indicial response functions cope with high non-linearities such as flow separation appearing in the flow. This will therefore be elaborated upon in more detail in chapter 4. Concluding the sensitive analysis, a statement can be made regarding the ROM accuracy and the number of samples (indicial functions) included within the dataset. This will be done in the next section, together with results on the the computational effort by discussing the ROM building method investigated.

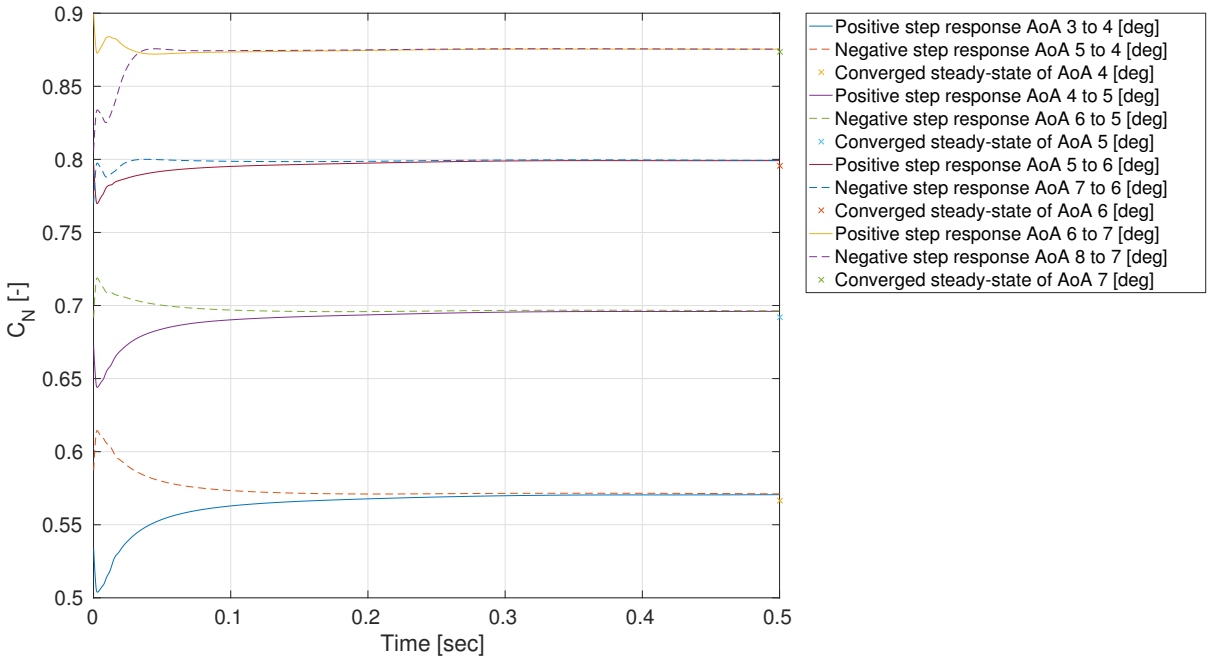

Figure 3.30: Comparison between positive and negative indicial step response functions of the angle of attack effect on the normal force coefficient by applying a one degree step change on a steady RANS solution at various angle of attack and zero pitch rate

3.6. Discussion of the method

Knowing where the differences between the ROMs and the full-order model might come from, a statement regarding the accuracy of models can be made. Intermediate conclusions and a small discussion will be given. This will be done in section 3.6.1. The amount of computational effort, along with the effect on CFD computational efficiency using ROMs, will be discussed in section 3.6.3. This section will close off the investigation on the 2D testcase. Conclusions and lessons learnt are applied to the 3D testcase, described within the next chapter.

3.6.1. Model accuracy

Continuing on the ROM results for the estimation of the normal force coefficient, the assumptions were made that the effect on angle of attack is non-linear, whereas the pitch rate effect was assumed to be linear during the motion. However, the sensitivity analysis showed that the last assumption may only hold for low angles of attack. Also, the ability to accurately approximate flow hysteresis highly depends on the frequency of the motion and the amount of negative indicial step responses taken into account This section will explore whether certain indicial step response functions in the dataset can be removed or altered such that the ROM remains as accurate, or improves in accuracy, with respect to the full-order model.

Linear regions

Due to the nature of the ROM method it is obvious that the linear part of the normal coefficient versus angle of attack (fig. 3.17) might be approximated by only one function. Concluding from fig. 3.15 the assumption can be made that the effect of angle of attack on the lift coefficient up to an angle of attack of roughly four degrees might be approximated by one indicial response function as the unsteady aerodynamic behaviour of the functions in that region is similar. However, it might be interesting to check whether there exists a difference between approximating this section using a step size of one degree or increasing the step size to the value of interest. The result on this small research topic is found in fig. 3.31.

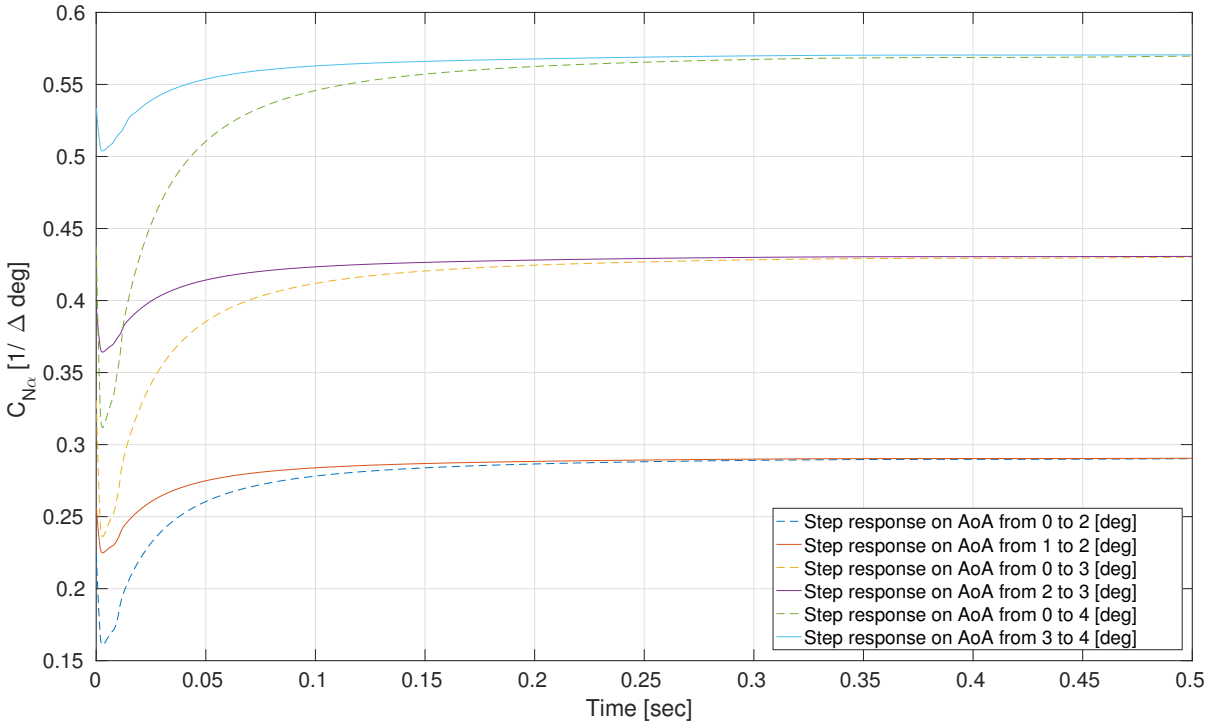

Figure 3.31: Indicial step response functions of the angle of attack effect on the normal force coefficient by applying various changes in degrees step change on a steady RANS solution starting at various angle of attack having a zero pitch rate

When looking at the results on the step amplitude it clearly shows that the step size does not affect the final steady state solution at lower angles of attack. This is as expected due to the fact that the configuration ends up in the same flow state in laminar attacked flow independent of the step size. However, for the research performed the unsteady effects are of high importance. It can be seen that all indicial responses behave as expected and at larger step magnitudes the disturbance in the flow field steady state solution increases, resulting in bigger starting peaks. In theory, the indicial function from zero to four degrees angle of attack, when divided by four (the step size), should correspond with an indicial response function in the linear domain, e.g. the function from zero to one degree angle of attack. It can be seen in fig. 3.32 that this is not the case. A cause for this difference may lie in the fact that a higher step response introduces a bigger disturbance in the steady state flow field starting solution. If accurate convergence is wanted smaller time steps or more sub-iterations per time step are needed. As the time steps were taken at similar sizes this produces a delay in convergence for the bigger step size, this could not be compensated by increasing the number of sub-iterations per time step. This shows that the accuracy in lower angles of attack at a laminar attached flow is a trade-off between computational time and accuracy wanted. In this case one indicial response function stepping from zero to one degrees is accurate enough to approximate the effect of angle of attack on the normal coefficient in low angle of attack ranges, where the flow is laminar and attached. Whether it is computationally efficient will be explored in section 3.6.3.

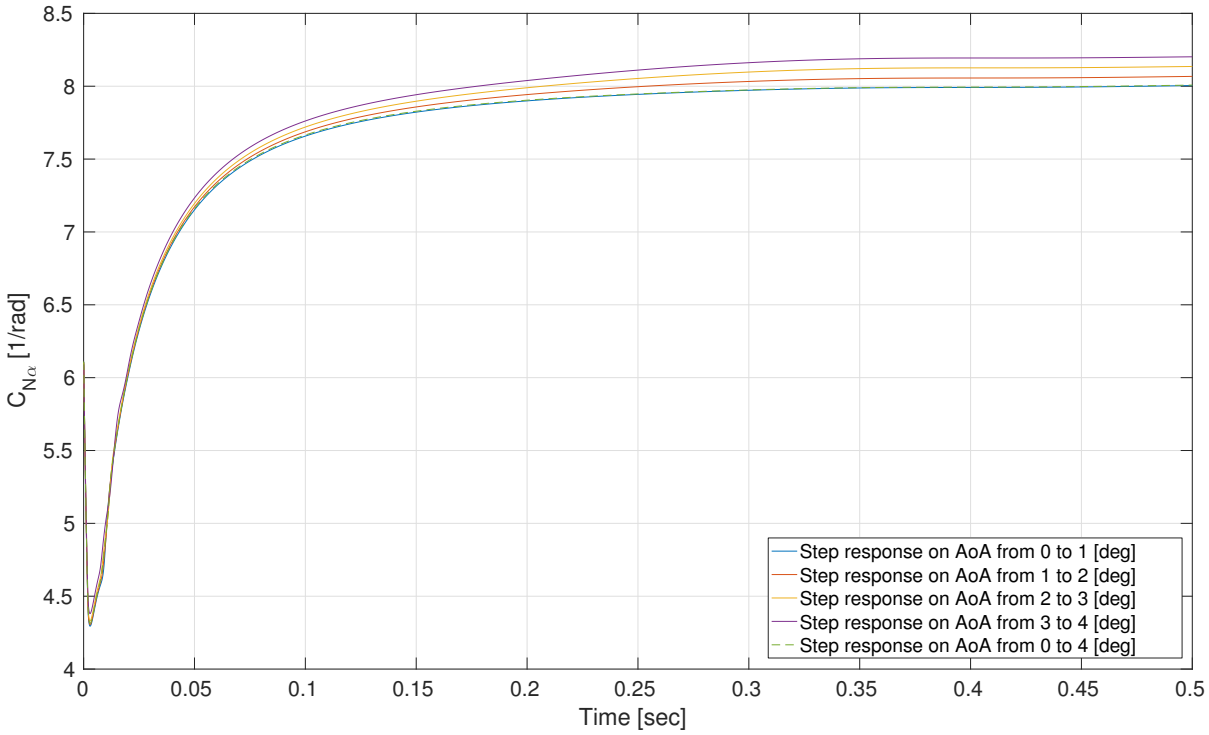

Figure 3.32: Indicial step response functions of the angle of attack effect on the normal force coefficient by applying a unit degree size step change and subtracting the steady RANS solution of interest at various starting angles of attack having a zero pitch rate

3.6.2. SAMPLING SPACE

From the sensitive analysis conducted and the step size research it is clear that the accuracy of ROMs becomes a sampling space problem. The accuracy as well as computational time involved to produce ROMs of the loads highly depend on the samples included within the datasets to approximate the full-order model. In the case explored within the section it was assumed that two effects influence the longitudinal loads.

The linear region of the angle of attack effect can be approximated using one indicial function using a step size of one degree. Several indicial functions are needed to approximate the non-linear region. For a fully accurate model also the negative step responses are needed. However, to effectively reduce the absolute error it is only needed to include the negative step responses at high angles of attack. This makes sure that the ROM can approximate flow hysteresis more accurately.

The pitch rate was assumed to be linear over the flight parameters of the motion. This is partially correct. The effect of rotating the configuration over a pitch angle at different angles of attack slightly affects the approximation of the unsteady flow behaviour. However, there is a hard to reduce numerical error involved when the indicial step response of pitch rate is wanted at different angles of attack. Furthermore, the pitch rate step size as a function of angle of attack shows slight non-linear behaviour. Overall, the ROMs produced can be made more accurate. however, this comes at a cost of computational time to expand the datasets. To what scale this expands and how the trade-off becomes beneficial is explored within the last part of this chapter.

3.6.3. COMPUTATIONAL EFFICIENCY

Resulting from previous parts of the report it is clear that a ROM based on indicial step response functions is able to relatively accurately predict the loads on the NACA profile, based on the functions used in the dataset. However, the question remains whether it is computational efficient to do this.

The results on the absolute error are once again given in table 3.2. For each performed frequency of the motion the normal force and pitching moment coefficients are given. As was clear from the previous section on ROM accuracy it is suspected that the main origin of the difference lies in the assumption of linearity of the pitch rate effect and the absence of negative step responses at higher angles of attack. The calculation of the ROMs only took a couple of minutes for each frequency. However, the setup time of the ROMs, meaning the calculation of the indicial functions to create the dataset, took approximately 1116 hours. This is due to the following calculations (note that the exact calculations of the dataset are found in appendix D). Each indicial step response starts from a steady state solution. Finding this steady state solution, provoking a step response and finding the next steady state solution takes approximately 124 [hours] per indicial function. Having 9 indicial functions in the dataset (8 for the angle of attack effect and one for the pitch rate effect) to approximate any of the six aircraft loads result in 1116 [hours] of ROM setup time.

To validate the ROMs, the full-order CFD calculations were performed. From table 3.2 it is found that each motion took approximately 160 hours to calculate. This means, finding an accurate solution of the Navier-Stokes solution inducing the forced motion in ENSOLV. It clearly shows that in this case it is not computational efficient to setup a ROM and approximate the loads for the frequencies of interest. The ROMs even get worse in terms of accuracy when the frequency is increased due to the assumptions made. This is one of the main drawbacks of this ROM building method. The setup time may take too much time. However, these are only the results of a 2D NACA case where the flow does not contain much non-linearities. Also, the dataset is not optimised in terms of redundant indicial step functions.

From the sensitivity analysis performed in section 3.5 the loads at lower angles of attack can be approximated by using only one function. However, to increase the accuracy at higher angles of attack or in the case of flow hysteresis , extra functions are needed to setup the ROMs. At this point it becomes a trade-off between the accuracy wanted and the computational time needed to setup the ROMs. In a case such as the current NACA profile it is not beneficial to use a ROM in terms of computational effort. However, imagine a more complex configuration which performs a very fast manoeuvre at high angles of attack. Unsteadiness and non-linearities dominate the flow at certain points. Vortices appear and flow hysteresis must be taken into account. A full-order CFD solution might take weeks to find a solution for the forced motion. At this point it might be beneficial in terms of computational effort as well as accuracy to setup a ROM. Especially when the manoeuvre needs to be optimised to adhere to certain flight qualifications. This is closely related to the use of conventional stability derivatives to approximate a flight mechanics model. It might therefore not be beneficial to use a ROM in the case of a forced motion, but it might be beneficial to use the dataset to estimate the conventional stability derivatives as well as taking into account the unsteady effects. To continue this research the second testcase was used and the conducted research in described within the next chapter.

Table 3.2: Computational effort in calculating and setting up the ROMs in comparison to the full-order model solutions and the absolute errors

Load [-]	**Frequency [Hz]**	**Max error[-]**	**Overall error [-]**	**ROM [sec]**	**Datasets [h]**	**Full-order [h]**
C_N	2.63	0.026	0.007	293	-	~ 160
	5.27	0.043	0.014	293	~ 1116	~ 160
	10.54	0.059	0.023	296	-	~ 161
C_m	2.63	3.20E-03	9.05E-04	290	-	-
	5.27	3.80E-03	1.80E-03	301	-	-
	10.54	9.10E-03	3.10E-03	302	-	-

4

REDUCED-ORDER MODELLING FOR THREE-DIMENSIONAL FLIGHT MANOEUVRES

The previous chapter was concerned with the investigation of ROMs of an oscillating two-dimensional airfoil in subsonic flow. Results gave rise to the question how accurate this ROM method is when extending the research to a three-dimensional configuration in a more complex manoeuvre. The results on this continuing research, by applying the ROM method to a more realistic configuration and flight manoeuvre prediction, are presented within this chapter.

This chapter will start off with the description of the three-dimensional testcase in section 4.1. The testcase will include design qualifications and reference values the design should adhere to. Based on these requirements, the manoeuvre can be selected which is interesting to investigate and apply the ROM to. This can be found in section 4.2. Having the requirements and dataset needed for the manoeuvre, a first ROM can be created to investigate whether the results correspond to the findings and conclusions made in the previous chapter. The results are given in section 4.3. Finally, in section 4.4, the manoeuvre selected is iterated by applying the investigated ROM method to a flight dynamics model and make a comparison between the researched ROM method and conventional use of stability derivatives.

4.1. TESTCASE DESCRIPTION

As already mentioned in section 2.5.2 the AVT-251 work-group is concerned with the multi-disciplinary design and performance assessment of effective, agile NATO air vehicles [40]. The configuration under investigation named MULDICON is based on a redesign of the DLR-F19/SACCON configuration [81]. The shape is seen in fig. 4.1. The goal of the work-group is to asses the baseline design performance and iterate it such that an agile UCAV bomber aircraft is obtained. Due to the shape of the aircraft and the mission requirements, unsteadiness and non-linearity will be involved in assessing aerodynamic performance in air combat manoeuvres such as an Immelmann turn (see fig. 2.11) [12]. This testcase will therefore be ideal to asses the use of the ROM method under investigation in a flight dynamics prediction. Besides, the work-group is also concerned with the aforementioned ROM method, meaning more results are produced for validation purposes. The research is therefore highly relevant as results from this testcase aid the progress of the work-group.

First the configuration and reference values will be described in more detail in section 4.1.1. In section 4.1.2, the mission design that the configuration should perform is described. Several flight loads characteristics of the baseline design are analysed in section 4.1.3. The final design qualifications selected for this research are summarised in section 4.1.4.

4.1.1. CONFIGURATION

The details and general shape of the MULDICON UCAV bomber baseline design are visualised in fig. 4.1. Due to its shape its called a lambda wing which is closely related to the well known delta wing. Therefore the common knowledge on the characteristics of flying wings and delta wings will be used during the research. These type of aircraft typically generate vortices at higher angles of attack, which might lead to stability issues. Therefore, it is interesting to investigate to see whether indicial step response functions can capture accurate samples of this high non-linear flow behaviour. The reference values of the baseline design are summarised in table 4.1.

The location of the bomber bays, fuel tanks and engine location are estimated, but details are not known at this point of design. Also, the Maximum Take-Off Weight (MTOW) and payload mass values are estimations such that detailed thrust to weight ratios are not known at this moment, references values of the previous design (the SACCON configuration) will be used when required MULDICON parameters are unknown. Furthermore, the biggest impact on the design is the absence of control surfaces. The conducted research will actively contribute to the aerodynamics shaping sub-group within the work-group. The research on control surfaces it therefore not considered, as another sub-group is covering this. Due to this, detailed calculations on stability and control are now minimal when assessing the performance of the aircraft. This has no impact on the ROM research as this research is only concerned with the prediction of the aerodynamic loads due to flow behaviour over the aircraft. However, the addition of control surfaces and thereby higher dependency on unsteady aerodynamics has an impact on the use of ROMs, but this will be a topic for future research (section 5.4.3). For now, the aerodynamic moments in this six degree of freedom model will be described instead of predicted during the manoeuvre to simulate the deflection of control surfaces. This is highly relevant when discussing the flight dynamics model in section 4.4.2. Details of the impact of this assumption on the results will be discussed when needed. The next section will describe the mission design proposed.

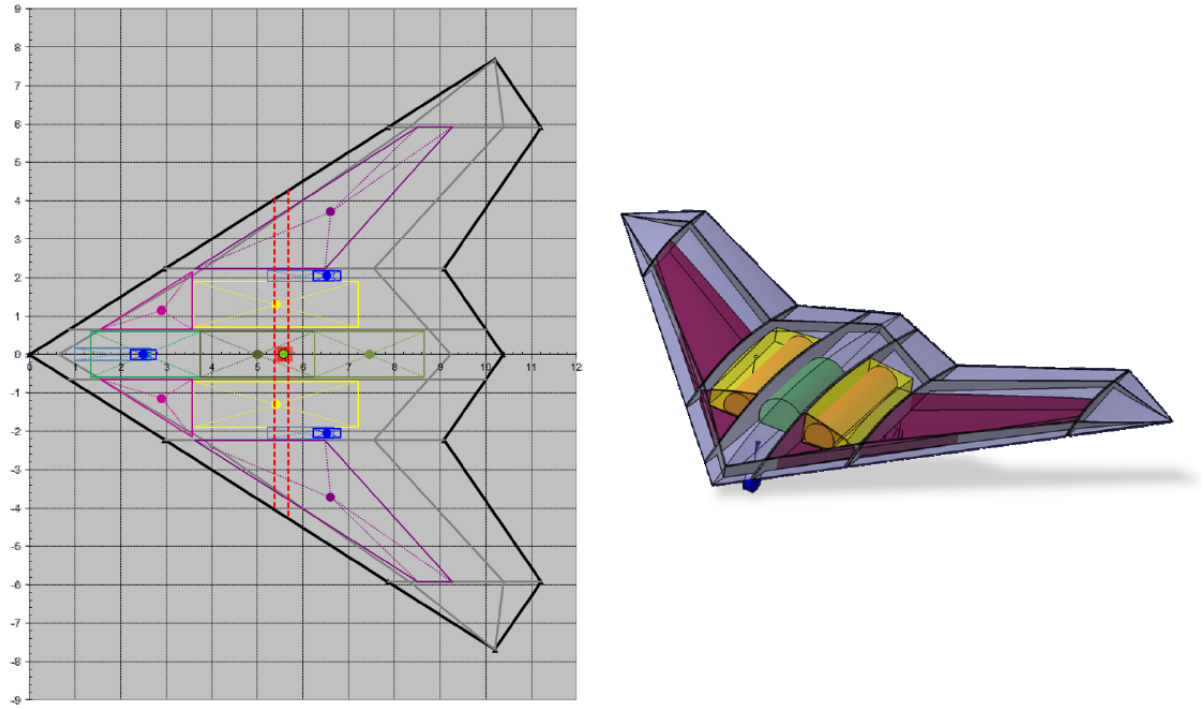

Figure 4.1: General shape of the MULDICON UCAV bomber baseline design showing the general aerodynamic shape (black), landing gear (blue), fuel tanks (purple), bomber bays (yellow) and engine location (green) created by work-group AVT-251 [40]

Table 4.1: MULDICON baseline configuration reference values created by work-group AVT-251 [40]

Parameter	**Value**
Outer shape	Based on DLR-F19, but with 30 [deg] trailing edge sweep
Propulsion	1 turbofan engine without afterburner
Engine integration	Buried (due to signature reasons)
Payload storage	Buried (due to signature reasons)
Payload mass [kg]	2 x 1000
Design range [km]	3000 (without aerial refuelling)
Fuel reserve [min]	≈ 45
Cruise altitude [km]	11
Cruise Mach number [-]	0.8
Stability margin	0 - 3 % MAC (stable)
MTOW [kg]	15,000
Reference Area [m^2])	77.8
Reference chord length [m]	6
Reference half span [m]	7.69
Moment reference point (from nose) [m]	6

4.1.2. MISSION DESIGN

The basic mission design is closely related to a "Bomber Low Level Penetration" as described by MIL-STD 3013 documents [92]. This is identical to the mission defined for the previous design configuration (DLR-F19/SACCON). Based on the set 3000 [km] range requirement, the mission radius is 1500 [km] without aerial refuelling. The requirement to increase speed to Mach 0.9 close to the target is considered an option (and maximum). If the engine still has a power reserve at Mach 0.8 at low altitude, it shall be used to make the final approach to target faster than Mach 0.8. The mission design is well defined and multiple design points can be chosen. In order to keep the research realistic and add contribution to the work-group, this mission design will be closely followed to asses aerodynamic performance of the design. However, before a design point can be chosen where a manoeuvre will be investigated, the steady state flight characteristics of the design should be analysed in order to create reference load values as well as to validate the use of the ENSOLV CFD solver for this configuration. This analysis now follows.

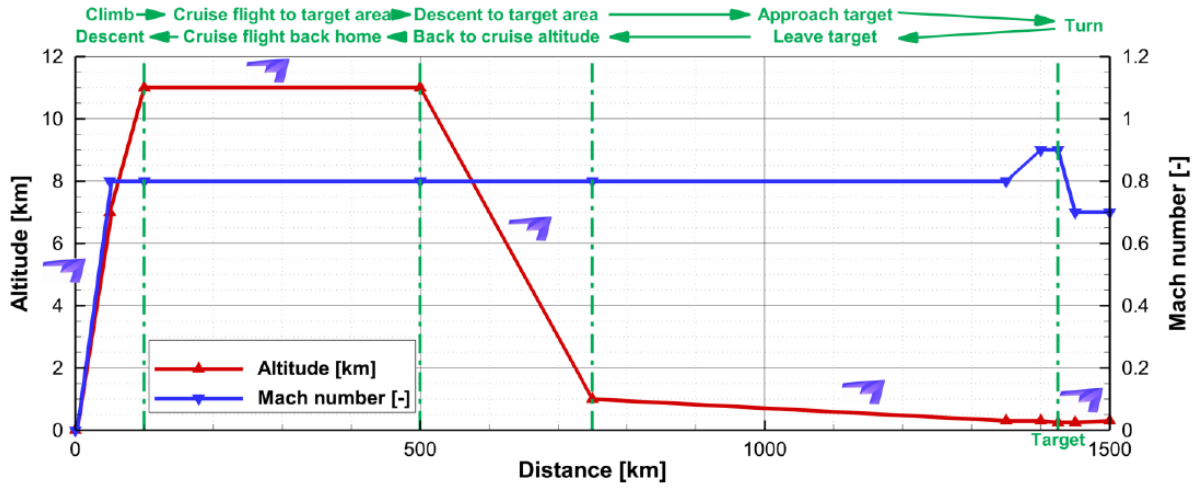

Figure 4.2: Basic mission design of the MULDICON created by work-group AVT-251 [40]

4.1.3. FLOW BEHAVIOUR ANALYSIS

To analyse the steady aerodynamic loads of the baseline design, several data points are needed. To reduce complexity only the longitudinal aerodynamic loads are analysed, in line with research performed on the NACA profile in previous chapter. Again, the RANS are used to predict flow behaviour of the configuration. Purely steady calculations are relatively fast, as the calculations are time-independent and only the final flow solution will be used. As with the NACA research, the settings of the unsteady calculations are chosen in such a way that accurate convergence at each time step is obtained (non-dimensional step size of 0.01 and 30 sub-iterations per time step). In order to be consistent with the fidelity used for the NACA research, these calculations will also include an Explicit Algebraic Reynolds Stress Model (EARSM) in K-omega form [86] to cope with turbulence in the flow. The dimensionless wall distance for proper turbulence modelling $y+ \approx 1$.

As only longitudinal manoeuvres will be investigated only one half of the grid will be used due to symmetry of the MULDICON design. This block-structured grid was produced by NLR using NLR's in-house domain modeller and grid generation tools Endomo [87] and Engrid [88] and consist out of 660 blocks and 16,357,376 cells. For this initial design, convergence issues of the RANS appeared when finding a solution at higher Mach numbers (≈ 0.8). Lower Mach number showed more accurate convergence in the solution. Therefore it is chosen to use a constant Mach number of 0.2 during the manoeuvre. This limits the manoeuvre selection, but that will be explored in section 4.1.4. For an accurate investigation of the flow behaviour the work-group states that at this flow speed a reference value of 28,000,000 for the Reynolds number should be used.

Based on initial research performed by the work-group the decision is made to investigate the aerodynamic loads in the range of 0 to 22 degrees angle of attack. To limit computational effort, time intervals of 2 degrees

are used. The resulting steady RANS lift and drag force coefficients as a function of angle of attack are visualised in fig. 4.3. The lift and drag show characteristics similar to those of a low-speed delta wing. Lift slowly increases as the angle of attack is increased. At roughly 15 degrees angle of attack the lift (as well as the drag) increases more rapidly. This might originate from typical high swept delta wing leading edge vortices, which start to form and flow over the wings. At roughly 10 to 12 degrees, flow vortices at the leading edge may occur. These vortices increase flow velocity, thereby energising the flow resulting in a higher suction peak. These vortices stay attached to the wing and as the angle of attack increases the lift also increases. This so called vortex lift [93] can be seen in the steady lift over angle of attack plot by a sudden increase in lift increment. This is in line with more recent research on an iteration of the MULDICON baseline design [94], confirming the suspicion on vortex lift generation. A drawback of this sudden increase in lift is an increase of drag, originating from the formed vortices also seen in the figure. Due to the appearance of these vortices, flow separation is postponed resulting in higher angles of attack where the flow is still attached. At higher angles of attack the flow behaviour becomes more unsteady due to these vortices, which will eventually break down from the wing resulting in stall. This unsteady flow behaviour may be approximated more accurately by the ROM method and will be further explored in section 4.3.

In line with the research on ROM accuracy in two-dimensional subsonic flow, again the normal and axial force coefficient are investigated to remove angle of attack dependency. For sake of completion these results are seen in fig. 4.4, based on the straightforward transformation between reference systems (eq. (3.2)). A final result on the steady longitudinal aerodynamic loads predictions is given in fig. 4.5, where the pitching moment coefficient is plotted against the angle of attack. As the angle of attack increases the pitching moment also increases, whereas a positive pitching moment corresponds to a nose up rotation. It seems that when the angle of attack is increased, the resulting force is situated more forward towards the leading edge, thereby increasing the pitching moment with respect to the reference value (aerodynamic centre) of 6 [m]. This increases more rapidly at the angle of attack where vortices begin to form. Around 16 to 18 degrees angle of attack the vortices apparently become unstable and more unsteadiness is introduced which might decrease the ability of the steady calculations to predict the actual flow behaviour. This means that the regions where vortices become unstable is of high interest in the analysis of flight performance of the design, especially the unsteadiness associated with it. Based on knowledge of the steady flow characteristics and the mission, a design point can be chosen where a manoeuvre will be specified to further inspect aerodynamic behaviour of the MULDICON. This will be done in the next part.

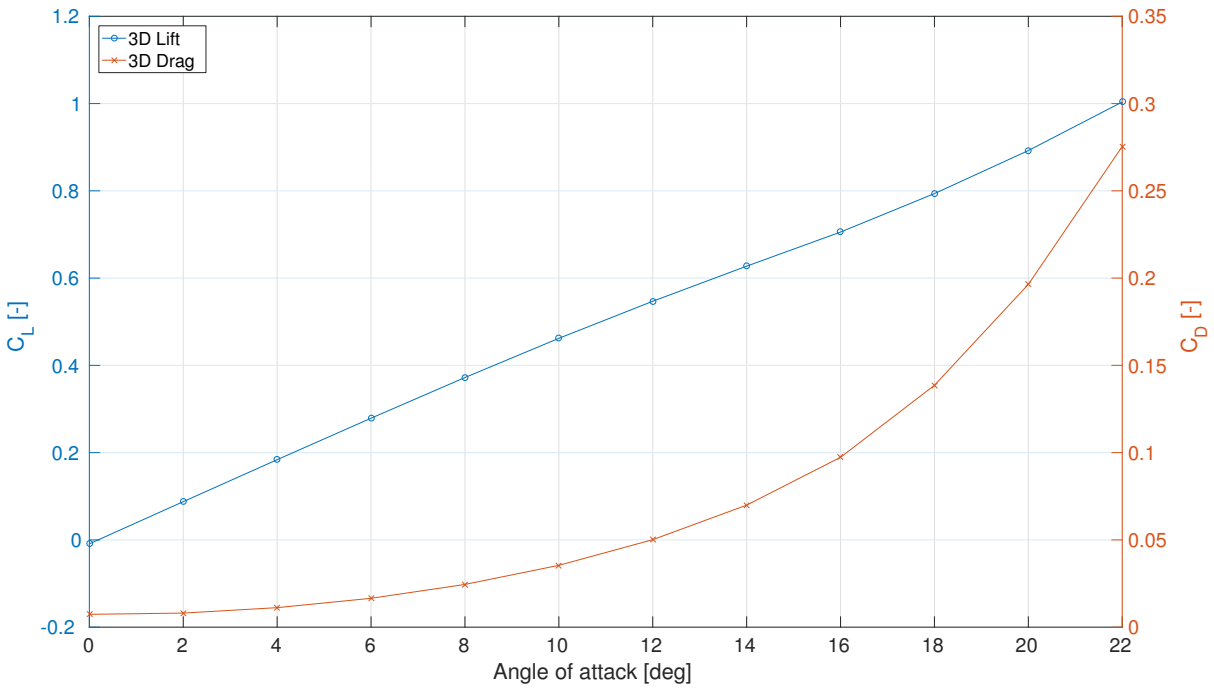

Figure 4.3: Steady RANS 3D lift and drag coefficients as a function of angle of attack of the MULDICON configuration at a Mach number of 0.2 and Reynolds number of 28,000,000

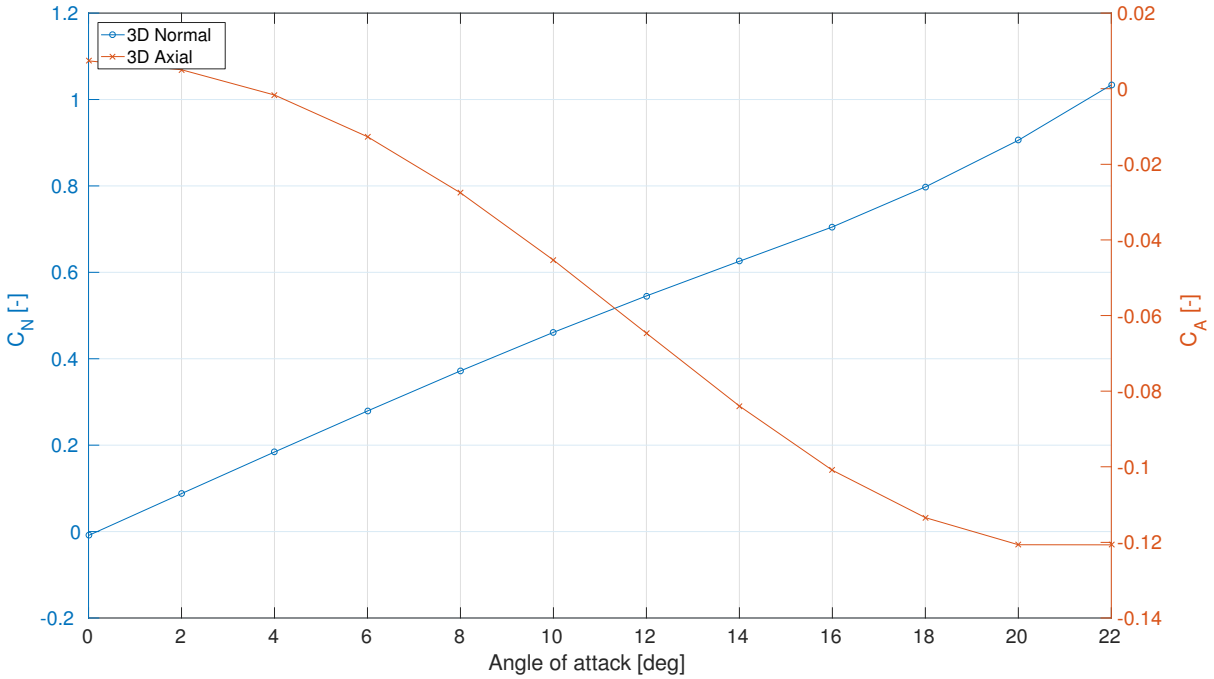

Figure 4.4: Steady RANS 3D normal and axial force coefficients as a function of angle of attack of the MULDICON configuration at a Mach number of 0.2 and Reynolds number of 28,000,000

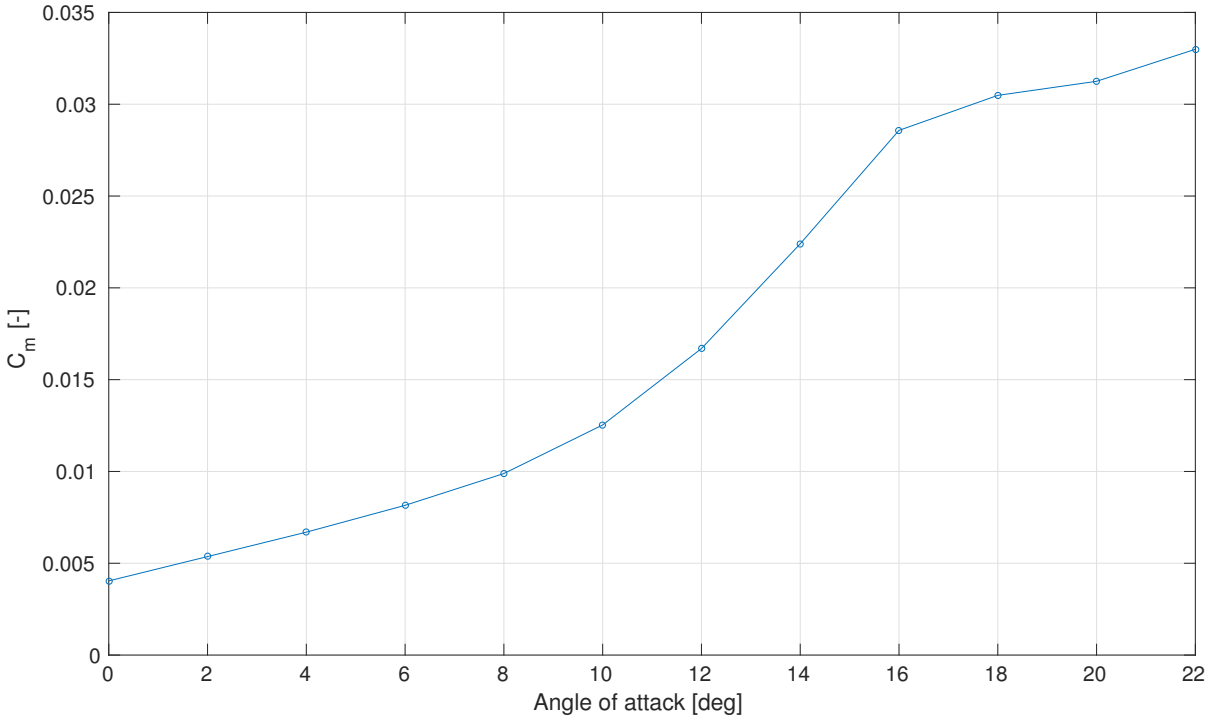

Figure 4.5: Steady RANS 3D pitching moment coefficient as a function of angle of attack of the MULDICON configuration at a Mach number of 0.2 and Reynolds number of 28,000,000

4.1.4. Design point

As was mentioned, a Mach number of 0.2 will be used during the manoeuvre. A quick study showed that the initial design could not cope with higher Mach numbers. Therefore, other velocities can be investigated in later design iterations, but for now the low Mach number will suffice. To reduce complexity it is chosen to only investigate longitudinal manoeuvres, in line with the research conducted on the NACA airfoil in previous chapter. Furthermore, the research performed in chapter 3 showed that ROMs based on indicial response functions may be able to accurately take into account unsteady effects of attached flow during relatively rapid motions. To strengthen this statement it is therefore interesting to investigate whether a three-dimensional and rapid manoeuvre provides similar results. What has not been investigated is whether the ROM method can cope with highly unsteady and non-linear flow behaviour, which might occur in the case of this MULDICON design approaching 15 to 16 degrees angles of attack. Therefore it is chosen to use the take-off design point, as specified by the work-group, to perform a climbing manoeuvre. This manoeuvre will minimise complexity yet still provide enough results to make a statement regarding the use of ROMs in flight dynamics predictions involving highly unsteady and non-linear flow behaviour at high angles of attack as well as relatively steady and linear flow behaviour at lower regions. A summary of the flight conditions and qualifications the manoeuvre should adhere to is given in table 4.2. Details on the manoeuvre details and dataset needed to build to ROMs is further discussed in section 4.2.

Table 4.2: MULDICON baseline configuration take-off design point values formulated by work-group AVT-251 [40] where the pitch rate requirement is based on a MIL-STD 1797A, level 1, Class IV classification [92]

Parameter	Value
Altitude [km]	0
Air density [kg/m^3]	1.225
Pressure [Pa]	101325
Temperature [K]	288.15
Speed of sound [m/s]	340.3
Gravitational constant [m/s^2]	9.81
Dynamic viscosity [Pa*s]	1.79E-05
Mach number [-]	0.2
Velocity [m/s]	68.06
Dynamic pressure [Pa]	2837.17
Reynolds number [-]	2.80E+07
Pitch rate requirement [deg/sec]	20
Design lift coefficient	1.1
Load factor [-]	1.5
Expected drag coefficient [-]	0.143
Expected lift over drag [-]	7

4.2. Experimental setup

As explained, the manoeuvre under investigation will be a take-off. This research will thereby strengthen the statements made in previous chapter as well as providing enough data to answer the research questions proposed in section 2.5.1. To create ROMs a dataset is needed. It is therefore necessary to first describe the experimental setup of the testcase. First the assumptions made will be given in section 4.2.1. The resulting dataset consisting out of samples of the full-order model, the indicial response functions, based on the assumptions will be described in section 4.2.2. To conclude the description the results of the verification of the dataset is given. This will be done in section 4.2.3.

4.2.1. Assumptions

Based on the requirements set on the manoeuvre several assumptions can be made. First of all, the manoeuvre will be a purely longitudinal motion. Side-slip angles and lateral-directional Euler rates will not be taken into account. In line with research conducted on the NACA airfoil the three loads (normal, axial and pitching moment) are again only considered to be affected by changes in angle of attack and pitch rate. One could debate whether higher order terms, such as the first derivative of angle of attack, should be taken into account. However, the impact of this assumption will become clear when the results are discussed. Furthermore, as limited by the design point, the value of the low speed Mach number is 0.2. Details on the effect of a constant speed during a take-off manoeuvre and the resulting reality of the corresponding predictions are further elaborated in section 4.4. For accurate flow behaviour prediction at this design point a Reynolds number of 28 million should be used according to the work-group. Finally an assumption should be made on the range of flight parameters the manoeuvre should adhere to. As seen from steady aerodynamic loads predictions in section 4.1.3, investigating flow behaviour and how a ROM copes with this, the angle of attack should be in the ranges between 0 and roughly 20 degrees angle of attack. The pitch rate requirement will be used such that the design should rotate in pitch with a constant 20 degrees per second. By keeping this pitch rate constant a possible error in pitch rate step size indicial function is reduced.

4.2.2. Indicial step response functions

To create the ROMs, a dataset consisting out of indicial step response functions is needed. Based on the assumptions the manoeuvre should cover a range from 0 to roughly 20 degrees angle of attack while under a constant pitch rate of 20 degrees per second. The research on the NACA airfoil showed that the indicial step responses might take a while to calculate which has a negative effect on the computational efficiency of the ROMs. Therefore, to reduce computational effort, step sizes of one degrees in angle of attack are used for a range of two degrees angle of attack. As example, the unsteady behaviour captured within the indicial response from 0 to 1 degree is used for the range of 0 to 2 degrees angle of attack in the load prediction of the take-off. This means that 11 indicial functions are computed to capture the angle of attack effect. To capture the pitch rate effect one indicial function is calculated by applying a 20 degrees per second step size. The URANS results of the calculated indicial functions and how the unsteady flow behaviour is captured can be seen in fig. 4.6 to fig. 4.9. To reduce the amount of figures within this analysis the axial force results are found in appendix F.

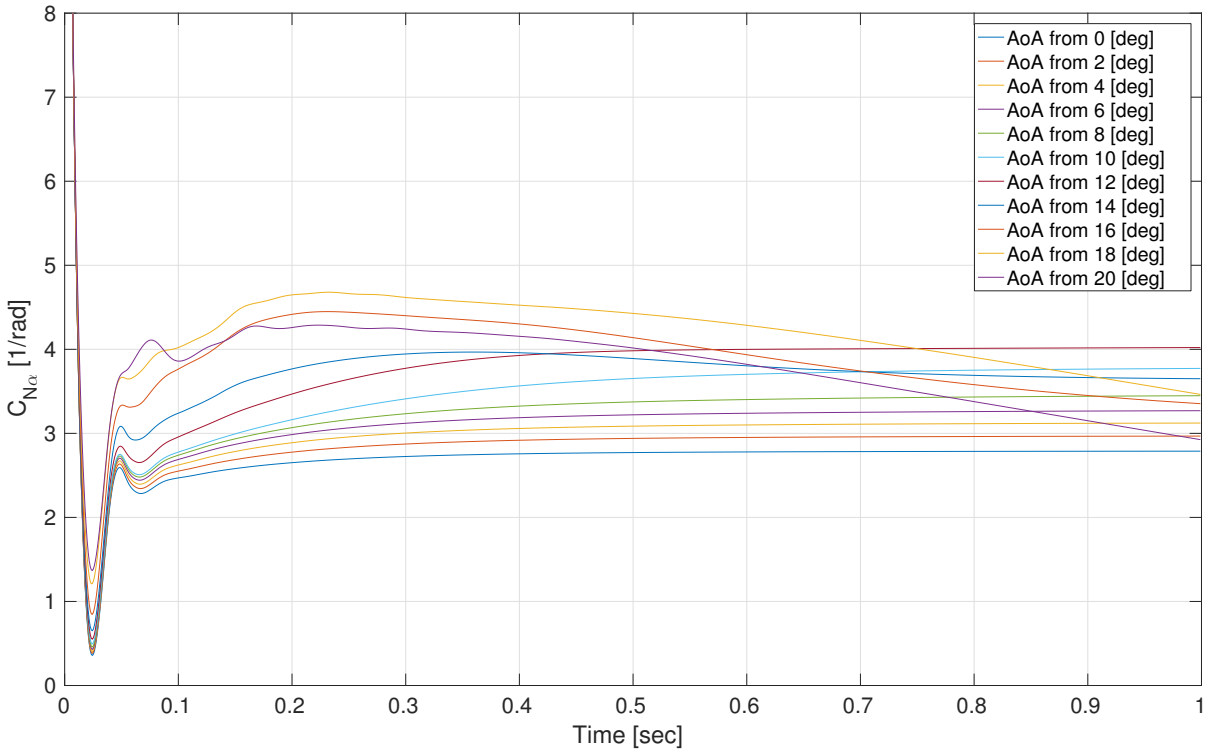

Figure 4.6: Indicial step response functions of the angle of attack effect on the normal force coefficient by applying a one degree step change on a steady RANS solution at various starting angles of attack and zero pitch rate

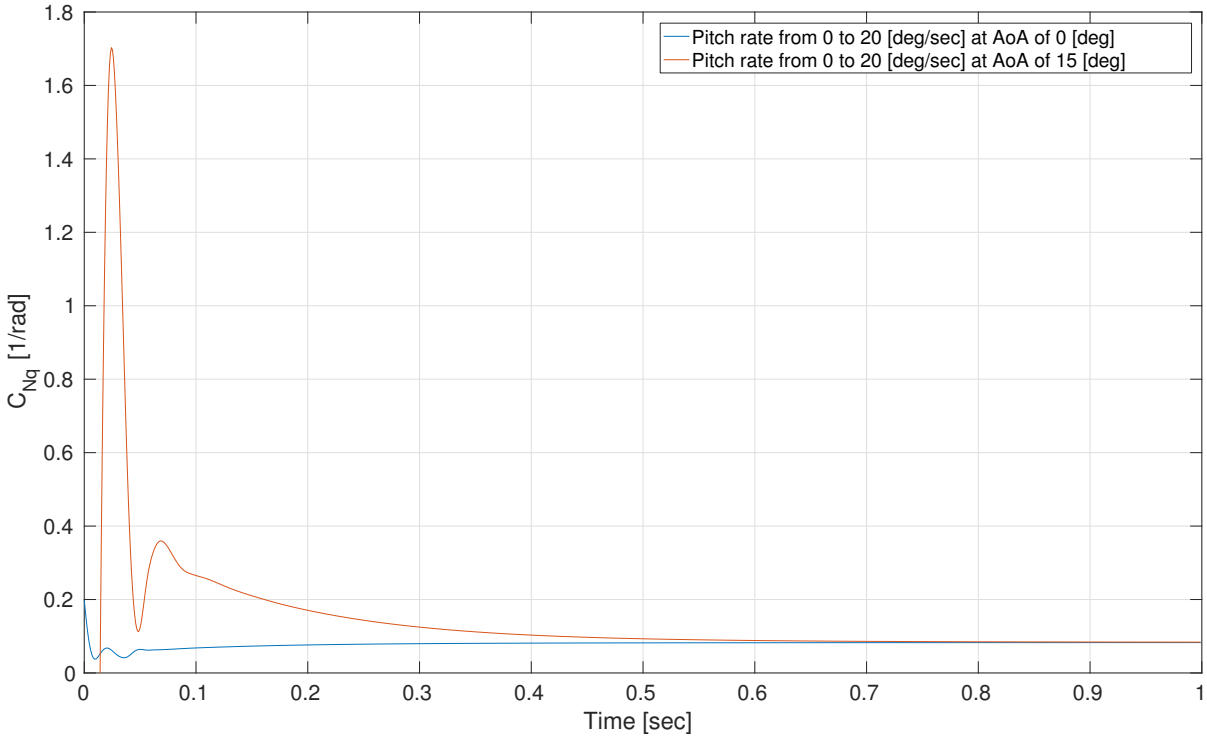

Figure 4.7: Indicial step response functions of the pitch rate effect on the normal force coefficient by applying a 20 degrees per second step change on a steady RANS solution at various starting angles of attack and zero pitch rate

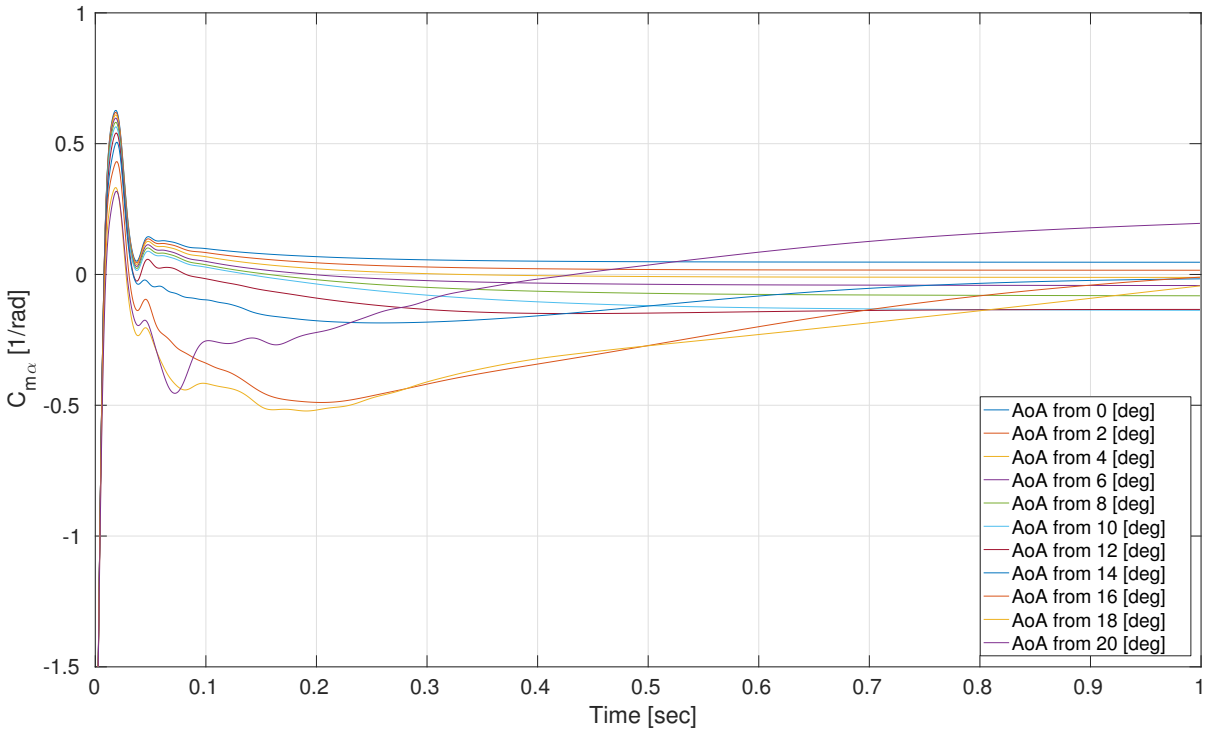

Figure 4.8: Indicial step response functions of the angle of attack effect on the pitching moment coefficient by applying a one degree step change on a steady RANS solution at various starting angles of attack and zero pitch rate

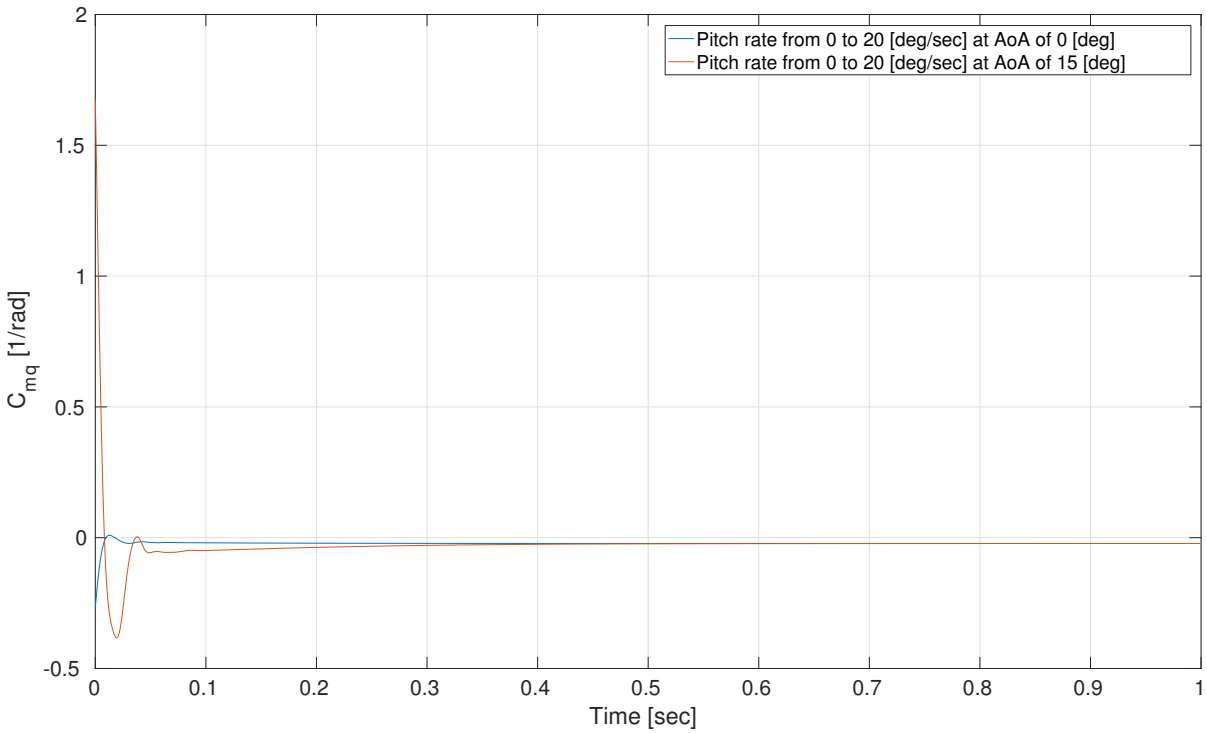

Figure 4.9: Indicial step response functions of the pitch rate effect on the pitching moment coefficient by applying a 20 degrees per second step change on a steady RANS solution at various starting angles of attack and zero pitch rate

When looking at the angle of attack effect on one of the loads, for example the normal force coefficient in fig. 4.6, the unsteady behaviour is as expected up to the angle of attack where vortices begin to form. Up to roughly 12 degrees the flow eventually reaches a steady state solution after one second. However, as the angle of attack increases, vortices appear which results in the steady state flow condition not yet being reached after one second. This might become an issue when creating the ROMs as the indicial response functions might not be able to accurately sample the effect of vortices. To verify whether these results are accurate, a verification of the results is needed which will be provided in section 4.2.3. When looking at the pitch rate effect on for example the normal force in fig. 4.7 the behaviour is as expected. To reproduce the conclusions of the NACA airfoil research, the step is applied at two different angle of attack RANS flow solutions. As a step of 20 degrees per second is used as input, a flow disturbance is added in the flow solutions which needs a certain time to damp out to a steady state flow condition. As the angle of attack increases the damping time required becomes larger, but might also contain the aforementioned numerical error in convergence at each time step. To minimise this error, the step response from an angle of attack of zero degrees is used for the pitch rate indicial effect.

4.2.3. Dataset verification

The dataset needs verification to verify and investigate the unexpected behaviour of the indicial responses at higher angles of attack. The results on the three loads are seen in fig. 4.10 to fig. 4.12. The final value of the URANS indicial step response and the RANS calculated steady state values are compared. These two should correspond as the aircraft will end up in the same flow state for both situations. When looking at the results it can be seen that up to roughly 12 degrees angle of attack, where vortices begin to form, the indicial functions are verified to be relatively accurate. After this point the datasets begin to differ. The discrepancies between the solutions when vortices begin to form can have multiple origins. When looking at the pitching moment results it can be seen that the datasets do not correspond accurately. This means that both datasets need verification. The steady RANS data points might have convergence errors, meaning the steady state flow condition is not reached, while the indicial response functions might need more time to reach a possible steady state solution. These two possible error origins will be researched in more detail to make a statement regarding the verification and accuracy of the indicial functions. It is important that these are verified as the ROM accuracy is based on the ability of the samples to accurately capture and represent the full-order model flow behaviour.

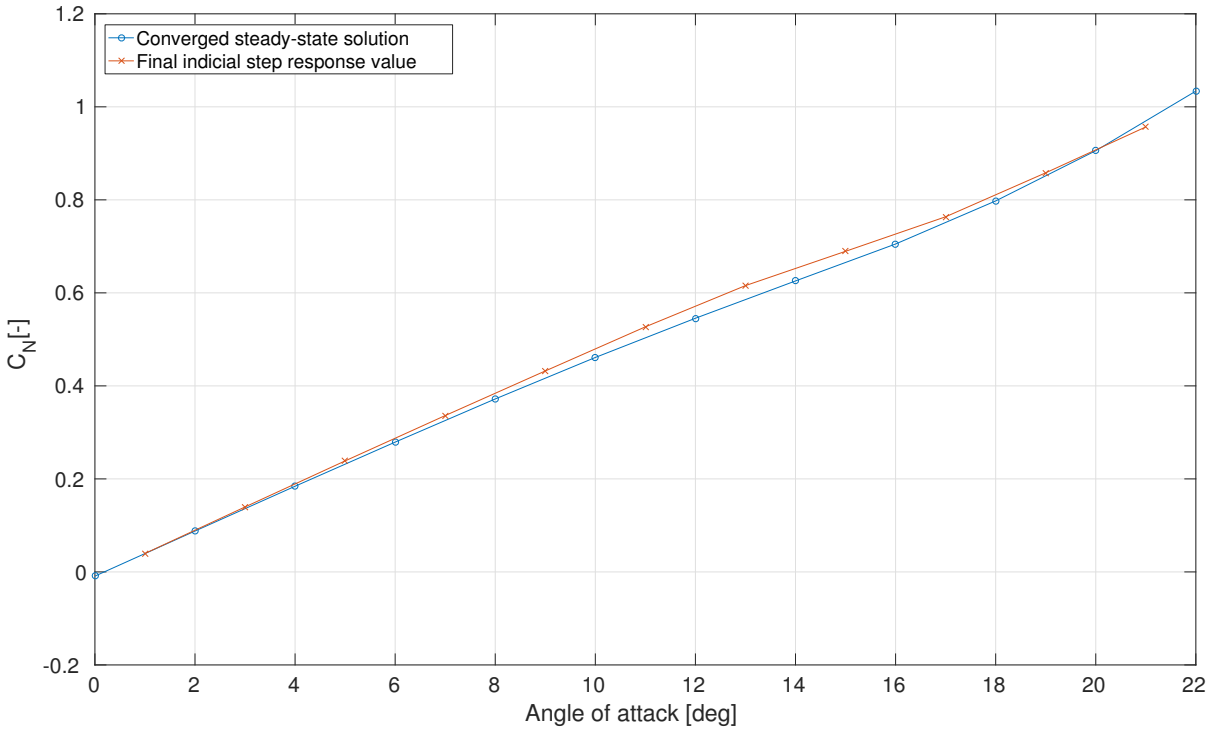

Figure 4.10: Final values of the angle of attack indicial step response functions on the normal force coefficient generated by approximating the unsteady RANS compared to the MULDICON directly configuring in the angle of attack of interest and finding the steady RANS solution

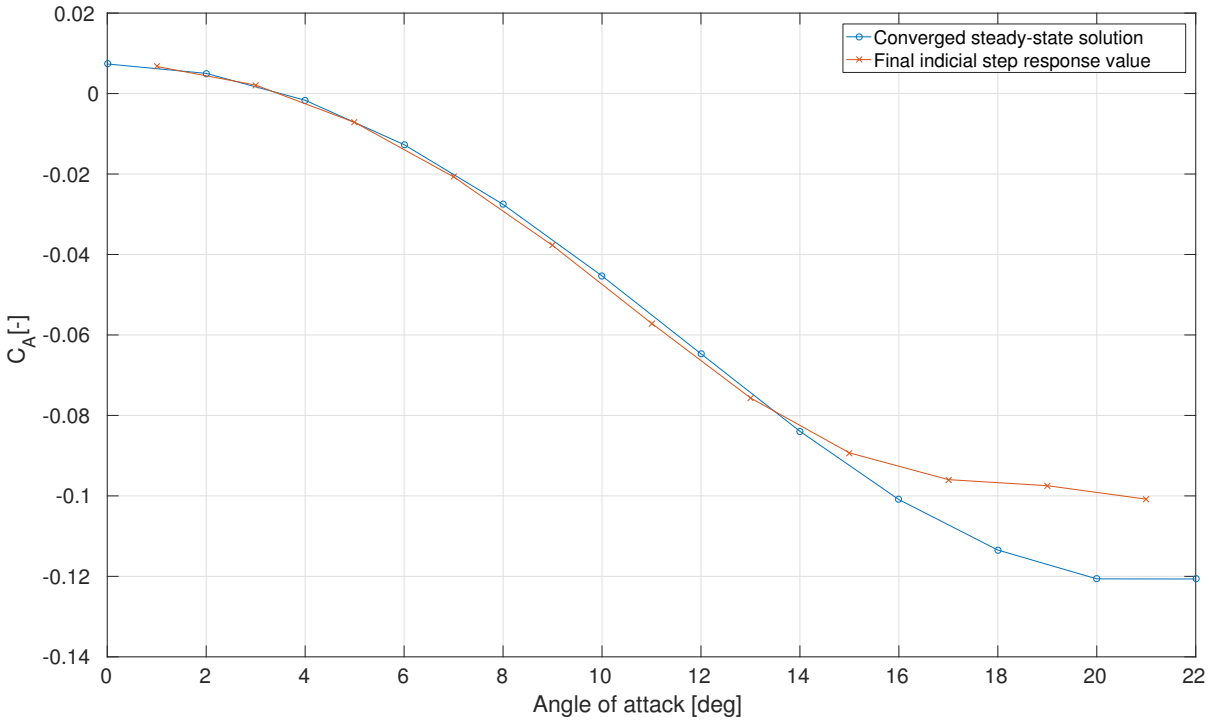

Figure 4.11: Final values of the angle of attack indicial step response functions on the axial force coefficient generated by approximating the unsteady RANS compared to the MULDICON directly configuring in the angle of attack of interest and finding the steady RANS solution

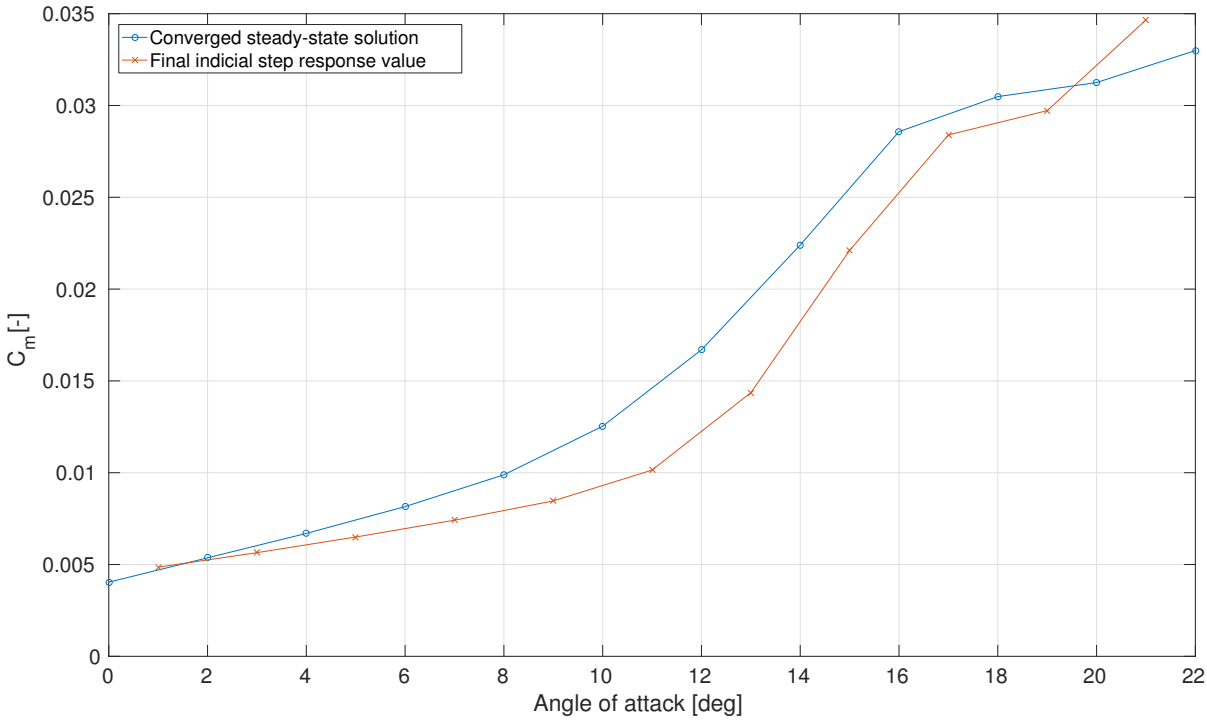

Figure 4.12: Final values of the angle of attack indicial step response functions on the pitching moment coefficient generated by approximating the unsteady RANS compared to the MULDICON directly configuring in the angle of attack of interest and finding the steady RANS solution

Steady RANS dataset error

The first logical step in finding the error between the datasets is to look at the convergence history of the CFD. It might be the case that the steady RANS solutions, which are needed to verify the indicial step functions, are not completely converged to a steady state solution after the specified time. The number of iterations used to simulate the air flowing over the wing might not be enough. In a steady calculation one is only interested in the final value of the CFD solution. However, to investigate the solution history, unsteady calculations were performed to get to a final RANS solution, which is used as a steady state flow solution. This was done in order to keep output data consistent for ease of comparison between the RANS solutions. The unsteady RANS calculations were based on 300 time steps in three grid levels, ranging from coarse to fine, whilst each time step had 100 sub-iterations leading to 30,000 iterations in total. As this convergence error might have occurred at every angle of attack, the three most critical angles of attack, 20, 21 and 22 degrees, are looked at in more detail. These flow states were recalculated, now having 200 time steps per grid level, while still having 100 sub-iterations resulting in 60,000 total iterations. The resulting final (steady-state) RANS solutions and errors between the number of iterations for each flight load are summarised in table 4.3. A significant error of 10.8 percent was found for the pitching moment coefficient at an angle of attack of 20 degrees. To analyse this error in more depth the convergence history of the unsteady calculations of this load for the two datasets for different total number of iterations is given in fig. 4.13. The history shows that the RANS solutions might not have fully reached a steady state flow condition for higher angles of attack as the figure clearly shows that each grid level has not been fully damped out. A more accurate approximation of the RANS was found for a higher number of iterations, but still does not yield in a perfectly converged solution. This might imply that unsteady and unstable vortices might be the cause for the RANS not finding a perfectly converged solution, thereby not reaching a steady state flow condition. The convergence histories of the other loads can be found in appendix E.

Table 4.3: Errors between the steady RANS final solutions having different number of iterations

Alpha [deg]	Total iterations	C_N [−]	C_A [−]	C_L [−]	C_D [−]	C_m [−]
20	30,000	0.906	-0.121	0.892	0.196	0.031
	60,000	0.932	-0.116	0.916	0.210	0.028
	error [%]	***2.9***	***4.1***	***2.6***	***6.7***	***10.8***
21	30,000	0.969	-0.121	0.948	0.234	0.031
	60,000	0.984	-0.118	0.961	0.243	0.032
	error [%]	***1.6***	***2.7***	***1.4***	***3.6***	***1.9***
22	30,000	1.034	-0.121	1.004	0.275	0.033
	60,000	1.039	-0.116	1.006	0.281	0.036
	error [%]	***0.5***	***3.9***	***0.3***	***2.2***	***7.3***

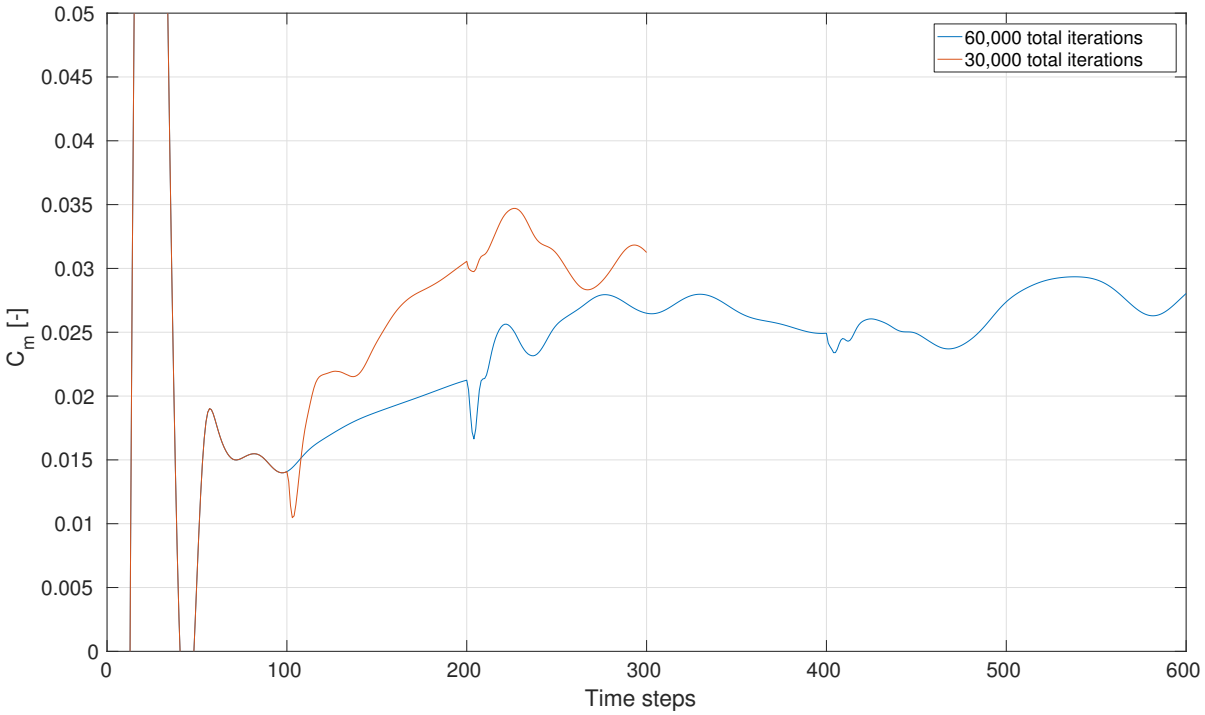

Figure 4.13: ENSOLV RANS convergence history results for MULDICON load at a Mach of 0.2, Reynolds number of 2.80E+07 and an angle of attack of 20 [deg] showing two different number of iterations

Unsteady RANS dataset error

Presuming that the higher angles of attack steady state values are not representative of the flow as unsteady behaviour is not taken into account, the indicial functions themselves are analysed in more depth. It can be seen in fig. 4.6 that the indicial functions at higher angles of attack need more iterations (read: time to let the air flow over the configuration) to reach a possible steady state. An extended indicial function of the angle of attack effect running for 5 seconds, as well as the original indicial function of 1 second is plotted in fig. 4.14 to fig. 4.16 for all three loads. Also, both final unsteady RANS solutions (representing a steady state condition) for the different number of iterations are shown in the figure. As stated before these values should agree as the aircraft, in theory, ends up in the same flow state. However, the results clearly shows that this is not the case.

Looking back at the steady flow behaviour of the aircraft design at higher angles of attack, analysed in section 4.1.3, it was stated that vortices appear at roughly 12 degrees angle of attack. Unsteadiness might become more dominant in the flow around 15 degrees angle of attack. As the angle of attack increases, the vortices become more unstable and might result in complete flow separation and lift loss. This unsteady behaviour might result in not finding a steady state flow solution. This can also be concluded from the difference between the final value of the unsteady RANS calculations. It could be seen that a complete steady-state solution is not even reached for 60,000 iterations. Therefore, the indicial response function, which does capture unsteady flow behaviour, might provide a more accurate solution to the flow behaviour at these angles of attack. A complete verification of the calculated indicial functions cannot be made as steady state flow conditions are not found at higher angles of attack. To investigate the (unsteady) flow behaviour in the testcase a basic full-order URANS calculation is needed to show how the loads differ, compared to the calculated 'steady state' RANS solutions. This will help in the verification process of the indicial functions at higher angles of attack. This will be described in the next part.

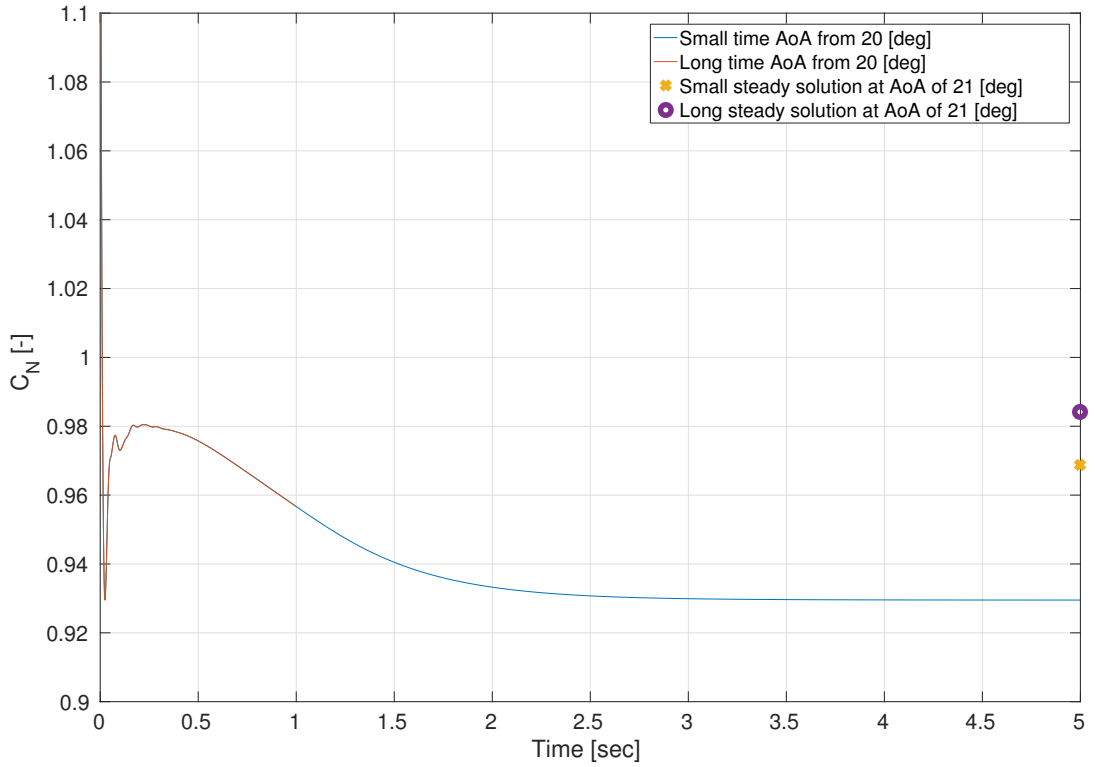

Figure 4.14: Indicial step response functions of the angle of attack effect on the normal force coefficient by applying a one degree step change on a steady RANS solution at 20 degrees angles of attack and zero pitch rate for the original 1 second and an extended 5 seconds as well as the data points for the 30,000 number (small) of iterations steady RANS solution and the 60,000 one(long)

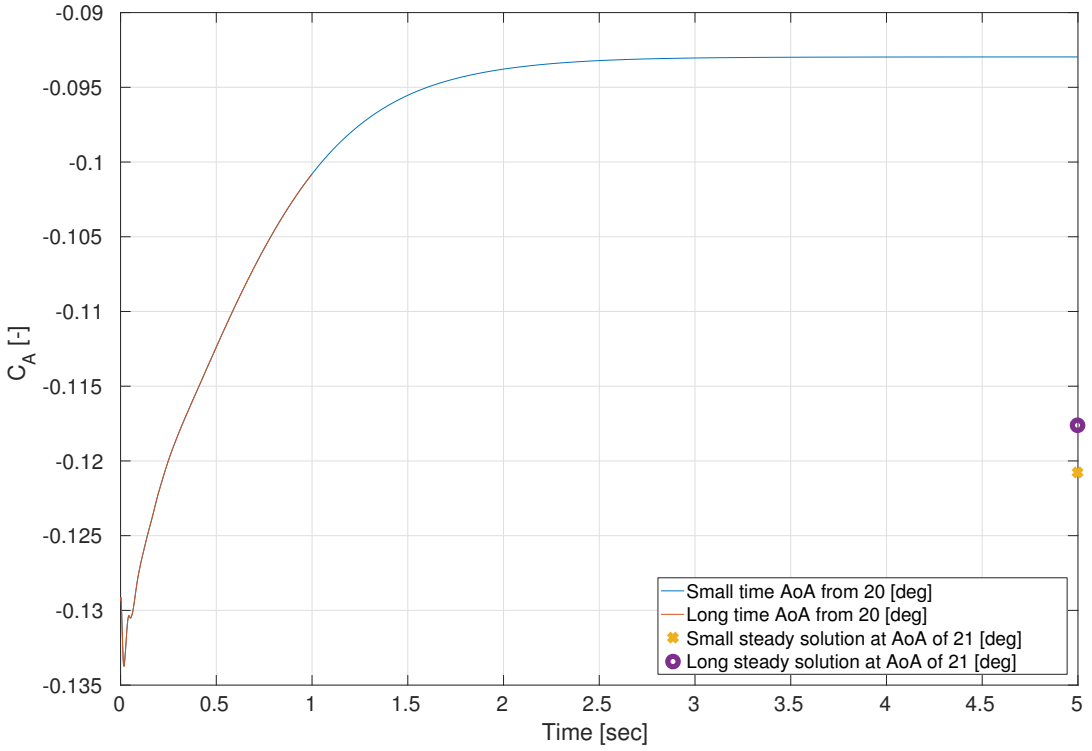

Figure 4.15: Indicial step response functions of the angle of attack effect on the axial force coefficient by applying a one degree step change on a steady RANS solution at 20 degrees angles of attack and zero pitch rate for the original 1 second and an extended 5 seconds as well as the data points for the 30,000 number (small) of iterations steady RANS solution and the 60,000 one(long)

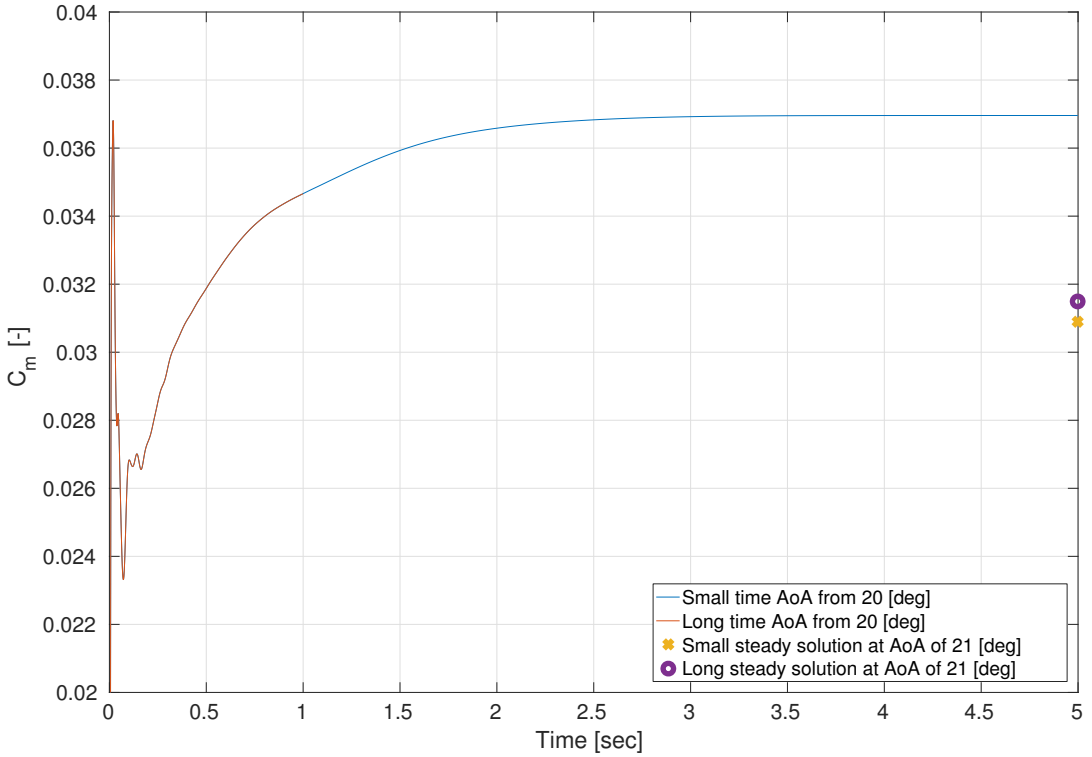

Figure 4.16: Indicial step response functions of the angle of attack effect on the pitching moment coefficient by applying a one degree step change on a steady RANS solution at 20 degrees angles of attack and zero pitch rate for the original 1 second and an extended 5 seconds as well as the data points for the 30,000 number (small) of iterations steady RANS solution and the 60,000 one(long)

4.3. UNSTEADY FLOW BEHAVIOUR

To investigate the actual unsteady flow behaviour of the aircraft within the limits of the defined testcase a full-order time-marching URANS calculation is performed. To minimise the number of unknown effects on the flow behaviour, the MULDICON is oscillated around a non-moving point, resulting in a similar pitch oscillation motion as specified for the airfoil testcase. To analyse possible unsteady flow behaviour at the design point, a maximum pitch rate of 20 degrees per second is applied. The motion starts at a steady RANS flow solution at 10 degrees angle of attack where it is known that vortices are not present. The angle of attack (and thereby pitch attitude due to the nature of the motion) is increased to 20 degrees to investigate the flow behaviour at high angles of attack and is then rotated back to zero degrees. The visualisation of this pitching motion is visualised in fig. 4.17. By calculating the URANS solution of this motion the unsteady flow behaviour encountered at the design point becomes more clear.

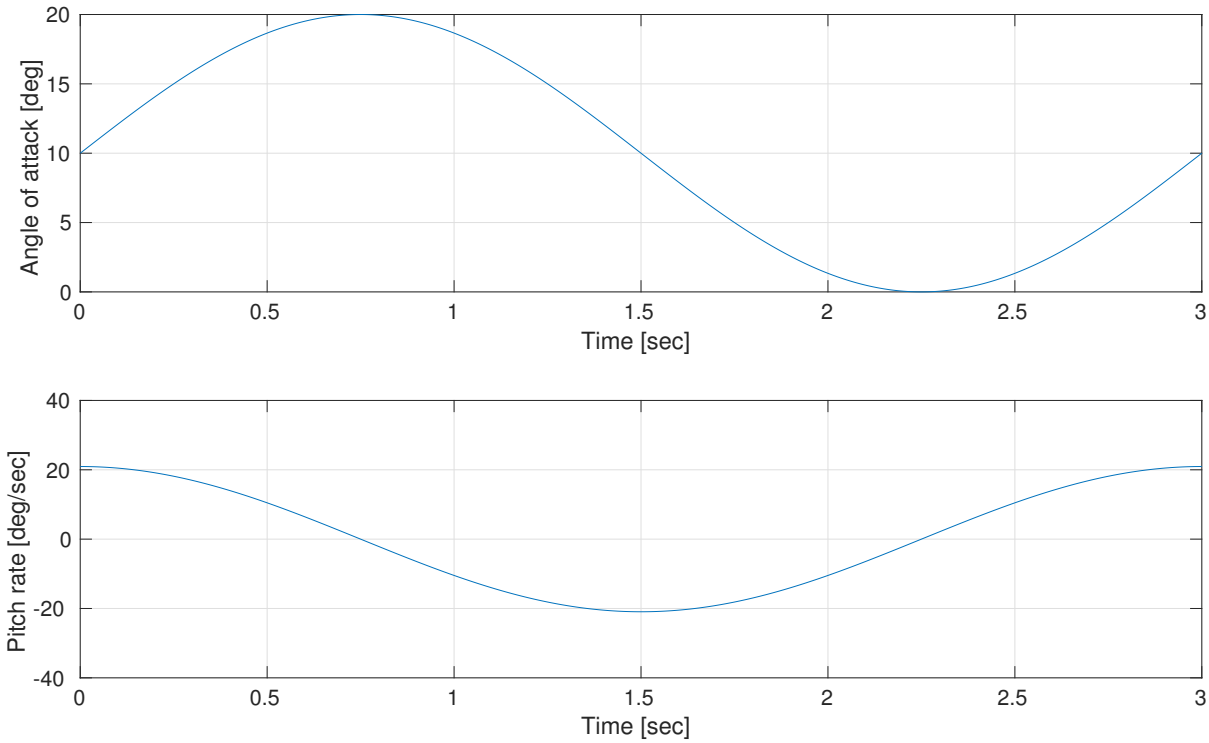

Figure 4.17: Longitudinal flight parameters of a one period pitching oscillation motion for the 3D MULDICON testcase of the frequency encountered in the take-of design point

First take a look at fig. 4.18 where the results for the normal force coefficient are depicted as well as the individual effects of the angle of attack and pitch rate on the load. The full-order CFD solution clearly shows a hysteresis loop due to the nature of the pitching motion. However, as the maximum pitch rate is only 20 [deg/sec], the unsteady effects in flow behaviour are not as apparent. Nevertheless, unsteady effects are still present as the solution differs from the steady calculations. Using the 11 calculated indicial functions a ROM was built which can also be seen in the figure. It clearly shows that at higher angles of attack this ROM differs from the actual unsteady flow behaviour. The normal force load prediction is too high. This means that the indicial functions calculated at higher angles of attack, which needed more time to settle at a steady state solution, are not representative samples of the flow behaviour at highly non-linear regions. This might be explained in a flow physics perspective. Consider a steady RANS flow field solution at an angle of attack of 20 degrees in the current testcase. At this point, unstable and highly unsteady vortices are present. When this flow field is disturbed by a sudden increase of one degree angle of attack the suction peak increases significantly and can cause the vortices to break down, resulting in a sudden drop in lift. This is exactly the behaviour seen in the indicial function calculated in fig. 4.14. In contrast, the full-order CFD motion oscillates at a relatively low frequency. This results in the vortices staying attached to the configuration during the motion. However,

at lower angles of attack the ROM does correspond with the full-order model. This means that the dataset can be considered accurate up to roughly 15 degrees angle of attack, but afterwards the flow physics and unsteady behaviour is not correctly captured within the indicial functions. The step size of the samples have changed the flow behaviour of the full-order model. Similar discrepancies and results can be drawn from the other two loads which are added in appendix F.

These observations are merely done for one motion at one frequency. Therefore the strength of the drawn conclusions on the dataset and the ability of the indicial functions to correctly sample flow physics at highly unsteady flow can be arguable. In order to add strength to the statements made, the research using the same dataset is continued in the next part. A take-off manoeuvre is defined where the indicial functions and corresponding ROMs shall be used to asses load prediction accuracy and computational time, taking into account previous findings on steady and unsteady flow behaviour from zero to 20 degrees angle of attack.

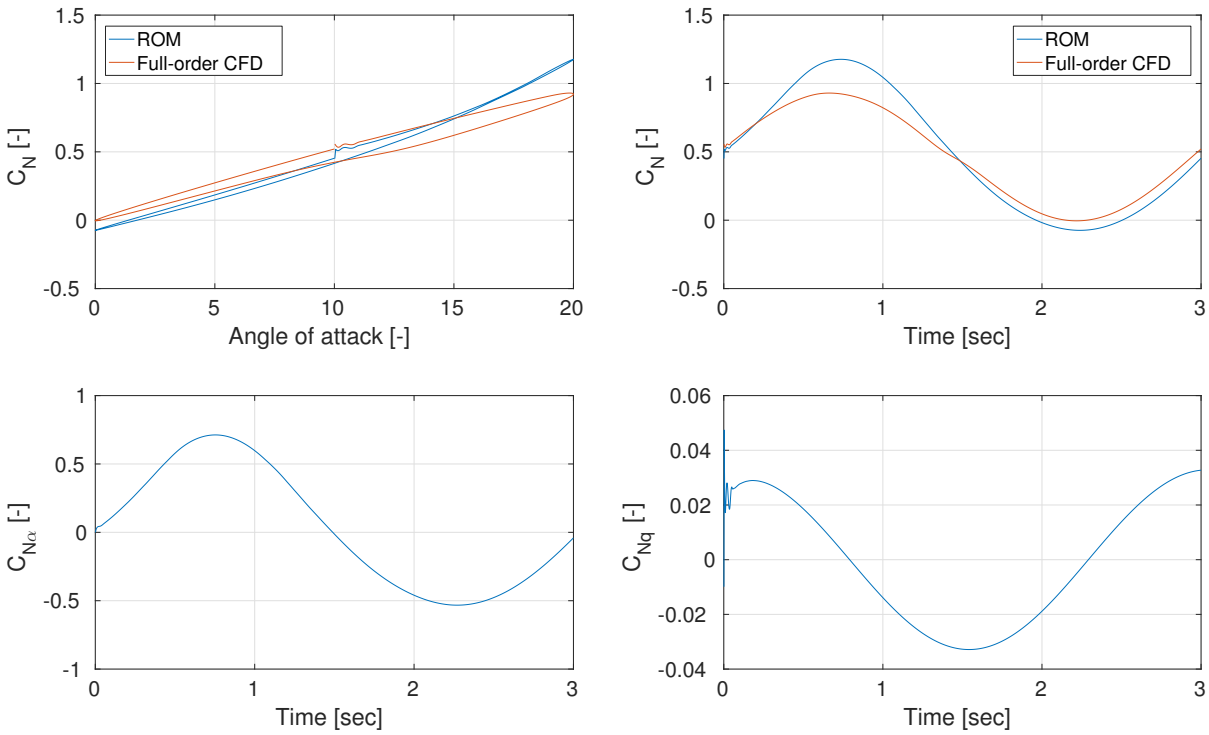

Figure 4.18: Comparison between the full-order CFD URANS and the ROM normal force coefficient solutions undergoing a pitching oscillation at a pitch rate of 20 [deg/second], Mach of 0.2 and a Reynolds number of 28 million, also showing the two individual contributions of angle of attack $C_{N\alpha}$ and pitch rate C_{Nq}

4.4. Flight dynamics predictions

Having a testcase, design point, manoeuvre, assumptions and knowing how the steady and unsteady flow behaves in the design limits a detailed manoeuvre can be created. A take-off manoeuvre at steady Mach number of 0.2 undergoing a pitch rate of 20 degrees per second was specified. First off, based on these requirements, a basic back-off the envelope manoeuvre can be specified using the following straightforward calculations.

4.4.1. Requirements

The manoeuvre should start at a straight and level steady flight (lift equals weight) and preferably end up in the same state. Having a Maximum Take-Off Mass (MTOM) of 15,000 [kg] at take-off and by assuming this to be constant during the manoeuvre, the required lift coefficient can be calculated by:

$$C_L = \frac{mg}{\frac{1}{2}\rho V^2 S} \tag{4.1}$$

Based on the design point requirements in table 4.2 and assuming a constant speed of Mach 0.2 this results in a required lift coefficient of 0.67. Looking at the steady data in fig. 4.3 this corresponds to an angle of attack of roughly 15 degrees. The assumption of constant speed and mass have a significant impact of the reality of a take-off manoeuvre. However, as this research will assess the validity of the ROMs, the reality of the manoeuvre itself will not be as important. Besides, these assumptions will lower the complexity of the ROM analysis as the full-order model aerodynamic load predictions will be based on the same manoeuvre. To investigate a relatively large take-off climb manoeuvre it is assumed that the take-off reaches a climb angle of 45 degree after rotation. The climb angle, together with the gravitational force (weight) of the aircraft and assuming the climb is straight at this point, results in a lift coefficient of 0.94. From the steady RANS data this corresponds to an angle of attack of roughly 22 degrees the manoeuvre should reach. This corresponds to a pitch attitude of 67 degrees. Knowing that the manoeuvre starts from a straight and level steady flight at 15 degrees angle of attack (= pitch attitude) while under a constant pitch rate of 20 degrees per second, this gives the basic take-off manoeuvre visualised in fig. 4.19. Note that the maximum load factor, being the design lift over weight ratio, reaches a value of 1.4 at the 45 degree climb line. This is within the specified limit load factor of 1.5.

This forms the basic manoeuvre of the aircraft which takes into account linear and non-linear regions of the flight parameters as well as steady and highly unsteady flow behaviour. By comparing a ROM, based on the calculated dataset, to the full-order URANS of this motion, a statement can be made regarding the limitations and capabilities of ROMs based on indicial response functions. However, as the flight path is forced into the ENSOLV CFD solver (by describing what the flight parameters are at each time step) the results will not show whether this manoeuvre is actually performed. This is due to the fact that the predicted loads are dependent on the flight path and the other way around. Besides, this manoeuvre is calculated based on steady solutions not taking into account possible unsteady effects. Lastly, the pitch rate and history of flight parameters are instant in the current manoeuvre. This will enforce a large flow disturbance in the RANS equation ensuring either inaccurate results or large computational effort when solving for the unsteady RANS.

To achieve a more realistic manoeuvre it is chosen to describe this take-off by using a simple flight dynamics model, based on conventional stability derivatives. This ensure that a more valid comparison can be made between conventional and ROM based flight dynamics predictions, as it will show the effects of taking into account unsteadiness during flight path and aerodynamic loads predictions. The calculated back-off-the-envelope manoeuvre will be used to empathise the ability of ROMs to represent unsteadiness in the flow during the final validation in section 4.4.4.

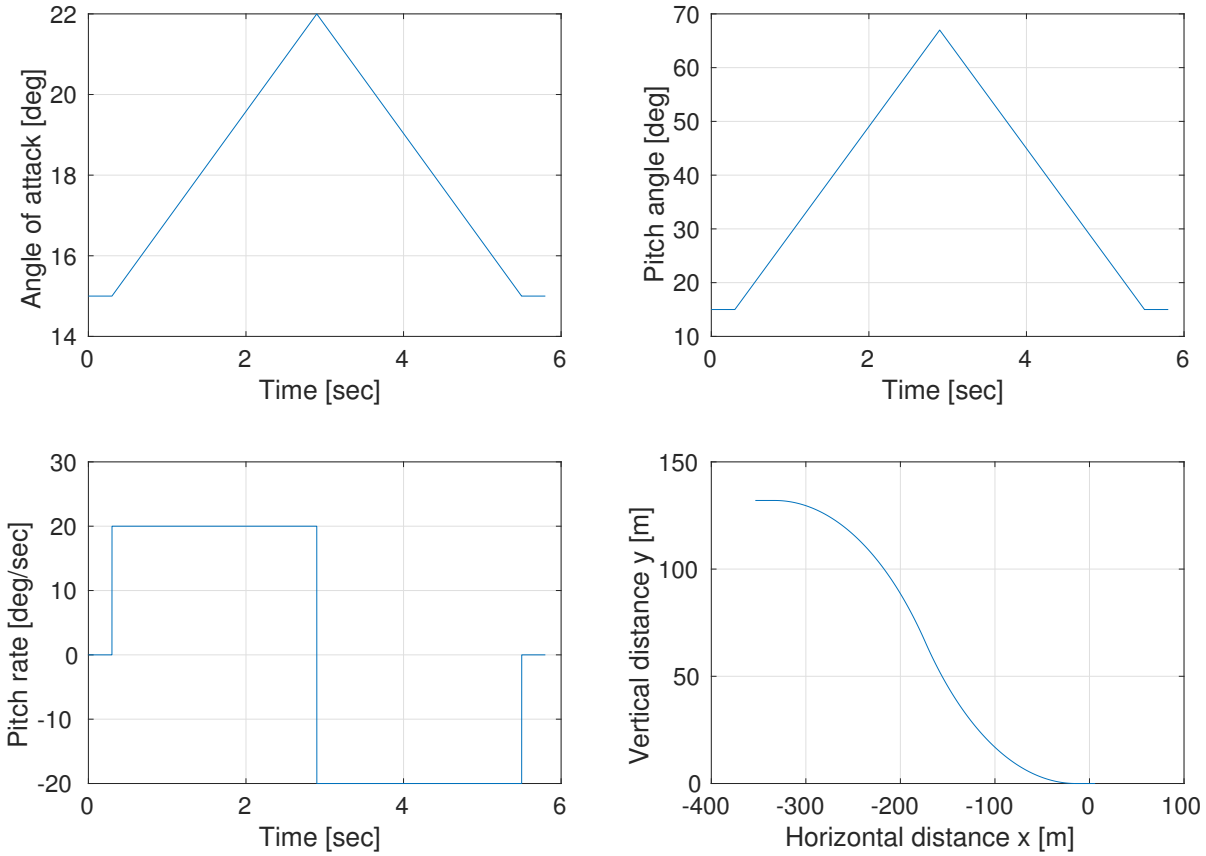

Figure 4.19: Basic take-off having a constant mass and constant Mach number of 0.2 describing the requirements the manoeuvre should adhere to

4.4.2. Model

Conventionally, a flight dynamics model couples the aerodynamic flight loads and flight path parameters. Depending on the input given on the control surfaces the path and loads are iteratively calculated, resulting in a manoeuvre. Actuators, feedback controllers and flight control systems can be added to manipulate the output manoeuvre and influence the stability and controllability of the aircraft. Conventionally, look-up tables based on the steady-state data are used to couple the loads with the flight path. A problem occurs when unsteady effects become dominant, as the look-up tables are instantaneous values at a pre-described number of flight conditions. By building a relatively straightforward model based on the equations of motion given in section 2.2.2 the limitations of basic look-up tables in this testcase becomes clear. A flight dynamics model will be created such that it fits the requirements specified for the manoeuvre. Using the knowledge gained in ROM building, the indicial response functions are integrated within the model to investigate whether the addition of unsteady effects improves it. By doing this, the capabilities and limitations of ROM building based on indicial response functions will become more clear as more results are gathered to eventually answer the main research question. What follows is a quick description of the flight dynamics model and the output of the manoeuvre using conventional flight behaviour coupling (look-up tables based on steady state data).

Implementation

The flight dynamics model is built in SIMULINK and a flow diagram implementing the equations of motion is seen in fig. 4.20. The complete equations of motion are already given in section 2.2.2. Under the assumptions of the manoeuvre, the three rigid body equations of motion given in eq. (4.2) to eq. (4.4) are implemented in the model, which works as follows:

1. An input is given to the elevator deflection.

2. The flight parameter states and the elevator control deflection δ_e are initiated. This deflection only affects the pitching moment and not the normal and axial forces. This has a significant impact on the reflection on reality, as the deflection will obvious affect the two loads. However, by making this assumption the need for iterations on the flight dynamics, in order to create a take-off manoeuvre, is removed. The elevator deflection is chosen such that a take-off manoeuvre occurs, thereby neglecting stability and control issues. This can be added in the future, but for now this will reduce complexity of the model, while still coupling the two other loads with the flight path manoeuvre.

3. The gravitational forces in x and z directions are calculated based on the pitch rate (eq. (2.8)). The current angle of attack and pitch rate correspond to a certain normal and axial coefficient based on the steady state plots. These values are used to estimate the aerodynamic forces in the current time step. In order to minimise complexity it is chosen that the pitching moment is based on the elevator deflection only, in such a way that the take-off manoeuvre at a pitch rate of 20 degrees per second is utilised. A 'thrust' value is added to the aerodynamic forces to keep the velocity acceleration in x-direction ($\dot{u}$) zero. This makes sure that the total velocity of the manoeuvre stays relatively constant, minimising possible Mach effect when applying the ROM method.

4. Based on the calculated forces and moments, the velocity acceleration in x direction (u) and z direction (w) as well as the pitch rate acceleration are calculated (eq. (2.10)).

5. The velocity components expressed in the body system and the pitch rate acceleration are integrated and fed back in the loop.

6. Based on the flight parameters and velocity components a manoeuvre is described in terms of x and z values.

Details of the SIMULINK model are added in appendix G. The resulting manoeuvre is visualised in fig. 4.21.

$$-mgsin(\theta) + \mathbf{X^b_{aero}} = m(\dot{u}^b + qw^b) \tag{4.2}$$

$$mgcos(\theta) + \mathbf{Z^b_{aero}} = m(\dot{w}^b - qu^b) \tag{4.3}$$

$$\mathbf{M^b} = I_{yy}\dot{q} \tag{4.4}$$

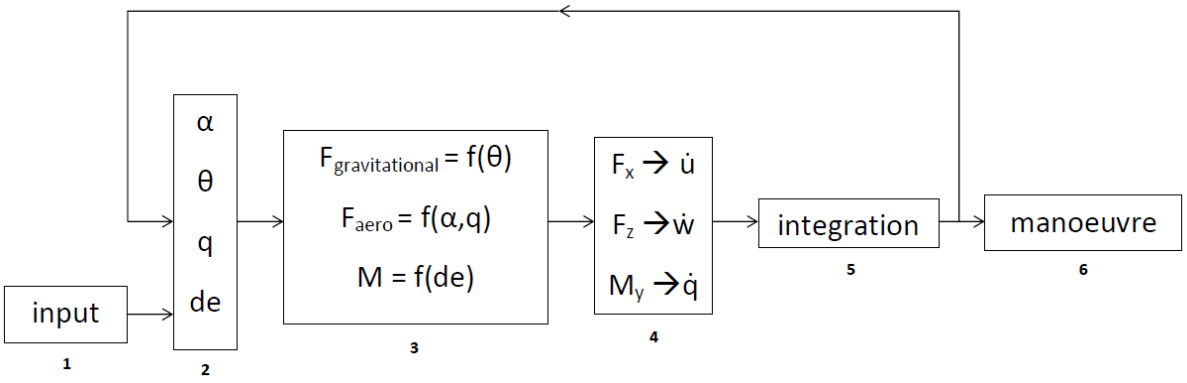

Figure 4.20: Flow diagram showing the implementation of the three rigid body equations of motion in a (non-linear) flight dynamics model utilised using SIMULINK

MANOEUVRE

As mentioned before, the elevator deflection has a direct effect on the pitching moment coefficient in the model. This makes sure that the pitch rate accelerates towards a pitch rate of 20 degrees per second, initiating the climb, and after 2 seconds starts pitching down ensuring the manoeuvre ends in the same flow condition, but at a higher altitude. Starting from a straight and level steady flight at 10 degrees angle of attack, this increases towards roughly 20 degrees and afterwards lowers to roughly 3 degrees as the aircraft pitches down again. To achieve this manoeuvre, the mass and moment of inertia had to be changed. These might not be representative, but are not unrealistic for the configuration. This ensures the range of interest for both flight parameter effects (angle of attack and pitch rate) conforms to the set of requirements in section 4.4.1. To ensure a constant velocity of Mach = 0.2 during the manoeuvre, the acceleration in x-direction of the aircraft should be zero. In reality this means that the engine will behave unrealistically, but it ensures that the total velocity during the manoeuvre stays relatively constant, minimising Mach effects when the ROM is built. Due to the varying loads during the manoeuvre the load factor in z-direction, being lift over weight, varies as well. Due to the nature of the climb-manoeuvre path and the aerodynamic forces predicted, the maximum load factor of 1.5, as specified at the design point, is exceeded.

In general, the manoeuvre seems to have a take-off nature (ignoring certain assumptions made regarding thrust and mass). However, as mentioned before the aerodynamic forces are based on values taken from the steady states. These are the so called conventional stability derivatives and are by definition instantaneous values of the pitch rate and angle of attack effects on the three loads. These values are gathered by taking the final value of the indicial response functions and are summarised in table 4.4. Having a path description for this manoeuvre a ROM can be built to calculate the loads, taking into account unsteady effects. The results on this are described next.

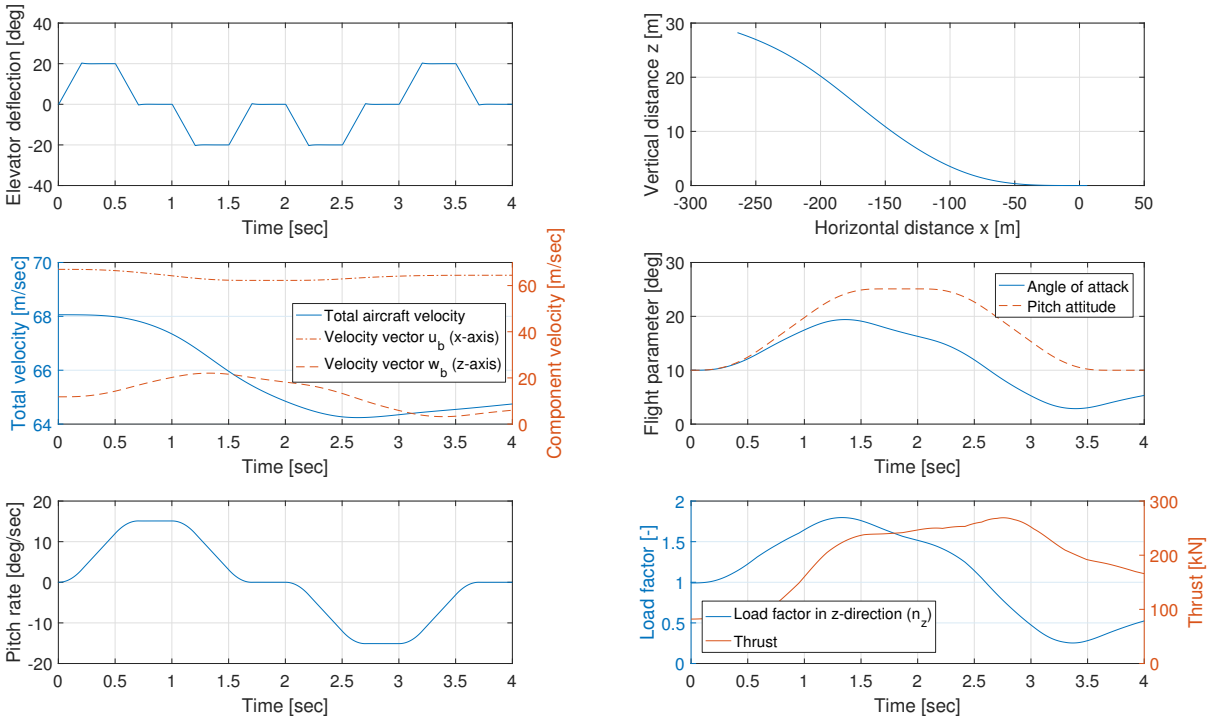

Figure 4.21: Results of the take-off manoeuvre based on the steady state data (conventional stability derivatives) by manually describing the pitch rate based on the elevator deflection and keeping the total velocity quasi-constant by adding thrust

Table 4.4: Conventional stability derivatives used in the first take-off manoeuvre creation based on the final value of the URANS calculated indical step response functions

Angle of attack	**static [1/rad]**		**dynamic [sec/rad]**	
	C_{X_α}	C_{Z_α}	C_{X_q}	C_{Z_q}
1	0.384	2.269	0.020	0.083
3	0.040	2.668	0.020	0.083
5	-0.083	2.735	0.020	0.083
7	-0.169	2.752	0.020	0.083
9	-0.241	2.751	0.020	0.083
11	-0.297	2.744	0.020	0.083
13	-0.333	2.713	0.020	0.083
15	-0.341	2.633	0.020	0.083
17	-0.324	2.574	0.020	0.083
19	-0.294	2.588	0.020	0.083
21	-0.275	2.610	0.020	0.083

4.4.3. Results

In the same manner as before a ROM is built based on the calculated indicial functions within the dataset. For sake of consistency these samples are the original 11 indicial step response functions. As concluded before, the accuracy of the higher angles of attack functions is debatable, but the lower ones are verified to include the correct unsteady flow behaviour of the full-order model. The goal of this manoeuvre analysis was to asses whether the ROM can accurately predict unsteady aerodynamics loads, specifically compared to the use of conventional ROM modelling based on instantaneous stability derivatives. Therefore, first the predicted loads based on stability derivatives will be compared to the prediction of a ROM based on the indicial functions. Later on, in section 4.4.4, the method will be validated against the full-order URANS calculations.

AERODYNAMIC LOADS PREDICTION COMPARISON

The resulting ROM compared to the conventional flight dynamics model predicted loads are seen in fig. 4.22.

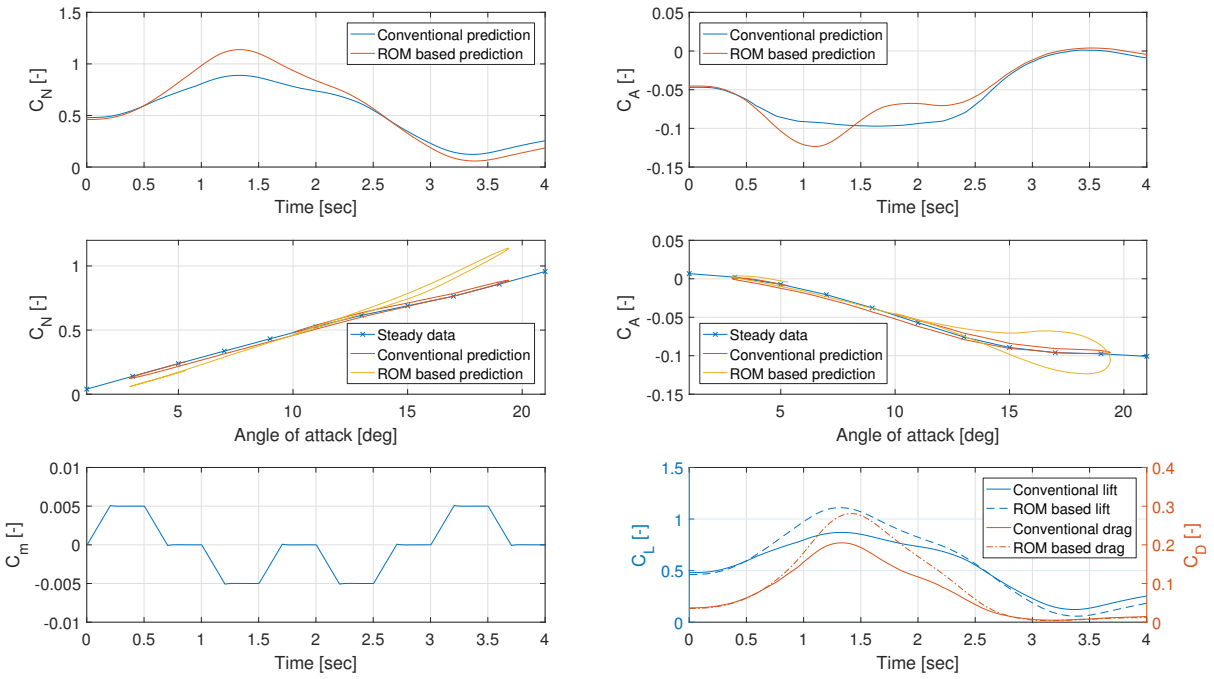

Figure 4.22: Flight loads prediction based on conventional use of stability derivatives compared to using a ROM of the take-off manoeuvre

Comparison between the two results clearly shows that the ROM based prediction, which takes into account unsteady effects, predict higher loads as is expected for this manoeuvre. However, from the unsteady flow behaviour in fig. 4.17 it was also stated that the a ROM built using the same dataset under similar flight conditions is less accurate at higher angles of attack as the flow samples are affecting the full-order model flow behaviour. Based on the results it can be seen that the ROM predicts a bigger normal force from 0.5 up to 2.5 seconds. When looking at fig. 4.21 this corresponds with the manoeuvre being at roughly 12 degrees angle of attack. At this point vortices begin to form, but it was concluded that the used indicial functions become inaccurate in flow sampling around 15 degrees. This means that the ROM based load prediction is indeed taking into account unsteady flow behaviour, resulting at higher lift prediction when vortices begin to form resulting in vortex lift. This means that, while the ROM predicted loads during the manoeuvre are inaccurate for high angles of attack from 15 degrees onward, unsteady effects are taken into account for lower angles of attack, leading to more accurate load predictions. This shows the benefits of using indicial functions over conventional stability derivatives for this testcase. The results in optimising the flight path by using the ROM predicted loads instead of the stability derivatives are described in the next part.

Flight path prediction comparisons

The ROM load predictions are used to iterate to a new flight path, similar to the style used in fig. 4.21. The results, compared to the first iteration are given in fig. 4.23. Important observations are that the pitch rate and attitude behaviour are still the same as in the first iterations as this is basically pre-described to ensure the climbing nature of the manoeuvre. However, it can be seen that the ROM based flight path reaches a higher flight altitude at a lower reached angle of attack, at a lower total velocity and higher load factor. This is logical as the ROMs take into account unsteady effects which results in a more accurate representation of vortex lift prediction at higher angles of attack. This results in a higher lift at the same angles of attack. This also means that the load factor becomes much higher as the nature of the take-off manoeuvre is not changed. It shows that it is critical to take into account unsteady effects when analysing aircraft performing fast manoeuvres at higher angles of attack where unsteady flow behaviour becomes dominant. When conventional flight analysis methods, such as the stability derivatives, are used to design an aircraft it can now be said that the actual flight behaviour in this manoeuvre will exceed design limits. Load prediction using indicial response functions will help in identifying issues early on in the design as it will take into account unsteady effects. The ROM accuracy based on the indicial functions will be discussed in more detail in section 4.4.5, but first some notes on results validation with respect to the complete full-order model will be given in the next part.

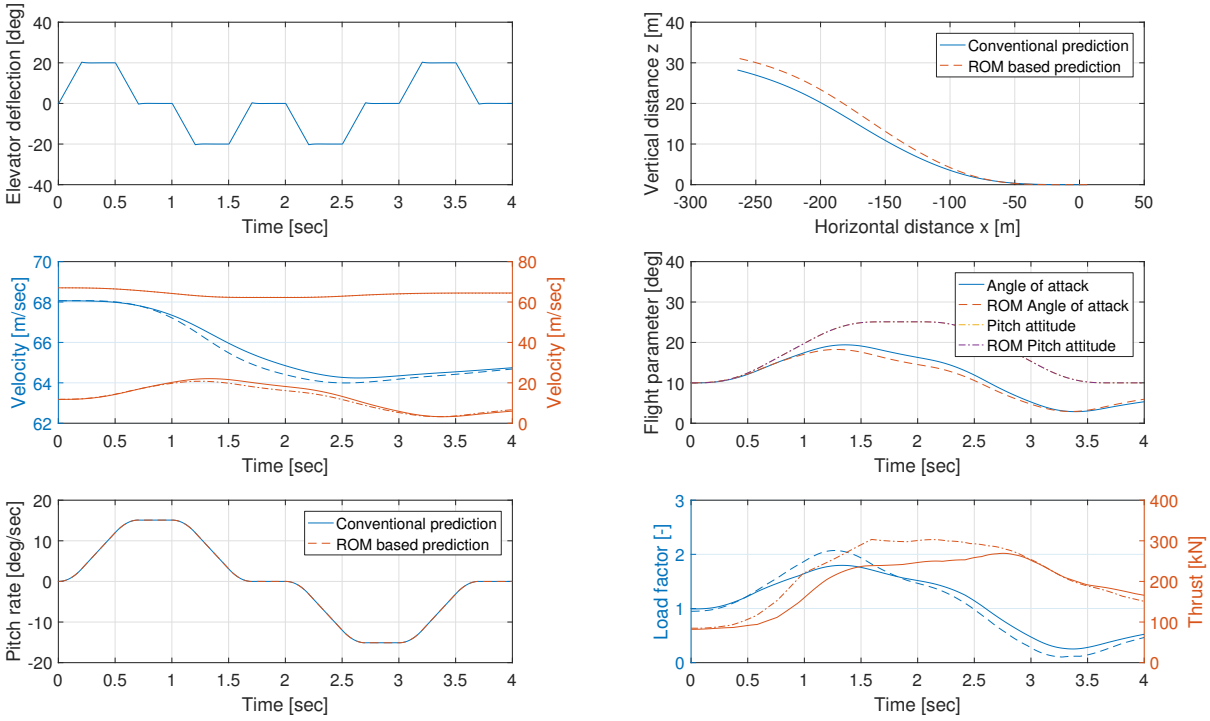

Figure 4.23: Results of the take-off manoeuvre based on the steady state data (conventional stability derivatives) compared to the flight path based on the ROM predicted loads by manually describing the pitch rate based on the elevator deflection and keeping the total velocity quasi-constant by adding thrust

4.4.4. VALIDATION

The ROM method based on indicial response step functions proved to take into account unsteady effects. This is not taken into account by flight dynamics predictions based on conventional stability derivatives. Therefore, differences were observed between the two flight dynamics predictions. However, to investigate whether it is needed to take into account unsteady effects and whether the ROM is an accurate representation of the actual flow behaviour, a full-order time-marching URANS calculation is needed for validation purposes. The results of this, compared to the ROM prediction of aerodynamics loads during the manoeuvre, are seen in fig. 4.24. The comparisons for the other two loads are added in appendix H.

There exist clear differences between the solutions. First of all, the full-order CFD clearly shows a hysteresis loop. This implies that the instantaneous stability derivatives, conventionally used for flight dynamics prediction, are not able to accurately predict the aerodynamic loads of the design undergoing this manoeuvre. This adds strength to the relevance of this research. The ROM does show a loop, but the predictions are far from the full-order data, especially at higher angles of attack. This was as expected, based on the observations made in previous part. The indicial step response functions used are not representative samples of the full-order models at higher angles of attack from 15 degrees onwards. However, in the lower angles of attack regions, the datasets find better agreement. Discrepancies are still present due to the conclusions found in Chapter 3 in sampling space. This means that the investigated ROM method could improve flight dynamics prediction compared to the use of stability derivatives for this test case when better sampling of the full-order model is used.

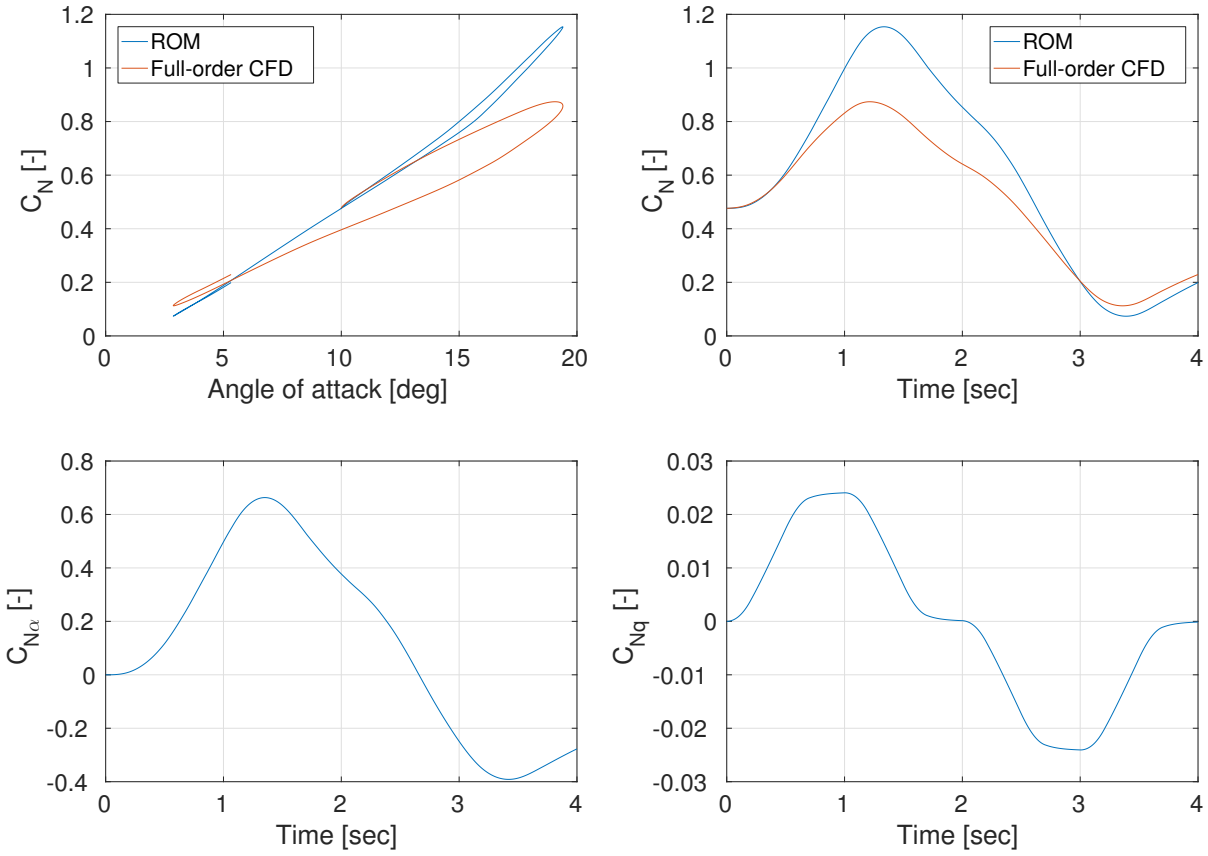

Figure 4.24: Comparison between the full-order CFD URANS and the ROM normal force coefficient solutions undergoing the climbing manoeuvre as predicted by the flight dynamics model for validation purposes, also showing the two individual contributions of angle of attack $C_{N\alpha}$ and pitch rate C_{Nq}

To emphasise on the ability of ROMs to accurately predict flight dynamics, also a validation on the back-of-the-envelope manoeuvre calculations was made. The ROM and full-order CFD results are compared in fig. 4.25. Again, the validation results for the other two loads are given in appendix H. Due to the sudden change in pitch rate, suction peaks are added during the motion. This clearly shows from the results. Again, the datasets find good agreement at lower angles of attack, but are off at higher angles of attack. However, the flow behaviour is relatively similar, empathising that unsteady behaviour is taken into account. This means that the accuracy of the ROM method based on indicial step response functions in predicting flight dynamics is based on the accuracy in full-order model sampling. More details as well as the answer to the main question and sub-questions is found in chapter 5. The research on this test case will close off with some final results on the computational efficiency of the method. This now follows in the next part.

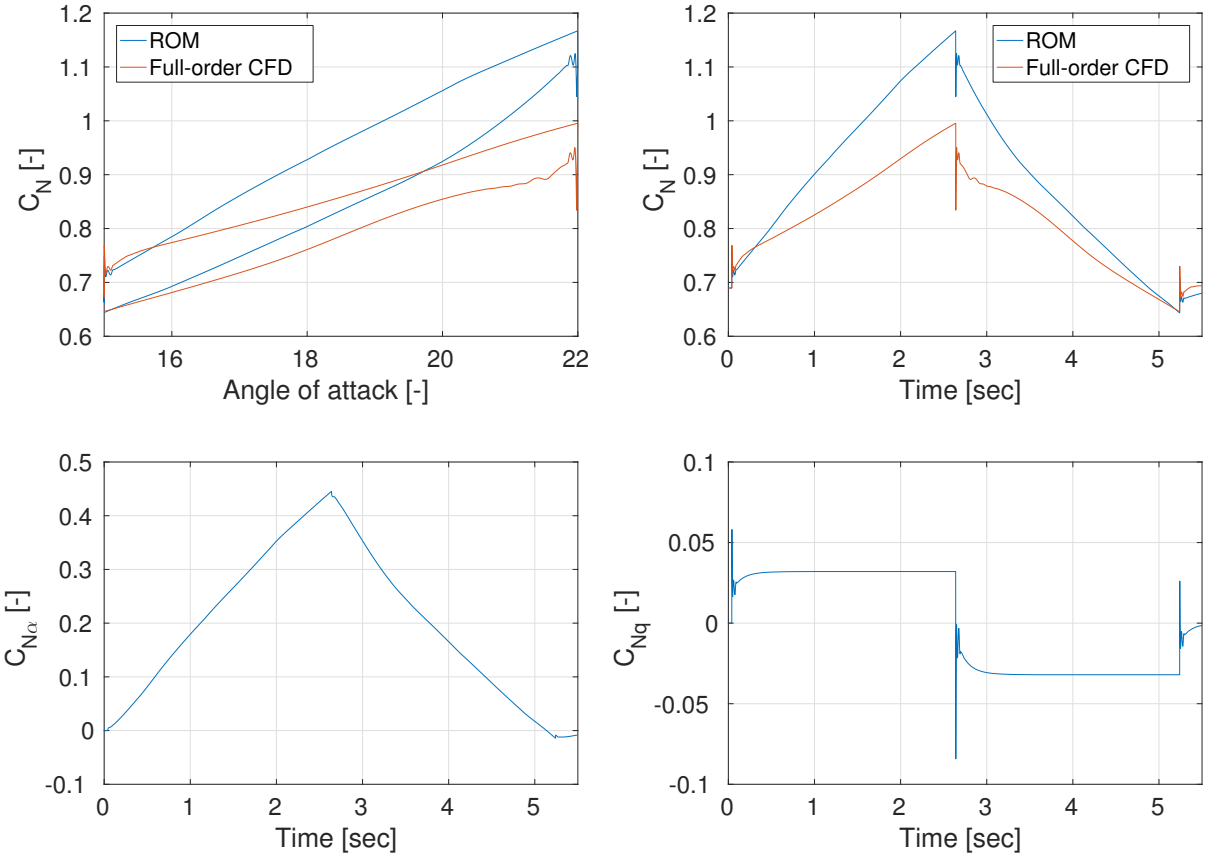

Figure 4.25: Comparison between the full-order CFD URANS and the ROM normal force coefficient solutions undergoing the back-of-the-envelope manoeuvre for validation purposes, also showing the two individual contributions of angle of attack $C_{N\alpha}$ and pitch rate C_{Nq}

4.4.5. COMPUTATIONAL EFFICIENCY

So far only the ROM accuracy has been mentioned while nothing has been stated regarding the computational effort required to create the results. A summary of the calculation times required is given in table 4.5 while more details can be found in appendix I.

Before any research could be conducted a ROM dataset containing the indicial functions had to be set-up. To cover the flight conditions of interest and take into account unsteady effects 11 indicial functions, starting from 10 steady state flow solutions, were calculated. On average this took 70 hours per function, while the ROMs could be created within minutes based on a script performing the ROM building method detailed in section 2.4.5 and provided in appendix A. An investigation continuing the steady flow behaviour resulted in a full-order URANS pitching motion flow calculation taking 220 hours.

A flight dynamics model was developed using the conventional stability derivatives. These derivates where taken from the final values of the indicial functions, meaning the whole ROM setup time was needed to fill in the conventional look-up tables. The same flight path was iterated, now using the complete indicial response functions. This takes the same amount of computational effort, but now unsteady effects are taken into account. Meaning that it is more computational efficient in terms of flow accuracy versus computational effort to use indicial response functions instead of stability derivatives when building a ROM to predict flight loads. Besides, validation showed that conventional flight prediction methods are not even able to accurately predict aerodynamics loads, whereas the ROMs based on indicial functions might.

This validation full-order manoeuvre has been created in order to accurately investigate how the actual flow behaves. The take-off manoeuvre, approximated by the ROM, took 235 hours to solve. The ROM itself took 840 hours to setup, with the ROM itself being created within minutes. At this point it is not computational efficient to setup a ROM and approximate the loads. However, one can imagine that multiple manoeuvres needs analysing during an aircraft design iterations. At this point it becomes a trade-off between indicial functions taken into account and accuracy wanted in the manoeuvre. Even after performing a similar manoeuvre which covers the same flight conditions it becomes computational efficient to set-up a ROM. This means that a ROM based on indicial response functions can be used to discretise flow behaviour and approximate the full-order model. One can even interpolate new indicial functions, as unsteady behaviour seems similar in-between flight parameter ranges. This is being done using so called surrogate modelling, but more on that is given on future research proposals in section 5.4.2. Combining the result of the first NACA testcase and this second MULDICON testcase an answer can be given to the research question(s). This follows in the last chapter.

Table 4.5: Summary of relevant computational effort for the MULDICON testcase calculations made in NLR's CFD solver ENSOLV [95], more details are added in table I.1

Calculation specification	*CPU effort [h]*	*Notes*
Setup		
One indicial function	70	Average based on calculated indicial functions
ROM setup	840	10 steady state RANS + 11 URANS indicial functions
ROM per load	few minutes	
Flow investigation		
Full-order pitching motion	220	Accurate converged URANS starting at 10 [deg] AoA
Manoeuvre optimisation		
Back-of-the-envelope manoeuvre	> 235	URANS to emphasise on unsteadiness
Conventional ROM	840	Flight flight dynamics Model using stability derivatives
ROM based on indicial functions	840	Flight flight dynamics Model using indicial responses
Full-order model manoeuvre	235	URANS to show accuracy of indicial functions
Expected		
New manoeuvres based on ROM	few minutes	Based on samples from full-order model
New manoeuvres full-order model	~250	Each URANS starts anew

5

CONCLUSIONS

The research conducted in the two test cases provide enough data to answer the main research question and thereby conclude the project. Following an extensive literature research on the topic described in chapter 2 this question has formed the research described within this report and was:

How can Reduced-Order Modelling based on indicial step response functions improve flight dynamics prediction?

As was suspected when this question was formed, one does not simple stumble upon an answer. Three sub-questions and two test cases have formed the main research of this project. Therefore, this chapter will first provide answers to the three sub questions before concluding this research and answer the main research question. The challenges found in load prediction are addressed in section 5.1. The investigated capabilities and limitations of ROM building based on indicial step response functions are described in section 5.2. Finally, in section 5.3, the conclusions on the comparison between conventional reduced-order modelling and the method investigated in this project will be given. By combining the answers, a final statement is made regarding the main research question which will close this project. Future research recommendations are written down in section 5.4.

5.1. LOAD PREDICTION CHALLENGES

One of the main challenges to overcome in modelling aerodynamic loads for next generation aircraft is to accurately estimate the aircraft flight dynamics at a reasonable computational effort. In practise, design of new aircraft is limited by a budget. It is therefore of high importance to select the right analysis methods in predicting how the aircraft will behave in real flight and whether it meets the design requirements. Especially for agile aircraft undergoing rapid manoeuvres. The challenges found in load prediction during the research will become clear when answering the first sub-question:

What are the requirements in modelling aerodynamic loads for agile aircraft undergoing rapid manoeuvres?

The research performed on the NACA0012 profile showed that a simple longitudinal manoeuvre at constant Mach number already forms a flow hysteresis loop due to unsteady aerodynamics (As the angle of attack is changed, the disturbance at the leading edge of the airfoil flows downstream). The full-order model URANS calculation was validated with experimental data confirming this unsteady flow behaviour. The motion was also performed at different frequencies, resulting in different load paths at the same angle of attack range, but different pitch rate. Conventional stability derivatives are not able to accurately predict the load as they do not take into account the frequency dependency whereas full-order URANS calculations were able to do this. In order to investigate whether a ROM can represent this flow behaviour several indicial step response functions were calculated. Multiple step responses were used to model the non-linear load behaviour over the angle of attack range, whereas one function was used to assume linear load behaviour over a changing pitch rate in accordance with literature. These assumptions resulted in a relatively accurate ROM of the three longitudinal loads, the normal and axial (or lift and drag) force and pitching moment (coefficients). Conclusions on the validity of this assumption are needed to answer the next sub-question in section 5.2. This showed that for the 2D NACA airfoil in subsonic flow testcase it is sufficient enough to assume the longitudinal loads to be dependent on a non-linear angle of attack and linear pitch rate effect in a relative rapid motion having weak non-linearities.

To continue the research, a more complex flow of the MULDICON baseline design was investigated. A steady aerodynamic loads analysis at roughly 12 degrees angle of attack showed that leading edge vortices began to form, which stay attached to the surface, resulting in a sudden increase in lift and drag. This also meant more convergence issues were encountered at higher angles of attack, when finding accurate solutions for the steady-state flow conditions. To investigate this flow in more detail an unsteady RANS calculation was performed by invoking a simple pitch oscillation motion on the aircraft as was done with to the first testcase. Also in this testcase a clear hysteresis loop was formed which is hard to approximate using conventional stability derivatives. An accurate flow solution and thereby load prediction for the unsteady flow behaviour was found using a full-order time-marching URANS calculation, but took a relatively long time due to the unsteadiness and non-linearity involved. As was clear from the NACA research, the first part of the flight dynamics, up to an angle of attack of 12 degrees, can be predicted with a ROM. Challenges arise when more unsteadiness and non-linearity dominates the flow, opening up the discussion whether steady RANS predictions are an accurate representation of the actual flow behaviour as a steady-state flow condition might not be reached. This gives rise to the question whether indicial step response functions might provide more accurate information regarding aerodynamic loads prediction when unsteady phenomena are dominant in flight. This involves more detailed research on the limitations and capabilities of the response functions. The conclusions of these abilities are written down in the next section by answering the second sub-question.

5.2. INDICIAL STEP RESPONSE FUNCTION ABILITIES

The accuracy of a ROM is highly dependent on the samples taken from the full-order model. In the case of using indicial step response functions to approximate the aircraft loads over time it is of the essence that these represent flow behaviour accurately. Combining the results from the two test cases an answer can be found for the second sub-question:

What are the limitations of indicial response functions in accurately sampling flow behaviour?

The samples which should accurately represent the full-order model flow behaviour were calculated using the verified grid motion approach. In the first testcase all indicial functions eventually reached a steady-state solution, as expected using classical unsteady aerodynamic fundamentals. As the speed of the NACA airfoil testcase was 0.6 Mach, the investigated range of angles of attack covered flow behaviour up to stall. The functions were able to capture the found weak non-linear flow behaviour accurately as observed from the accuracy in the ROMs. Some small discrepancies were found when a frequency analysis was performed, resulting in extra research on the assumptions made in literature. It was concluded that the pitch rate effect can indeed be assumed linear over time, but shows some non-linearities at higher angles of attack and step sizes where flow starts to separate. Especially the unsteady behaviour changes significantly in these regions. It was assumed that more computational effort will help in calculating accurate samples of the full-order model. As the indicial step response functions are able to capture the unsteady flow behaviour of the full-order model, it is worth investigating whether this can be done in a more computational efficient way. Recommended research on this topic is described in more detail in section 5.4.1. The research also showed that negative indicial step responses are different from their positive counterparts. This means that in theory, flow hysteresis can be predicted, as this flow behaviour results in different load paths at decreasing angles of attack. In order to perform a more detailed research on the ability of the indicial step functions to capture highly unsteady flow and accurately predict flow hysteresis, a more complex flow was analysed in the second testcase.

As with the NACA research, also the second testcase (the MULDICON lambda wing) showed accurate ROM predictions of the aerodynamic loads in the linear regions of motion, based on indicial step response functions to sample full-order model. The samples proved to accurately capture the unsteady behaviour of the full-order model at higher angles of attack, where highly unsteady and non-linear flow was present, but did not accurately represent full-order model flow behaviour. This was validated by comparing results to a full-order time-marching CFD URANS calculation. From steady aerodynamics loads analysis, as well as recent research on the design, it was found that vortices begin to occur at an angle of attack of 12 degrees at low speed (Mach of 0.2). The step magnitude chosen to calculate the indicial effects of angle of attack and pitch rate proved to affect the flow behaviour of the full-order model. A sudden step was induced, destabilising the vortices and lowering sampling accuracy. This means that the indicial step response functions were able to capture the highly unsteady aerodynamics of non-linear flow behaviour. However, more research is needed to obtain accurate sampling of the full-order model at these regions. A solution might be found in using so called training manoeuvres. These are basically smaller full-order model motions which capture the flow behaviour at different frequencies. However, this was beyond the scope of this research and will therefore be discussed as recommended future research in section 5.4.2. Knowing what the capabilities and limitations are of ROM building based on indicial step response function, a comparison can be made to conventional flight dynamics analyses. The conclusions drawn by answering the remaining sub-question concerned with this will be given in the next section.

5.3. ROM ACCURACY AND COMPUTATIONAL EFFICIENCY

In understanding the strength of the method investigated, a comparison can be made to existing techniques in analysing flight dynamics. So far, the first research conducted by answering the first two sub-questions dealt with the comparison of ROMs versus the full-order CFD calculations in terms of forcing a flight path. In an actual flight dynamics prediction the aerodynamic loads are dependent on the flight path and vice versa. As stated in the start of this report, the conventional stability derivative model breaks down completely at rapid manoeuvres, where linearisation of the equations of motion is not representative of the flight dynamics. Indicial step response functions take into account unsteady effects and might be a solution for these type of manoeuvres in flight models. Based on the results from the two test cases the third sub-question can be answered:

When are ROMs based on indicial step response functions more useful than conventional flight dynamics prediction methods in terms of accuracy and computational effort?

Research performed on the first testcase eventually compared the full-order models of a 2D NACA0012 airfoil, undergoing a pitch oscillation, to a ROM. The time-marching URANS calculation took approximately 160 hours. However, setting up the ROM took a significant amount of 1116 CPU hours. At first glance this means that these ROMs are not computationally efficient as they approximate the full-order model at a much higher computational effort. However, as was concluded from the results this ROM building is a trade-off between accuracy wanted and the number of samples calculated. As every sample which contains the same or at least periodic unsteady flow behaviour might be redundant, a surrogate model might be beneficial to use when filling up the remaining sampling space. More on the subject of surrogate modelling is recommended for future research, detailed in section 5.4.2. A benefit of ROMs based on indicial step responses was found when multiple similar manoeuvres need analysing. For example in the case of investigating the flying qualities of an aircraft. The use of a ROMs becomes interesting when this is the case, as the dataset already contains representative samples of the full-order model. This is one of the reasons why conventional methods such as the use of stability derivatives came to existence to approximate the full-order model in flight dynamics models. To implement the ROM method and investigate whether this is more useful than using stability derivatives, a flight dynamics model was developed during the second testcase research.

The second testcase involved the use of a prediction model based on conventional stability derivatives to built a ROM of the aerodynamic loads prediction and flight path. These values were taken as the final values of the indicial step response functions. However, these are instantaneous values, meaning that simple hysteresis loops and rapid manoeuvres are not predicted accurately. This was also seen when performing validation analyses by investigating the full-order time-marching URANS solution. It is more useful to include the complete history of URANS calculation (the indicial step response) in order to incorporate unsteady effects and cope with changes in frequency in the flight dynamics model. It was shown that, even though not the whole dataset was an accurate representation of the full-order model, a flight dynamics model based on indicial functions was more accurate at unsteady and weak non-linear flow behaviour prediction than the conventional method. A take-off manoeuvre was investigated of which the full-order model took roughly 235 hours to calculate. The ROM setup took 840 hours, taking into account some surrogate modelling (using one degree step functions to cover a range of 20 degrees in angle of attack). Based on the NACA research this calculation effort can even be reduced by samples which capture similar of periodic unsteady flow behaviour. Besides, the ROM can be made more accurate by adding more samples, each taking approximately 70 hours to calculate.

In conclusion, this means that ROMs based on indicial response functions can already improve flight dynamics prediction at the most basic level by replacing the instantaneous stability derivatives. This lowers the need for complete time-marching solutions. At unsteady and weak non-linear flow behaviour these functions proved to sample the full-order model correctly, resulting in accurate ROMs at these regions. The step size of the indicial function calculations proved to change the flow behaviour of the full-order model at higher angles of attack. This gave inaccurate results of the ROM compared to the full-order time-marching CFD solution at regions involving vortices and flow separation. More research is needed on the topics of sampling highly non-linear flow behaviour. A discussion on the recommended research on the topic of reduced-order modelling and how indicial step response functions can help in improving flight dynamics predictions will be given in the next part, thereby concluding this project.

5.4. RECOMMENDATIONS

Based on the research performed an answer has been found to the main research question, thereby satisfying the main objective of this project. However, during the project several minor research paths came up as well as possible future research topics. Either due to time restrictions or simply being out of scope these topics were only briefly addressed during the description of the research. This final part of the report will restate those topics and describe them in the form of recommendations for future research.

During the research, the CFD solver ENSOLV has been used. In section 5.4.1 several possible improvements shall be discussed which apply to CFD solving in general. Afterwards, in section 5.4.2, future research on the topic of the discussed ROM method will be described. Surrogate modelling and sampling space will be further elaborated upon. Lastly, in section 5.4.3, the applicability of the ROM method in an actual design process will be described.

5.4.1. CFD FLOW FIELD DISTURBANCE OPTIMISATION

All CFD calculations performed in this research were based on the highest required flow fidelity modelling by solving the Reynolds-Averaged Navier-Stokes (RANS) equations, including an Explicit Algebraic Reynolds Stress Model (EARSM) in K-omega form and a dimensionless wall distance $y+ \approx 1$, to cope with accurate turbulence modelling [34]. During the research on the pitch rate linearity assumption in section 3.5.1 it was stated that a numerical error occurred in the unsteady RANS calculations. This error occurred when a step size of one radian per second on the pitch rate was given on the NACA profile at a constant angle of attack. This error increased as the aircraft was set at a higher angle of attack flow condition. It was also observed that each calculation converged to the same final (stability derivative) value, independent of the starting angle of attack. The assumption was made that this flow behaviour is correct, as this is the objective of the indicial step response function. The URANS calculations, started from a steady RANS solution. Consider this thought experiment. A solution is found for the NACA profile being in a flow condition at zero degrees angle of attack. The pitch rate effect is found by applying a one radian per second step input on the system. In CFD terms this means adding a disturbance to the flow field solution which eventually damps out (the unsteady aerodynamics) to a steady state solution. The CFD solver used is set up in such a way that the step size in time remains constant. Assume that this time-step and the addition of optional sub-iterations per time step are sufficient enough to find an accurate flow field solution at each point in time. Now consider the same profile angled at a one degree angle of attack. The normal force coefficient has a higher value than it had for zero angle of attack, but still needs to attain an equal final value (stability derivative), as found for the previous calculation when performing the pitch rate step input. Assume that the step size and number of sub iterations per time level is still unchanged. The same disturbance is added to the flow, but a larger step in normal force coefficient has to bridged to come to the same final steady-state. This means that the time-step should be taken smaller or the number of sub-iterations increased in order to cope with the bigger change in flow field solution. The CFD solver is set-up in such a way that the step-size as well as the number of sub-iterations remains constant during the whole unsteady RANS calculation. It would be computationally beneficial to decrease the step-size near the beginning of the URANS calculation, increase it near the end and/or change the number of sub-iterations over time. Therefore, a future research topic could be to investigate whether implementing and changing this has an effect on the calculation of the indicial step response functions in terms of load prediction accuracy and computational effort.

5.4.2. Reduced-order modelling of flight loads

The main research question has been set up to fill gaps in found literature as well as continue research on the topic. Even though this question has been answered it is recommended to conduct more research on the topic of reduced-order modelling with a specific interest in flight dynamics prediction.

The main limitation in capturing representative flow behaviour by sampling the full-order model was found near high angles of attack where highly non-linear flow dominates flow behaviour. When flow starts to separate and vortices form it is not trivial to capture an accurate sample of this behaviour and predict flight dynamics. Therefore it might seem more logic to investigate whether indicial step response functions with an increased step size might be able to accurately sample the full-order model. This could be extended to a small indicial response motion in which a possible hysteresis loop might be fully captured at a specific frequency. Due to the nature of the functions this could then be used for a bigger frequency range. Similarities are found with the use of training manoeuvres in unsteady flow prediction. These training manoeuvres are basically bigger flight samples of the aircraft, instead of relatively small flow behaviour samples of the indicial functions [96] [97] [98]. Using a hybrid form of indicial step response functions and training manoeuvres might be an interesting research topic to continue reduced-order modelling. Also, it might be interesting to incorporate the indicial step response functions directly in a flight dynamics model, thereby replacing the instantaneous stability derivative values by the indicial step response functions in look-up tables .

Another topic which came up several times during the research was the use of surrogate modelling. What this implies is that one captures several samples of the full-order model and then sets up a (surrogate) model which can predict the remaining sampling space. This is basically a ROM of the ROM. From the results it could be seen that several calculated indicial step response functions are equal or at least show similar unsteady flow behaviour, in accordance with classical unsteady aerodynamics theory. Therefore, one or two responses near the limits of predictable unsteady flow behaviour might be sufficient to set up a surrogate model which then calculates (inter- and extrapolates) the remaining samples. This would decrease computational effort and potentially increase ROM accuracy, thereby improving computational efficiency of the method. Recommended research would be to investigate whether such a surrogate model could accurately fill in remaining sampling space including more parameters than investigated in this research such as side-slip angle and varying Mach number.

5.4.3. ROM IN AN AERODYNAMIC DESIGN FRAMEWORK

One of the main reasons to use reduced-order modelling is to provide a quicker and as accurate flight dynamics prediction as it would take several full-order model manoeuvre calculations. From the research it can be concluded that it is possible to use higher-fidelity CFD methods (URANS) earlier in the design, where the configuration is more flexible to changes. This has also been researched before, as found in literature. Research by Mason et al. [99] describes the need to use CFD earlier in the design process while looking at it from an Multi-Disciplinary Optimisation (MDO) perspective. This was done by using stability derivatives, which the investigated indicial functions could replace in order to asses flight dynamics of rapid manoeuvres more accurately. The investigated ROM method thus has the capability of addressing the need to bring higher fidelity CFD tools forward in the design process [100]. A question remains is how this method would fit in during an actual (aerodynamic) design process.

It is known that aircraft design can generally be divided in three separate design phases. Conceptual, preliminary and final design. The first stage anticipates on the market, determines the general aircraft configuration and makes first estimates in weight and performance. The preliminary design phase is concerned with more detailed design, ensuring the designed aircraft meets the mission requirements. The final phase calculates final details and fits in subsystems such as control systems and landing gear. At this point, high-fidelity CFD methods are used to predict aircraft flight behaviour. A small overview of the aerodynamic tools, e.g. CFD analysis, in the general design can be seen in fig. 5.1. As is seen from the figure, design of aircraft is a highly iterative process involving a CFD analysis every time the configuration changes. Trade-offs must be made between the accuracy of CFD modelling and maximum computational time in order to finish the design in a certain timespan. After aerodynamic design is done, a bigger loop includes other disciplines such as propulsion and control systems. Due to the high computational time of high-fidelity CFD methods such as the URANS approximations it is often not feasible to simulate every manoeuvre done. This results in aerodynamic issues not found until flight testing [2]. Besides, low-order fidelity CFD methods, such as the Vortex Lattice Method [101], are used to define the general configuration of an aircraft. Once this has been decided it is less flexible to changes in matured design stages. This results in an aircraft shape that might fit the mission needs, but can show unexpected stability and control issues. One method of optimising for aircraft design is found in the area of multi-disciplinary optimisation, where different discipline design tools are re-ordered to ensure more efficient aircraft design. Recommended research would be to investigate how a ROM tool based on indicial step response functions would fit in such a framework. On top of that it would be interesting research to find out how indicial step response functions are affected by changes in the design. This means that the ROM would have a direct impact on the design space and detailed CFD analysis near the end of the design to assess stability and control, would not be needed as the design has already been fit to adhere to the set requirements.

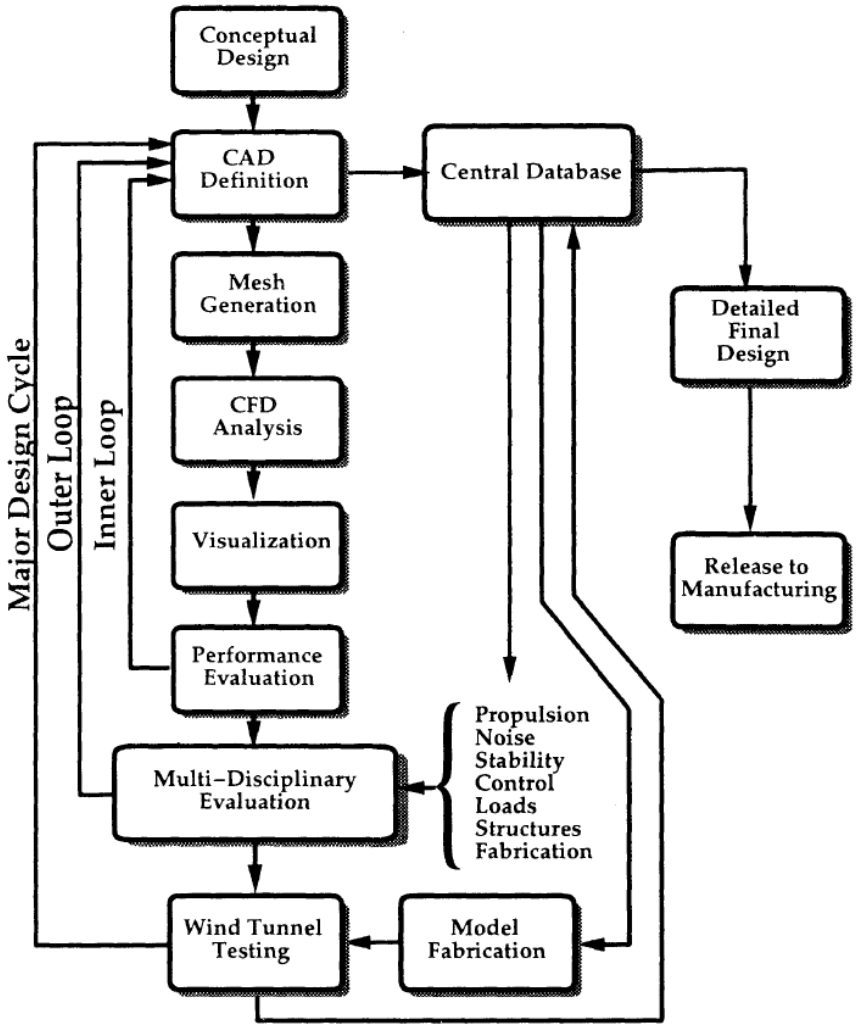

Figure 5.1: Conventional aerodynamic design process [15] by Pradeep Raj

A

ROM BUILDING MATLAB CODE

```
%% -------------------- ROM code -------------------- %%
%  MAIN CODE
%  Optimised for MULDICON baseline design and ENSOLV
%  This code is developed by M.J.M. Ketelaars
%  Based on the scripts by M. Ghoreyshi
%  Tested for MATLAB R2016a
%# ------------------------------------------------- #%

clear all
close all
clc

%% INPUT
% Specify what ROMs are needed, what flight conditions etc.
% motionData in format: [time [sec], aoa [deg], q [deg/s]
% coeffNames gives string array in the 6 loads order
% coeffType specifies of what aerodynamic load a ROM should be built
% indicialEffects specifices what flight parameters affect the chosen
  load
% effectNames specified what the names are of the indicialEffects
% IMPORTANT: AERODYNAMIC LOADS SHOULD BE TAKEN WRT BODY FRAME -> CA
  AND CN

% Constant parameters
mach            =   0.2;        %[-]
speedOfSound    =   340.2980;   %[m/s]
referenceLength =   6;          %[m]

[motionData,coeffNames,coeffType,indicialEffects,effectNames,mach,
  speedOfSound,referenceLength] = ROMInit(mach,speedOfSound,
  referenceLength);

%% READ IN full-order model CFD solution
[CFDData,steadyValue] = CFDReader(coeffType,referenceLength,mach,
  speedOfSound,motionData);

%% INTERMEDIATE MOTION PLOT
figure(1)
```

```
34      subplot(3,1,1)
35          plot(motionData(:,1),motionData(:,2));
36          ylabel('Angle of attack [deg]');
37          grid on
38          xlabel('Time [sec]')
39      subplot(3,1,2)
40          plot(motionData(:,1),rad2deg(motionData(:,3)));
41          ylabel('Pitch rate [deg/sec]');
42          grid on
43          xlabel('Time [sec]')
44      subplot(3,1,3)
45          plot(CFDData(:,1),CFDData(:,2));
46          ylabel('Aerodynamic load coefficient [-]');
47          grid on
48          xlabel('Time [sec]')
49
50  %% READ IN INDICIAL FUNCTIONS
51  % Read in the needed datasets
52  % Correct (inter- and extra-polate) samples to fit against motion data
53  % Store datasets in datastructure 'effects'
54  % Datastructure: effect.aoa.data (parameter,indicialfunctions)
55  [effect] = storeIndicialData(motionData,indicialEffects,effectNames,
      coeffType,mach,speedOfSound,referenceLength);
56
57  %% ROM BUILDING
58  tic
59  [parameterEffects, ROM] = ROMbuilderV3(motionData, effect,
      indicialEffects, steadyValue);
60  toc
61
62  %% Write ROM output file
63
64  %write motion file
65  fid = fopen('muldicon-half-CN.rom', 'w');
66
67  for i=1:length(motionData(:,1))-1
68
69      fprintf(fid, '%12.8f\t', motionData(i,1));          % Time [-]
70      fprintf(fid, '%12.8f\t', motionData(i,2));          %Angle of
          attack [deg]
71      fprintf(fid, '%12.8f\t', motionData(i,3));          %Pitch rate [
          rad/sec]
72      fprintf(fid, '%12.8f\t', parameterEffects(1,i));    %aoa-effect on
            load [-]
73      fprintf(fid, '%12.8f\t', parameterEffects(4,i));    %q-effect on
          load [-]
74      fprintf(fid, '%12.8f\t\n', ROM(i));                       %ROM
          load [-]
75  end
76  fclose('all');
77
78  %% PLOTS
79  figure()
80      subplot(2,2,1)
81          plot(motionData(2:end,2),ROM);
82          hold on
```

```
            if CFDData ~= 0
                plot(motionData(:,2),CFDData(:,2));
            end
        hold off
        grid on
        ylabel('C_N [-]')
        xlabel('Angle of attack [-]')
        legend('ROM', 'Full-order CFD','location','NorthWest')
        xlim([15 22])
        set(gca,'fontsize',20)
    subplot(2,2,2)
        plot(motionData(2:end,1),ROM);
        hold on
            if CFDData ~= 0
                plot(CFDData(:,1),CFDData(:,2));
            end
        hold off
        grid on
        ylabel('C_N [-]')
        xlabel('Time [sec]')
        legend('ROM', 'Full-order CFD','location','NorthEast')
        set(gca,'fontsize',20)
        xlim([0 5.5])
    subplot(2,2,3)
        plot(motionData(2:end,1),parameterEffects(1,:));
        grid on
        ylabel('C_N_{\alpha} [-]')
        xlabel('Time [sec]')
        set(gca,'fontsize',20)
        xlim([0 5.5])
    subplot(2,2,4)
        plot(motionData(2:end,1),parameterEffects(4,:));
        grid on
        ylabel('C_N_q [-]')
        xlabel('Time [sec]')
        set(gca,'fontsize',20)
        xlim([0 5.5])
```

```
%% -------------------- ROM code -------------------- %%
%  FUNCTION TO DEFINE MOTION OF INTEREST
%  Optimised for MULDICON baseline design and ENSOLV
%  This code is developed by M.J.M. Ketelaars
%  Based on the scripts by M. Ghoreyshi
%  Tested for MATLAB R2016a
%# ------------------------------------------------- #%

function [motionData,coeffNames,coeffType,indicialEffects,effectNames,
  mach,speedOfSound,referenceLength] = ROMInit(mach,speedOfSound,
  referenceLength)

%% Manoeuvre selection
% Read in motion data
fprintf('Select motion file [ENSOLV FORMAT]..\n');
[fileName,workFolder] = uigetfile('*.motion');
fileID = strcat(workFolder,fileName);

```

```
motion = dlmread(fileID,'',6,0);

    motionData(:,1) = motion(:,1).*referenceLength/(mach*speedOfSound)
      ; % time history[sec]

pitchAngle = motion(:,6);            % pitch angle[rad]
uSpeed = abs(motion(:,8));           % horizontal speed[-]
wSpeed = abs(motion(:,10));          % vertical speed[-]
climbAngle = atan(wSpeed./uSpeed);   % climb angle[rad]
climbAngle(isnan(climbAngle))=0;     % correct for stationary motions
  [0]
aoa = pitchAngle - climbAngle;       % angle of attack[rad]

    motionData(:,2) = rad2deg(aoa);     % angle of attack history [deg
      ]
    motionData(:,3) = motion(:,12).*mach*speedOfSound/referenceLength;
       %pitch rate history [rad/sec]

    % Remove initialization row at t = 0 from dataset
    if motionData(1,1)==0
        motionData(1,:)=[];
    end

%% Coefficient selection
% select (load) coefficient of interest
coeffNames = {'C_A', 'C_S', 'C_N', 'C_l', 'C_m', 'C_n'};
coeffType = input('Select coefficient:\n 1 - CA\n 2 - CS\n 3 - CN\n 4
  - Cl\n 5 - Cm\n 6 - Cn\n .. ');

    % default case is normal load coefficient
    if isempty(coeffType)==1
        coeffType = 3;
    end

    % link effects to loads in format: [alpha,beta,p,q,r]
    effectNames = {'aoa', 'beta', 'p', 'q', 'r'};

        % In case of longitudinal loads (CA, CN or Cm)
        if coeffType == 1 || coeffType == 3 || coeffType == 5
            % ASSUMPTION: angle of attack and pitch rate affect loads
            indicialEffects = [1 0 0 1 0 0];
        end

        % In case of lateral loads (CS, Cl or Cn)
        if coeffType == 2 || coeffType == 4 || coeffType == 6
            % ASSUMPTION: sideslip, roll and yaw rate affect loads
            indicialEffects = [0 1 1 0 1 0];
        end
end
```

```
%% -------------------- ROM code -------------------- %%
%  FUNCTION TO READ IN FULL-ORDER MODEL CFD DATA
%  Optimised for MULDICON baseline design and ENSOLV
%  This code is developed by M.J.M. Ketelaars
%  Based on the scripts by M. Ghoreyshi
%  Tested for MATLAB R2016a
```

```
%# ------------------------------------------------- #%

function [CFDData, steadyValue] = CFDReader(coeffType,referenceLength,
  mach,speedOfSound,motionData)

% Link load to correct column in ENSOLV .conv file format
        %                   [CA, CS, CN, Cl, Cm, Cn]
        loadConventions =   [10, 11, 9,  18, 17, 19];

% Read in .conv file
sprintf('Load full-order time-marching CFD solution..\n')
[fileName,workFolder] = uigetfile('*.conv');

    % In case of no selection: no data
    if fileName == 0
        sprintf('No CFD data selected\n')
        CFDData = 0;
            % Select steady data
            sprintf('Load steady data from aoa of %d [deg]..\n',
              motionData(1,2))
            [fileName,workFolder] = uigetfile('*.conv');
            fileID = strcat(workFolder,fileName);
            rawData = dlmread(fileID);
            steadyValue = rawData(end,loadConventions(coeffType));
    else
        fileID = strcat(workFolder,fileName);
        rawData = dlmread(fileID);


        % Find indices of final subiterations values in ENSOLV *.conv
          format
        [~, index] = unique(rawData(:,1),'legacy');
        ENSOLVTime = rawData(index,3);

        % Convert ENSOLV nondim time [-] to physical time [sec]
        CFDData(:,1) = ENSOLVTime.*referenceLength/(mach*speedOfSound)
          ;
        CFDData(:,2) = rawData(index,loadConventions(coeffType));

        steadyValue = CFDData(1,2);
    end
end
```

```
%% -------------------- ROM code -------------------- %%
%  FUNCTION TO READ IN REQUIRED SAMPLES
%  Optimised for MULDICON baseline design and ENSOLV
%  This code is developed by M.J.M. Ketelaars
%  Based on the scripts by M. Ghoreyshi
%  Tested for MATLAB R2016a
%# ------------------------------------------------- #%

function [effect,steadyData] = storeIndicialData(motionData,
  indicialEffects,effectNames,coeffType,mach,speedOfSound,
  referenceLength)

%% Initialise data structure
```

```
% ASSUMPTION: only positive angles of attack and step respones of 1 degree

% Loop trough indicial effects
for i = 1:length(indicialEffects)
    if indicialEffects(i) == 1;

        %initialise figure
        figure()
        hold on
        % In case of AoA or Beta effect take correct motionData column [deg]
        stepData = 2;
        % The case of p, q or r [rad/s]
        if i > 2
            stepData = 3;
        end

        % find minimum parameter value
        parameterMin = floor(min(motionData(:,2)));
            if parameterMin < 0
                parameterMin = 0;
            end
        % find maximum parameter value
        % p,q,r are defined linear
        parameterMax = floor(max(motionData(:,2)));
        if stepData == 3
            parameterMin = 0;
            parameterMax = 0;
        end
        parameterStep = 1;

        % Loop trough angles of attack
        for parameter = parameterMin:parameterStep:parameterMax+parameterStep

            % Select indicial file
            if i > 2
                sprintf('Load indicial function - %s effect - from q of %d [deg]..\n', effectNames{i}, parameter)
            elseif i <=2
                sprintf('Load indicial function - %s effect - from aoa of %d [deg]..\n', effectNames{i}, parameter)

            end
                % Read in data
                [fileName,workFolder] = uigetfile('*.conv');
                    % In case of no selection: use previous dataset (assume linearity)
                    if fileName == 0
                        % Fit function to the motion data
                        fittedLoadCoeff = interp1(time, loadCoeff, motionData(:,1),'nearest','extrap');
                        % Store data in structure
                        effect(i).aoa(parameter+1).data(:,1) = motionData(:,1);
```

```
60                      effect(i).aoa(parameter+1).data(:,2) =
                          fittedLoadCoeff;
61                      steadyData(parameter+1,i) = steadyValue;
62                      continue
63                  end
64              fileID = strcat(workFolder,fileName);
65              rawData = dlmread(fileID);
66                  % Find indices of final subiterations values in
                      ENSOLV *.conv format
67                  [~, index] = unique(rawData(:,1),'legacy');
68
69              % ENSOLV time [non-dimensionalised]
70              rawTime = rawData(index,3); %[-]
71              % Revert to physical time [dimensionalise]
72              time = (rawTime-rawTime(1,1)) .* (referenceLength/(
                  mach*speedOfSound)); %[sec]
73
74              % Link load to correct column in ENSOLV .conv file
                  format
75              loadConventions = [10,11,9,18,17,19];
76              % ENSOLV load [non-dimensionalised]
77              rawLoad = rawData(index,loadConventions(coeffType));
78
79                  % Select steady data
80                  sprintf('Load steady data from aoa of %d [deg]..\n
                      ', parameter)
81                  [fileName,workFolder] = uigetfile('*.conv');
82                  % In case of no selection: use previous dataset (
                      assume linearity)
83                  fileID = strcat(workFolder,fileName);
84                  rawData = dlmread(fileID);
85
86                  % Select steady value of chosen load
87                  steadyValue = rawData(end,loadConventions(
                      coeffType));
88                  steadyData(parameter+1,i) = steadyValue;
89
90              % Subtract steady data from dataset for pure indicial
                  response
91              if i < 2
92                  loadCoeff = rawLoad - steadyValue; %[1 1/deg]
93              else
94                  loadCoeff = rawLoad/(deg2rad(20)) - steadyValue; %
                      [1 sec/rad]
95              end
96
97          % Fit function to the motion data
98          fittedLoadCoeff = interp1(time, loadCoeff, motionData(:,1)
              ,'nearest','extrap');
99
100         % Store data in structure
101         effect(i).aoa(parameter+1).data(:,1) = motionData(:,1);
102         effect(i).aoa(parameter+1).data(:,2) = fittedLoadCoeff;
103
104         % Plot indicial functions of effect
105         if i < 2
```

```
106                 plot(motionData(:,1),fittedLoadCoeff.*180/pi);
107                 ylabel('C_{load} [1/rad]');
108                 xlabel('Time [sec]');
109                 grid on
110             else
111                 plot(motionData(:,1),fittedLoadCoeff.*mach*
                      speedOfSound/referenceLength)
112                 ylabel('C_{load} [1/rad]');
113                 xlabel('Time [sec]');
114                 grid on
115             end
116             hold on
117         % next indicial effect parameter (e.g. aoa or q)
118         end
119     end
120 % all indicial functions are read
121 sprintf('All samples stored in dataset\n')
122 end
123 % end function
124 end
```

```
1  %% -------------------- ROM code -------------------- %%
2  %  NUMERICAL ROM BUILDING PROCEDURE
3  %  Optimised for MULDICON baseline design and ENSOLV
4  %  This code is developed by M.J.M. Ketelaars
5  %  Based on the scripts by M. Ghoreyshi
6  %  Tested for MATLAB R2016a
7  %# ------------------------------------------------- #%
8
9  function [parameterEffects, ROM] = ROMbuilderV3(motionData, effect,
     indicialEffects, steadyValue)
10
11 %% Initialising
12 % Link load to correct column in ENSOLV .conv file format
13
14 parameterMin = floor(min(motionData(:,2)));
15
16 % Initialising
17 motionTimeStep = motionData(2,1)-motionData(1,1);
18
19 %% ROM building loops
20     % Loop trough effects
21     for k = 1:length(indicialEffects)
22         if indicialEffects(k) == 1;
23
24             % In case of AoA or Beta effect take correct motionData
                 column [deg]
25             stepData = 2;
26                 % The case of p, q or r [rad/s]
27                 if k > 2
28                     stepData = 3;
29                 end
30
31             j = 1;
32
33             %% ROM building
```

```
34
35              for i = 2:length(motionData)
36
37                  %Time integration span of interest
38                  X = 0 : motionTimeStep : motionData(i,1);
39
40                  %Flip time vector for convolution purposes
41                  XFlip = motionData(i,1) - X;
42
43                      %Flipp and order indicial data vectors for
                          convolution purposes
44                      if k == 1
45                          for n = parameterMin+1:length(effect(k).aoa)
46                              Y2(n).step  =   interp1(effect(k).aoa(n).
                                  data(:,1), ...
47                                              effect(k).aoa(n).data(:,2)
                                                , ...
48                                              XFlip,'nearest','extrap');
49                          end
50                      elseif k == 4
51                              Y2(1).step  =   interp1(effect(k).aoa(1).
                                  data(:,1), ...
52                                              effect(k).aoa(1).data(:,2)
                                                , ...
53                                              XFlip,'nearest','extrap');
54                      end
55
56                      % Calculate individual effect data (e.g. Cla, Clq
                          etc.)
57                      Y = zeros(length(X),1);
58
59                          for n = 1:i
60                              value = motionData(n,stepData);
61                               % HARDCODED FOR ROUGH MOTION 14-22 AOA
                                   from 15
62                               % case aoa effect
63                               if k == 1
64                                      if      value >= 15 &&  value < 16
65                                         Y(n) =  Y2(16).step(n) * (value
                                             -15);
66                                      elseif value >= 16 &&  value < 17
67                                         Y(n) =  Y2(16).step(n) * 1 +
                                             ...
68                                                 Y2(17).step(n) * (value
                                                     -16);
69                                      elseif value >= 17 &&  value < 18
70                                         Y(n) =  Y2(16).step(n) * 1 +
                                             ...
71                                                 Y2(17).step(n) * 1 +
                                                     ...
72                                                 Y2(18).step(n) * (value
                                                     -17);
73                                      elseif value >= 18 &&  value < 19
74                                         Y(n) =  Y2(16).step(n) * 1 +
                                             ...
75                                                 Y2(17).step(n) * 1 +
```

```
                                                    ...
76                                                Y2(18).step(n) * 1 +
                                                    ...
77                                                Y2(19).step(n) * (value
                                                     -18);
78                                        elseif value >= 19 &&  value < 20
79                                           Y(n) =  Y2(16).step(n) * 1 +
                                                ...
80                                                Y2(17).step(n) * 1 +
                                                    ...
81                                                Y2(18).step(n) * 1 +
                                                    ...
82                                                Y2(19).step(n) * 1 +
                                                    ...
83                                                Y2(20).step(n) * (value
                                                     -19);
84                                        elseif value >= 20 &&  value < 21
85                                           Y(n) =  Y2(16).step(n) * 1 +
                                                ...
86                                                Y2(17).step(n) * 1 +
                                                    ...
87                                                Y2(18).step(n) * 1 +
                                                    ...
88                                                Y2(19).step(n) * 1 +
                                                    ...
89                                                Y2(20).step(n) * 1 +
                                                    ...
90                                                Y2(21).step(n) * (value
                                                     -20);
91                                        elseif value >= 21 &&  value < 22
92                                           Y(n) =  Y2(16).step(n) * 1 +
                                                ...
93                                                Y2(17).step(n) * 1 +
                                                    ...
94                                                Y2(18).step(n) * 1 +
                                                    ...
95                                                Y2(19).step(n) * 1 +
                                                    ...
96                                                Y2(20).step(n) * 1 +
                                                    ...
97                                                Y2(21).step(n) * 1 +
                                                    ...
98                                                Y2(22).step(n) * (value
                                                     -21);
99                                       elseif value >= 14 && value < 15
100                                         Y(n) = -Y2(15).step(n) * (15-
                                                value);
101                                      end
102                                % case q effect (assume always linear)
103                                elseif k == 4
104                                    Y(n) = Y2(1).step(n) * value;
105                                end
106
107                        end
108                %% ROM building remainder
109
```

```
110                 %Resulting convolution integral
111                 convolutionResult(j) = trapz(X,Y);
112 
113                 %Indicial effects on the normal load coefficient
114                 individualEffect = gradient(convolutionResult,
                      motionTimeStep);
115 
116                 j = j+1;
117             end
118             parameterEffects(k,:) = individualEffect;
119             % next effect
120             sprintf('Next effect')
121         end
122     % done effects
123     end
124 
125     ROM = sum(parameterEffects) + steadyValue;
126 
127 %% End function
128 end
```

B

ADDITIONAL ROMS AND ERROR ANALYSIS OF NACA0012

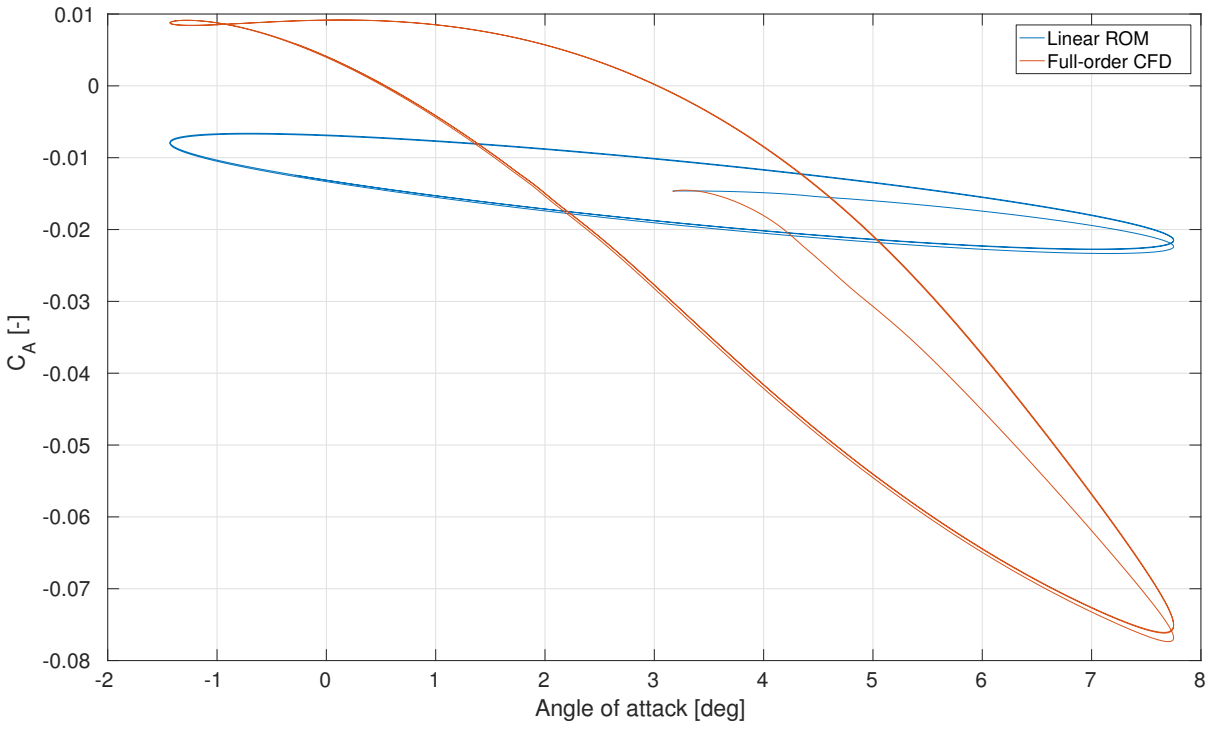

Figure B.1: Comparison between AGARD CT2 wind-tunnel data, the full-order CFD URANS and the linear ROM axial force coefficient solutions undergoing a pitching oscillation at a frequency of 5.27$[Hz]$, Mach of 0.6 and a Reynolds number of 4.8$E6$

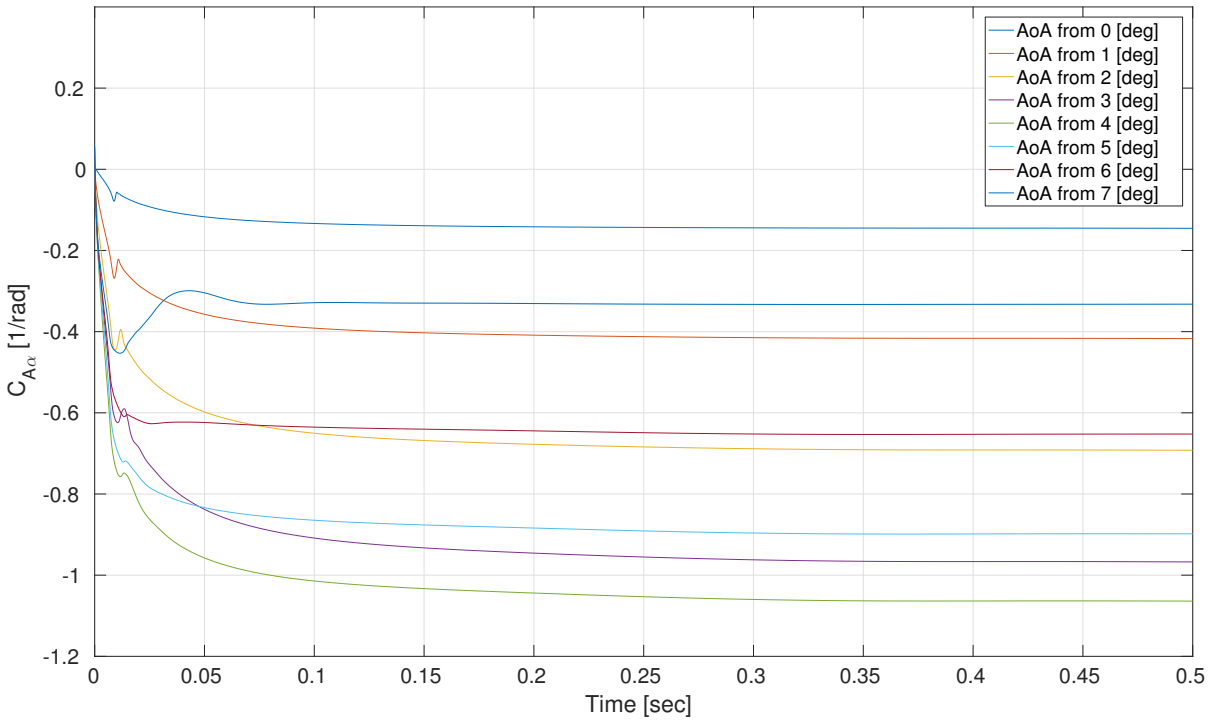

Figure B.2: Additional indicial step response functions of the angle of attack effect on the axial force coefficient to capture the non-linear unsteady flow behaviour by applying a one degree step change on a steady RANS solution at various angles of attack while keeping the pitch rate zero

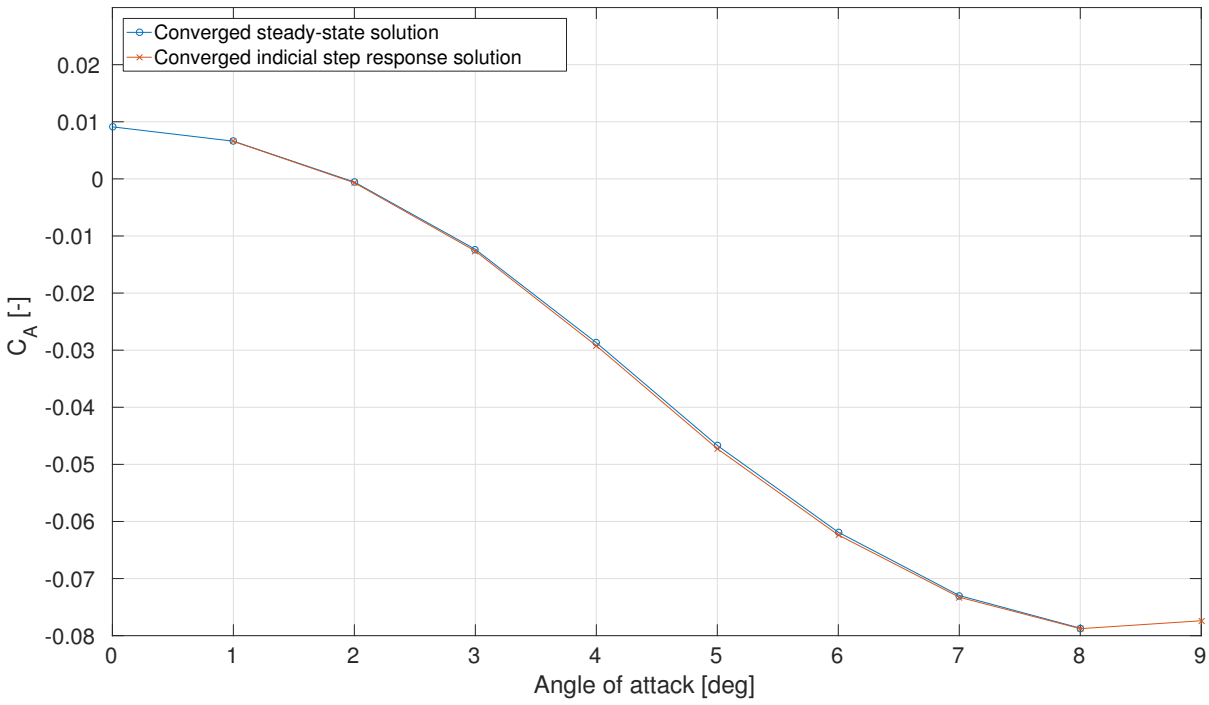

Figure B.3: Final values of the angle of attack indicial step response functions on the axial force coefficient generated by approximating the unsteady RANS compared to the airfoil directly configuring in the angle of attack of interest and finding the steady RANS solution

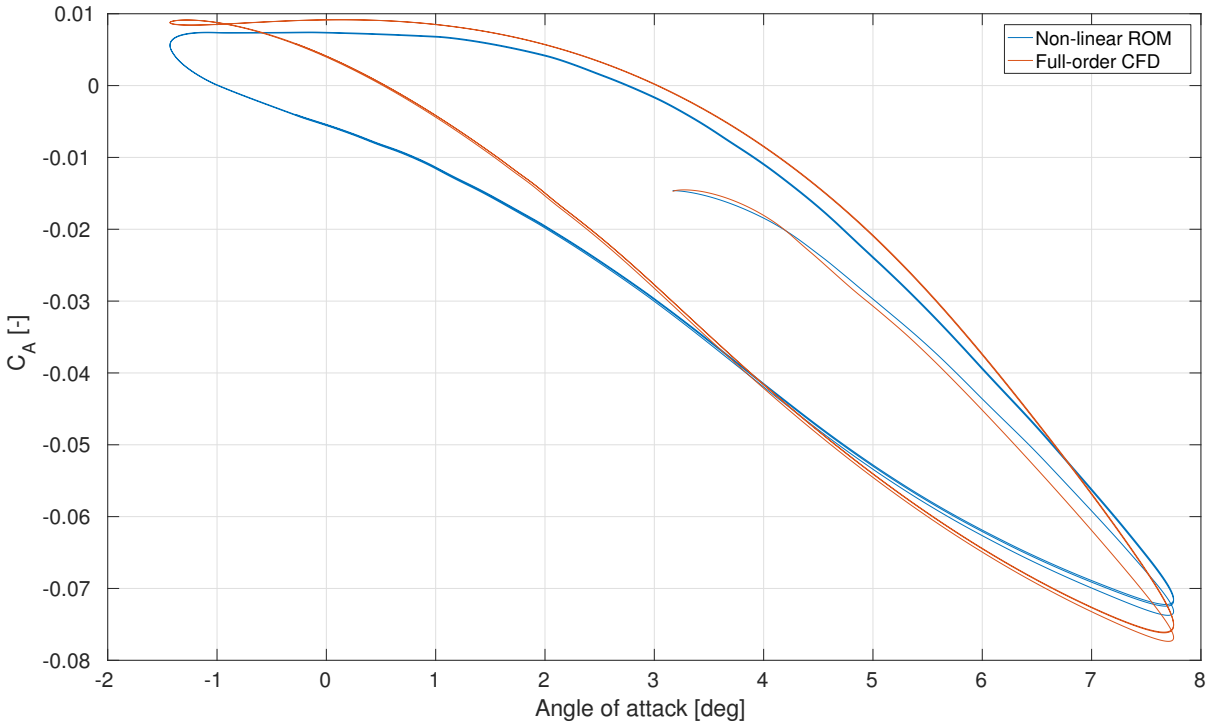

Figure B.4: Comparison between the full-order CFD URANS and the non-linear ROM axial force coefficient solutions undergoing a pitching oscillation at a frequency of 5.27$[Hz]$, Mach of 0.6 and a Reynolds number of 4.8E6

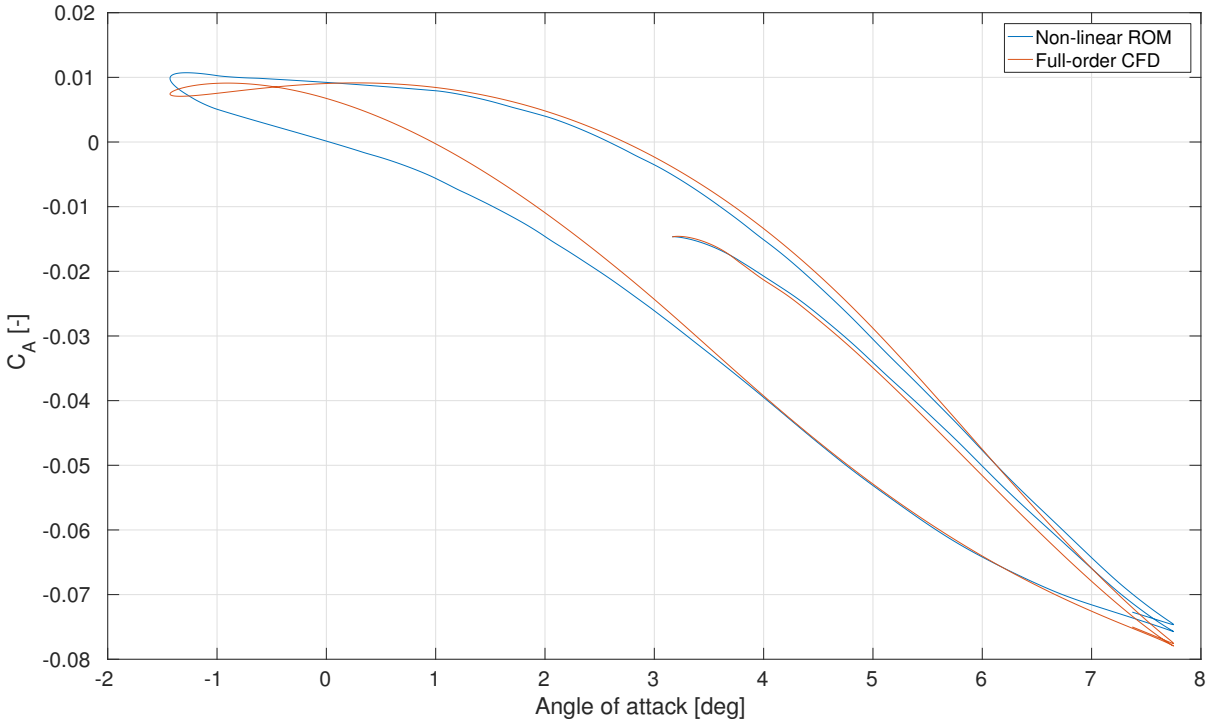

Figure B.5: Comparison between the full-order CFD URANS and the non-linear ROM axial force coefficient solutions undergoing a pitching oscillation at a frequency of 2.63$[Hz]$, Mach of 0.6 and a Reynolds number of 4.8E6

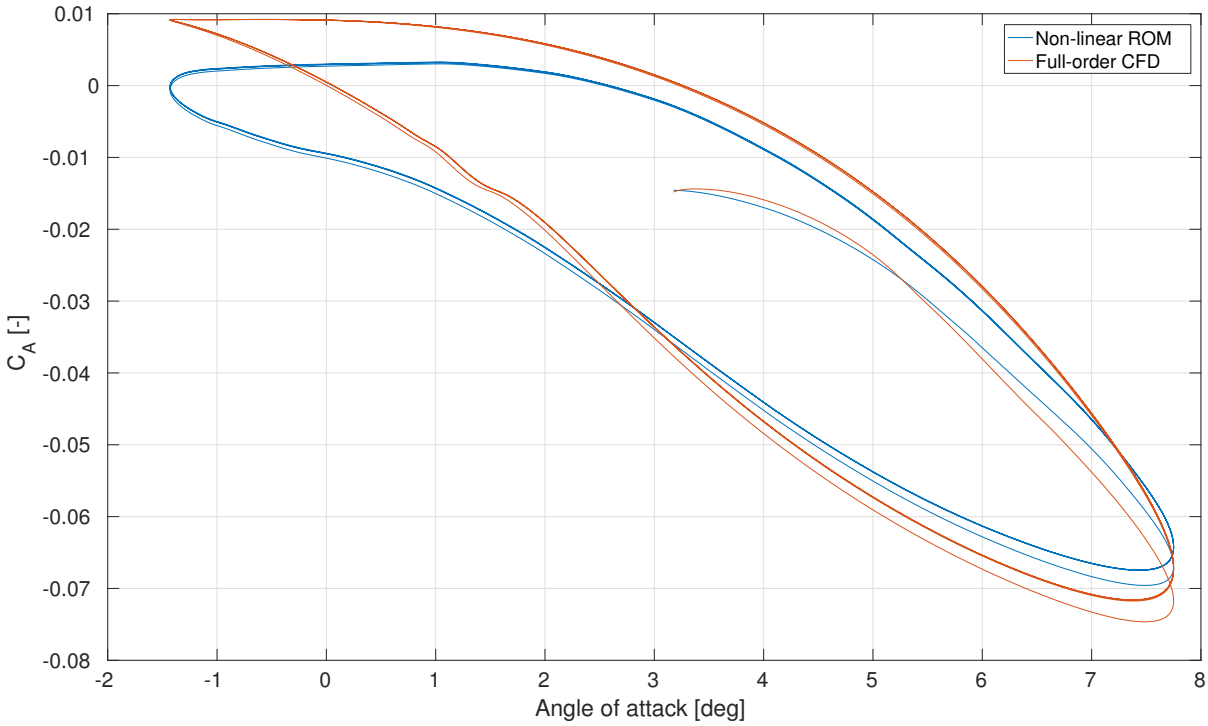

Figure B.6: Comparison between the full-order CFD URANS and the non-linear ROM axial force coefficient solutions undergoing a pitching oscillation at a frequency of 10.54$[Hz]$, Mach of 0.6 and a Reynolds number of 4.8E6

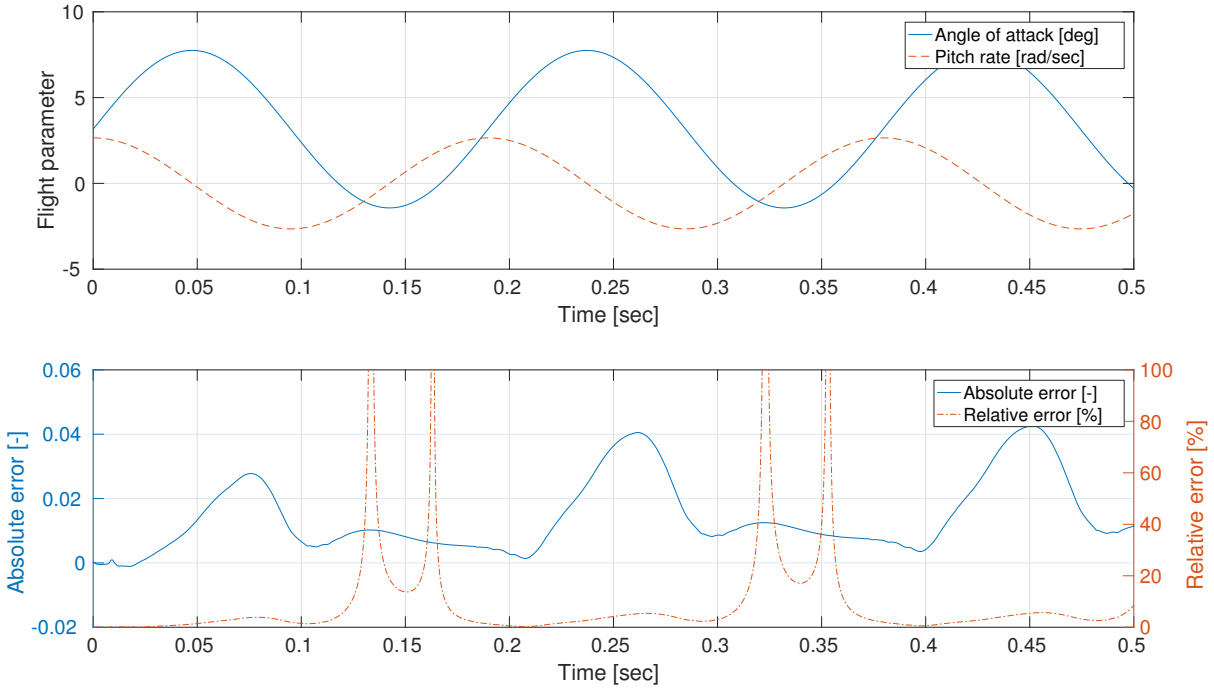

Figure B.7: Flight parameter history (top) during the oscillating motion at a frequency of 5.27 [Hz] including the differences between the normal force ROM and the full-order model (bottom) expressed in the absolute and relative error histories

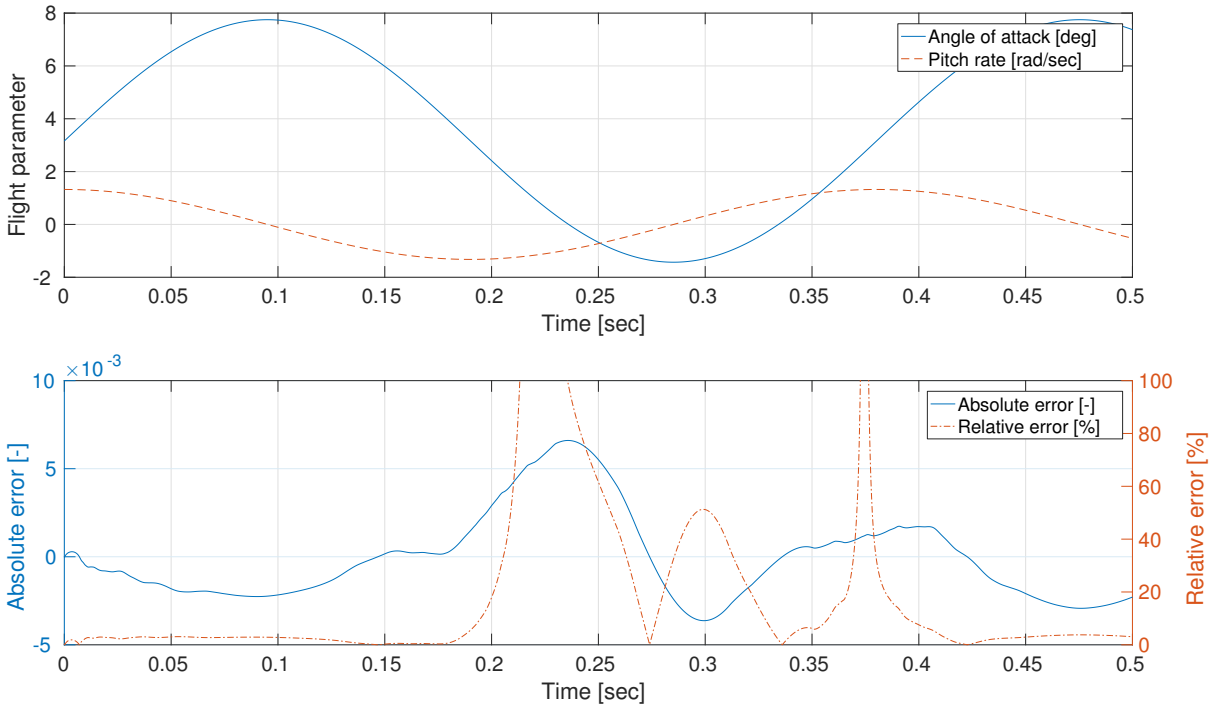

Figure B.8: Flight parameter history (top) during the oscillating motion at a frequency of 2.63 [Hz] including the differences between the axial force ROM and the full-order model (bottom) expressed in the absolute and relative error histories

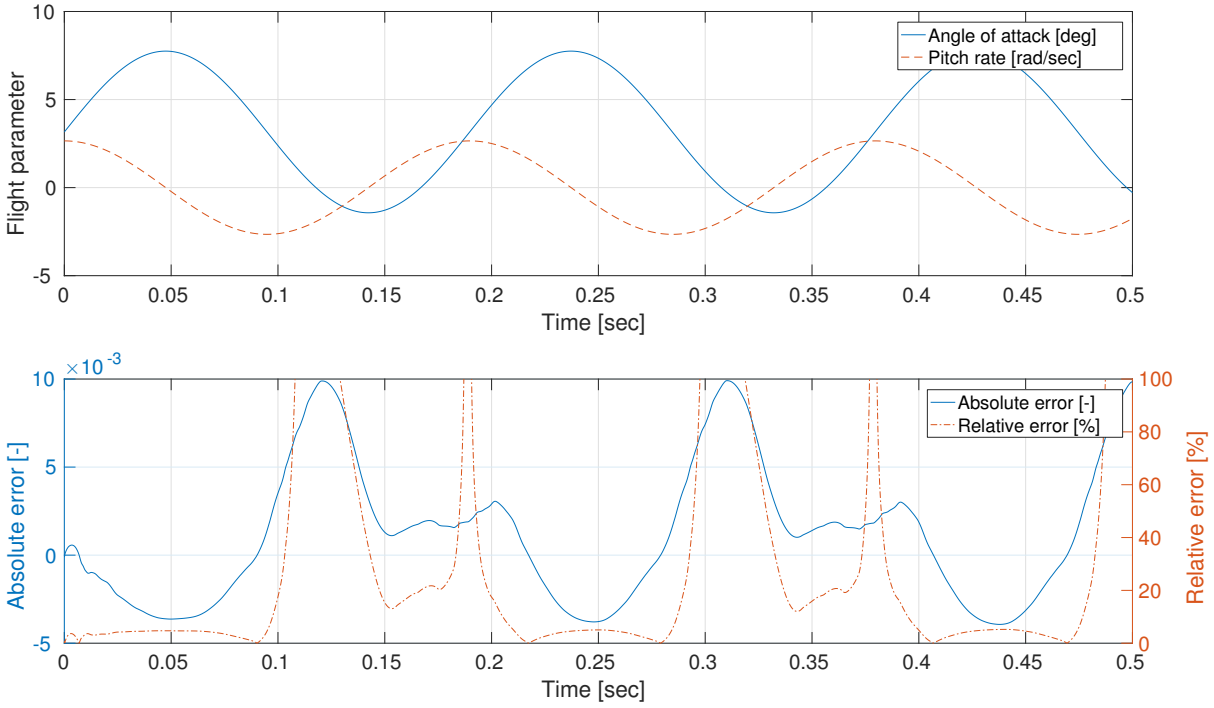

Figure B.9: Flight parameter history (top) during the oscillating motion at a frequency of 5.27 [Hz] including the differences between the axial force ROM and the full-order model (bottom) expressed in the absolute and relative error histories

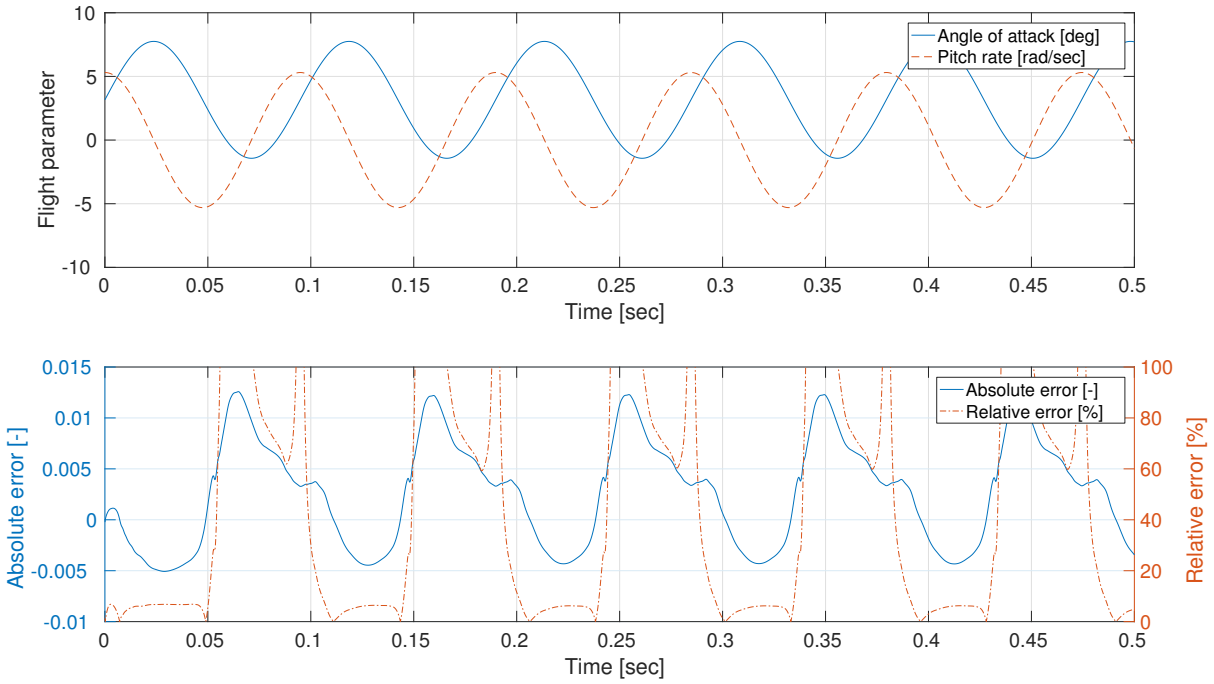

Figure B.10: Flight parameter history (top) during the oscillating motion at a frequency of 10.54 [Hz] including the differences between the axial force ROM and the full-order model (bottom) expressed in the absolute and relative error histories

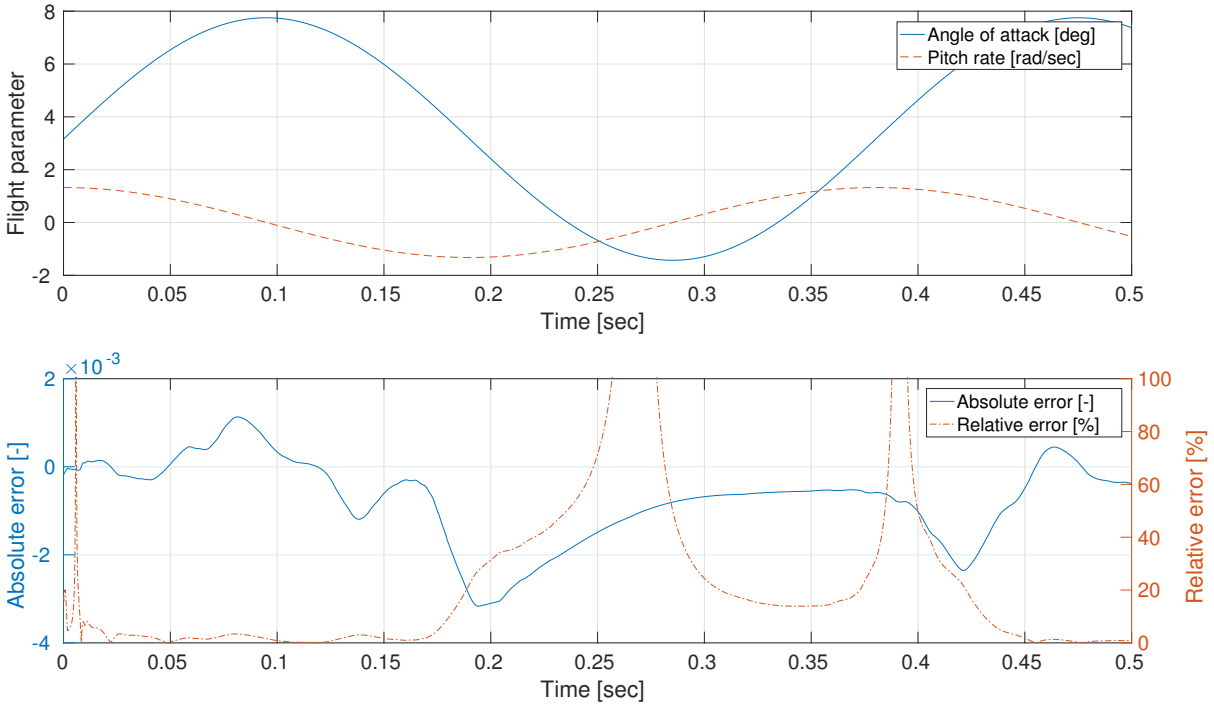

Figure B.11: Flight parameter history (top) during the oscillating motion at a frequency of 2.63 [Hz] including the differences between the pitching moment ROM and the full-order model (bottom) expressed in the absolute and relative error histories

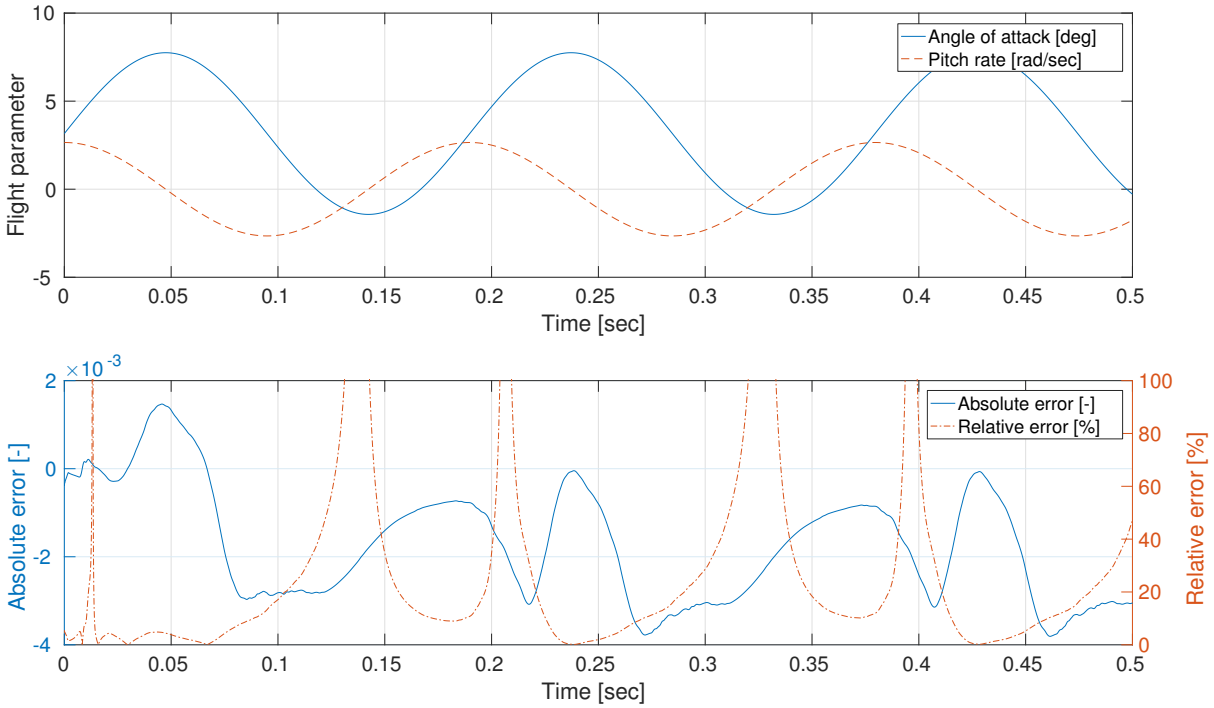

Figure B.12: Flight parameter history (top) during the oscillating motion at a frequency of 5.27 [Hz] including the differences between the pitching moment ROM and the full-order model (bottom) expressed in the absolute and relative error histories

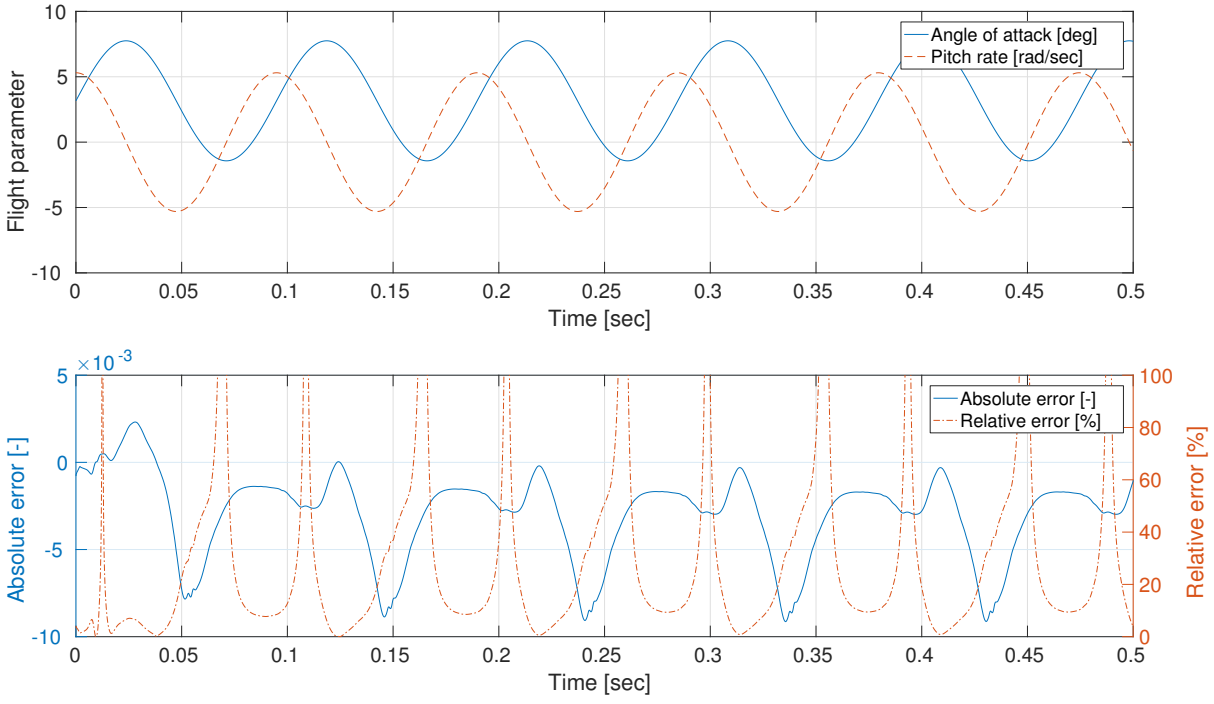

Figure B.13: Flight parameter history (top) during the oscillating motion at a frequency of 10.54 [Hz] including the differences between the pitching moment ROM and the full-order model (bottom) expressed in the absolute and relative error histories

C

ADDITIONAL SENSITIVITY ANALYSIS RESULTS OF NACA0012

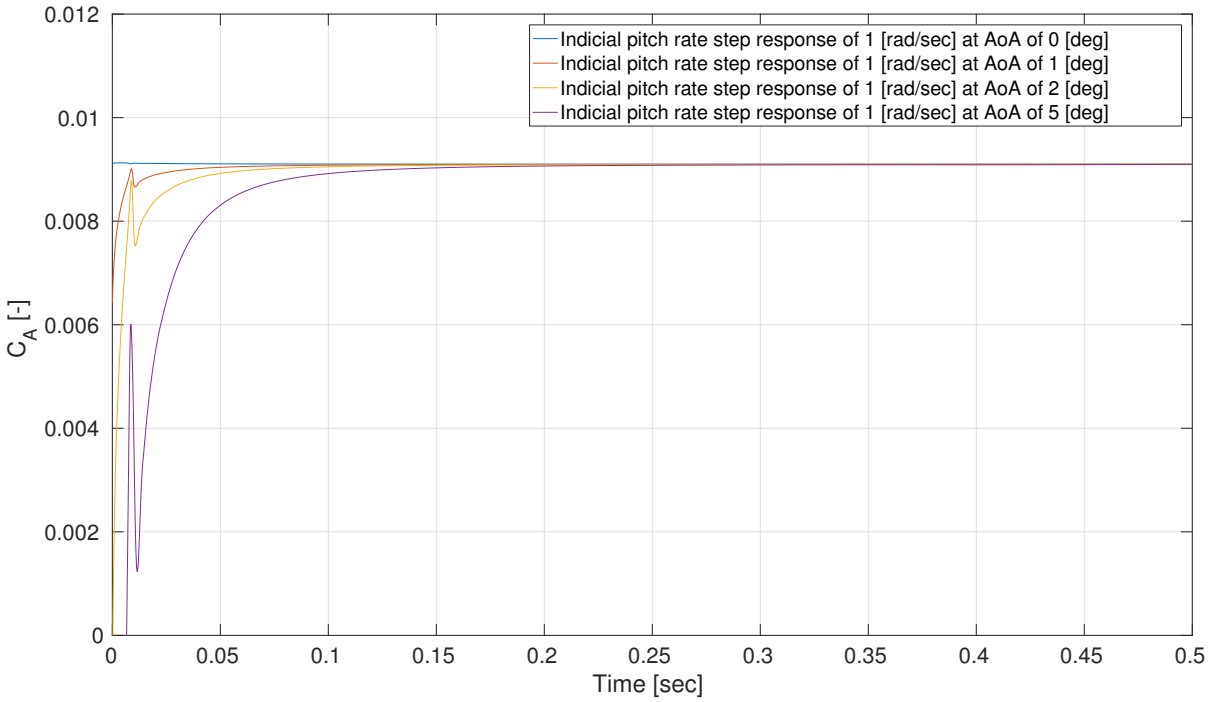

Figure C.1: Indicial step response function of the pitch rate effect on the axial force coefficient by applying a one radians per second step change on a steady RANS solution at starting various angles of attack having a constant pitch rate

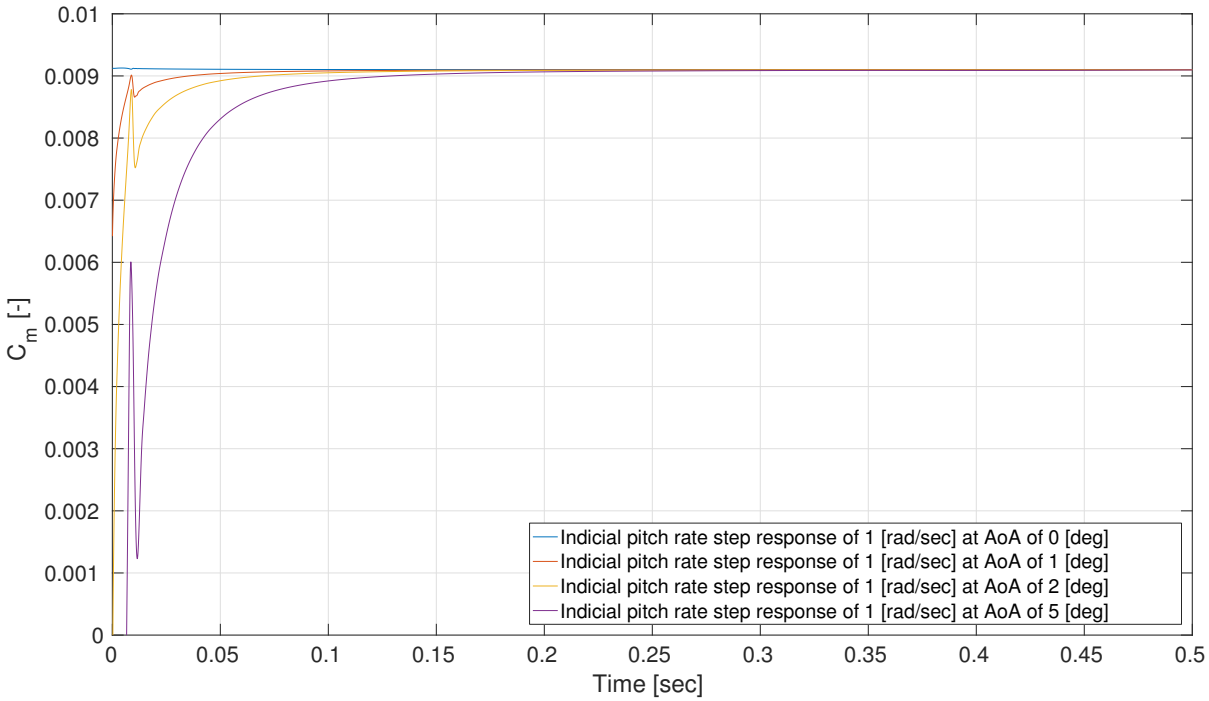

Figure C.2: Indicial step response function of the pitch rate effect on the pitching moment coefficient by applying a one radians per second step change on a steady RANS solution at starting various angles of attack having a constant pitch rate

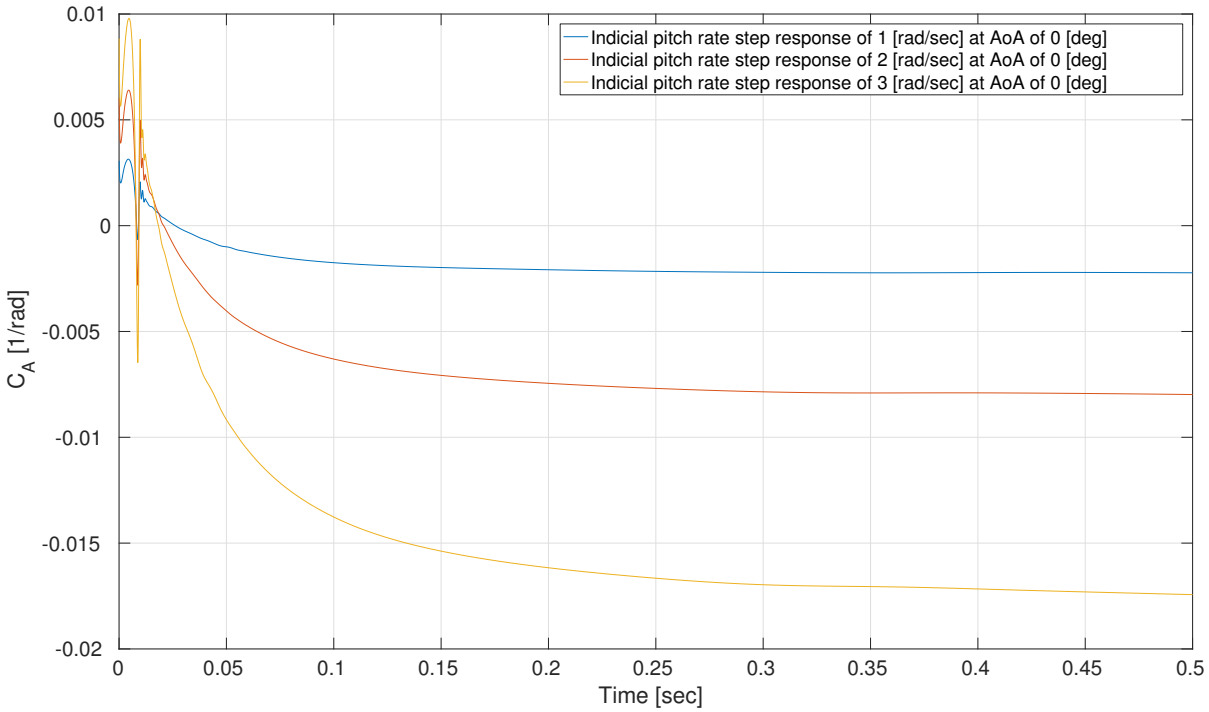

Figure C.3: Indicial step response function of the pitch rate effect on the axial force coefficient by applying various radians per second step changes on a steady RANS solution at zero angle of attack having a constant pitch rate

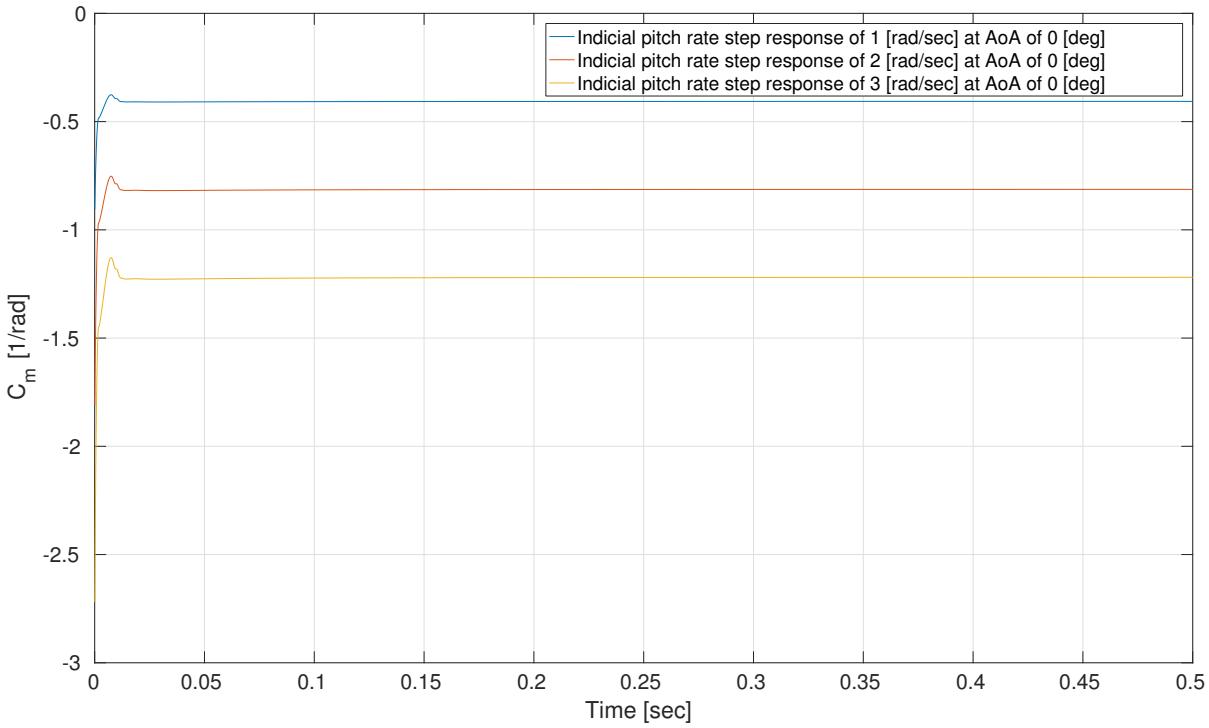

Figure C.4: Indicial step response function of the pitch rate effect on the pitching moment coefficient by applying various radians per second step changes on a steady RANS solution at zero angle of attack having a constant pitch rate

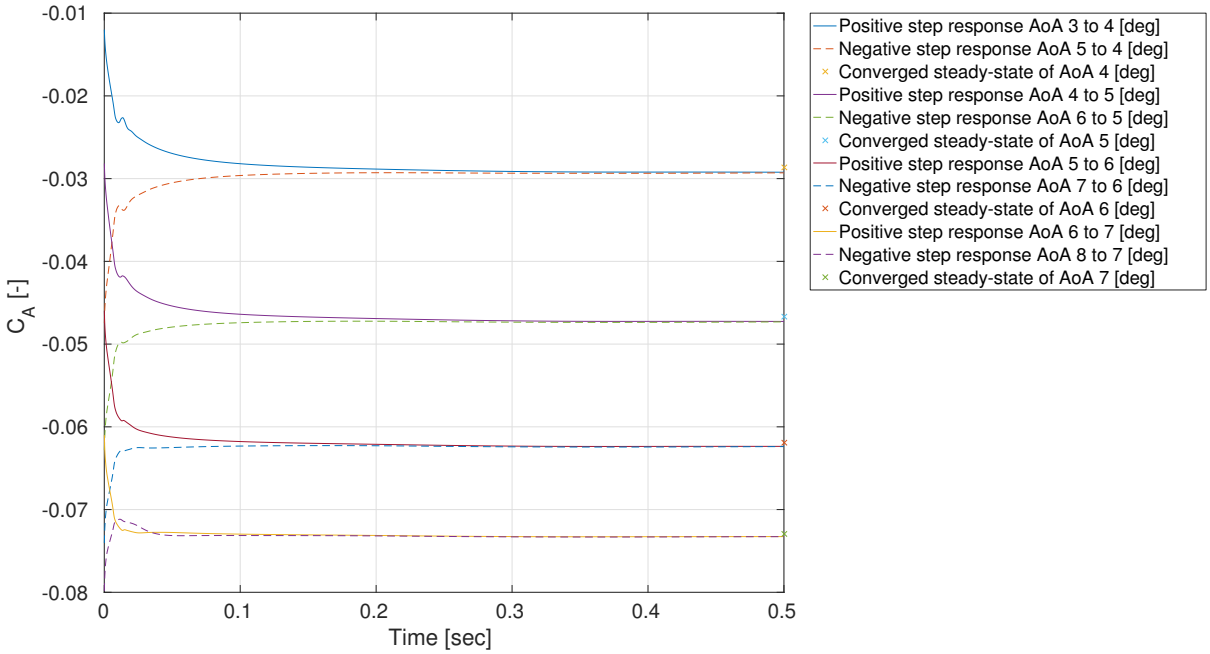

Figure C.5: Comparison between positive and negative indicial step response functions of the angle of attack effect on the axial force coefficient by applying a one degree step change on a steady RANS solution at various angle of attack and zero pitch rate

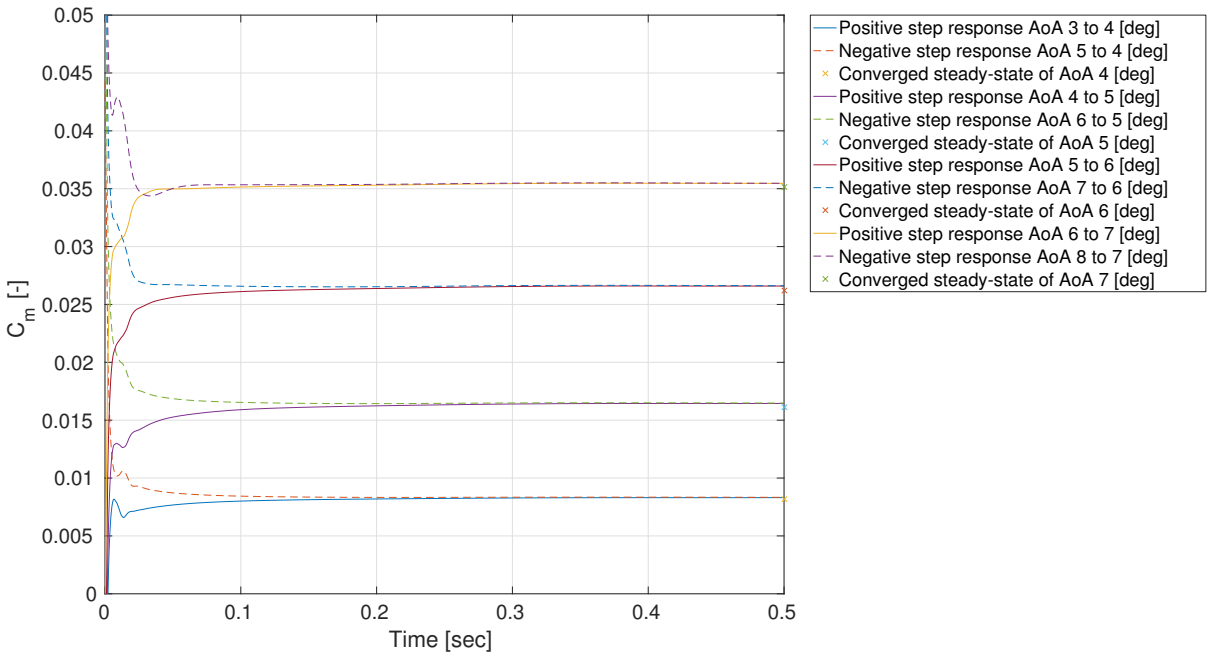

Figure C.6: Comparison between positive and negative indicial step response functions of the angle of attack effect on the pitching moment coefficient by applying a one degree step change on a steady RANS solution at various angle of attack and zero pitch rate

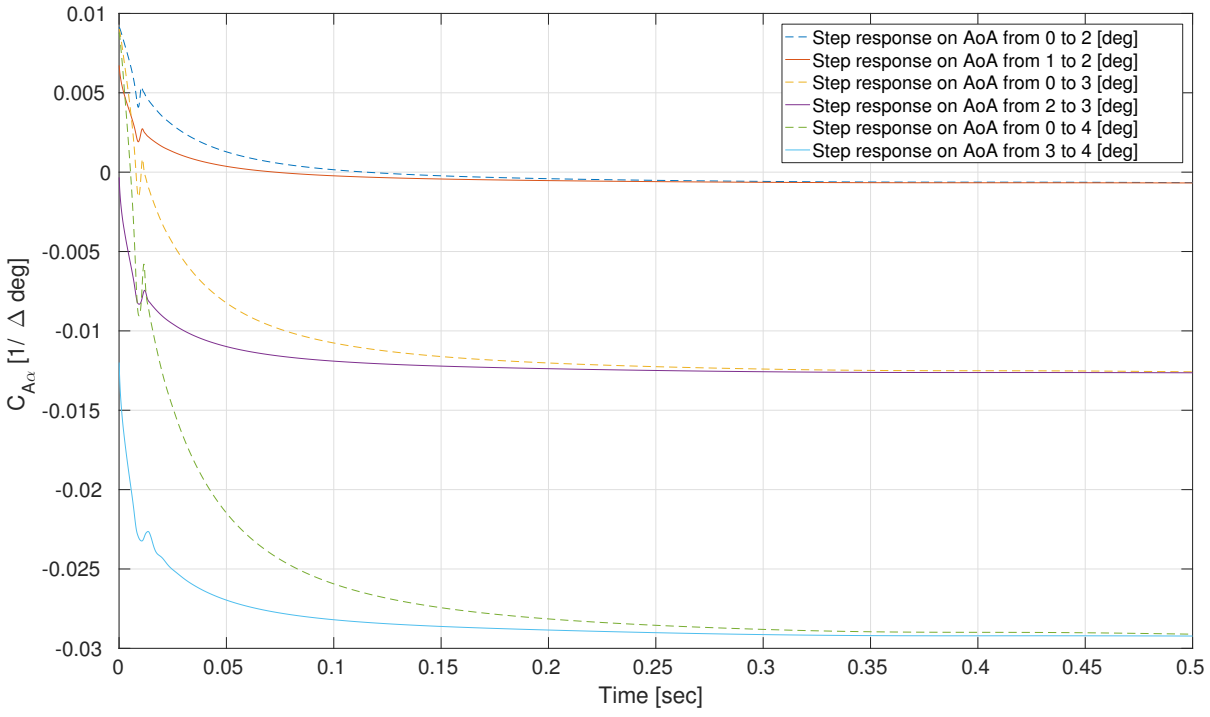

Figure C.7: Indicial step response functions of the angle of attack effect on the axial force coefficient by applying various changes in degrees step change on a steady RANS solution starting at various angle of attack having a zero pitch rate

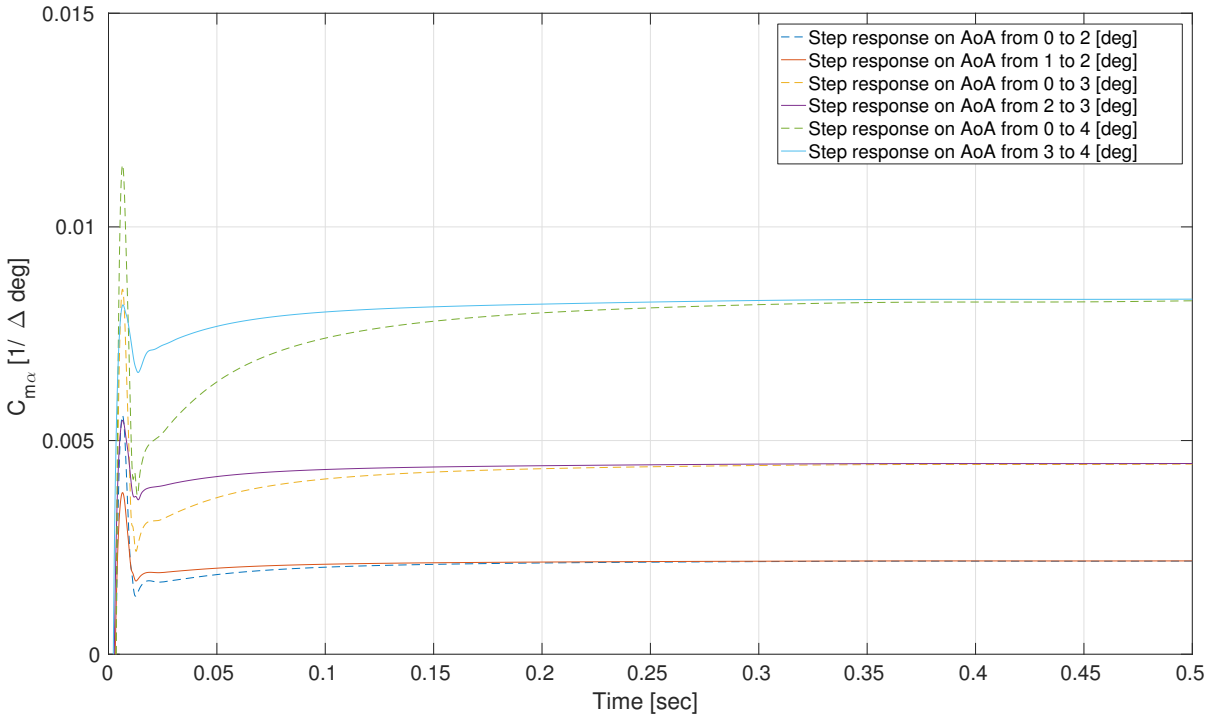

Figure C.8: Indicial step response functions of the angle of attack effect on the pitching moment coefficient by applying various changes in degrees step change on a steady RANS solution starting at various angle of attack having a zero pitch rate

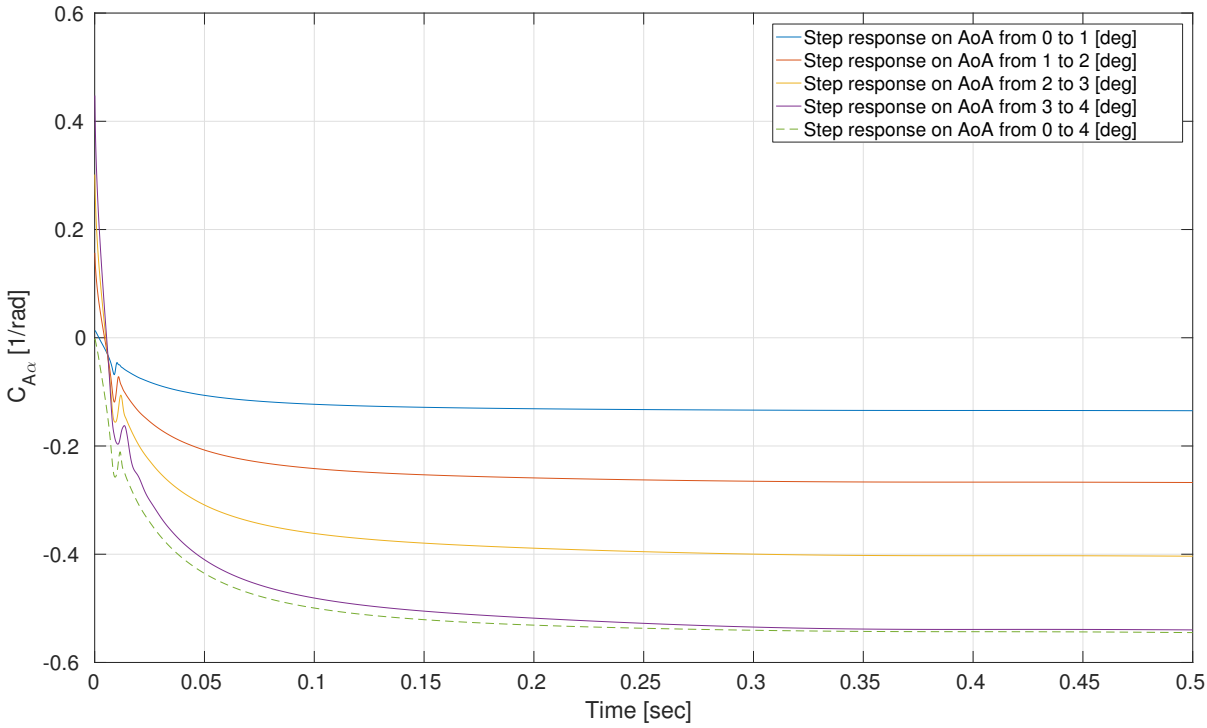

Figure C.9: Indicial step response functions of the angle of attack effect on the axial force coefficient by applying a unit degree size step change and subtracting the steady RANS solution of interest at various starting angles of attack having a zero pitch rate

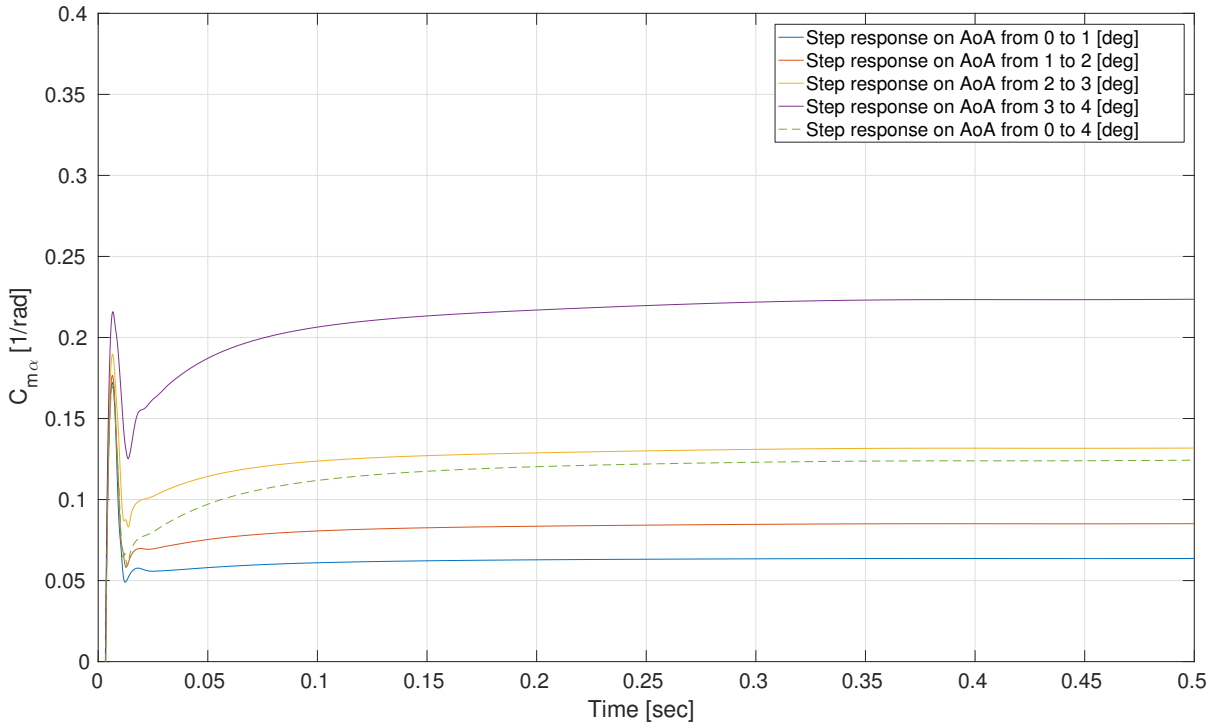

Figure C.10: Indicial step response functions of the angle of attack effect on the pitching moment coefficient by applying a unit degree size step change and subtracting the steady RANS solution of interest at various starting angles of attack having a zero pitch rate

D

Details on computational effort of NACA0012 results

Table D.1: Computational data on CFD calculations

Steady-state calculations							
Indicial step response	*CPU hours [h,m,s]*			*Levels*	*Iterations*	*Sub iterations*	*Total iterations*
SS A00	23	50	54.58	3	2000	30	180000
SS A01	28	6	57.41	3	2000	30	180000
SS A02	27	51	35.71	3	2000	30	180000
SS A03	27	48	39.61	3	2000	30	180000
SS A04	27	48	4.65	3	2000	30	180000
SS A05	27	47	4.58	3	2000	30	180000
SS A06	23	50	37.04	3	2000	30	180000
SS A07	23	54	47.62	3	2000	30	180000
SS A08	24	58	51.65	3	2000	30	180000
One degree indicial step responses							
Indicial step response	*CPU hours [h,m,s]*			*Levels*	*Iterations*	*Sub iterations*	*Total iterations*
step A00	96	31	46.29	1	10000	30	300000
step A01	96	27	36.91	1	10000	30	300000
step A02	96	20	34.66	1	10000	30	300000
step A03	96	27	15.24	1	10000	30	300000
step A04	96	16	53.37	1	10000	30	300000
step A05	96	21	21.4	1	10000	30	300000
step A06	100	32	32.6	1	10000	30	300000
step A07	96	23	51.39	1	10000	30	300000
step A08	96	38	1.03	1	10000	30	300000
Pitch rate responses of 1 [rad/s]							
step q00	96	22	2.99	1	10000	30	300000
step q01	96	18	59.87	1	10000	30	300000
step q02	96	45	25.58	1	10000	30	300000
step q05	96	24	33.77	1	10000	30	300000
Varying indicial step responses							
Indicial step response	*CPU [h,m,s]*			*Levels*	*Iterations*	*Sub iterations*	*Total iterations*
Step A00-02	192	39	11.76	1	10000	60	600000
Step A00-03	192	45	16.05	1	10000	60	600000
Step A00-04	192	23	48.32	1	10000	60	600000
Negative indicial step responses							
Indicial step response	*CPU [h,m,s]*			*Levels*	*Iterations*	*Sub iterations*	*Total iterations*
Step A08-07	96	21	49.87	1	10000	30	300000
Step A07-06	96	29	25.49	1	10000	30	300000
Step A06-05	96	28	47.45	1	10000	30	300000
Step A05-04	96	40	21.89	1	10000	30	300000
Full motion pitch oscillation calculations							
Calculation	*CPU [h,m,s]*			*Levels*	*Iterations*	*Sub iterations*	*Total iterations*
Frequency of 2.63 [Hz]	160	18	43.09	1	10000	50	500000
Frequency of 5.27 [Hz]				1	10000	50	500000
Frequency of 10.54 [Hz]	161	20	2.37	1	10000	50	500000

E

ADDITIONAL CFD STEADY STATE RESULTS

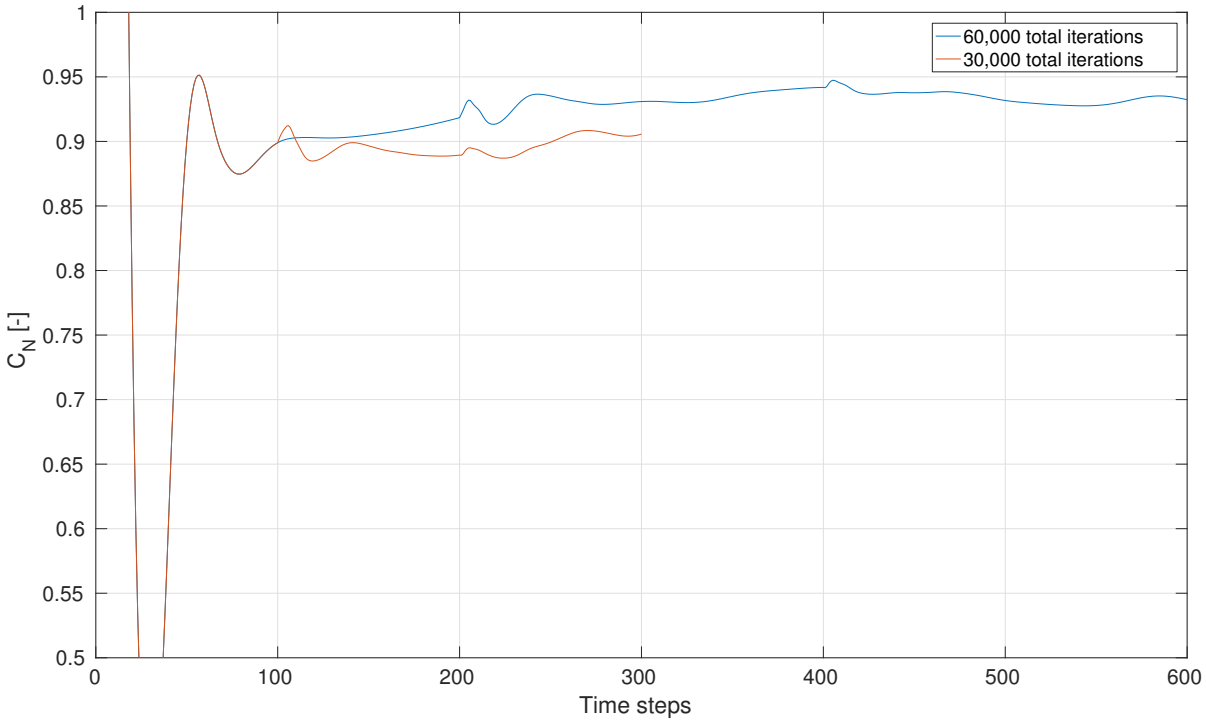

Figure E.1: ENSOLV URANS convergence results for MULDICON load at a Mach of 0.2, Reynolds number of 2.80E+07 and an angle of attack of 20 [deg]

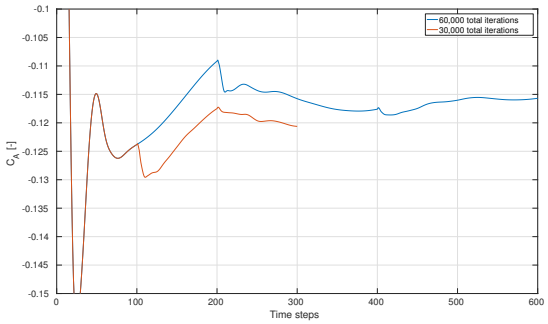

Figure E.2: ENSOLV URANS convergence results for MULDICON load at a Mach of 0.2, Reynolds number of 2.80E+07 and an angle of attack of 20 [deg]

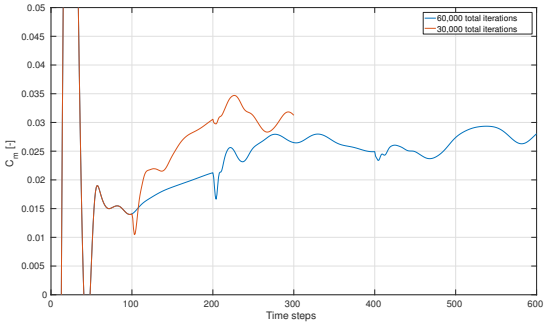

Figure E.3: ENSOLV URANS convergence results for MULDICON load at a Mach of 0.2, Reynolds number of 2.80E+07 and an angle of attack of 20 [deg]

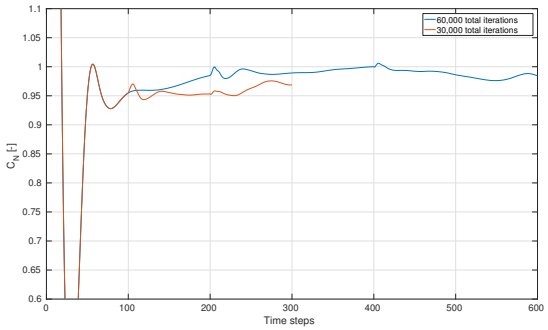

Figure E.4: ENSOLV URANS convergence results for MULDICON load at a Mach of 0.2, Reynolds number of 2.80E+07 and an angle of attack of 21 [deg]

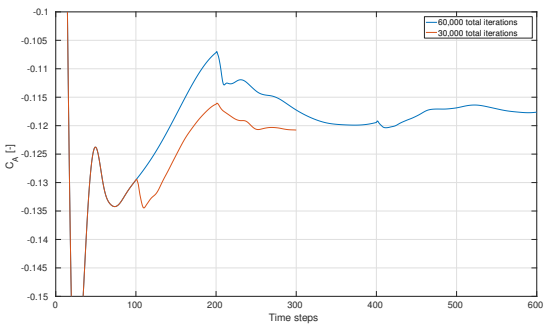

Figure E.5: ENSOLV URANS convergence results for MULDICON load at a Mach of 0.2, Reynolds number of 2.80E+07 and an angle of attack of 21 [deg]

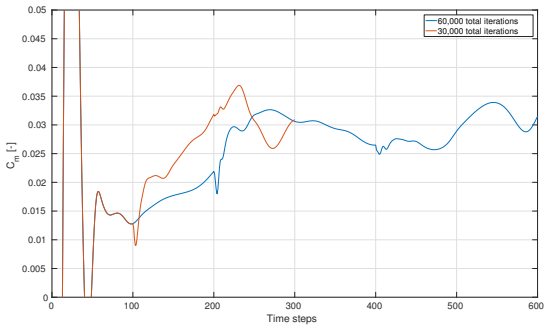

Figure E.6: ENSOLV URANS convergence results for MULDICON load at a Mach of 0.2, Reynolds number of 2.80E+07 and an angle of attack of 21 [deg]

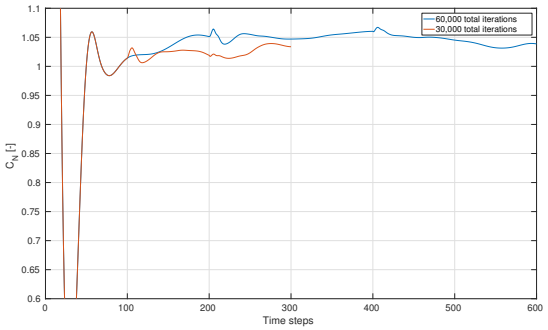

Figure E.7: ENSOLV URANS convergence results for MULDICON load at a Mach of 0.2, Reynolds number of 2.80E+07 and an angle of attack of 22 [deg]

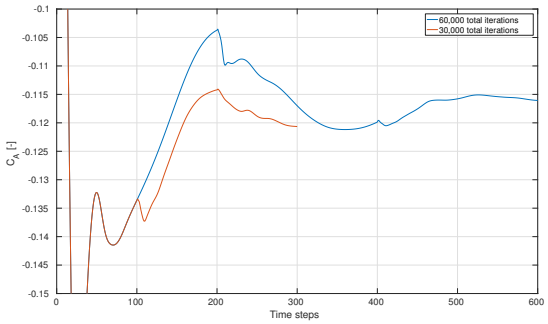

Figure E.8: ENSOLV URANS convergence results for MULDICON load at a Mach of 0.2, Reynolds number of 2.80E+07 and an angle of attack of 22 [deg]

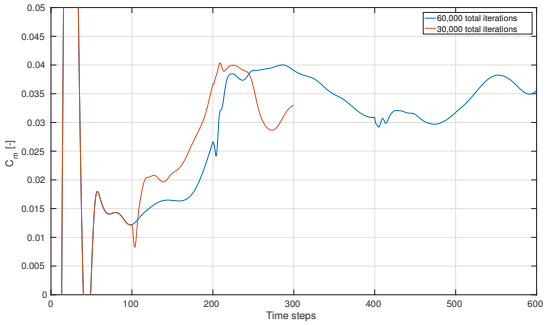

Figure E.9: ENSOLV URANS convergence results for MULDICON load at a Mach of 0.2, Reynolds number of 2.80E+07 and an angle of attack of 22 [deg]

F

ADDITIONAL ROM RESULTS OF MULDICON

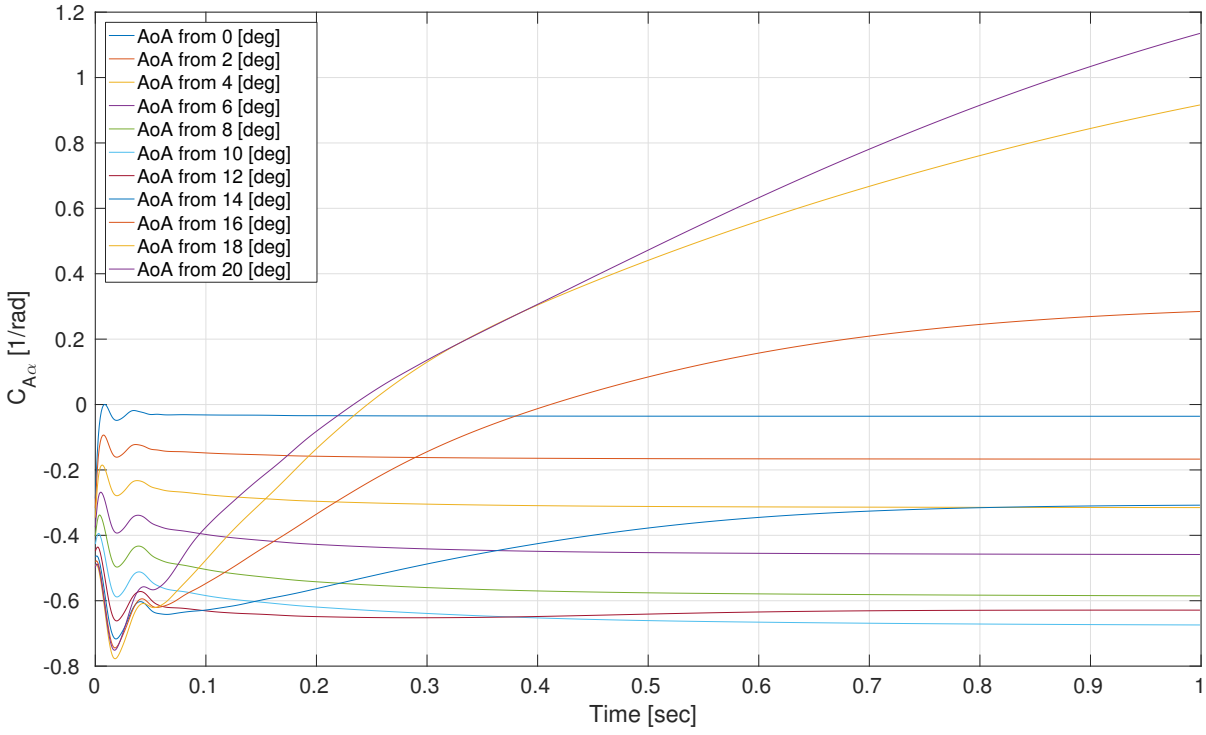

Figure F.1: Indicial step response functions of the angle of attack effect on the axial force coefficient by applying a one degree step change on a steady RANS solution at various starting angles of attack and zero pitch rate

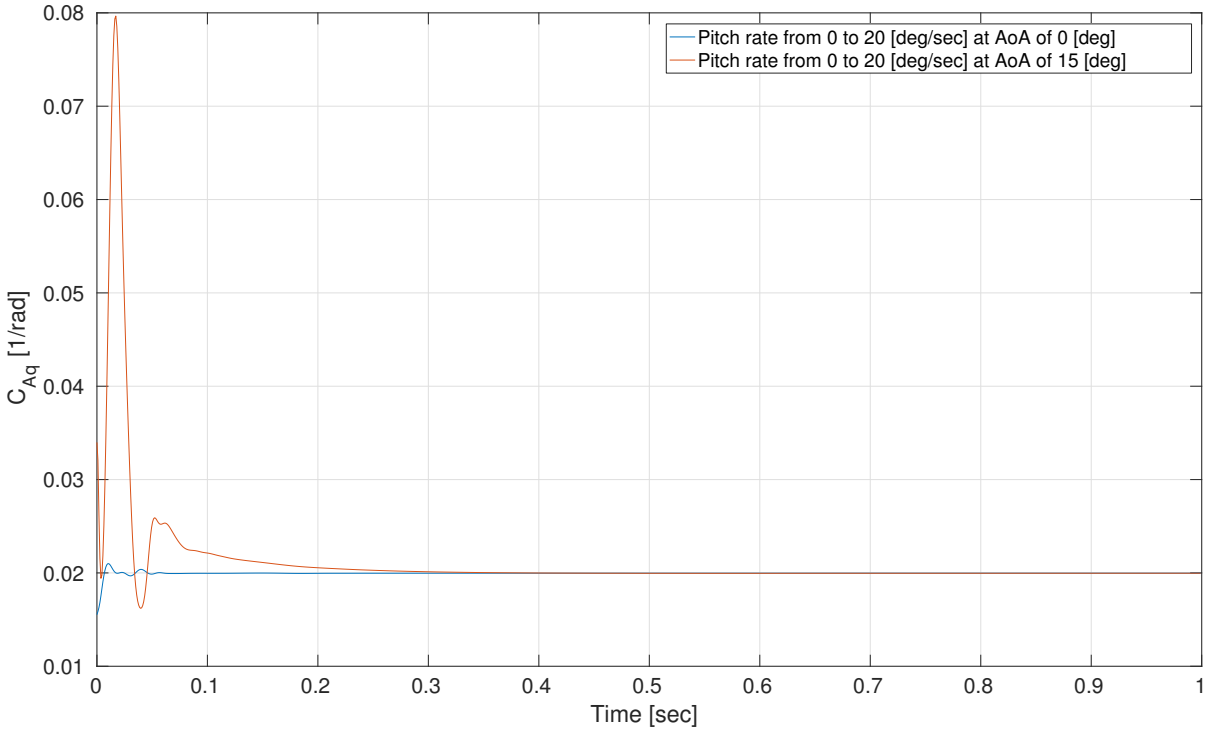

Figure F.2: Indicial step response function of the pitch rate effect on the axial force coefficient by applying a 20 degrees per second step change on a steady RANS solution at various starting angles of attack and zero pitch rate

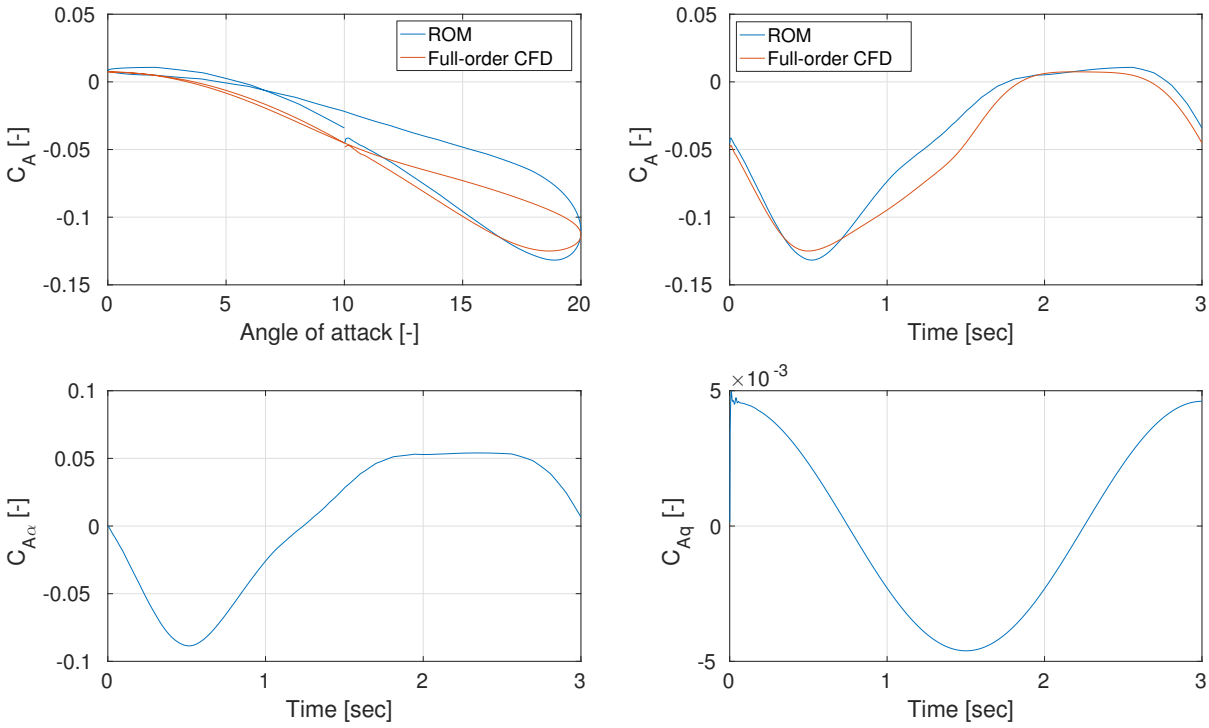

Figure F.3: Comparison between the full-order CFD URANS and the ROM axial force coefficient solutions undergoing a pitching oscillation at a pitch rate of 20$[deg/second]$, Mach of 0.2 and a Reynolds number of 2.8$E7$, also showing the two individual contributions of angle of attack $C_{N\alpha}$ and pitch rate C_{Nq}

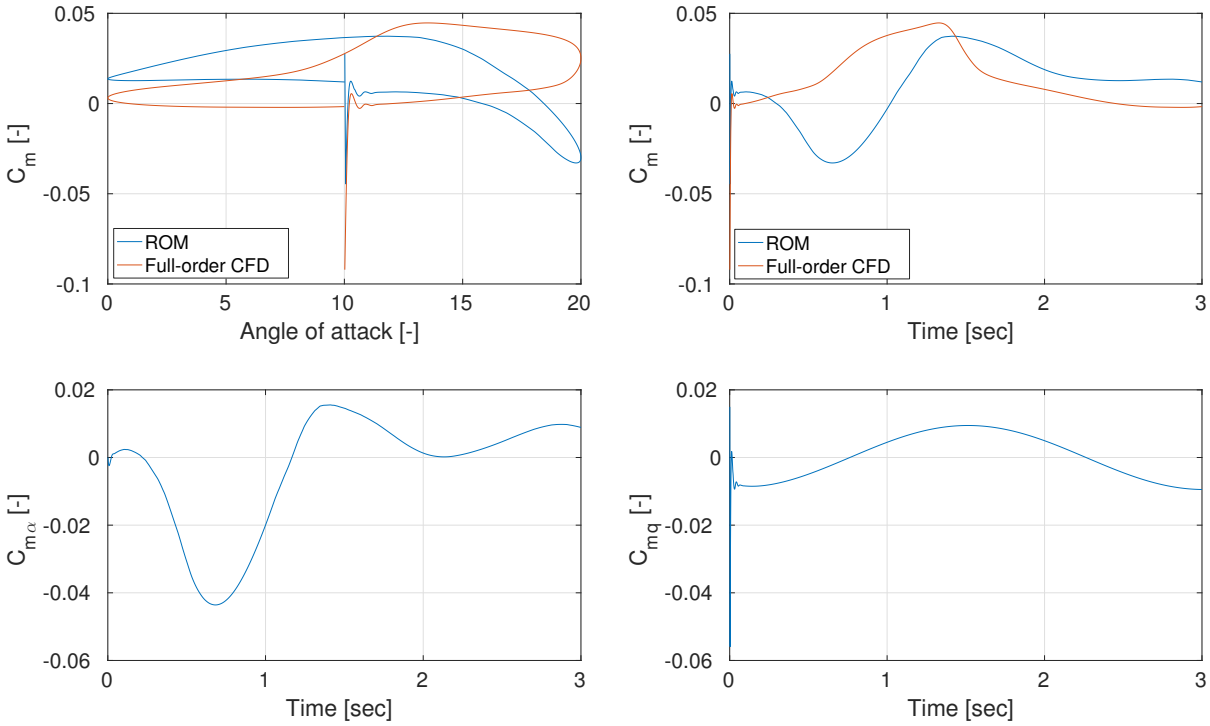

Figure F.4: Comparison between the full-order CFD URANS and the ROM pitching moment coefficient solutions undergoing a pitching oscillation at a pitch rate of 20$[deg/second]$, Mach of 0.2 and a Reynolds number of 2.8$E7$, also showing the two individual contributions of angle of attack $C_{N\alpha}$ and pitch rate C_{Nq}

G

SIMULINK MODEL FOR FLIGHT DYNAMICS PREDICTION

```
%% Accompayning script for SIMULINK manoeuvre model
% Made by Martijn Ketelaars - 2017

clear all
close all
clc

%Initializing
rho             = 1.225;              % air density [kg/m^3]
m               = 10900;              % aircraft mass[kg]
g               = 9.81;               % gravitational acceleration [m/s
  ^2]
speedOfSound    = 340.3;              % speed of sound [m/s]
mach            = 0.2;                % freestream mach number [-]
Vref            = mach*speedOfSound; % reference speed [m/s]
surface         = 77.8;               % reference chord [m^2]
chord           = 6;                  % reference surface [m]
Iyy             = 12564;              % aircraft pitch moment of
  inertia [kg*m^2]
lRef            = 6;                  % reference length[m]

%           [u               w                theta       q]
initial =   [-Vref*cosd(10) -Vref*sind(10)  deg2rad(10) 0];

%Actuator
omega0  =   30;  %natural frequency [rad/sec]
zeta    =   0.7; %damping [-]

%Stabilty derivatives
CXu     =   0;
CXAoALookUpArray = [ 0.0067/deg2rad(1), ...
                     0.0021/deg2rad(3), ...
                    -0.0072/deg2rad(5), ...
                    -0.0207/deg2rad(7), ...
                    -0.0378/deg2rad(9), ...
                    -0.0571/deg2rad(11), ...
```

```
                    -0.0756/deg2rad(13), ...
                    -0.0893/deg2rad(15), ...
                    -0.0960/deg2rad(17), ...
                    -0.0975/deg2rad(19), ...
                    -0.1008/deg2rad(21)];       %[1/rad] non-linear
CXq     =   0.007/deg2rad(20);                  %[sec/rad] linear
CXde    =   0;
CXdt    =   0;

CZu     =   0;
CZAoALookUpArray = [0.0396/deg2rad(1), ...
                    0.1397/deg2rad(3), ...
                    0.2387/deg2rad(5), ...
                    0.3362/deg2rad(7), ...
                    0.4321/deg2rad(9), ...
                    0.5269/deg2rad(11), ...
                    0.6156/deg2rad(13), ...
                    0.6893/deg2rad(15), ...
                    0.7636/deg2rad(17), ...
                    0.8581/deg2rad(19), ...
                    0.9567/deg2rad(21)];        %[1/rad] non-linear
CZq     =   0.0289/deg2rad(20);                 %[sec/rad] linear
CZde    =   0;
CZdt    =   0;

Cmu     =   0;
Cmaoa   =   0;%  [0.0049/deg2rad(1), ...
%                   0.0056/deg2rad(3), ...
%                   0.0065/deg2rad(5), ...
%                   0.0074/deg2rad(7), ...
%                   0.0085/deg2rad(9), ...
%                   0.0101/deg2rad(11), ...
%                   0.0144/deg2rad(13), ...
%                   0.0221/deg2rad(15), ...
%                   0.0284/deg2rad(17), ...
%                   0.0297/deg2rad(19), ...
%                   0.0347/deg2rad(21)];        %[1/rad] non-linear
Cmq     =   0;%-0.0078/deg2rad(20);             %[sec/rad] linear
Cmde    =   0.005/deg2rad(20);
Cmdt    =   0;

%breakpoints for lookup tables
AoALookUpArray = deg2rad([1 3 5 7 9 11 13 15 17 19 21]);

% start SIMULINK model
sim('manoeuvreSIMULINK');

% Receive data from model
time1    = aoa(:,1);

x1       = x(:,2);                  % position w.r.t. initial axis
y1       = zeros(length(time1),1);
z1       = z(:,2);                  % position w.r.t. initial axis

phi1     = zeros(length(time1),1);
theta1   = theta(:,2);              % angle between body and initial
```

```
  axis
psi1      = zeros(length(time1),1);

aoa1      = aoa(:,2);
u1        = u(:,2);                    % u w.r.t. body axis
v1        = zeros(length(time1),1);    %
w1        = w(:,2);                    %w w.r.t. body axis
V1        = V(:,2);

uInit1    = -V1.*cosd(theta1-aoa1);    % u w.r.t. initial axis
wInit1    = V1.*sind(theta1-aoa1);     % w w.r.t. initial axis

p1        = zeros(length(time1),1);
q1        = q(:,2);                % rotatation between body and initial
   axis
r1        = zeros(length(time1),1);

de1       = de(:,2); %[rad]
dt1       = dt(:,2);

%nx       = nx(:,2);
nz1       = nz(:,2);
thrust1   = thrust(:,2);

% Plots
figure()
subplot(3,2,1)
    plot(time1,rad2deg(de1));
    grid on
    ylabel('Elevator deflection [deg]');
    xlabel('Time [sec]');
    set(gca, 'fontsize', 15)
subplot(3,2,2)
    plot(x1,z1);
    grid on
    ylabel('Vertical distance z [m]');
    xlabel('Horizontal distance x [m]');
    set(gca, 'fontsize', 15)
subplot(3,2,3)
    yyaxis left
    plot(time1,V1);
    ylabel('Total velocity [m/sec]');
    hold on
    yyaxis right
    plot(time1,abs(u1),'-.')
    hold on
    plot(time1,abs(w1),'--')
    legend('Total aircraft velocity','Velocity vector u_b (x-axis)', '
      Velocity vector w_b (z-axis)','location','Best')
    ylim([0 70]);
    grid on
    ylabel('Component velocity [m/sec]');
    xlabel('Time [sec]');
    set(gca, 'fontsize', 15)
subplot(3,2,4)
    plot(time1,aoa1);
```

```
144     hold on
145     plot(time1,theta1,'--');
146     legend('Angle of attack', 'Pitch attitude','location','NorthEast')
147     grid on
148     ylabel('Flight parameter [deg]');
149     xlabel('Time [sec]');
150     set(gca, 'fontsize', 15)
151 subplot(3,2,5)
152     plot(time1,q1);
153     grid on
154     ylabel('Pitch rate [deg/sec]');
155     xlabel('Time [sec]');
156     set(gca, 'fontsize', 15)
157 subplot(3,2,6)
158     yyaxis left
159     plot(time1,nz1);
160     ylabel('Load factor [-]')
161     hold on
162     yyaxis right
163     plot(time1,thrust1.*10e-3);
164     grid on
165     legend('Load factor in z-direction (n_z)','Thrust','location','
          SouthWest')
166     ylabel('Thrust [kN]');
167     xlabel('Time [sec]');
168     set(gca, 'fontsize', 15)
```

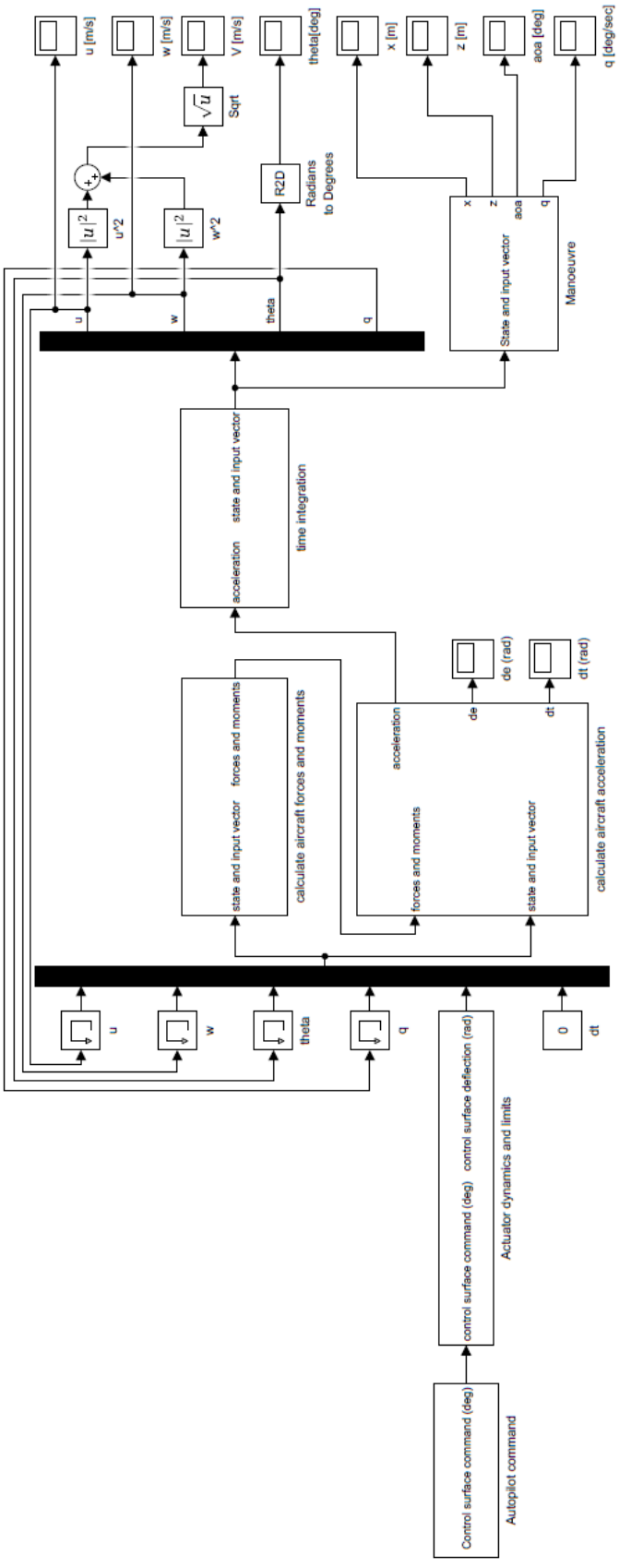

Figure G.1: Main system of SIMULINK flight mechanics model

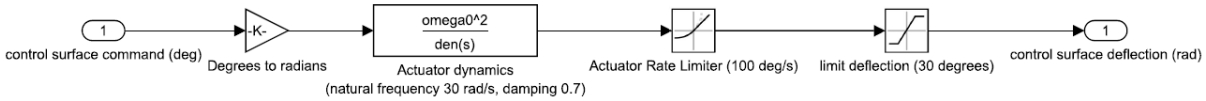

Figure G.2: Actuator dynamics Sub-system of SIMULINK flight mechanics model transferring control command to elevator surface deflection

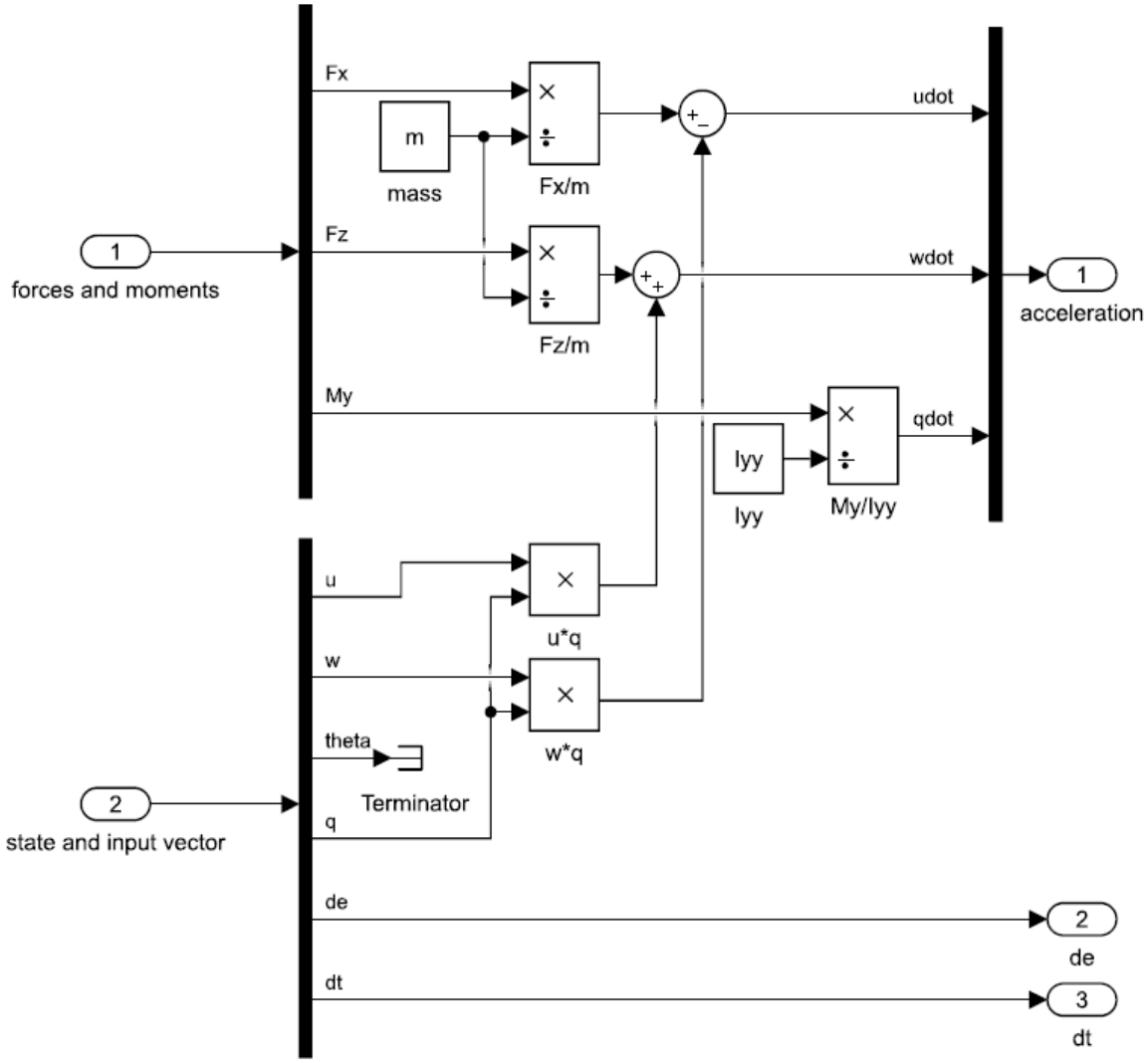

Figure G.3: Sub-system of SIMULINK flight mechanics model transferring forces, moments and states to aircraft acceleration

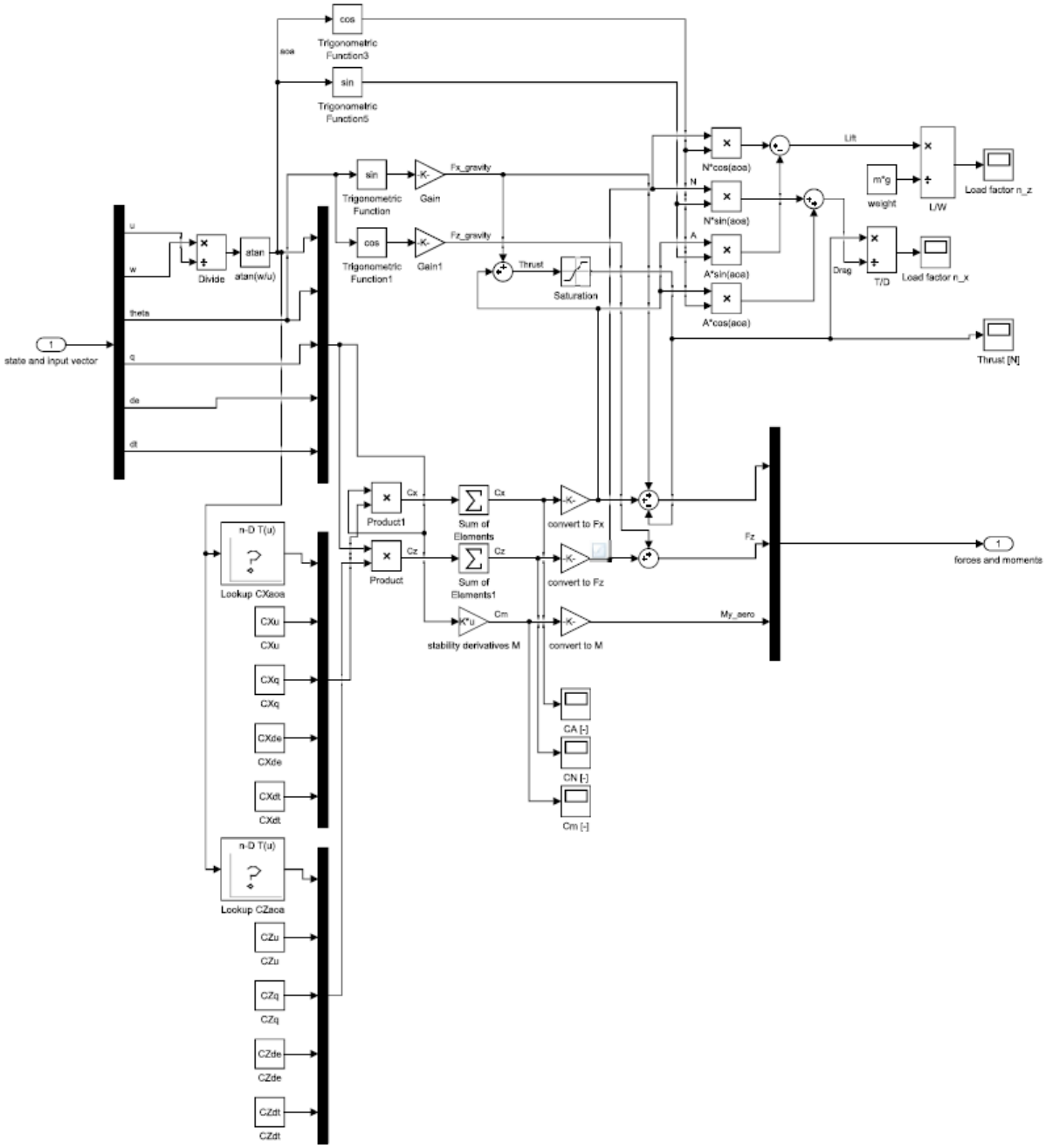

Figure G.4: Sub-system of SIMULINK flight mechanics model transferring aircraft states, applying stability derivatives and adding thrust, to forces and moments

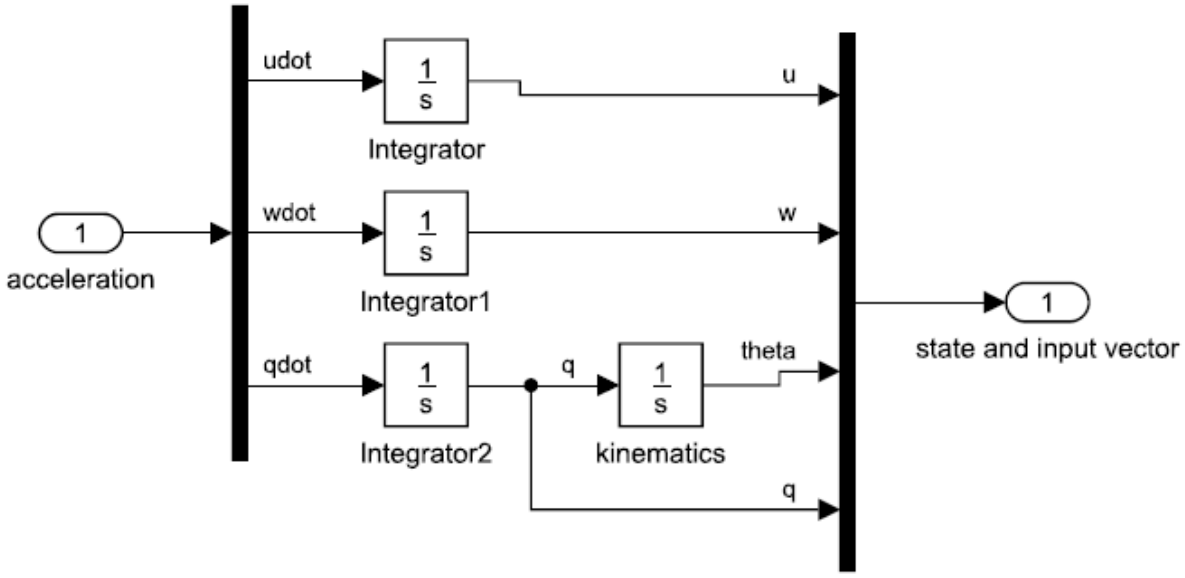

Figure G.5: Sub-system of SIMULINK flight mechanics model integrating the acceleration parameters back to state parameters

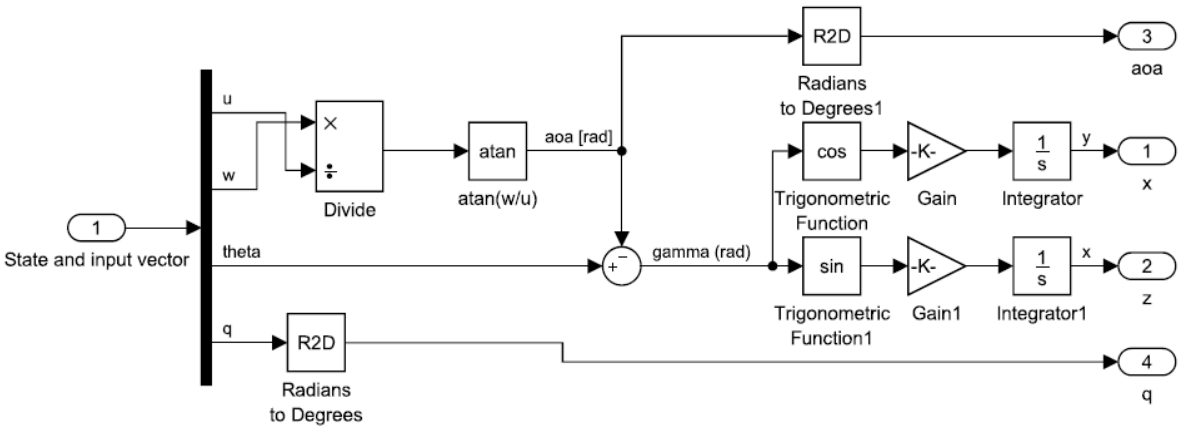

Figure G.6: Sub-system of SIMULINK flight mechanics modelling calculating the manoeuvre based on state and input history

H

ADDITIONAL VALIDATION RESULTS OF MULDICON

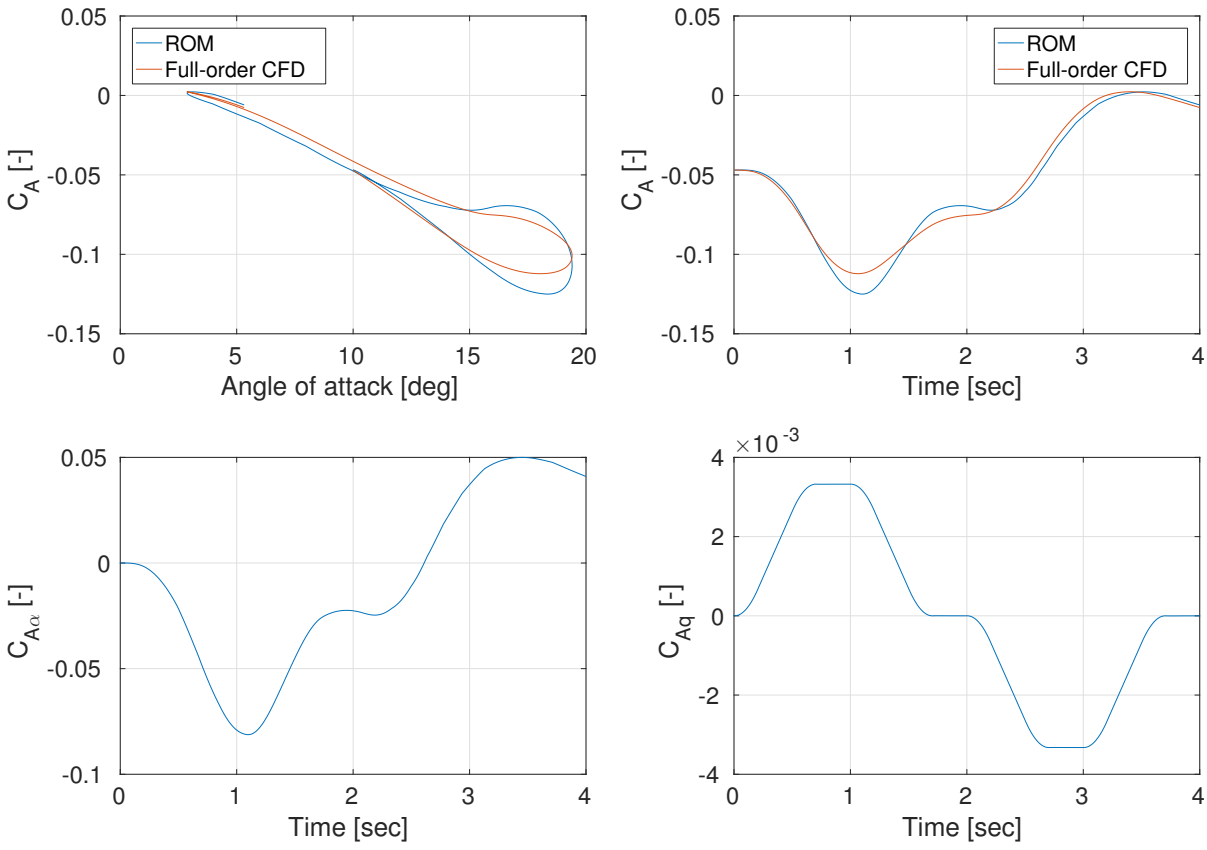

Figure H.1: Comparison between the full-order CFD URANS and the ROM axial force coefficient solutions undergoing the climbing manoeuvre as predicted by the flight dynamics model for validation purposes, also showing the two individual contributions of angle of attack $C_{N\alpha}$ and pitch rate C_{Nq}

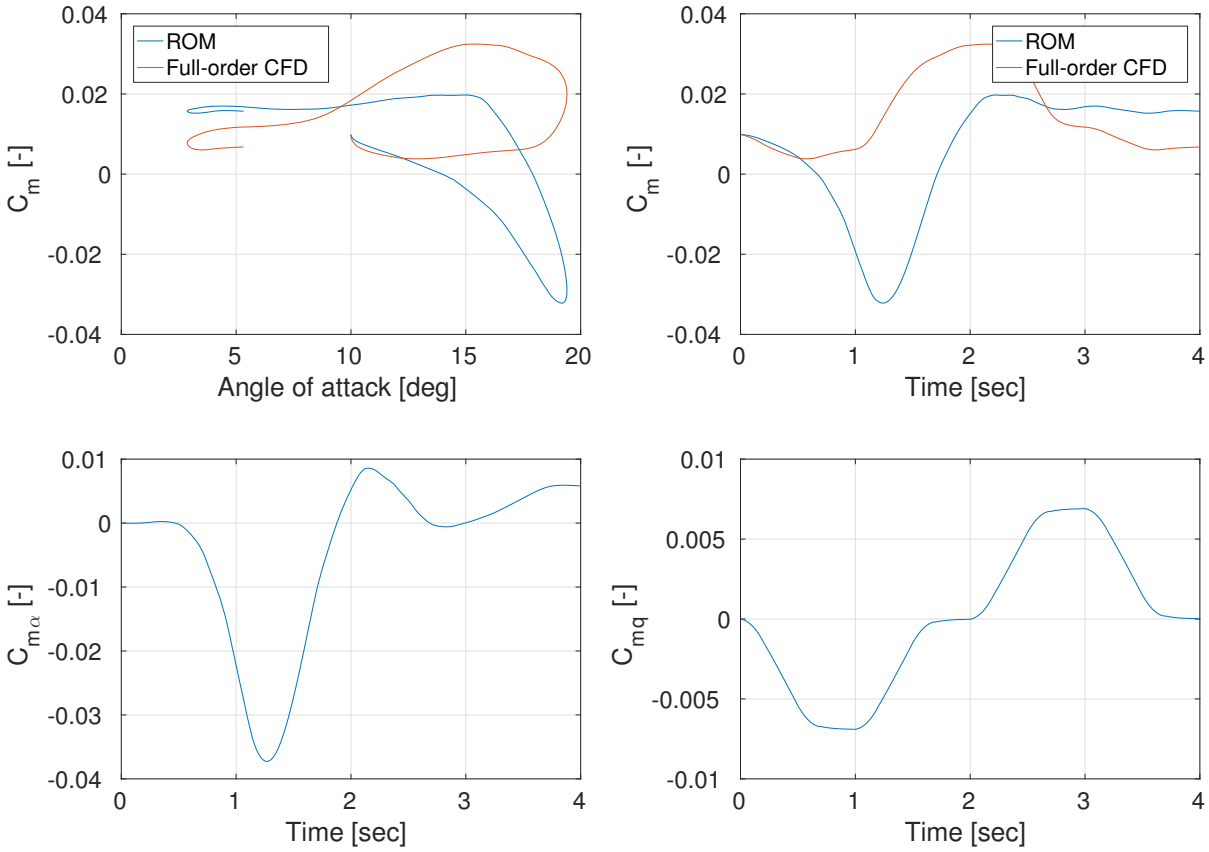

Figure H.2: Comparison between the full-order CFD URANS and the ROM pitching moment coefficient solutions undergoing the climbing manoeuvre as predicted by the flight dynamics model for validation purposes, also showing the two individual contributions of angle of attack $C_{N\alpha}$ and pitch rate C_{Nq}

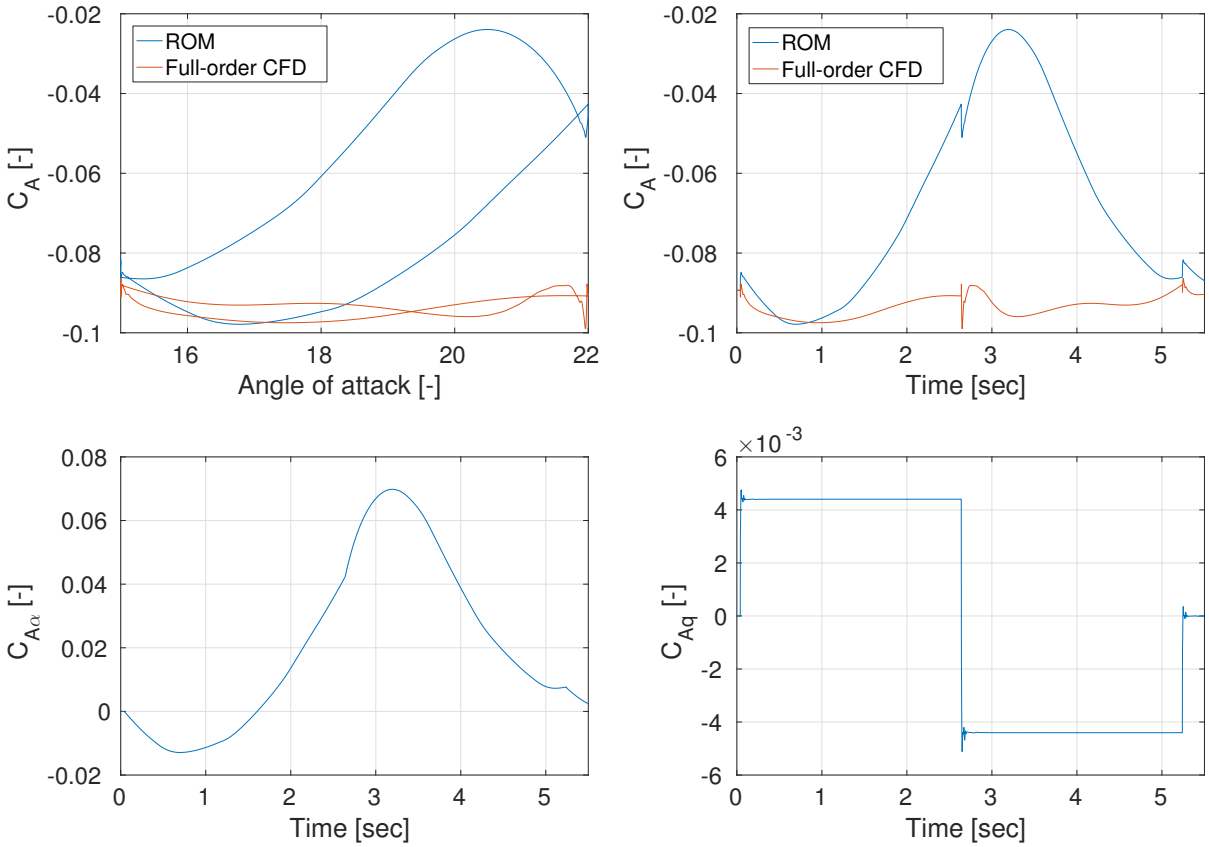

Figure H.3: Comparison between the full-order CFD URANS and the ROM axial force coefficient solutions undergoing the back-of-the-envelope manoeuvre for validation purposes, also showing the two individual contributions of angle of attack $C_{N\alpha}$ and pitch rate C_{Nq}

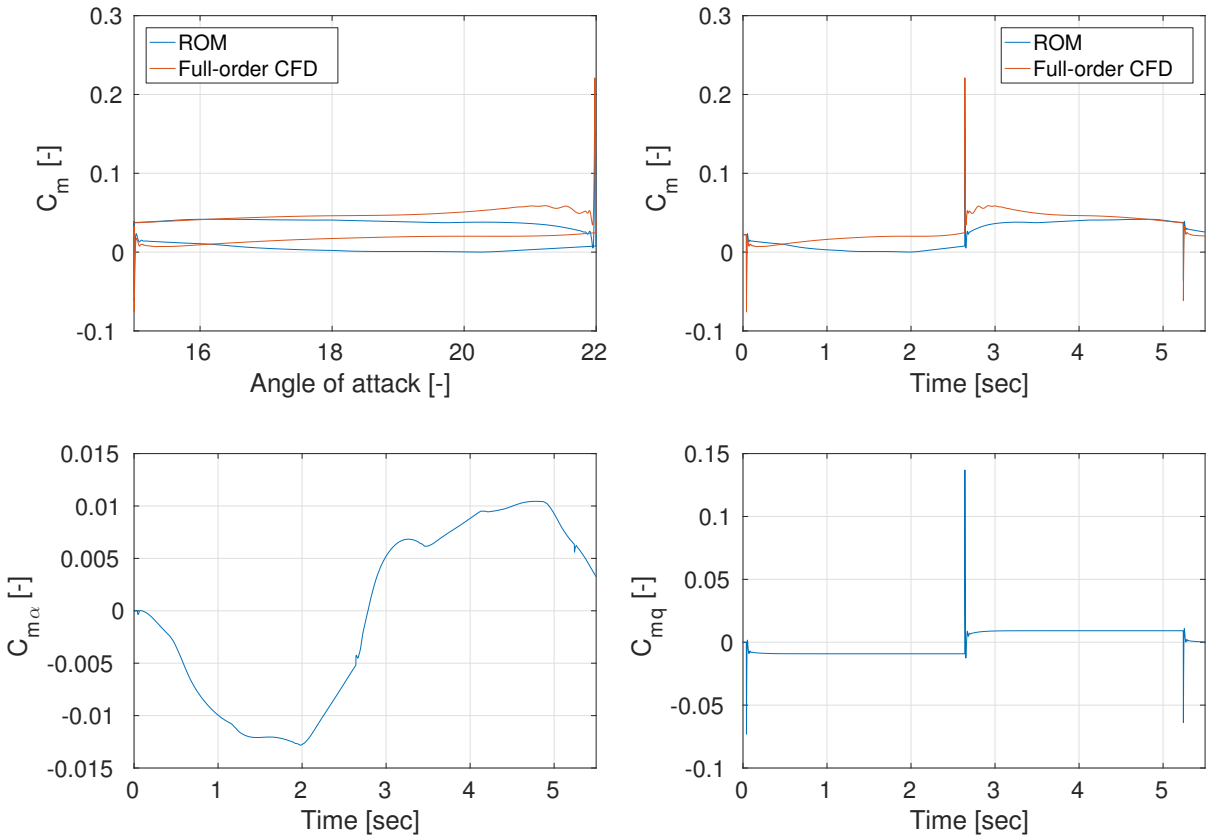

Figure H.4: Comparison between the full-order CFD URANS and the ROM pitching moment coefficient solutions undergoing the back-of-the-envelope manoeuvre for validation purposes, also showing the two individual contributions of angle of attack $C_{N\alpha}$ and pitch rate C_{Nq}

I

DETAILS ON COMPUTATIONAL EFFORT OF MULDICON RESULTS

Table I.1: Detailed results on the computational effort required for the MULDICON testcase calculations made in NLR's CFD solver ENSOLV [95]

Steady-state calculations			
Specification	*CPU hours [h,m]*		*Notes*
AoA = 0 [deg]	4	12	RANS
AoA = 2 [deg]	4	12	RANS
AoA = 4 [deg]	4	9	RANS
AoA = 6 [deg]	4	15	RANS
AoA = 8 [deg]	4	17	RANS
AoA = 10 [deg]	4	11	RANS
AoA = 12 [deg]	4	18	RANS
AoA = 14 [deg]	4	14	RANS
AoA = 16 [deg]	4	14	RANS
AoA = 18 [deg]	4	16	RANS
AoA = 20 [deg]	4	13	RANS
AoA = 22 [deg]	4	16	RANS
Indicial step responses			
Specification	*CPU hours [h,m]*		*Notes*
AoA = 0 to 1 [deg]	67	39	URANS
AoA = 2 to 3 [deg]	68	2	URANS
AoA = 4 to 5 [deg]	68	29	URANS
AoA = 6 to 7 [deg]	68	30	URANS
AoA = 8 to 9 [deg]	67	29	URANS
AoA = 10 to 11 [deg]	69	2	URANS
AoA = 12 to 13 [deg]	69	13	URANS
AoA = 14 to 15 [deg]	58	59	URANS
AoA = 16 to 17 [deg]	68	23	URANS
AoA = 18 to 19 [deg]	58	58	URANS
AoA = 20 to 21 [deg]	61	6	URANS
q = 0 to 20 [deg/sec] at Aoa of 0 [deg]	67	52	URANS
Full-order calculations			
Specification	*CPU hours [h,m]*		*Notes*
Steady state theta and AoA = 2 [deg]	6	5	RANS pitch and AoA are equal
Steady state theta and AoA = 10 [deg]	8	24	RANS pitch and AoA are equal
Steady state theta and AoA = 15 [deg]	11	6	RANS pitch and AoA are equal
Manoeuvre starting from 15 [deg] RANS	>234		URANS based on design requirements
Manoeuvre starting from 15 [deg] RANS	234	40	URANS based on flight dynamics model
Manoeuvre starting from 2 [deg] RANS	393	27	Extra URANS to investigate flow
Pitching motion starting from 10 [deg] RANS	211	12	URANS to investigate unsteady flow
Verification calculations			
Specification	*CPU hours [h,m]*		*Notes*
q = 0 to 20 [deg/sec] at Aoa of 15 [deg]	119	26	URANS to investigate NACA conclusions
Long steady state theta and AoA = 15 [deg]	36	58	URANS to investigate flow divergence
Long AoA = 20 [deg]	7	24	RANS to investigate damping
Long AoA = 21 [deg]	7	27	RANS to investigate damping
Long AoA = 22 [deg]	7	24	RANS to investigate damping

BIBLIOGRAPHY

[1] Cummings, Russell M and Schütte, Andreas, *Integrated computational/experimental approach to unmanned combat air vehicle stability and control estimation,* Journal of Aircraft **49**, 1542 (2012).

[2] Ghoreyshi, M., Cummings, R.M., *Unsteady aerodynamics modeling for aircraft maneuvers: A new approach using time-dependent surrogate modeling,* Aerospace Science and Technology **39**, 222 (2014).

[3] Chambers, J.R. and Hall, R.M., *Historical review of uncommanded lateral-directional motions at transonic conditions,* Journal of Aircraft **41**, 436 (2004).

[4] Hall, R.M., Woodson, S.H., and Chambers, J.R., *Accomplishments of the abrupt-wing-stall program,* Journal of Aircraft **42**, 653 (2005).

[5] Yurkovich, R., *Status of unsteady aerodynamic prediction for flutter of high-performance aircraft,* Journal of Aircraft **40**, 832 (2003).

[6] Cover picture, *B2 bomber infographic,* http://wallpoper.com/wallpaper/stealth-bomber-262100 (2012), "[Viewed on 16-07-2017]".

[7] Jacobson, S.B., Britt, R.T., Freim, D.R., and Kelly, P.D., *Residual pitch oscillation flight test analysis on the b-2 bomber,* AIAA Paper (1998).

[8] Fink, R.D., Hoak, D.E., *Usaf stability and control datcom,* Air Force Flight Dynamics Laboratory, Wright-Patterson AFB, Ohio (1975).

[9] Anderson, J.D., Wendt, J., *Computational fluid dynamics*, Vol. 206 (Springer, 1995).

[10] Raveh, D.E., Karpel, M., *Structural optimization of flight vehicles with computational-fluid-dynamics-based maneuver loads,* Journal of aircraft **36**, 1007 (1999).

[11] Nixon, D., *Conceptual design method for wings at transonic speeds,* AIAA paper , 97 (1997).

[12] Ghoreyshi, Mehdi and Cummings, Russell M., *Aerodynamics modeling of a maneuvering Aircraft Using Indicial Funtions,* Aerospace Science and Technology (2012).

[13] Ghoreyshi, M., Lofthouse, A. J., Cummings, R. M., *Sampling strategies for reduced-order modeling of nonlinear and unsteady aerodynamics,* (American Institute of Aeronautics and Astronautics Inc., 2014).

[14] Ghoreyshi, M., Vallespin, D., Da Ronch, A., Badcock, K.J., Vos, J., and Hitzelf, S., *Simulation of aircraft manouvres based on computational fluid dynamics,* AIAA Paper (2010).

[15] A. Jameson, *Re-engineering the design process through computation,* Journal of Aircraft **36**, 36 (1999).

[16] E. Oktay and H. U. Akay, *Cfd predictions of dynamic derivatives for missiles,* AIAA Paper **276**, 14 (2002).

[17] Da Ronch, A., Ghoreyshi, M., Badcock, K.J., *On the generation of flight dynamics aerodynamic tables by computational fluid dynamics,* Elsevier Progress in Aerospace Sciences **47**, 597 (2011).

[18] Ghoreyshi M., Badcock K., Da Ronch A., Marques S., Swift A., Ames N., *Framework for Establishing Limits of Tabular Aerodynamic Models for Flight Dynamics Analysis,* Aerospace Science and Technology (2011).

[19] Chaderjian, N.M., and Pandya, S.A., *Automation of a navier-stokes s&c database generation for the harrier in ground effect,* AIAA Paper **259** (2002).

[20] Ghoreyshi, Mehdi and Vallespin, David and Da Ronch, Andrea and Badcock, KJ and Vos, Jan and Hitzel, Stefan, *Simulation of aircraft manoeuvres based on computational fluid dynamics,* in *AIAA Atmospheric Flight Mechanics Conference* (2010) p. 8239.

[21] D. I. Greenwell, *A review of unsteady aerodynamic modelling for flight dynamics of manoeuvrable aircraft,* AIAA paper **5276**, 2004 (2004).

[22] Cowley, W.L. and Glauert, H., *The effect of the lag of the Downwash on the Longitudinal Stability of an Airplane and on the Rotary Derivative,* Reports and Memoranda (1921).

[23] Wagner, H., *Über die Entstehung des dynamischen Auftriebes von Tragflügeln,* Zeitschrift fur angewandte Mathematik und Mechanik **1**, 17 (1925).

[24] H. Lomax, *Indicial aerodynamics,* (1961).

[25] Silva, W.A., Bartels, R.E., *Development of reduced-order models for aeroelastic analysis and flutter prediction using the cfl3dv6. 0 code,* Journal of Fluids and Structures **19**, 729 (2004).

[26] Lucia, D.J. ,Beran, P.S., Silva, W.A., *Reduced-order modeling: new approaches for computational physics,* Progress in Aerospace Sciences **40**, 51 (2004).

[27] H. Kussner, *Stresses produced in airplane wings by gusts,* NACA (1932).

[28] Theodorsen, T., *General theory of aerodynamic instability and the mechanism of flutter,* NACA (1949).

[29] Sears, W.R., *Some aspects of non-stationary airfoil theory and its practical application,* Journal of the Aeronautical Sciences **8**, 104 (1941).

[30] Giesing, J.P., Kalman, T.P., Rodden, W.P., *Subsonic unsteady aerodynamics for general configurations, part i. direct application of the nonplanar doublet lattice method.* Air Force Flight Dynamics Laboratory Report AFFDL-TR-71-5 (1971).

[31] Silva, W.A., *Discrete-time linear and nonlinear aerodynamic impulse responses for efficient CFD analyses.*, Ph.D. thesis, College of William and Mary (1997).

[32] Ghoreyshi, M., Jirasek, A., and Cummings, R.M., *Computational investigation into the use of response functions for aerodynamic-load modeling,* AIAA **50**, 1314 (2012).

[33] Ghoreyshi, Mehdi and Cummings, Russell M, *Challenges in the aerodynamics modeling of an oscillating and translating airfoil at large incidence angles,* Aerospace Science and Technology **28**, 176 (2013).

[34] MIT, *Avl - vortex-lattice model,* http://web.mit.edu/drela/Public/web/avl/ (2015), "[Viewed on 27-10-2016]".

[35] Ghoreyshi, M., Jirasek, A., Cummings, R.M., *Reduced order unsteady aerodynamic modeling for stability and control analysis using computational fluid dynamics,* Progress in Aerospace Sciences **71**, 167 (2014).

[36] Schütte, A., Einarsson, G., Raichle, A., Schoning, B., Mönnich, W., and Forkert, T., *Numerical simulation of manoeuvreing aircraft by aerodynamic, flight mechanics, and structural mechanics coupling,* Journal of Aircraft **46**, 53 (2009).

[37] Ghoreyshi, M., Jirasek, A., and Cummings, R.M., *Cfd modeling for trajectory predictions of a configurations,* AIAA Paper (2011).

[38] Stark, V.J.E., *Indicial coefficients for a cropped delta wing in incompressible flow,* Journal of Aircraft **23**, 370 (1985).

[39] Lisandrin, P., Carpentieri, G., and van Tooren, M., *Investigation over cfd-based models for the identification of nonlinear unsteady aerodynamic responses,* AIAA Journal **44**, 2043 (2006).

[40] NATO-AVT-251, *Multi-disciplinary design and performance assessment of effective, agile nato air vehicles,* https://www.cso.nato.int/ACTIVITY_META.asp?ACT=6144 (2016), "[Viewed on 27-10-2016]".

[41] D. Vallespin, M. Ghoreyshi, and K. Badcock, *Assessment of the limits of tabular aerodynamic models for flight dynamics analysis using the saccon ucav configuration,* in *Royal Aeronautical Society aerodynamics conference* (2010).

[42] J. Kalviste, *Aircraft stability characteristics at high angles of attack,* AGARD Dyn. Stability Parameters 18 p(SEE N 79-15061 06-08) (1978).

[43] J. Roskam, *Airplane flight dynamics and automatic flight controls* (DARcorporation, 1995).

[44] S. M. Murman, *Reduced-frequency approach for calculating dynamic derivatives,* AIAA journal **45**, 1161 (2007).

[45] Parrish, Jeff and Rais-Rohani, Masoud and Janus, M, *Reduced-order techniques for sensitivity analysis and design optimization of aerospace systems,* AIAA Journal **53**, 3567 (2015).

[46] Dowell, E.H., Hall, K.C., Thomas, J.P., Florea, R., Epureanu, B.I., Heeg, J., *Reduced order models in unsteady aerodynamics,* AIAA (1999).

[47] E. H. Dowell, *Eigenmode analysis in unsteady aerodynamics: Reduced-order models,* AIAA journal **34** (1996).

[48] Q. Wang, K.-F. He, W.-Q. Qian, T.-J. Zhang, Y.-Q. Cheng, and K.-Y. Wu, *Unsteady aerodynamics modeling for flight dynamics application,* Acta Mechanica Sinica **28**, 14 (2012).

[49] V. Volterra, *Theory of Functionals of Integral and Integro-Differential Equations* (Dover Publ., 1959).

[50] Silva, W. A., *Discrete-time linear and nonlinear aerodynamic impulse responses for efficient CFD analyses,* Ph.D. thesis, College of William and Mary (1997).

[51] W. A. Silva, P. S. Beran, C. E. Cesnik, R. E. Guendel, A. Kurdila, R. J. Prazenica, L. Librescu, P. Marzocca, and D. E. Raveh, *Reduced-order modeling: cooperative research and development at the nasa langley research center,* (2001).

[52] W. A. Silva, *Identification of nonlinear aeroelastic systems based on the volterra theory: progress and opportunities,* (2009).

[53] Kvaternik R Silva W, *A computational procedure for identifying bilinear representations of nonlinear systems using volterra kernels,* (2008).

[54] N. K. Leishman J, *State-Space Representation of Unsteady Airfoil Behavior,* (1998).

[55] D. Findeisen, *System dynamics and mechanical vibrations: an introduction* (Springer Science & Business Media, 2013).

[56] Tobak, M., Schiff, L.B., *On the formulation of the aerodynamic characteristics in aircraft dynamics,* (1976).

[57] Ballhaus, W. F., Goorjian, P. M., *Computation of unsteady transonic flows by the indicial method,* AIAA Journal **16**, 117 (1987).

[58] Singh, R. and Baeder, J.,, *Direct Calculation of Three-Dimensional Indicial Lift Response Using Computational Fluid Dynamics,* journal of Aircraft **34** (1997).

[59] Ghoreyshi, M., Cummings, R.M., Da Ronch, A., Badcock, K.J., *Transonic Aerodynamic Load Modeling of X-31 Aircraft Pitching Motions,* AIAA Journal **51**, 2447 (2013).

[60] Ghoreyshi, M., Post, M.L., Cummings, R.M., *Cfd calculation of aerodynamic indicial functions for a generic fighter configuration,* ITEA J. Test Eval. **33**, 348 (2012).

[61] Ghoreyshi, M., Cummings, R. M., *Unsteady aerodynamic modeling of aircraft control surfaces by indicial response methods,* **52**, 2683 (2014).

[62] Simpson, T.W., Mauery, T.M., Korte, J.J., Mistree, F., *Kriging models for global approximation in simulation-based multidisciplinary design optimization,* AIAA journal **39**, 2233 (2001).

[63] Ghoreyshi, M., Badcock, K.J., Woodgate, M.A., *Accelerating the numerical generation of aerodynamic models for flight simulation,* Journal of aircraft **46**, 972 (2009).

[64] Tobak, M., Murray, *National Advisory Committee for Aeronautics*, Tech. Rep. (NACA).

[65] N. Hariharan and J. G. Leishman, *Unsteady aerodynamics of a flapped airfoil in subsonic flow by indicial concepts,* Journal of Aircraft **33**, 855 (1996).

[66] M. Queijo, W. R. Wells, and D. A. Keskar, *Approximate indicial lift function for tapered, swept wings in incompressible flow,* (1978).

[67] D. Nixon, P. Reisenthel, T. Torres, and G. Klopfer, *unsteady transonic flow around missile configurations,* (1990).

[68] P. REISENTHEL and D. Nixon, *Application of indicial theory to the prediction of unsteady separation,* in *22nd Fluid Dynamics, Plasma Dynamics and Lasers Conference* (1991) p. 1742.

[69] P. Reisenthel, D. LESIEUTRE, and D. Nixon, *Prediction of aeroelastic effects for sea-skimming missiles with flow separation,* in *32nd Structures, Structural Dynamics, and Materials Conference* (1991) p. 1052.

[70] D. J. Lesieutre, P. H. Reisenthel, and M. F. Dillenius, *Alaa 94-0059 a practical approach for calculating aerodynamic indicia1 functions with a navier-stokes solver,* (1994).

[71] K. Yiu and P. Stow, *Aspects of the transpiration model for aerofoil design,* International Journal for numerical methods in fluids **18**, 509 (1994).

[72] P. H. Reisenthel, *linear indicial model for maneuvering fighter aircraft,* AIAA paper **896**, 1996 (1996).

[73] Reisenthe, P., Bettencourt, M., *Data-based aerodynamic modeling using nonlinear indicial theory,* (1999).

[74] P. Reisenthel, W. Xie, I. Gursul, and M. Bettencourt, *Aim 99-0136 an analysis of fin motion induced vortex breakdown,* (1999).

[75] Reisenthel, P.H., Bettencourt, M.T., *Extraction of nonlinear indicial and critical state responses from experimental data,* AIAA Paper , 99 (1999).

[76] P. Reisenthel, *Development of a nonlinear indicial model using response functions generated by a neural network,* 35th Aerospace Sciences Meeting and Exhibit (1997).

[77] Nielsen Engineering and Research, INC. , *Nonlinear indicial prediction (ips),* http://www.nearinc.com/index.cfm?fuseaction=page.display&page_id=108, "[Viewed on 25-11-2016]".

[78] P. H. Reisenthel, M. T. Bettencourt, J. H. Myatt, and D. S. Grismer, *A nonlinear indicial prediction tool for unsteady aerodynamic modeling,* AIAA Paper **9814350** (1998).

[79] NATO-AVT-161, *Assessment of stability and control prediction methods for nato air and sea vehicles,* https://www.cso.nato.int/ACTIVITY_META.asp?ACT=929 (2011), "[Viewed on 06-12-2016]".

[80] Cummings, R.M., Schütte, A., and Hübner, A., *Overview of stability and control estimation methods from nato sto task group avt-201,* (2013).

[81] NATO-AVT-201, *Extended assessment of reliable stability and control prediction methods for nato air vehicles,* http://www.cso.nato.int/Activity_Meta.asp?Act=2060 (2012), "[Viewed on 22-11-2016]".

[82] M. Ghoreyshi, D. Vallespin, A. Da Ronch, K. Badcock, J. Vos, and S. Hitzel, *Simulation of aircraft manoeuvres based on computational fluid dynamics,* AIAA paper **8239** (2010).

[83] Ghoreyshi, M., Frink, N.T., v. Rooij, M., Lofthouse, A.J., Cummings, R.M., Nayani, S., *Collaborative evaluation of cfd-to-rom dynamic modeling,* (2016).

[84] Ghoreyshi, Mehdi and Young, Michael E and Lofthouse, Andrew J and Jirásek, Adam and Cummings, Russell M, *Numerical simulation and reduced-order aerodynamic modeling of a lambda wing configuration,* Journal of Aircraft , 1 (2016).

[85] Ghoreyshi, M., French, P.L., Findlay, D., Lee, J., Jirasek, A., Lofthouse, A.J., *Indicial methods for the numerical calculation of dynamic derivatives of a finned projectile,* in *46th AIAA Fluid Dynamics Conference* (2016) p. 3199.

[86] NASA - Langley Research Center, *The explicit algebraic stress k-omega turbulence model,* https://turbmodels.larc.nasa.gov/easmko.html (2016), "[Viewed on 30-06-2017]".

[87] N. G. Spekreijse, S.P., *Usser guide of Endomo Version 2.60, A Graphical Interactive Domain Decomposer For Multi-Block Domain Decomposition of Arbitrary Flow Domains*, NLR ().

[88] N. G. Spekreijse, S.P., *Usser guide of Engrid, Version 4.20, A Graphical Interactive Grid Generator For Arbitrary Multi-Block Domains*, NLR ().

[89] M. Ghoreyshi, N. T. Frink, M. van Rooij, A. J. Lofthouse, R. M. Cummings, and S. Nayani, *Collaborative evaluation of cfd-to-rom dynamic modeling,* in *54th AIAA Aerospace Sciences Meeting* (2016) p. 1077.

[90] R. Landon, *Compendium of unsteady aerodynamic measurements,* AGARD Report **702** (1982).

[91] Aerospace web - Jeff Scot, *Lift and drag vs. normal and axial force,* http://www.aerospaceweb.org/question/aerodynamics/q0194.shtml] (2004), "[Viewed on 14-06-2017]".

[92] Appendix B, page 82, figure B-12, *MIL-STD-3013, Glossary of Definitions, Ground Rules, and Mission Profiles to Define Air Vehicle Performance and Capability*, Tech. Rep. (US Department of Defense).

[93] E. C. Polhamus, *A concept of the vortex lift of sharp-edge delta wings based on a leading-edge-suction analogy,* (1966).

[94] A. J. Lofthouse and K. N. Cotton, *Computational simulation of a generic ucav configuration with control surfaces,* .

[95] J. Kok and B. Prananta, *User guide of ensolv version 7.21, a flow solver for aerodynamic, aeroelastic, and aeroacoustic applications using 3d multi-block structured grids,* (2010).

[96] S. A. Morton and D. R. McDaniel, *Cfd based model building of the f-16xl static and dynamic loads using kestrel,* AIAA Paper **286** (2017).

[97] A. Jirásek, T. L. Jeans, M. Martenson, R. M. Cummings, and K. Bergeron, *Improved methodologies for maneuver design of aircraft stability and control simulations,* in *48th AIAA Aerospace Sciences Meeting* (2010) pp. 2010–515.

[98] A. Jirasek and R. M. Cummings, *Saccon static and dynamic motion flow physics simulations using cobalt,* in *Proceedings of the 29th AIAA Applied Aerodynamics Conference* (2011) pp. 1–11.

[99] Mason, William H and Knill, Duane L and Giunta, Antony A and Grossman, Bernard and Watson, Layne T and Haftka, Raphael T, *Getting the full benefits of cfd in conceptual design,* in *16th AIAA Applied Aerodynamics Conference, Albuquerque, NM, Paper No. AIAA* (1998) pp. 98–2513.

[100] J. R. Snyder, *Aim-90-3209 cfd needs in conceptual design,* (1990).

[101] C. E. Lan, *A quasi-vortex-lattice method in thin wing theory,* Journal of Aircraft **11**, 518 (1974).